INVESTIGATING THE EFFECT OF ENANTIOMERIC RATIO AND PREPARATION METHOD ON CRYSTALLINE FORMS OF PROLINE USING SOLID-STATE NMR SPECTROSCOPY
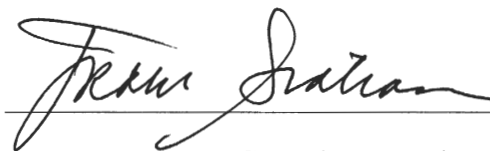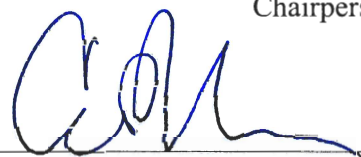
BY

ROBERT T. BERENDT II

Submitted to the graduate degree program in Pharmaceutical Chemistry and the Graduate Faculty of the University of Kansas in partial fulfillment of the requirements for the degree of Doctor of Philosophy.

_____

Chairperson

_____

_____

_____

_____

Committee members

Date Defended: August 19, 2010

The Dissertation Committee for Robert T. Berendt II

certifies that this is the approved version of the following dissertation:

INVESTIGATING THE EFFECT OF ENANTIOMERIC RATIO AND
PREPARATION METHOD ON CRYSTALLINE FORMS OF PROLINE
USING SOLID-STATE NMR SPECTROSCOPY

_____

Chairperson

Date approved: August 26, 2010

ii

Abstract

Chiral molecules are prevalent among currently marketed pharmaceutical products, many of which are solid formulations. The solid-state form of a drug can have a dramatic effect on its solubility, dissolution rate (hence bioavailability), physical stability, and interaction with excipients; therefore, understanding the solid forms that exist for a drug molecule is critical to ensure product performance and safety. Analysis of solid systems typically requires the application of several analytical techniques, one or two of which may be particularly helpful. In this thesis work, solid-state NMR spectroscopy (SSNMR) was found to be a particularly powerful method for characterizing proline enantiomers in the solid state.

Using SSNMR, we evaluated the differences in crystal forms of proline that resulted from changes in enantiomeric ratio and crystallization conditions. Various ratios of D- and L-proline (0–50% L-proline with 100–50% D-proline) were crystallized from aqueous solution and by lyophilization, spray drying, and cryogrinding. These methods produced multiple crystalline forms, including previously unreported polymorphs and chiral defects, in which the L-proline molecules were kinetically trapped in the D-proline crystal lattice.

This thesis work has significant implications for the development of pharmaceutical solids. Whereas typical solid-form screening assays involve crystallizing from various solvents, we used lyophilization, spray drying, and cryogrinding. These nontraditional crystallization methods produced high-energy solids (e.g., metastable polymorphs, defects, and amorphous material) and an unreported more

thermodynamically stable co-crystal polymorph. Additionally, the presence of L-proline enantiomeric impurity altered the crystallization process of D-proline, therein affecting the crystal product. "Chiral doping" is potentially a valuable addition to current solid-form screening processes, as it may produce forms that would not be observed during normal screening methods.

SSNMR was highly suited for investigating proline enantiomers in the solid state. Different solid forms, including crystal defects and amorphous material, possessed different peaks in ^{13}C CP-MAS NMR spectra. Also, isotopic labeling, combined with spectral subtraction, allowed for identification and relative quantitation of solid forms within a wide range of enantiomeric ratios. Phase separation among these forms was confirmed by ^{1}H T_1 relaxation measurements, and 2D-SSNMR experiments demonstrated the potential to provide in-depth structural information.

Dedicated to:

My Family

Acknowledgements

Thank you very much to my graduate advisor, Dr. Eric Munson. His support during my graduate work was essential for my success in both the classroom and the laboratory. I look forward to many future interactions with him and the Munson lab.

The members of the Munson lab have become some of my closest friends. Dr. Joseph Lubach, Dr. Loren Schieber, Ben Nelson, Dr. Diana Sperger, Eric Gorman, Sarah Pyszczynski, and Elodie Dempah: Thank you for all of our science-related discussions, your help within the laboratory, and especially your friendship outside of the lab. In particular, I would like to acknowledge Diana, who has been a tremendous source of support and friendship over the last six years of studying, conference traveling, and late nights/weekends working in lab. Also, thanks to Sarah for reading and providing feedback on my dissertation, as well as for sharing her mad baking skills with us lab members. And Elodie, your 100%–natural-abundance happiness made even frustrating days a bit brighter *here* in the lab.

Thanks to my dissertation committee, Dr. Valentino Stella, Dr. Susan Lunte, Dr. Teruna Siahaan, and Dr. Stevin Gehrke, for serving on my committee. Thank you especially to Dr. Stella for reading my dissertation and providing valuable feedback and guidance during the writing process.

Thank you to all of the faculty and staff of the Department of Pharmaceutical Chemistry. I am especially thankful to Dr. Elizabeth Topp and her graduate students for hosting me as a summer undergraduate research student in the summer of 2003. My decision to come to this department and to pursue research in the area of solid-state

characterization was due in large part to the positive experience that they provided. Thank you to the faculty for course/seminar lectures, which have provided me with a broad foundation that has been helpful in performing my dissertation research and will no doubt be invaluable to me in the future. I also extend my gratitude to the departmental staff, Nancy Helm, Ann Heptig, Nicole Brooks, and Karen Hall, for all of their help, support, and kindness.

Dr. Bradley Hanson provided me with an opportunity to intern at Schering-Plough Research Institute during the summer of 2008. I appreciate all of his efforts to ensure that I had a positive experience.

I would also like to thank Dr. Raj Suryanarayanan and Dr. Paroma Chakravarty for their collaboration in characterizing thiamine hydrochloride hydrates. This collaborative work provided valuable insight into my own dissertation project. Thanks especially to Paroma for her time and effort in helping me acquire diffraction patterns of proline and to Dr. Sury for time on the powder X-ray diffractometer at the University of Minnesota Characterization Facility.

I am greatly indebted to Al and Lila Self. The programming of the Madison & Lila Self Graduate Fellowship enriched my time here at the University of Kansas, and the lessons learned during the skill sessions will contribute greatly to future successes. Special thanks to Jimmy Morrison, Cathy Dwigans, Sharon Graham, and Patty Dannenberg for all of their work in creating and organizing the development program.

I had the pleasure of mentoring two undergraduate students, Matt Durban and Maya Lipert. Thanks to both of them for their work in assessing the feasibility of using pseudoephedrine as a model chiral molecule for SSNMR studies.

Special thanks to my family for all of their support, encouragement, and love. Dad, thank you for always encouraging me to seek balance in my life while also demonstrating the importance of a strong work ethic. Nick, my *little* brother, thank you for interjecting humor into everyday life and helping me laugh at myself when I take things too seriously. And Mom, thank you for instilling in me a great desire to learn and the value of education. I love you and am very proud of all of you.

Table of Contents

Chapter 1

Chiral Molecules in the Solid State: Pharmaceutical Relevance

1.1   Purpose of this work

The purpose of this work was to selectively identify and characterize the crystallographic locations of L-proline molecules upon crystallization with the opposite enantiomer, D-proline. Concurrent crystallization of opposite enantiomers can produce a wide range of solid phases, including cocrystals, solid solutions, polymorphic forms, hydrates/solvates, and chiral defects. Despite the fact that crystallization processes are commonplace due to their use as separation methods in the production of enantiopure pharmaceuticals, the manner in which one enantiomer can become incorporated into or affect the crystallization of the opposite enantiomer has not been thoroughly studied. This lack of understanding is particularly true for the formation of chiral defects, which occur when one enantiomer is present as a substitutional defect in the crystal lattice of its antipode. The lack of knowledge in this area has been largely due to analytical limitations and challenges associated with studying such complicated solid-state systems. In this body of work, we applied ^{13}C solid-state NMR spectroscopy and complementary solid-state analytical methods to investigate the presence of polymorphism and the incorporation of chiral defects as a function of D- and L-proline enantiomeric ratio and preparation method.

1.2   Introduction

Chiral molecules have become increasingly popular within the pharmaceutical industry. According to a recent study, more than 50 percent of all drugs currently under development contain at least one chiral center.[1,2] The main reason that chiral centers are present within drugs is to create specificity for a known drug target.[3] By imposing a particular spatial arrangement of functional groups within the drug molecule, it will be less likely to bind/interact with non-target proteins/enzymes, therein reducing the possibility of side effects and toxicity. However, this specificity comes at a cost. Each chiral center results in the formation of stereoisomers, which can be very difficult to separate from one another to produce a chemically pure product of one specific stereoisomer. The presence of a stereoisomeric impurity can affect the production of the desired drug, which has implications for both safety and product performance.[4,5] Therefore, characterization of a drug in the solid state is essential if the desired product is a solid formulation. An overview of chirality as it pertains to the pharmaceutical industry, including challenges associated with developing and characterizing a chiral drug in the solid state follows.

1.3   Defining chirality

Stereoisomers are molecules that possess the same molecular formula and bond structure but differ in the geometric arrangement of functional groups. Chiral molecules are stereoisomers that result from the presence of one or more chiral centers. In organic chemistry, the chiral center often exists at a carbon atom bonded to four different

substituents. In general, a chiral center exists wherever a molecule lacks an axis of symmetry due to the geometric arrangement of atoms and functional groups.

Each chiral center in a molecule creates a pair of enantiomers. Enantiomers are defined as molecules that are non-superimposable mirror images of one another. The word "chiral" is derived from the Greek word for "hand," and the image of right and left hands is often used as an illustration of the relationship between enantiomers. When enantiomers are present together in a 1:1 ratio, the mixture is referred to as a racemic mixture. There are several methods for designating the "right and left handedness" of molecules forming an enantiomeric pair. These are described below and exemplified in Figure 1.1.

1.3.1   Assignment based on molecular configuration

The Cahn-Ingold-Prelog classification (R-/S-) is the standard nomenclature for chiral organic compounds, with some exceptions among amino acids and carbohydrates. This naming system assigns priority, based on atomic number, to the substituents bonded to the chiral center. When the molecule is oriented such that the lowest-priority group is pointed away from the viewer, the chiral center is labeled according to whether the decreasing order of priority is in a clockwise (R, *rectus*) or counter-clockwise (S, *sinister*) direction.

The D-/L- assignment system is based on the reference molecule glyceraldehyde, a small chiral molecule that is fairly stable to configurational change or racemization. This system historically was used for labeling amino acids and carbohydrates, and the

4
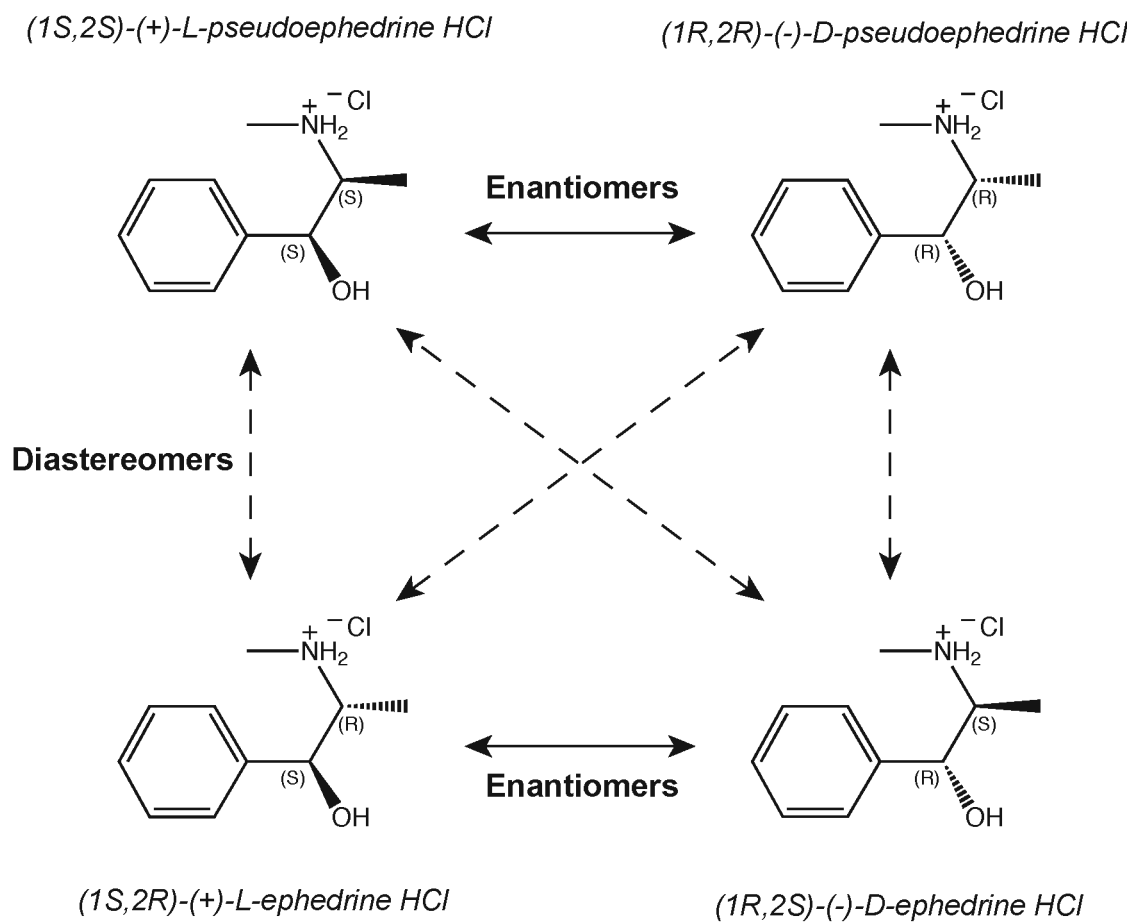
Figure 1.1. Solid and dashed arrows indicate enantiomeric and diastereomeric relationships, respectively, between molecules of ephedrine HCl and pseudoephedrine HCl. All three nomenclatures for designating stereochemistry are shown for each molecule.

notation continues to be used for these systems. In this assignment system, racemic mixtures are often noted by DL-*compound name*.

1.3.2   Assignment based on rotation of polarized light

Enantiomers are able to rotate a plane of polarized light in opposite directions. If the plane of polarized light is rotated in a clockwise direction (with the light coming towards the observer), then the enantiomer is labeled (+) or (*d*) for *dextrorotatory*. If the light is rotated in a counter-clockwise direction, the enantiomer is (-) or (*l*) for *levorotatory*. This method of identification requires transmittance of the polarized light; therefore, solutions of the enantiomers are typically used, but identification using single crystals is possible. The magnitude and direction of the light rotation is often used to determine the relative ratio (optical purity) of two enantiomers. A racemic mixture, noted as (±), produces no rotation, and a single enantiomer will produce a maximum rotation. Note that there is no direct relationship between the *d/l*, D-/L-, or R-/S- naming conventions. For instance, the fact that L-proline can also be noted (*l*) or (-)-proline, or (S)-proline, is purely coincidental.

1.3.3   Enantiomers and diastereomers

As defined previously, enantiomers are non-superimposable mirror images of one another, and they arise from the presence of a chiral center. When multiple chiral centers are present in the same molecule, each chiral center gives rise to a separate pair of enantiomers, and these sets of enantiomers are related diastereomerically to each other. Figure 1.1 demonstrates the relationship between enantiomeric pairs [(+)- versus (-)-

6

ephedrine] and diastereomeric pairs (ephedrine versus pseudoephedrine) in ephedrine HCl, which has two chiral centers.

One of the most notable properties of enantiomeric pairs is that both molecules have the same physicochemical properties (e.g., dissolution rate, melting temperature, NMR spectrum, etc.) when in an achiral environment. This can create challenges in the separation and analysis of chiral systems. Diastereomers, on the other hand, differ in their physicochemical properties. One of the ways in which enantiomers are separated is by chemically modifying both enantiomers to include another chiral center. This creates a diastereomeric relationship between the molecules, and separation is relatively easy to perform. Following separation, the additional chiral center is cleaved to produce the original molecule of interest.

1.4   Biological and pharmaceutical importance of chirality

One of the defining characteristics of enantiomers is that they possess the same physicochemical properties in an achiral environment. However, the human body is *not* an achiral environment. Therefore, enantiomers within the body potentially have different properties.

One of the models for understanding the method by which drugs interact in the body is the lock-and-key model.[6] According to this model, the drug target (typically a protein receptor) is the "lock," and the desired drug is the "key" that fits into this lock. When the drug interacts with the target, the original behavior of the target is modified and produces a therapeutic effect. Just like a key and lock, drugs are intended to be specific

for only one target, as undesired interactions with non-target molecules can produce undesirable side effects.

Due to the differences in spatial arrangement of functional groups, enantiomers interact differentially with biological molecules, as represented in Figure 1.2.[3,7] There are many examples of this, including the differences in the smell and taste of different enantiomers, such as the sweetener aspartame, the enantiomer of which tastes bitter.[8] In the case of pharmaceuticals, this means that one of the enantiomers may produce a favorable therapeutic effect, while the other elicits a completely different response.[9] The drug thalidomide is a famous example of this property. Whereas one enantiomer of thalidomide had a sedative effect, the other was teratogenic and caused significant birth defects among pregnant women.[10] The observation of this differential effect underscored the importance of chirality in the pharmaceutical industry and led to many of the guidelines and regulations that are used to ensure drug safety in the United States today.

Although the thalidomide disaster highlights dramatic and negative differences between the effects of enantiomers, sometimes the differences in their interactions are benign.[9] For instance, in some cases, only one enantiomer elicits any notable biological response. In others, both enantiomers are able to produce the desired therapeutic effect, but may differ only in potency. Cases have existed in which a drug initially has been marketed as a mixture of the two enantiomers, and then later switched to a single-enantiomer formulation. This has been coined "chiral switching" and has been used as a strategy to prolong the patent life of an active pharmaceutical ingredient.[9,11] In any case, current regulations and guidelines typically make it more favorable to market only a single enantiomer.[5,12-15]
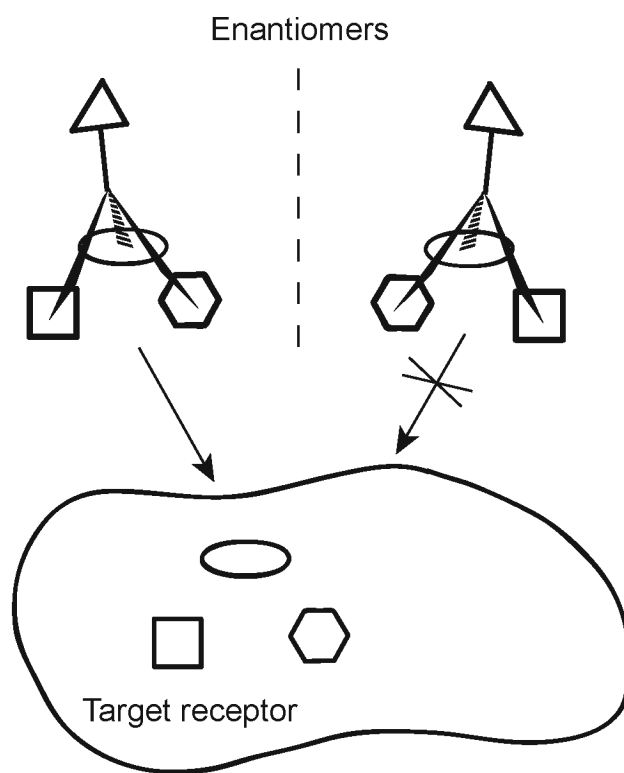
Figure 1.2. The lock-and-key model demonstrates differences in biological and therapeutic activity among enantiomers.

1.5   Production of single enantiomers

There are multiple methods for producing a single enantiomer, including stereoselective synthesis, chiral separations, and preferential crystallization.[2,5]   The optimal method often depends on the properties of the molecule. For instance, if an enantiomer has a tendency to racemize (reversibly convert between both enantiomers to form a racemic mixture) certain synthetic steps or separation methods might not be possible.

1.5.1   Stereoselective synthesis

Stereoselective synthesis is a method for producing only the enantiomer of interest, without the need for subsequent separation.[2] These methods typically require a catalyst that selectively produces only one of the stereoisomers. Such catalysts exist in natural biological systems. A prime example of this is the stereoselective synthesis of L-amino acid enantiomers, which are used as fundamental building blocks for proteins. Much attention has been devoted to harnessing these naturally stereoselective processes for use in the manufacture of fine chemicals and pharmaceutical products.   Such processes are referred to as "bio-catalysis."   Although traditional and bio-catalytic processes can be very efficient and stereoselective, they also require special conditions, and it is not always possible to find a naturally-occurring enzyme that can produce the desired product. However, in many cases, traditional and/or biological catalysis is used to selectively produce a single enantiomer that can be used as starting material for the production of the desired product.

When stereoselective synthesis is not possible, the stereoisomers can be separated at one of the steps in the synthesis of the compound. Ideally, the separation step occurs at an early stage in the synthetic process, as this typically produces a higher yield of the desired enantiomer. Chromatographic and crystallization methods are the main pathways for separating stereoisomers.

1.5.2   Chiral separations

Chiral separation science has made many advances in the past decades.[16]   Again, the main challenge associated with chiral separation is the fact that enantiomers have the same physicochemical properties in an achiral environment.[7]   This means that typical chromatography-based separation methods, such as standard HPLC, which use achiral stationary and mobile phases, are unable to distinguish between the two enantiomers, which elute at the same time.   Two common methods for separating enantiomers by chromatography are 1) converting the enantiomers into diastereomers and 2) modifying traditional chromatographic methods to create a chiral separation environment.

Whereas enantiomers have the same physicochemical properties, diastereomers do not.   By reacting both enantiomers with the same optically pure enantiomer, the enantiomeric pair becomes a diastereomeric pair, which can then be separated by standard, achiral chromatographic methods.   After separation, the enantiomer of interest can be recovered by cleaving the aforementioned additional enantiomer.   Although this method is effective for separating enantiomers, it still requires optically pure material in order to form the diastereomer.   It also requires the ability to create and subsequently cleave a bond between the enantiomeric pair and the diastereomer-former without

11

modifying the desired product. In addition, steps are added to the synthetic route, which may decrease percent yield.

Modification of the stationary phase and/or mobile phase of traditional chromatographic methods is another possible method. This has become fairly commonplace and is referred to as "chiral chromatography." Most often, the stationary phase is modified to include chiral functional groups, which interact differentially with the stereoisomers in the mobile phase, resulting in different elution times for the enantiomers. Including chiral molecules, such as cyclodextrins,[17] in the mobile phase can also be used to selectively modify retention times of the enantiomers. However, similar to separation by diastereomer formation, the modification of either stationary or mobile phase typically requires access to optically pure materials.

1.5.3   *Preferential crystallization*

Preferential crystallization is one of the primary methods by which enantiopure materials are prepared for pharmaceuticals and fine chemicals.[5,18-24] This separation method is based on the binary and ternary phase diagram for the enantiomers of the chiral molecule of interest. Thus, it requires an understanding of the thermodynamic relationship between enantiomers in the solid state. The next section provides a general overview of physical forms in the solid state, which will include a description of chiral molecules in the solid state.

1.6   Physical forms of solids

Many drugs on the market today are small-molecule drugs, formulated as solids. The physical form of these solids has a direct impact on the performance and safety of the drug due to distinct interactions between the molecules that compose the material.[25] The sum of these molecular interactions results in the observed pharmaceutically relevant properties, such as dissolution rate, apparent solubility, and physical and chemical stability. Therefore, understanding the physical form of a drug is very important to ensuring safety and efficacy. Figure 1.3 is a tree diagram that represents some of the physical forms in which a molecule "E" can exist in the solid state.

1.6.1   The amorphous state

The amorphous state is referred to as a super-cooled liquid, wherein molecules exist in a distribution of conformations and supramolecular arrangements. This molecular disorder results in faster dissolution of the amorphous material as compared to the corresponding crystalline form of a compound.[26] Thus, formulating a drug as an amorphous form is a feasible option to mitigate dissolution and solubility problems that might be observed for the crystalline material. However, the amorphous state is thermodynamically metastable to the crystalline state and therefore has the potential to crystallize. Much research is focused on creating and stabilizing the amorphous state for pharmaceutical solids.[27] Alternatively, crystallization from the amorphous state may be desired in order to assist discovery of high-energy crystal forms, as described in Chapters 5 and 6.
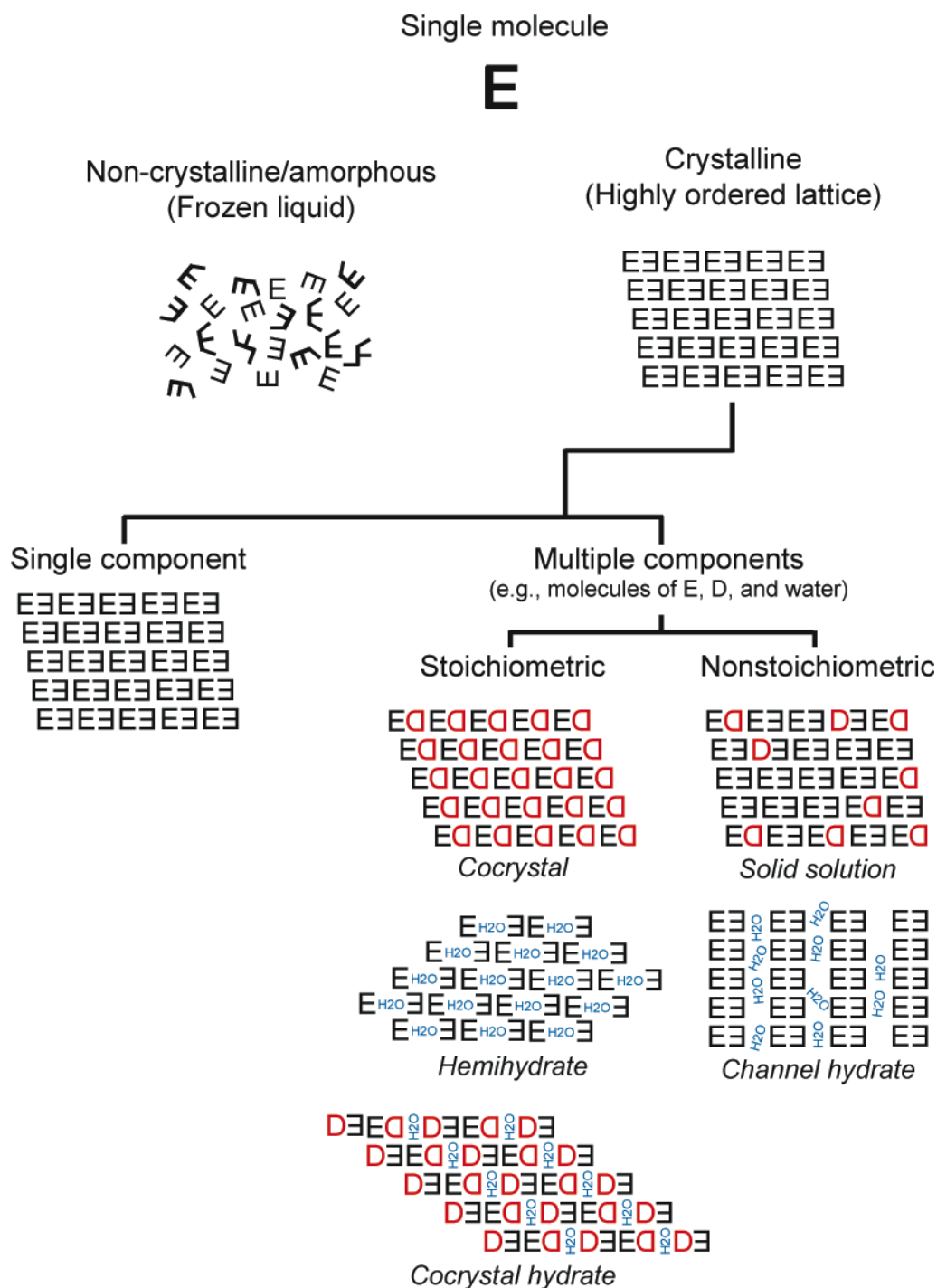
Figure 1.3. Tree diagram outlining the physical forms in which a single molecule "E" can exist in the solid state.

14

1.6.2   The crystalline state

As opposed to the molecular disorder of amorphous materials, crystalline materials are three-dimensional lattices that are formed by highly ordered packing of molecules.[25] In some cases, it is not possible for a molecule to crystallize. This is often the case for long polymeric molecules, the conformational flexibility of which can limit the highly ordered packing associated with a crystal lattice. Because of this, certain polymers exist as amorphous or semi-crystalline materials, and they can be used to stabilize the amorphous state of other compounds that do have a tendency to crystallize.

The formation of crystal lattices is highly dependent on intra- and intermolecular hydrogen bonding, van der Waals interactions, and ionic forces.[25] Crystals can be composed of a single component or multiple components, depending upon the available interactions between molecules. As indicated by the name, single-component crystalline materials are made from the packing of molecules of a single compound. Alternatively, multiple-component crystalline materials contain multiple compounds within the crystal lattice. These multiple-compound crystals can be formed by stoichiometric or nonstoichiometric ratios of the components. Examples of stoichiometric multiple-component systems include cocrystals, salts, hydrates, and solvates, as illustrated in Figure 1.3.

Cocrystals are defined as multiple-component crystals that contain stoichiometric ratios of the components, each of which exists as a solid at room temperature.[28] This is in contrast to hydrates and solvates, which include components that are liquids at room temperature (i.e., water or solvent molecules). Cocrystals are distinguished from salts in that salts are produced by *ionic* interactions between the components, while cocrystals are

produced predominantly via formation of complementary hydrogen bonding between components. Both salts and cocrystals are of interest in the pharmaceutical industry due to their ability to modify the solid-state properties of an active pharmaceutical ingredient without chemical modification. Of particular importance is increased dissolution rate, potential increased stability, and, in the case of cocrystals, the possibility of combining two active pharmaceutical ingredients together into the same crystal structure.

Nonstoichiometric multiple-component crystals do not contain specific ratios of the components. Instead, the components can exist in a range of ratios. The most common nonstoichiometric multiple-component crystalline systems are channel inclusion compounds (e.g., channel hydrates) and solid solutions. The term solid solution is most often used in the field of metallurgy to describe the formation of alloys, in which one metal is "dissolved" in another. The same term can be applied to molecular compounds. It is important to distinguish between a solid solution and a crystal that contains impurities or defects. True solid solutions are thermodynamically stable, while impurities/defects are not thermodynamically favored, but only exist because the impurity is kinetically trapped inside of the (host) crystal lattice of another component. Although solid solutions are more common in metallurgy, such systems also are occasionally observed among molecular compounds.

1.6.3   Polymorphism/allotropism

For each of the crystalline systems described above, there is the potential for polymorphism, which is the existence of the same chemical compound(s) in multiple crystal forms.[25,29] Representations of polymorphism for both single- and multiple-

component crystals are shown in Figure 1.4. The differences in crystal forms are the result of differences in crystal packing and/or molecular conformation.

Polymorphism is a subcategory of allotropism, in which a chemical entity can exist in more than one crystal form. Probably the most widely recognized example of allotropism is the ability for carbon to exist as diamond or graphite. These materials differ in their physical properties as a result of the distinct packing of the carbon atoms within the crystal structure. Similar to carbon allotropes, polymorphs of molecular compounds can differ significantly in their physicochemical properties, including pharmaceutically relevant properties such as dissolution rate and stability.[25]

Because different polymorphic forms possess different properties, it is very important to know what, if any, polymorphic forms exist for a given system. Polymorphic screening assays have become a standard procedure during the development of any new active pharmaceutical ingredient.[30] During these assays, the pharmaceutically relevant properties of each form are assessed in order to decide which form should be used in the development of a solid dosage form. An important factor in this decision is the relative physical stabilities of the various polymorphic forms.[31]

At a given temperature and pressure, one polymorphic form will be the most stable form. However, upon changing conditions, the relative stability of the polymorphic forms might change. E.g., in the case of two polymorphs, Form I and Form II, Form I might be more stable at room temperature, but Form II becomes the more stable form at 50ºC, at which point Form I is metastable to II. In such cases, where the relative stability of two forms "cross," the energetic relationship between the two polymorphs is called "enantiotropic."
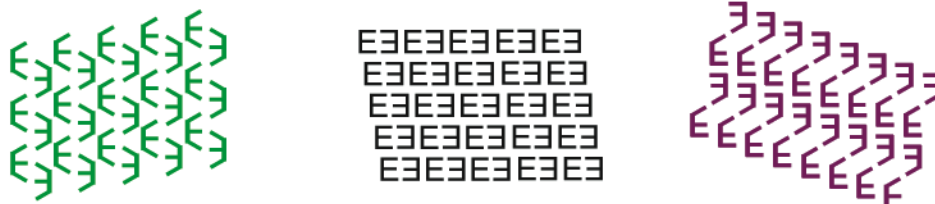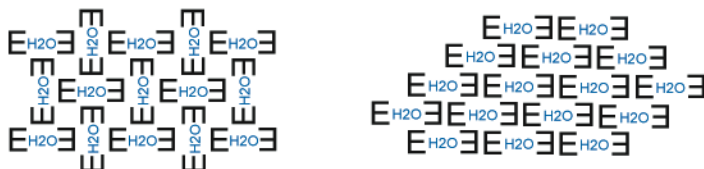
Figure 1.4. Representations of polymorphism for single-component and multiple-component crystals. The same molecules are present, but different molecular conformations and packing result it different crystal forms.

In other cases, however, a polymorphic form may be the stable form across the entire range of temperatures, and any other polymorphic forms are always metastable relative to this form. In this case, there is a "monotropic" relationship between the polymorphic forms.

The relative thermodynamic stabilities of polymorphs are usually described in terms of an energy diagram where either free energy or solubility (van't Hoff plot) of each polymorphic form is plotted as a function of temperature.[25] Examples of free energy diagrams and van't Hoff plots for both an enantiotropic and a monotropic system are shown in Figure 1.5. The terms *monotropic* and *enantiotropic* refer to the energy relationships between *two* polymorphs. Thus, if a system has three polymorphic forms, the relationship between Forms I and II, I and III, and II and III must be defined.

Before continuing with the discussion of relative stability of polymorphic forms, it is important to note that polymorphs are typically named in the order in which they are observed/discovered. Oftentimes, they are denoted using Roman numerals, such as Forms I, II, and III. However, Greek letters (α, β, δ, γ, etc.) and capital letters (A, B, C, etc.) are also commonly used. Because the order in which polymorphic forms are discovered does not necessarily correspond to their relative stability, one cannot assume that Form I is the most stable form. In fact Form II, III, or even IV may be the most stable form. In some cases, the most stable form may not even be known.

Understanding the relative stability of polymorphic forms is extremely important, as formulation of a pharmaceutical compound as a metastable form can cause problems with a drug product if it transforms to the more stable form during/after processing, as exemplified by the ritonavir case.[32] This drug was unknowingly formulated as a

19
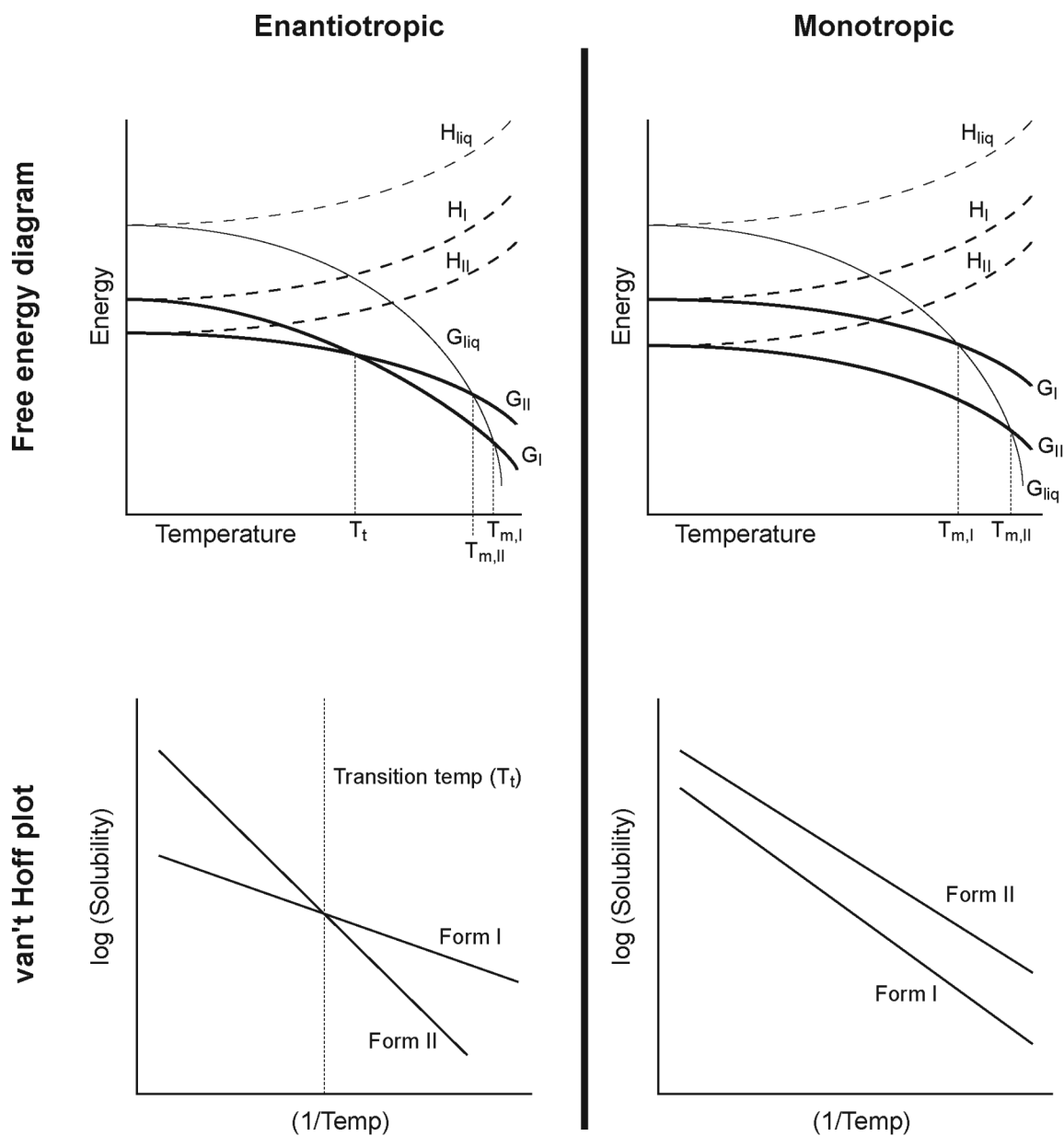
Figure 1.5. Free energy diagrams and van't Hoff plots are shown for both enantiotropically and monotropically related polymorphic systems. T_m, T_t, H, and G represent melting temperature, transition temperature, enthalpy, and free energy, respectively.

metastable polymorphic form. After a period of time, the drug started to convert/transform to the more stable form, which led to a dramatic reduction in dissolution rate/solubility and loss of therapeutic effect. The drug product had to be recalled and reformulated, resulting in large economic loss for the company.

There are a series of rules/guidelines that are used to identify enantiotropic versus monotropic relationships between polymorphic forms. Specifically, the Burger–Ramberger rules[33,34] are cited frequently in the literature. These rules are referred to as the "heat of transition" and "heat of fusion" rules, and they are based on calorimetric (DSC) measurements.

1) The heat of transition rule states that if an endothermic transition is observed, then there is an enantiotropic relationship; and if an exothermic transition is observed, there is a monotropic relationship.

2) The heat of fusion rule states that if the higher-melting form also has a higher heat of fusion, then there is a monotropic relationship; otherwise, it is an enantiotropic relationship.

These two rules are often referenced due to the ability to obtain the information quickly via DSC and also because they have been shown to be fairly reliable. Other guidelines that are sometimes cited include the entropy of fusion rule, the heat capacity rule, the density rule, and inferring stability based on melting data.[25,35,36] However, in cases where thermal degradation appreciably occurs during DSC analysis, energy relationships can be defined via solubility measurements or by adding an impurity to decrease the thermal transitions of interest.[37]

In many systems where polymorphism exists, crystallization initially produces a metastable form, which progressively converts to forms of increasing stability. This phenomenon is called Ostwald's rule of stages.[38] Whereas Ostwald's original publication described a step-wise transformation of stability from least-stable to the most-stable crystal form, the order of transformation doesn't always proceed in this manner, as it is possible for the least stable structure to transform directly to the most stable. The kinetics of this transformation are dependent upon many factors, including: 1) the quality of the crystals, where the presence of defects can allow for a faster transformation due to increased mobility around the defect or the defects' ability to act as nucleation sites for the other crystal form[39,40]; and 2) the conditions of storage, which can enhance or inhibit the transformation. In some cases, the metastable form may not transform at all. This situation is an example of kinetic stability. Thus, the thermodynamics as well as the kinetics of a system affect the formation and observation of crystalline polymorphism.

1.7   Solid-state chemistry of enantiomers

Now that we have an overview of physical forms of solids, this information can be applied to enantiomers in the solid state.

1.7.1   Physical forms of enantiomers

As previously noted, a racemic mixture refers to a 1:1 ratio of opposite enantiomers. If the enantiomers of a racemic mixture are concurrently crystallized, either by melting or dissolving the enantiomers together, followed by cooling or solvent removal, there are three main types of crystal forms that might be produced: a) a racemic

conglomerate, b) a racemic cocrystal, or c) a solid solution.[41] These potential crystal forms are represented in Figure 1.6.

Figure 1.6a shows a representation of a *racemic conglomerate*, which is a physical mixture of single-component crystals.

Figure 1.6b shows a *racemic cocrystal*. A racemic cocrystal (sometimes referred to as a racemic compound or racemate) is a stoichiometric, multiple-component system in which both enantiomers are present in a 1:1 stoichiometric ratio within the crystal lattice. Oftentimes, the two enantiomers form heterodimers that are then packed together to form the lattice. However, there also are examples where the enantiomers pack together in homochiral sheets or columns, which are then packed together.

Figure 1.6c shows a *solid solution* of enantiomers, which can be categorized as a non-stoichiometric, multiple-component system. In the case of enantiomers, solid solutions form when two enantiomers can substitute for one another within the crystal lattice. This creates a relatively random distribution of the enantiomers throughout the lattice, and the composition of the lattice can range anywhere from a homochiral (enantiopure) lattice to a 1:1 ratio of the two. Again, it must be emphasized that solid solutions are thermodynamic products that are at equilibrium. This differs from the presence of chiral defects, in which one enantiomer might be present in the crystal lattice of its antipode due to crystallization under non-equilibrium conditions.

The type of physical form in which a given compound will exist upon crystallization of the two enantiomers is compound specific.[18,41] Typically, crystallization of a racemic mixture will produce only one of these three crystal forms.
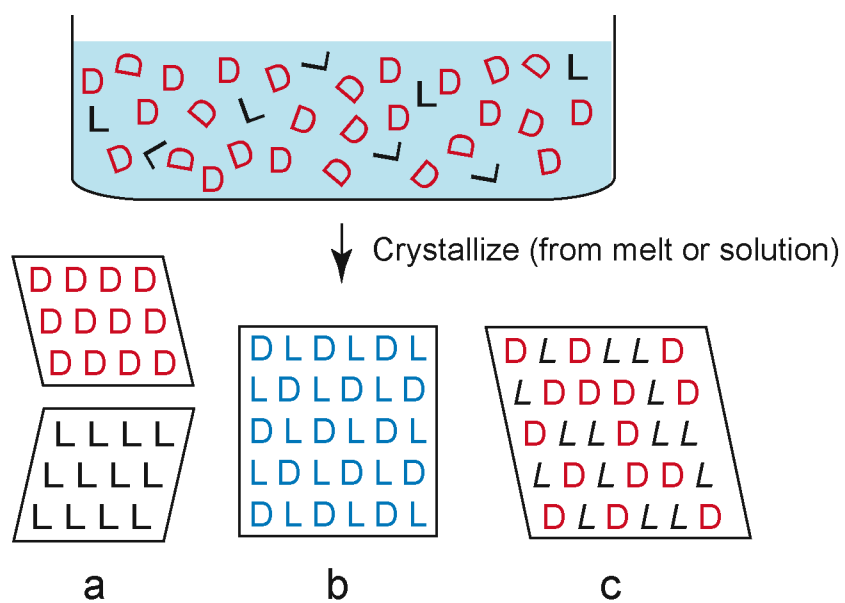
Figure 1.6. The three physical forms that can exist upon concurrent crystallization of enantiomers: a) racemic conglomerate, b) racemic cocrystal, and c) solid solution.

Jacques, Collet, and Wilen have estimated that approximately 10% of all racemic mixtures will form a racemic conglomerate, 90% will form a racemic cocrystal, and the formation of a solid solution is fairly rare.[18] Just like with polymorphism, where different forms can exist under different conditions, it is possible for a racemic system to transition between racemic conglomerate, cocrystal, and/or solid-solution forms as the temperature of the system is modified. In addition, there is the potential for the formation of polymorphic, hydrated, and/or solvated crystal forms, and multiple forms can be present at the same time in the same mixture.[7] In the presence of such a complicated system of physical forms, analysis can be a challenge. Typical analytical methods for characterizing enantiomeric systems in the solid state are briefly described in § 1.8.

1.7.2 Binary phase diagrams

The creation of melting-point binary phase diagrams has historically been the primary method for characterizing racemic systems.[41] These diagrams consist of melting-point data plotted as a function of enantiomeric composition. To create a binary phase diagram, various ratios of the two enantiomers are mixed, crystallized together (either from solution or a melt), and then analyzed by differential scanning calorimetry (DSC). For each sample, the DSC thermogram will possess two temperatures of interest: the melting onset temperature, which corresponds to the eutectic or solidus temperature, and the final melting peak temperature, which corresponds to the liquidus temperature. These temperatures are plotted as a function of the enantiomeric composition to create the binary phase diagram. Racemic conglomerates, racemic compounds, and solid solutions all have distinctive binary phase diagrams (Figure 1.7).[18,41] Thus, by creating a
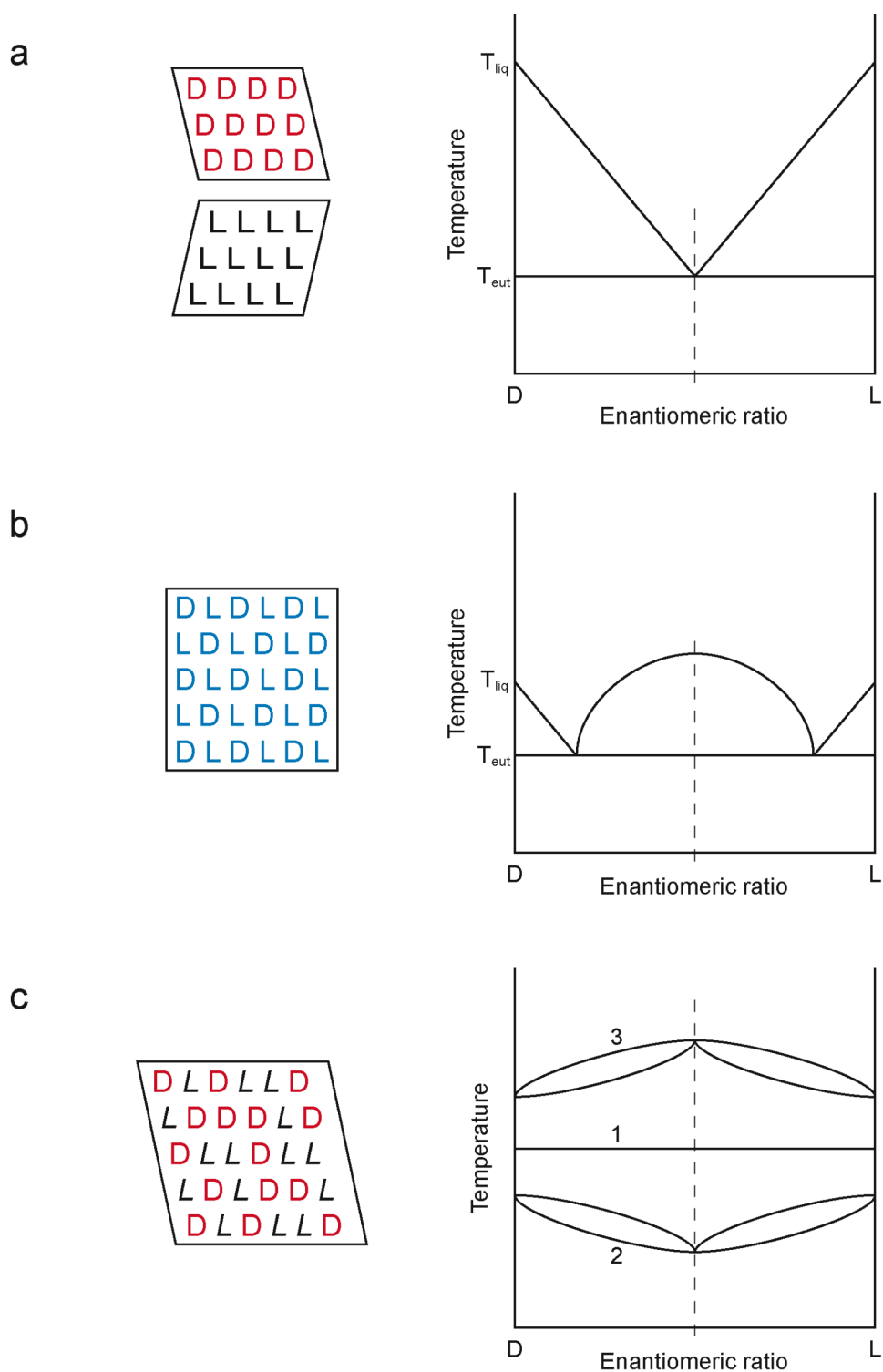
Figure 1.7. Melting binary phase diagrams that are characteristic for a) racemic conglomerates, b) racemic cocrystals, and c) solid solutions displaying 1) ideal behavior, 2) a minimum, and 3) a maximum.

binary phase diagram, one can determine the identity of the solid-state system. Of course, the fact that this method is non-isothermal means that changes in the sample can occur during analysis. Because of this, the analysis of solid chiral systems can benefit from the application of multiple analytical methods.

1.8   Methods for analyzing chiral molecules in the solid-state

Many of the methods for analyzing solid-state systems in general can be applied to chiral molecules in the solid state.[7,25,28] Those techniques that are particularly relevant to studying chiral systems are highlighted here.

1.8.1   Solution methods

Although this section is titled "Methods for analyzing chiral molecules in the solid state," several solution-based methods are very important for characterizing chiral systems. Thus, they have been briefly included here. However, it is important to note that there is a loss of information upon dissolution of a solid system. For instance, chiral HPLC cannot distinguish between a racemic conglomerate or a racemic compound, as both would show a 1:1 ratio of the two enantiomers in solution. Additionally, although different polymorphic forms can have different dissolution rates, upon complete dissolution, identification of polymorphism is impossible. Thus, solid-state characterization is extremely important for the development of any solid-state pharmaceutical system.

Dissolution rate is a common method for characterizing solid-state systems because different crystal forms have different intermolecular interactions, which may

give rise to differences in dissolution rate.[25] This is true for polymorphism as well as for different crystal forms of enantiomers.[42] Solubility measurements can also be helpful, as they can be used to create ternary phase diagrams, which can be used in place of melting binary phase diagrams in cases of chemical or physical thermal instability. Dissolution and solubility studies typically rely on an HPLC method or spectral assays to measure the concentration of species in solution. For the quantitation of enantiomers in solution, a chiral HPLC method is necessary due to the fact that both enantiomers will elute simultaneously using a standard achiral method. Alternatively, if the optical rotation for the enantiopure compound is known, the relative ratios of enantiomers can be measured via optical activity.

1.8.2   Thermal methods

Thermal methods, most notably DSC, are very important in the characterization of enantiomeric systems.[18,42] Some of the first characterizations of enantiomers were performed by visually assessing the melting of enantiomeric mixtures via hot stage microscopy (HSM).[18] Although HSM can still be valuable for investigating enantiomeric mixtures, DSC now provides much more sensitive and less biased measurements of thermal transitions. The creation of binary phase diagrams (§ 1.7.2) via DSC-measured melting temperatures, as reported by Jacques, Collet, and Wilen, has become a standard method for determining the formation of racemic conglomerate, cocrystal, or solid solution upon crystallization of enantiomeric mixtures. In general, DSC is commonly used to observe both exo- and endothermic events that occur upon heating a solid sample,

including polymorphic transitions, crystallization, dehydration/desolvation, or decomposition.[25]

In addition to measuring the temperatures associated with the eutectic melting of enantiomers, the heats of fusion of various crystal forms can be valuable. If the melting temperatures and heats of fusion associated with the enantiopure and racemic forms of a chiral compound are known, it is possible to construct the theoretical melting binary phase diagram.[18] This can be very helpful in supporting experimental data and also for calculating the eutectic composition, which can be difficult to accurately determine from the experimental phase diagram alone.

Heats of fusion can be used as a measure of the relative stability of a solid material.[25] In cases where the heat of fusion cannot be obtained from a DSC thermogram due to thermal decomposition or sublimation of the compound, isoperibol calorimetry can be used to measure the heat consumed/evolved upon isothermal dissolution of the solid, otherwise known as the heat of solution. The heat of solution is directly proportional to the heat of fusion of the crystal. Thus, this measurement can be used for determining the relative stability among different crystal forms.

1.8.3   Crystallography

Crystallography is one of the most powerful methods for analyzing crystalline materials.[25] Once the crystal structure for a compound has been "solved" by X-ray analysis, the conformation, arrangement, and intra- and intermolecular bonding patterns can be identified. This molecular-level view can provide tremendous insight into the macroscopic behavior (e.g., dissolution rate and stability) of crystalline materials. It is

for this reason that single-crystal X-ray diffraction analysis (XRD) is often referred to as the "gold standard" for the identification of crystal forms. In order to obtain XRD data, the sample of interest must exist as a single, macroscopic crystal. This crystal is then exposed to a monochromatic X-ray beam, which is reflected by the lattice planes of the crystal. These reflections are detected as a function of the angle of reflection, and the angles and intensities of the reflections are related to the spacing of the atoms within the crystal structure via the Bragg equation. Additional refinements produce a picture of the molecules that are in the crystal. Unfortunately, it is not always possible to crystallize a single crystal of a given material. In such cases, single-crystal X-ray diffraction cannot be performed. Instead, X-ray analysis is performed on a powdered sample via powder X-ray diffraction (PXRD).

Similar to XRD, in PXRD, the powdered sample is exposed to the X-ray beam, and the reflections of the X-rays are measured at different angles.[43] Unlike single-crystal XRD, the resulting PXRD pattern often is unable to provide detailed structural information but instead is used for identification of different crystal forms. There are a couple of potential issues with the use of powder, including preferred orientation, which can lead to dramatic differences in peak intensities. Additionally, the reduced crystal size means that the destructive interference that typically occurs in larger, single crystals is reduced, leading to broader diffraction peaks.[43] As particle size becomes extremely small, the peaks continue to broaden. The extreme case of this is observed for amorphous material. Because amorphous material by definition lacks the long-range order that is necessary to constructively diffract X-rays, the PXRD pattern of amorphous material consists of a very broad "peak," referred to as an amorphous halo. Thus,

30

disorder within the lattice, either due to molecular disorder (e.g., chemical impurity) or structural disorder (e.g., crystal defects) can be difficult to detect, or even may cause XRD or PXRD analysis to be of limited help in characterizing a material.

XRD and PXRD analysis can be very helpful in characterizing a chiral compound in the solid state. The differences in molecular packing in the various crystal structures result in different diffraction patterns.[4,42] Enantiopure materials possess different diffraction patterns than their corresponding racemic cocrystal counterparts, and polymorphic forms will also have different patterns. However, due to the achiral nature of X-ray analysis, enantiopure material has the same diffraction pattern as a racemic conglomerate.[4,7] Therefore, this technique cannot always determine the enantiomeric purity of a sample. The detection of solid solutions by X-ray diffraction is also potentially limited.[44] The disruption of order within a solid solution may lead to lack of resolution in the X-ray pattern, or the pattern might look very similar to the diffraction pattern of enantiopure material, in which case X-ray diffraction would be unable to distinguish between a racemic conglomerate and a solid solution.

1.8.4   Spectroscopic methods

Spectroscopic techniques are often used for the characterization of physical forms. The most common techniques are infrared (IR), Raman, and solid-state NMR (SSNMR) spectroscopies.[45] As with all analytical techniques described here, one of these spectroscopic techniques might be particularly relevant for a specific system, since each method measures a different type of interaction within the electromagnetic spectrum. IR spectroscopy measures the absorption of infrared wavelengths, Raman detects inelastic

scattering, and SSNMR measures the absorption of radiofrequency in a static magnetic field. All of these methods can be used for qualitative assessment of a sample, and they also can be quantitative.[45] Their use for characterization of both crystalline and amorphous solids is well represented in the literature.

Infrared spectroscopy is based on the absorbance of infrared light, which corresponds to the stretching and rotational resonances of molecular bonds. This technique is particularly useful in cases where hydrogen-bonding is present.[25] Measured absorbances are indicative of the molecular conformation and packing within the crystal lattice, and changes in crystal form can result in significant differences in the observed resonances. However, if the differences in molecular conformation/packing among physical forms do not differ significantly, distinguishing between these forms may not be possible. Additionally, resonances often overlap, which can make identification and quantitation a challenge.

Raman is somewhat complementary to IR spectroscopy in that it measures scattered light, as opposed to absorbed light. Many of the advantages and disadvantages in regard to the identification and quantitation of crystal forms are similar to IR spectroscopy.

Solid-state NMR spectroscopy is a very powerful technique for studying different crystal forms. The peak positions in the SSNMR spectrum are very sensitive to differences in molecular conformation and packing within the crystal structure, making it a very important technique for characterizing different solid forms.[25,46] The use of SSNMR for characterizing chiral molecules in the solid state will be discussed in detail in Chapter 2.

As with crystallographic techniques, IR, Raman, and SSNMR spectroscopies cannot distinguish between opposite enantiomers, as both enantiomers possess the same spectrum. As a result, it is also impossible to distinguish between an enantiopure sample and a racemic conglomerate.[4,7] However, the spectra of an enantiopure sample versus a racemic cocrystal or a solid solution should be different due to differences in the electronic environments that exist among the molecules in each form.

1.9   Overview of thesis work

Chiral molecules are prevalent among currently marketed pharmaceutical products, many of which are solid formulations. The challenges associated with producing and characterizing chiral small molecules in the solid state are not trivial. Analysis of these systems typically requires the application of several analytical techniques, one or two of which may be particularly helpful. In this thesis work, solid-state NMR spectroscopy (SSNMR) was found to be a particularly powerful method for characterizing proline enantiomers in the solid state.

Chapter 2 includes relevant background information on the use of solid-state NMR spectroscopy (SSNMR) for the analysis of pharmaceutical solids. A very basic description of the NMR method is provided, and the main advantages of the SSNMR technique are discussed. This chapter also includes explanations of SSNMR experiments that are particularly relevant for studying chiral molecules in the solid state.

In Chapter 3, we evaluate the differences in crystal forms of proline that result from changes in enantiomeric ratio and crystallization conditions. Various ratios of D- and L-proline were crystallized from solution and by lyophilization, and the resulting

materials were characterized by thermal, X-ray diffraction, and spectroscopic methods. During the course of these studies, evidence for a previously unreported polymorphic form was obtained. Characterization of this form, including assessment of its thermodynamic relationship to published crystal forms, is described.

Chapter 4 reports the use of ^{13}C SSNMR to observe and quantitate chiral defects that are produced during concurrent crystallization of both D- and L-proline enantiomers. Previous studies have investigated chiral defects, but no direct observations of these defects have been made. This chapter provides support for the observation of L-proline chiral defects in the host crystal lattice of D-proline through use of SSNMR methods.

Chapter 5 includes further examination of the crystallization of D- and L-proline obtained by lyophilization. Samples were maintained under dry-nitrogen conditions, which allowed observation of metastable crystal forms of proline. Observations of thermal- and water-induced crystallization of these forms demonstrated the importance of molecular mobility for the crystallization of the proline system and contributed to a greater understanding of previously observed polymorph formation.

In Chapter 6, crystallization of proline enantiomers from an amorphous phase was investigated. Samples of racemic cocrystals and D- and L-proline physical mixtures were partially amorphized by cryogrinding. The resulting samples were analyzed using variable-temperature SSNMR, PXRD, and DSC.

Chapter 7 is a brief discussion of the implications of this thesis work and the potential direction of future research. Pseudoephedrine HCl has been proposed as a future model chiral compound due to its pharmaceutical relevance and the presence of

two chiral centers within its structure, which leads to the existence of both enantiomers and diastereomers.

1.10   Summary

The study of chiral molecules is highly relevant to the pharmaceutical industry. Many drugs currently on the market and under development contain one or more chiral centers, which lead to the presence of enantiomeric pairs. It is often desirable to use only one enantiomer within a drug product, but producing a single enantiomer can be a challenge. Understanding the solid-state properties of the chiral molecule is essential to the successful development and production of a safe and efficacious drug product. Thus, characterization of the chiral material in the solid state with solution, thermal, crystallographic, and/or spectroscopic methods is critical.

1.11   References

1.   Carey JS, Laffan D, Thomson C, Williams MT 2006. Analysis of the reactions used for the preparation of drug candidate molecules. Org Biomol Chem 4(12):2337-2347.

2.   Murakami H 2007. From racemates to single enantiomers - chiral synthetic drugs over the last 20 years. Top Curr Chem 269:273-299.

3.   Holmstedt B, Frank H, Testa B 1990. Chirality and Biological Activity. New York: Alan R. Liss.

4.   Gu C-H, Grant DJW 2004. Effects of crystal structure and physical properties on the release of chiral drugs. Chirality Drug Des Dev:1-36.

5. Li ZJ, Grant DJW 1997. Relationship between physical properties and crystal structures of chiral drugs. J Pharm Sci 86(10):1073-1078.

6. Pandit NK 2007. Introduction to the Pharmaceutical Sciences. Baltimore, MD: Lippincott Williams & Wilkins.

7. Stahly GP, Byrn SR 1999. The solid-state structure of chiral organic pharmaceuticals. Mol Model Appl Cryst:313-345.

8. Bentley R 2006. The nose as a stereochemist. Enantiomers and odor. Chem Rev 106(9):4099-4112.

9. Caldwell J 1999. Through the looking glass in chiral drug development. Mod Drug Discovery 2(4):51, 54-55, 57, 59-60.

10. De Camp WH 1989. The FDA perspective on the development of stereoisomers. Chirality 1(1):2-6.

11. Darrow JJ 2007. The patentability of enantiomers: implications for the pharmaceutical industry. Stan Tech L Rev 2.

12. Shah RR, Branch SK 2003. Regulatory requirements for the development of chirally active drugs. Handb Exp Pharmacol 153:379-399.

13. Caner H, Groner E, Levy L, Agranat I 2004. Trends in the development of chiral drugs. Drug Discov Today 9(3):105-110.

14. Sahajwalla C, Chawla J, Reddy IK 2004. Scientific and regulatory issues in development of chiral drugs. Drugs Pharm Sci 141:503-524.

15. Ahuja S 1997. The importance of chiral separations in pharmaceuticals. Chem Anal (N Y) 142:287-315.

16. Thayer A 2005. Trial separations. Chem Eng News 83(36):49-53.

17. Grandeury A, Condamine E, Hilfert L, Gouhier G, Petit S, Coquerel G 2007. Chiral discrimination in host-guest supramolecular complexes. Understanding enantioselectivity and solid solution behaviors by using spectroscopic methods and chemical sensors. J Phys Chem B 111(25):7017-7026.

18. Jacques J, Collet A, Wilen SH 1981. Enantiomers, Racemates, and Resolutions. New York: Wiley.

19. Brittain HG 1990. Crystallographic consequences of molecular dissymmetry. Pharm Res 7(7):683-690.

20. Addadi L, Weinstein S, Gati E, Weissbuch I, Lahav M 1982. Resolution of conglomerates with the assistance of tailor-made impurities. Generality and mechanistic aspects of the "rule of reversal". A new method for assignment of absolute configuration. J Am Chem Soc 104(17):4610-4617.

21. Wang Y, LoBrutto R, Wenslow RW, Santos I 2005. Eutectic composition of a chiral mixture containing a racemic compound. Org Proc Res Dev 9(5):670-676.

22. Mersmann A 2001. Crystallization Technology Handbook. Second ed., New York, NY: Marcel Dekker, Inc.

23. Faigl F, Fogassy E, Nogradi M, Palovics E, Schindler J 2010. Separation of non-racemic mixtures of enantiomers: an essential part of optical resolution. Org Biomol Chem 8(5):947-959.

24. Wang Y, Chen AM 2008. Enantioenrichment by crystallization. Org Process Res Dev 12(2):282-290.

25. Byrn SR, Pfeiffer RR, Stowell JG 1999. Solid-State Chemistry of Drugs. 2nd ed., West Lafayette, Indiana: SSCI, Inc.

26.   Taylor LS, Shamblin SL 2009. Amorphous solids. Drugs Pharm Sci 192:587-629.

27.   Yu L 2001. Amorphous pharmaceutical solids: preparation, characterization and stabilization. Adv Drug Delivery Rev 48(1):27-42.

28.   Rodríguez-Hornedo N, Nehm SJ, Jayasankar A. 2007. Cocrystals: design, properties, and formation mechanisms.   Encylopedia of Pharmaceutical Technology. Informa Healthcare USA, Inc. p 615-635.

29.   Vippagunta SR, Brittain HG, Grant DJW 2001. Crystalline solids. Adv Drug Delivery Rev 48(1):3-26.

30.   Stahly GP 2007. Diversity in single- and multiple-component crystals. The search for and prevalence of polymorphs and cocrystals. Cryst Growth Des 7(6):1007-1026.

31.   Grant DJW, Byrn SR 2004. A timely re-examination of drug polymorphism in pharmaceutical development and regulation. Adv Drug Del Rev 56(3):237-239.

32.   Chemburkar SR, Bauer J, Deming K, Spiwek H, Patel K, Morris J, Henry R, Spanton S, Dziki W, Porter W, Quick J, Bauer P, Donaubauer J, Narayanan BA, Soldani M, Riley D, McFarland K 2000. Dealing with the impact of ritonavir polymorphs on the late stages of bulk drug process development. Org Proc Res Dev 4(5):413-417.

33.   Burger A, Ramberger R 1979. On the polymorphism of pharmaceuticals and other molecular crystals. II. Applicability of thermodynamic rules. Mikrochim Acta 2(3-4):273-316.

34.   Burger A, Ramberger R 1979. On the polymorphism of pharmaceuticals and other molecular crystals. I. Theory of thermodynamic rules. Mikrochim Acta 2(3-4):259-271.

35.   Bernstein J 2002. Polymorphism in Molecular Crystals. Oxford: Oxford University Press.

36.   Yu L 1995. Inferring thermodynamic stability relationship of polymorphs from melting data. J Pharm Sci 84(8):966-974.

37.   Yu L, Huang J, Jones KJ 2005. Measuring free-energy difference between crystal polymorphs through eutectic melting. J Phys Chem B 109(42):19915-19922.

38.   Ostwald W 1897. Studies on the formation and transformation of solid compounds: Report I. Supersaturation and practicing cooling. [machine translation]. Z Phys Chem 22:289-330.

39.   Brittain HG 2002. Effects of mechanical processing on phase composition. J Pharm Sci 91(7):1573-1580.

40.   Dunitz JD 1991. Phase transitions in molecular crystals from a chemical viewpoint. Pure Appl Chem 63(2):177-185.

41.   Roozeboom HWB 1899. Solubility and melting point as criteria for racemic compounds, pseudoracemic mixed crystals and inactive conglomerates. [machine translation]. Z Phys Chem 28:494-517.

42.   Gu CH, Grant DJW 2003. Physical properties and crystal structures of chiral drugs. Handb Exp Pharmacol 153:113-139.

43.   Jenkins R, Snyder R, Editors. 1996. Introduction to X-Ray Powder Diffractometry. New York: Wiley.

44. Stahly GP, McKenzie AT, Andres MC, Russell CA, Byrn SR, Johnson P 1997. Determination of the optical purity of ibuprofen using X-ray powder diffraction. J Pharm Sci 86(8):970-971.

45. Bugay DE 2001. Characterization of the solid-state: spectroscopic techniques. Adv Drug Delivery Rev 48(1):43-65.

46. Berendt RT, Sperger DM, Munson EJ, Isbester PK 2006. Solid-state NMR spectroscopy in pharmaceutical research and analysis. TrAC, Trends Anal Chem 25(10):977-984.

Chapter 2

Solid-State NMR Spectroscopy of Pharmaceutical Solids

2.1   Introduction

As described in Chapter 1, the physical form of a drug has important implications for its performance within a drug product.[1] The solid-state form of a drug can have a dramatic effect on its solubility, dissolution rate (and therefore bioavailability), physical stability, and interaction with excipients. There are many analytical techniques that can be used to identify and characterize solid-state pharmaceuticals. Because there are advantages and disadvantages to each method, most systems are analyzed by multiple techniques. However, in each case, there often are a couple of methods that are particularly helpful in studying the system of interest.

The use of solid-state NMR spectroscopy to study pharmaceutical solids is described in this chapter. The basic theory and analytical advantages of solid-state NMR spectroscopy will be explained, and literature on the application of SSNMR to solid chiral systems, the major subject of this dissertation, will be reviewed.

2.2   Basics of solid-state NMR

Solution NMR spectroscopy is widely viewed as the most powerful tool for structural elucidation of organic compounds. However, conventional solution NMR techniques produce only a broad, featureless spectrum when applied to most crystalline organic solids.[2,3] This largely arises from restricted molecular motion in the solid state. In solution, the rapid tumbling of molecules averages out most of the interactions that produce line broadening. The primary interactions that lead to line broadening in solids

are dipolar coupling and anisotropy. Fortunately, the techniques of high-power ^{1}H decoupling and magic-angle spinning allow narrow lines to be achieved for the solid-state analysis of most systems.

2.2.1 Dipolar coupling / High-power decoupling

Dipole–dipole interactions, which are through-space interactions that are both orientation and distance dependent, occur between magnetic nuclei. These interactions affect the electronic environment of a nucleus, therein modifying the observed chemical shift in the NMR spectrum. In solution NMR, the rapid tumbling of molecules in solution results in decoupling and averaging of the dipole–dipole interactions between NMR-active nuclei. However, in the solid state, molecular motions are restricted. This leads to pronounced dipolar coupling, resulting in broad peaks.

Although ^{1}H NMR is common for solution analysis, its use is limited in solids due to strong homonuclear ^{1}H dipolar coupling. ^{1}H has a high natural abundance (99.98%), which means that the probability of a particular ^{1}H being physically nearby and coupling to another ^{1}H is very high. Because of this coupling, the narrowest achievable ^{1}H peak widths for solids are ~1 ppm, but much broader peaks are typical. Thus, most solid-state NMR studies are performed on less abundant (or "dilute") nuclei such as ^{13}C, ^{15}N, ^{31}P, and ^{19}F. For instance, the natural abundance of ^{13}C is only 1.1%, making ^{13}C–^{13}C homonuclear coupling almost nonexistent. Although strong ^{1}H heteronuclear dipolar coupling to the observed nucleus still occurs, resulting in peak widths of >50 kHz for nuclei such as ^{13}C, narrow lines can be achieved by high-power ^{1}H decoupling.[4]

[1]H decoupling is commonly used in solution NMR spectroscopy. However, in solids, the decoupling power must be several orders of magnitude greater due to the strength of the ^{1}H dipolar couplings.

2.2.2 *Anisotropy / Magic-angle spinning*

The second source of line broadening is due to the fact that all molecular (i.e., crystal) orientations occur with equal probability in a powdered solid. The chemical shift (peak position) of a nucleus is dependent on its orientation relative to the static magnetic field. Thus, a range of molecular orientations is observed as a range of chemical shifts for a particular nucleus. Again, the rapid molecular movement in solution averages out this effect.

The shape of the broad peak resulting from the anisotropy in solids is referred to as a chemical shift anisotropy (CSA) powder pattern. For sp^2 hybridized carbons, such as those found in phenyl rings and carbonyl carbons, the width of the CSA powder pattern may be 200 ppm or more. The equation that describes the orientation dependence of the chemical shift is:

$$\sigma_{observed} \;=\; \sigma_{isotropic} \;+\; [\sigma_{anisotropic} \times (3\cos^2\theta - 1)],$$

where $\sigma_{observed}$ is the observed chemical shift, $\sigma_{isotropic}$ is what would be observed in solution, $\sigma_{anisotropic}$ is the magnitude of the anisotropic component, and θ describes the angular dependence of the chemical shift with respect to the static magnetic field. The observed spectrum is a superposition of all of the CSA powder patterns for all of the ^{13}C nuclei that have chemically different local environments.

As can be seen by looking at the above equation, the anisotropic contribution to the observed chemical shift is dependent on the angle of the sample relative to the static magnetic field, θ. When this angle is 54.7º, denoted the "magic-angle" setting, the anisotropic component becomes zero.[5] When the sample is spun at the magic angle (magic-angle spinning, MAS) at a rate faster than the width of the powder pattern (up to 20 kHz), only the isotropic peak is observed. However, such fast spinning rates typically are not feasible, and the remaining intensity is observed as additional peaks ("spinning sidebands") in the spectrum. These spinning sidebands are easily removed from the spectrum with techniques such as TOtal Suppression of Spinning Sidebands (TOSS).[6]

2.2.3 Quadrupolar coupling

Quadrupolar coupling is another important source of line broadening. In organic compounds, this heteronuclear coupling is often observed for ^{13}C nuclei bonded to the quadrupolar nucleus ^{14}N. This is a through-space interaction, so non-covalently bonded quadrupolar nuclei also can induce ^{13}C line broadening. For instance, drugs formulated as chloride salts may contain split ^{13}C peaks, since ^{35}Cl is a quadrupolar nucleus.[7,8] ^{13}C–^{14}N interactions give rise to characteristic peak splitting of the ^{13}C peak. The associated line broadening is reduced, but not removed, by MAS, and stronger magnetic fields and special pulse sequences can further reduce the observed splitting and peak width.

2.2.4 Dilute spins and increased spin–lattice relaxation / Cross polarization

In addition to the line-broadening effects of dipole–dipole interactions and chemical shift anisotropy, the lack of molecular motion in solids affects spin–lattice

relaxation. NMR spectra typically consist of the average of many pulses/acquisitions on the sample, where the more acquisitions, the greater the signal-to-noise ratio in the spectrum. Unfortunately, when observing dilute spins, such as ^{13}C nuclei, which are only 1.1% naturally abundant, a large number of acquisitions is necessary to achieve a quality spectrum because only 1.1% of the carbon nuclei in a sample are actually "seen" by the NMR method. One of the methods to mitigate this issue is to transfer magnetization from an abundant spin system, typically ^{1}H nuclei, to the dilute spin system of interest, often ^{13}C.[9,10] This magnetization transfer is referred to as cross-polarization (CP). The ^{1}H–^{13}C cross-polarization process produces a significant signal enhancement for the observed ^{13}C nucleus, leading to much shorter analysis times. In addition to increasing signal associated with dilute spin systems, CP also offers the advantage of shorter pulse delays during data acquisition. This requires a more detailed explanation of NMR relaxation.

As previously highlighted, many of the differences in the practical aspects of obtaining an NMR spectrum in solution versus the solid state arise from decreased mobility in the solid state. This decreased mobility also increases the spin–lattice relaxation (T_1) of nuclei.

The spin–lattice relaxation is a calculated constant that is based on the amount of time for nuclear magnetization to return to its equilibrium state after each radiofrequency pulse (acquisition). The term "spin–lattice" is based on the idea that, after the nucleus (spin system) is excited by the radiofrequency pulse, energy is released into the surrounding lattice as the nucleus returns to equilibrium.[11] The T_1 value is related to the relaxation process by the equation:

$$M = (1 - e^{(-\tau/T_1)}) \times 100\%,$$

where M is the percent of total relaxation (or recovery), τ is the experimental pulse delay, and T_1 is the relaxation time constant. When the experimental pulse delay (τ) is 5 times the T_1, 99.33% of relaxation will have occurred. Thus, in order to observe signal that is truly representative of the number of nuclei (i.e., to acquire a quantitative spectrum), a pulse delay of 5 times the T_1 is used to provide sufficient time to achieve equilibrium between each pulse.

Typically, ^{1}H nuclei have much shorter (seconds versus tens of seconds) relaxation times than ^{13}C. When using CP, it is the relaxation of the abundant spin that dictates the pulse delay during data acquisition. Thus, the use of CP allows experimental time to be reduced due to the ability to pulse more rapidly, and thus obtain a quality spectrum more rapidly, than the equivalent acquisition without CP. Although the use of CP dramatically improves the efficiency of SSNMR acquisition, it can make quantitation of different components in a mixture more challenging (§ 2.3.4).

2.2.5   Summary

The combination of high-power decoupling, CP, and MAS is often referred to as a CP-MAS NMR experiment. This combination was demonstrated by Stejskal and Schaefer in 1977,[12] and Figure 2.1 shows the additive improvement in spectral quality obtained through implementing these techniques. Table 2.1 lists common pulse sequences used in SSNMR. The development of techniques such as decoupling, magic-angle spinning, and cross polarization has greatly alleviated the line-broadening problem, as well as decreased the analysis times associated with analyzing solid-state systems
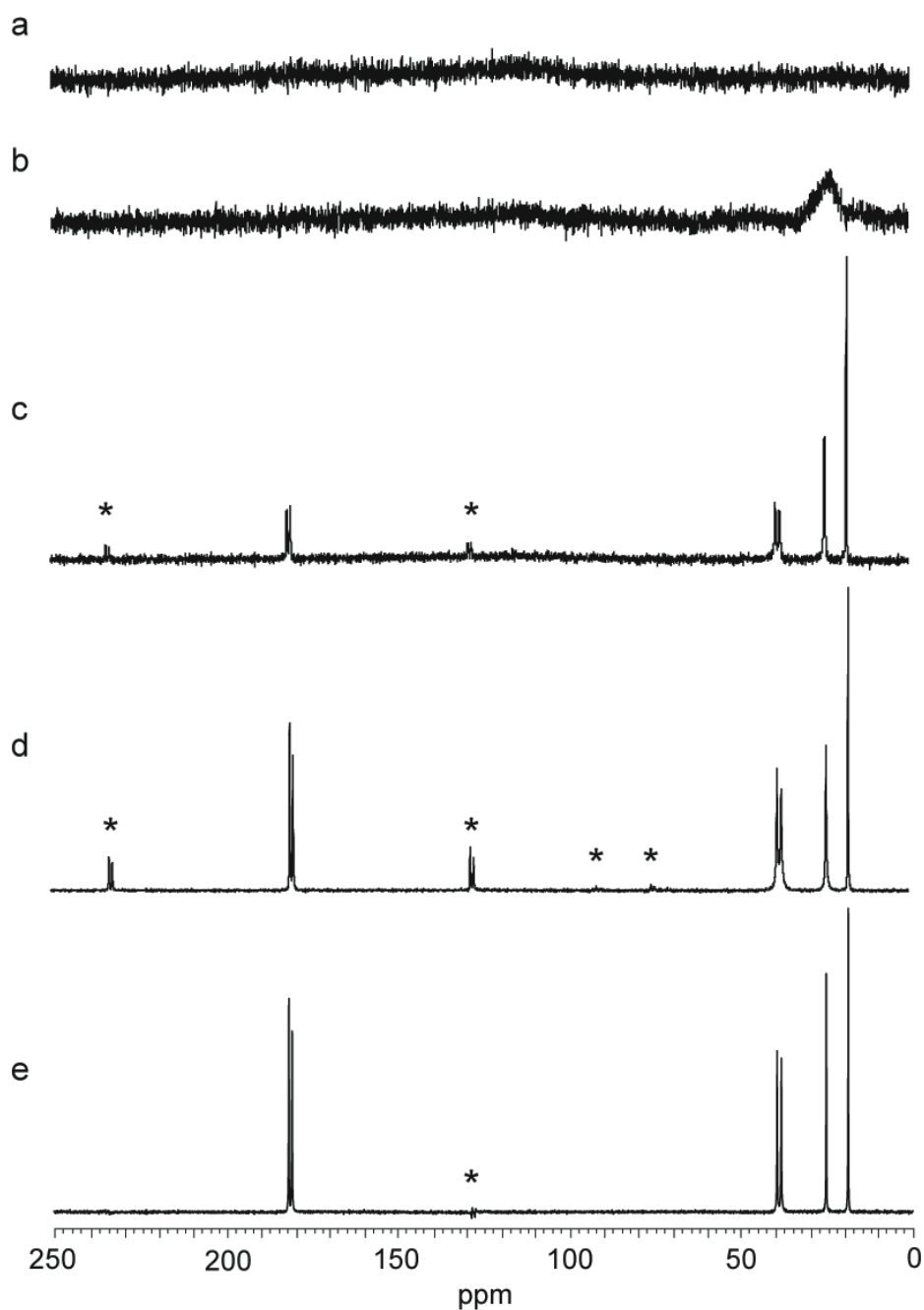
Figure 2.1. Solid-state ¹³C NMR spectra of 3-methylglutaric acid (MGA), obtained at 75 MHz. All spectra consist of 32 acquisitions under the following experimental conditions: a) 90° flip-angle carbon pulses with a 60-second pulse delay between scans, magic-angle spinning (MAS) at 4 kHz, and no decoupling; b) same as (a), without MAS and with high-power decoupling; c) same as (b), with MAS at 4 kHz; d) same as (c), with proton–carbon cross polarization and a 2-second pulse delay between scans; e) same as (d), only 12 acquisitions with TOSS. *denote spinning sidebands or artifacts.

Table 2.1. Descriptions of commonly used SSNMR pulse sequences[a]

Pulse Sequence	Description
Cross Polarization/Magic-Angle Spinning (CP-MAS)[5,11,13]	Used to obtain high-resolution NMR spectra from dilute, spin-1/2 nuclei
Single Pulse/Magic-Angle Spinning (SP-MAS)[14]	Used to obtain high-resolution NMR spectra from abundant spin systems
Dipolar Dephasing, Cross Polarization/Magic-Angle Spinning[15]	Used to detect non-protonated resonances
Cross Polarization combined with Polarization Inversion (CPPI)[16]	Used to distinguish different types of carbon resonances
Total Suppression of Spinning Sidebands (TOSS)[6]	A sideband suppression experiment used to simplify spectra
T_1 Measurement[17]	Used to determine the spin–lattice relaxation time
$T_{1\rho}$ Measurement [2]	Measures the spin–lattice relaxation time in the rotating frame
2-Dimensional Phase Adjustments of the Spinning Sidebands, Five Pi Replicated Magic-Angle Turning (PASS, FIREMAT) [18-20]	Used to correlate anisotropic and isotropic chemical shifts, which provide information on the molecular conformation

[a]Adapted from Bugay.[11]

using NMR spectroscopy. Please refer to other sources for more detailed information on both solution and solid-state NMR theory.[1,11,21,22]

2.3   Advantages of SSNMR

The motivation for using solid-state NMR spectroscopy for characterizing pharmaceuticals can be described by highlighting five areas for which SSNMR can provide unique information about a system. They are: 1) nondestructive and noninvasive analysis; 2) detection and identification of different phases/solid forms; 3) elucidation of structural information, such as conformation and arrangement of molecules within a solid; 4) quantitation of different solid forms; and 5) study of molecular dynamics.

The vast majority of pharmaceuticals are carbon-based. As a result ^{13}C is the nucleus most often observed when performing SSNMR analysis of a pharmaceutical compound. In the following examples, applications of SSNMR will focus on ^{13}C SSNMR.

2.3.1   Nondestructive

SSNMR is a nondestructive technique in that the sample is packed and sealed into a rotor, analyzed, and then can be removed from the rotor for further analysis. Unlike other techniques, SSNMR is capable of analyzing the drug molecule within the formulated drug product without additional sample preparation. In theory, intact tablets can be studied using SSNMR. However, a large tablet may be broken into pieces for ease of packing into the rotor. It is also possible to use SSNMR for the analysis of inclusion complexes, particularly to determine if there is any sort of interaction occurring between

the drug molecule and the host molecules.[23] The chemical reactions of a drug, including small molecules, peptides, or proteins, within a polymer matrix can also be followed.[24,25] In all of these cases, the analysis of a formulated product is aided by the fact that the drug molecule typically has a different chemical-shift range than the excipients, making it relatively easy to distinguish the peaks corresponding to the drug from those of the excipients.

2.3.2   *Identification of physical forms*

As with solution NMR, the position of each peak in the spectrum is indicative of the electronic environment of that particular nucleus, where a greater electron density around the nucleus produces a peak upfield (low ppm values) and less electron density results in a peak located downfield (high ppm values). Thus, just like in solution NMR, solid-state NMR can elucidate interactions such as H-bonding, in which the bonding modifies the electronic environment of the nucleus involved in or near the interaction, resulting in a change in peak position. However, due to the absence of solvent interactions, as well as the presence of "solute–solute" interactions in the solid state, the chemical shifts of a nucleus in the solid state can vary by more than 10 ppm relative to its position in solution. In general, for the ^{13}C nucleus, peaks from 220–200 ppm are due to ketone carbonyls, 180–160 ppm correspond to carbonyl groups of carboxylic acid derivatives, 160–100 are aromatic and olefinic carbons, 100–50 ppm correspond to sp^3-hybridized carbons attached to heteroatoms, and 40–10 ppm are aliphatic carbons attached to other carbons and/or hydrogens.

In both solution and solid-state NMR spectroscopy, differences in the chemical identity of a molecule can be observed in the spectrum. For instance, due to differences in the bonding structure, and therefore electronics, associated with the carbons in the molecules, the amino acids alanine, leucine, and proline (Figure 2.2) possess peaks in different locations. If these three distinct chemical entities were mixed together in solution, or as a physical mixture of solids, it would be possible to identify them based upon the number and locations of the peaks. However, whereas solution NMR typically gives only one signal for each observed nucleus, solid-state NMR provides signal for each crystallographically distinct nucleus, even when chemically identical. In order to illustrate this, a bit more information about crystal structures is required.

As mentioned in Chapter 1, a crystal lattice is formed by the highly ordered packing of molecules. The smallest repeating unit of a crystal lattice is called the "unit cell." The number of molecules that are present within a given unit cell is dependent upon the crystal form. In the case of an L-proline crystal, there are four molecules of L-proline in the unit cell. The conformation and arrangement of molecules in this unit cell is such that a particular carbon in a molecule (e.g., the carbonyl carbon, C-1) has the same electronic environment as any of the other C-1 nuclei in the other three molecules of the unit cell. Thus, there is only one peak for every carbon in the ^{13}C CP-MAS NMR spectrum of L-proline (Figure 2.2). Similar to L-proline, L-leucine has 4 molecules per unit cell. However, in the case of L-leucine, the conformations of the molecules within the unit cell differ slightly, and the carbonyl carbons of two of the molecules in each unit cell are slightly different from the other two. This is observed in the SSNMR spectrum as multiple peaks for each carbon (Figure 2.2) and is referred to as
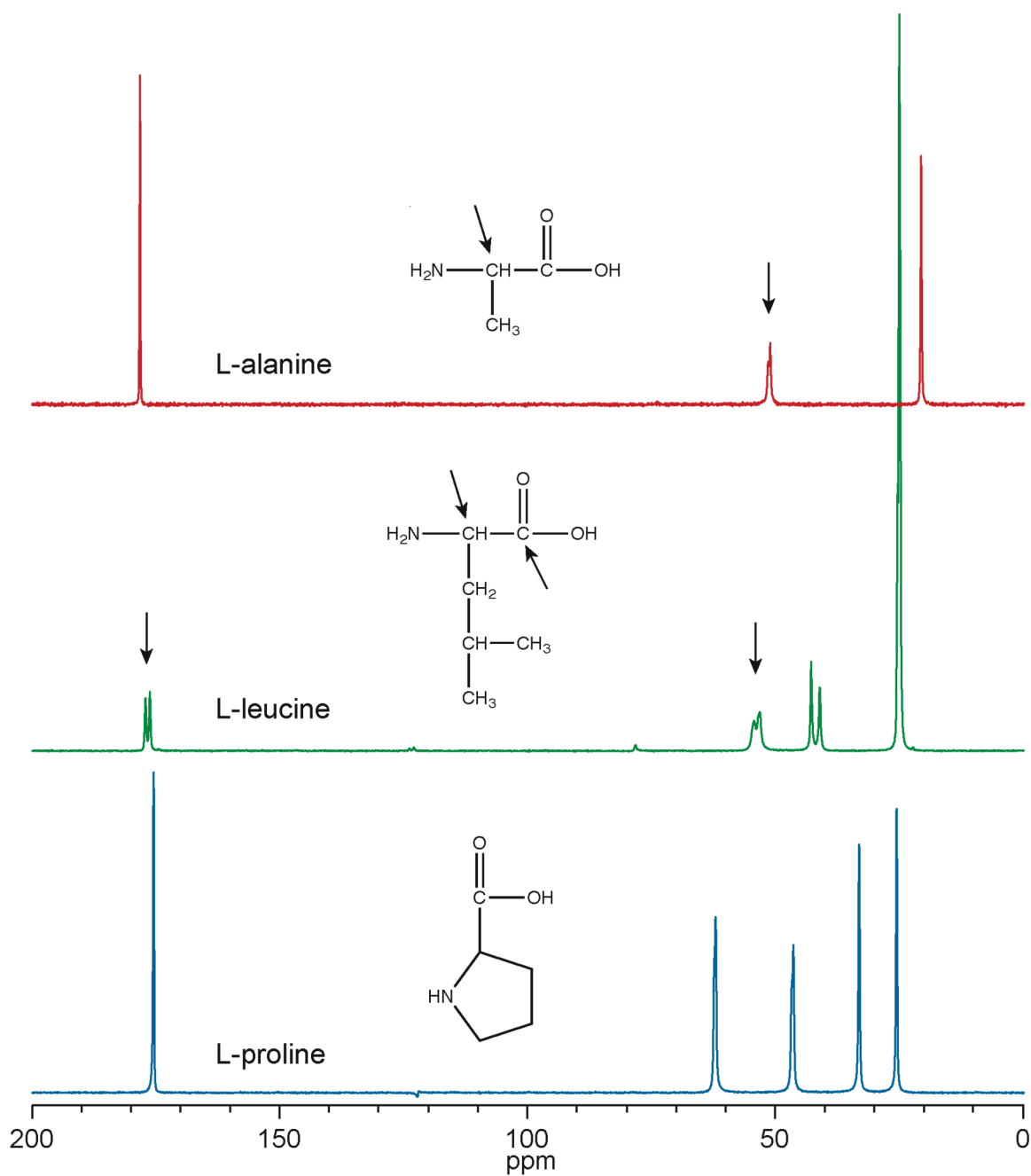
Figure 2.2. ^{13}C CP-MAS NMR spectra and molecular structures of L-alanine, L-leucine, and L-proline. Crystallographic inequivalence is denoted by arrows.

crystallographic inequivalence. This inequivalence provides information about the structure of molecules within the crystal lattice. Additionally, it serves as a demonstration for the effect of molecular conformation/packing on the peak positions observed in SSNMR.

Similar to the effect of crystallographic inequivalence, differences in the molecular conformation/packing among different crystal forms (including polymorphs, solvates, and hydrates) also produce differences in SSNMR peak locations. This means that SSNMR is very powerful for looking at different solid-state forms, where the chemical identity is the same, but the structural/crystallographic identity differs.

Significant differences exist between the SSNMR spectra of crystalline and amorphous materials as well. Whereas crystalline materials give rise to relatively narrow peaks within the CP-MAS spectrum, the distribution of molecular conformations and arrangements within an amorphous phase produces a range of electronic environments, which lead to very broad peaks,[1] typically >10 times the width of the corresponding crystalline peaks. In addition, the peaks of amorphous materials are not necessarily centered at the same spectral location as the corresponding crystalline peaks. As a result, SSNMR is a tool capable of identifying both amorphous and crystalline physical forms of solids. The differences in both peak width and peak location between crystalline and amorphous forms are demonstrated in Figure 2.3, which shows the ^{13}C CP-MAS NMR spectra for both crystalline and amorphous thiamine hydrochloride.

It is also possible to look at very small quantities of individual components of a system by isotopically labeling specific nuclei. As mentioned in § 2.2.1, the ^{13}C nucleus is only 1.1% naturally abundant, meaning that only 1.1% of the carbons in a sample are
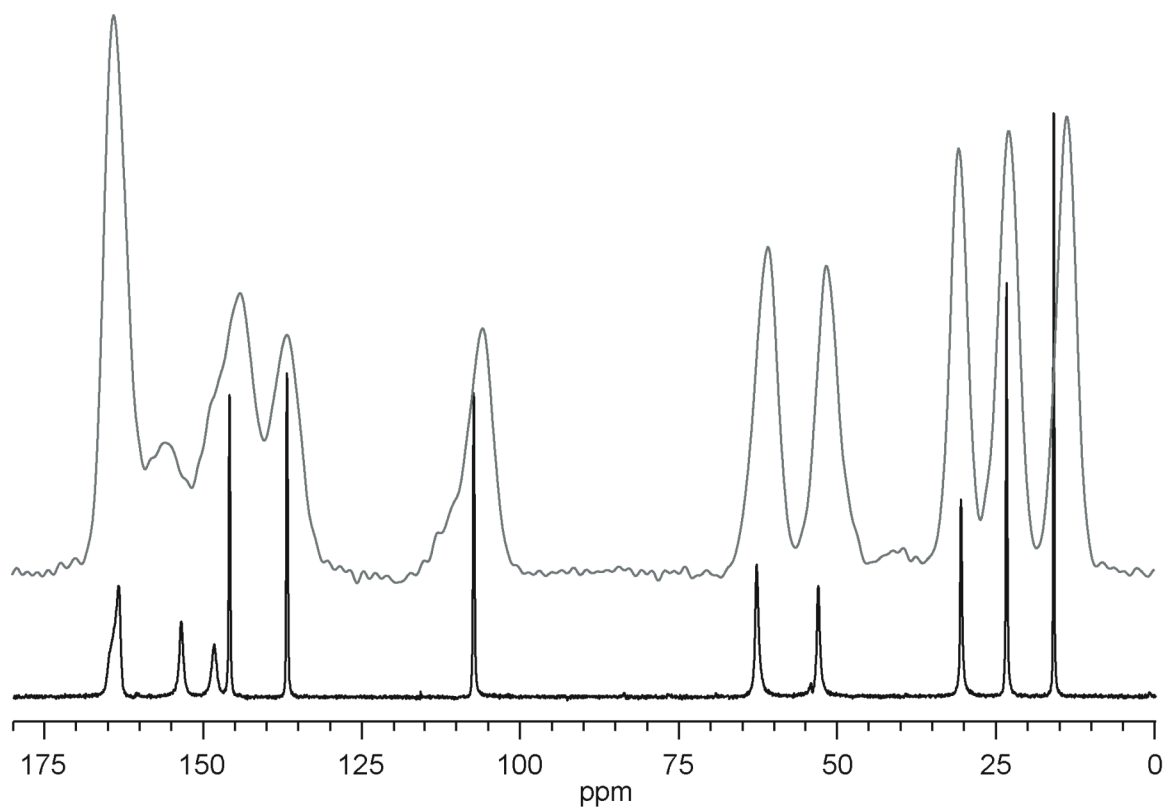
Figure 2.3. ^{13}C CP-MAS NMR spectra of anhydrous thiamine hydrochloride in its crystalline (black, lower spectrum) and amorphous (gray, upper spectrum) forms.

"visible" to the NMR technique. This can lead to sensitivity issues if the molecule or crystal form of interest is present at very low levels within the sample. In order to increase sensitivity, a molecule can be isotopically labeled, where the ^{12}C nuclei are replaced with ^{13}C nuclei. A molecule can be isotopically labeled at a specific carbon or uniformly labeled, in which case all the carbons in the molecule are ^{13}C nuclei. If a particular molecule or drug is ^{13}C labeled, the signal from the labeled carbon will be approximately 90 times greater than that of a natural-abundance signal. This makes it possible to follow interactions and detect forms that might occur at low levels.

Although X-ray diffraction techniques are often considered the gold standard for polymorph identification,[1] the requirement of long-range order can limit its applicability. Whereas SSNMR is based on short-range molecular interactions, X-ray diffraction techniques are based on the reflection of X-rays in a highly ordered lattice structure. Padden and coworkers performed a back-to-back comparison of PXRD and SSNMR in the analysis of neotame polymorphism.[26] Based on the SSNMR analysis, differences in the spectra provided evidence for ongoing polymorphic transformations. However, these crystal form changes were not observed by PXRD, since the transformations did not significantly alter the long-range order of the crystal lattice. The authors acknowledged the limitations of PXRD for identifying polymorphs and concluded that SSNMR should be used more frequently in the analysis of polymorphic systems, since it is not limited by the need for long-range order.

There are many examples of the use of SSNMR to determine/characterize differences in crystal form in the literature, including differences among chiral systems.[27-32] One of the first studies to do so was performed by Hill et al., who demonstrated that

56

the crystallographic differences of racemic (±)-tartaric acid and enantiopure (+)-tartaric acid produced different peaks within the ^{13}C CP-MAS NMR spectrum.[30] The authors noted that, due to the ability for SSNMR to quantitate the relative amounts of (±)- versus (+)-tartaric acid, SSNMR is a novel method for assessing optical purity of a solid material. Similar results have been shown by Munson and coworkers, who used ^{13}C SSNMR to study the enantiopure and racemic cocrystal forms of ephedrinium 2-naphthalenesulfonate.[31] In these studies, they were able to identify and quantitate the enantiopure and racemic cocrystal forms in a physical mixture at a 10:90 ratio. In the rare cases where the peaks of enantiopure and racemic cocrystals completely overlap, there are special SSNMR methods that can be used to distinguish between the two forms.[29]

Sometimes peak identification within a ^{13}C SSNMR spectrum can be difficult due to the presence of many peaks for a carbon site. As described previously, crystallographically inequivalent sites in a crystal structure can give rise to multiple peaks for a single carbon. Similarly, the presence of multiple phase-separated crystal forms typically produce distinct peaks corresponding to each crystal form. Sometimes, both of these situations are observed within a system, and determining whether multiple peaks for a single carbon are due to polymorphism and/or crystallographic inequivalencies is difficult. In such cases, two-dimensional exchange NMR experiments can be used. In these experiments, nuclei are excited and then allowed to "talk" to one another by exchanging magnetization through dipole–dipole interactions. The farther apart the nuclei are, the longer it takes for the exchange process to occur. By varying the exchange time, it is possible to determine which nuclei are near one another, as well as to identify

phase separation. Thus, such an experiment can be helpful in making peak assignments, as it is possible to determine carbon connectivity, as well as in determining if phase separation or crystallographic inequivalence is the cause of multiple peaks for a single carbon in the spectrum. Zell et al. used such 2D-exchange NMR experiments, along with high spin speed and decoupling power, in order to assign peaks to carbons of aspartame polymorphs.[33]

Although SSNMR alone can provide a large amount of information about a solid system, it can often benefit from complementary analysis. For instance, SSNMR can be used in combination with diffraction methods to determine the degree of disorder within a crystal lattice. The presence of defects within the crystal lattice, or the reduction of particle size, results in reduced coherence of the X-ray reflections, which leads to broad peaks of lower intensity, the extreme of which is an amorphous halo.[34] In contrast, the effect of crystalline particle size on SSNMR peak widths is typically much less. Thus, the comparison of PXRD and SSNMR analyses of a powder can give an idea as to the "degree of crystallinity" that exists in the sample: The sample is highly crystalline if both PXRD and SSNMR show sharp peaks; it is amorphous when both techniques show broad peaks; and it is disordered crystalline material when there are sharp SSNMR peaks, but broad peaks or an amorphous halo in the PXRD pattern. Chakravarty et al. used the combination of SSNMR and PXRD to show that the dehydration of thiamine hydrochloride hemihydrate (THCl HH) did not produce amorphous material. The PXRD pattern of dehydrated THCl HH contained a subtle amorphous halo. However, the ^{13}C CP-MAS NMR spectrum did not contain peaks corresponding to amorphous material. These observations led to the conclusion that THCl HH dehydration produced some

disorder/partial collapse of the crystal lattice, but not the formation of an amorphous phase.[7]

2.3.3   Structural elucidation

Up until this point, the discussion has focused on the information available from SSNMR peak location and shape within the spectrum. These sharp, isotropic peaks were achieved by spinning the sample rapidly at the magic angle, which reduced the influence of anisotropy on the observed line width (§ 2.2.2). However, this anisotropy contains information about the local molecular structure within the crystal lattice. Two-dimensional NMR techniques such as PASS (Phase Adjustments of the Spinning Sidebands)[35] and FIREMAT (Five Pi Replicated Magic-Angle Turning)[18] take advantage of this information. These techniques measure the shape of the chemical shift anisotropy (CSA) powder pattern by calculating the associated tensor values, which can be combined with computational molecular modeling to determine molecular conformation.[36] This process has been applied to a variety of chemical systems, such as measuring bond lengths and dihedral angles in protein and peptide backbones,[37,38] identifying structural differences in various forms of diamond,[39] and distinguishing conformational polymorphism.[40-42] This type of conformational analysis is particularly valuable when crystal-structure elucidation is not possible by traditional X-ray diffraction methods. This technique is also directly applicable to chiral compounds: Harper et al. characterized the stereochemistry and molecular conformation of diastereomers of terrein.[43] In their study, the authors showed that comparing the SSNMR data with ab initio computations made it possible to determine both the relative stereochemistry and

59

conformation of terrein. A comparison of this SSNMR–computational structure data was consistent with structure data achieved by XRD.

2.3.4 Quantitation

Not only can SSNMR identify both crystalline and amorphous forms in solid materials, but it also is capable of quantitating the amount of each form present. NMR is inherently a quantitative technique in that the signal that is observed is directly proportional to the relative number of like nuclei in the sample. This is unique compared to most other analytical techniques, and it allows for the quantitation of forms without the need for a standard.[44] SSNMR can be used to quantitate the amount of crystalline versus amorphous material present in a particular sample, as well as to quantitate mixtures of crystalline forms.[44-46] Changes that might occur upon formulation, such as the crystallization of an amorphous drug, also can be monitored.

SSNMR spectra usually are acquired with cross polarization. CP does not necessarily produce quantitative spectra because the signal that arises in a CP spectrum is dependent upon magnetization transfer from ^{1}H to ^{13}C nuclei. Thus, the signal enhancement for a particular carbon nucleus depends on the number and strength of ^{1}H–^{13}C interactions. These differences are accounted for in the relaxation constants T_{CH} and $T_{1\rho}$, which describe the rate of magnetization transfer from ^{1}H to ^{13}C nuclei and the rate of magnetization decrease due to ^{1}H relaxation, respectively.[47] Quantitation of different physical forms is possible by accounting for these differences through careful optimization of the experimental conditions and use of calibration curves.

Offerdahl et al. have used SSNMR to quantitate the different polymorphic forms of neotame present in physical mixtures.[44] Figure 2.4 shows the ^{13}C CP-MAS NMR spectrum of a 1:1 (wt/wt) physical mixture of the neotame polymorphs Form A and Form G. The two aromatic resonances selected for quantitation represent the same carbon in each form. The relative peak intensities are not the same for each form. This indicates that the cross-polarization rate for each form is different. By plotting the natural log of the relative peak area as a function of the contact time, the authors used the anti-log of the y-intercept to calculate the weight percent of each form. Table 2.2 displays the summary of the data obtained from quantitation experiments on physical mixtures of neotame polymorphic Forms A and G. It can be seen (Figure 2.5) that the relative weight percent determined by SSNMR corresponds with the weight percent values determined by mass. In some cases, the differences in CP dynamics may be negligible, which can simplify the acquisition of quantitative spectra. However, even in these cases, it is important to take into account T_1 relaxation differences that might exist between different forms.

Just as $T_{1\rho}$ and T_{CH} relaxation constants can differ among different forms, T_1 values also can differ. As mentioned in § 2.2.3, spectral acquisition parameters must include a pulse delay of 5 times the T_1 value in order to avoid saturation effects. When looking at a binary mixture of components, a given pulse delay may be sufficiently long as to avoid saturation of one component, but not long enough for the other. The resulting spectrum will contain an artificially low peak area for the component that did not have sufficient time between pulses to relax completely. Thus, when quantitative SSNMR spectra are desired, a pulse delay of at least 5 times the longest T_1 must be used.
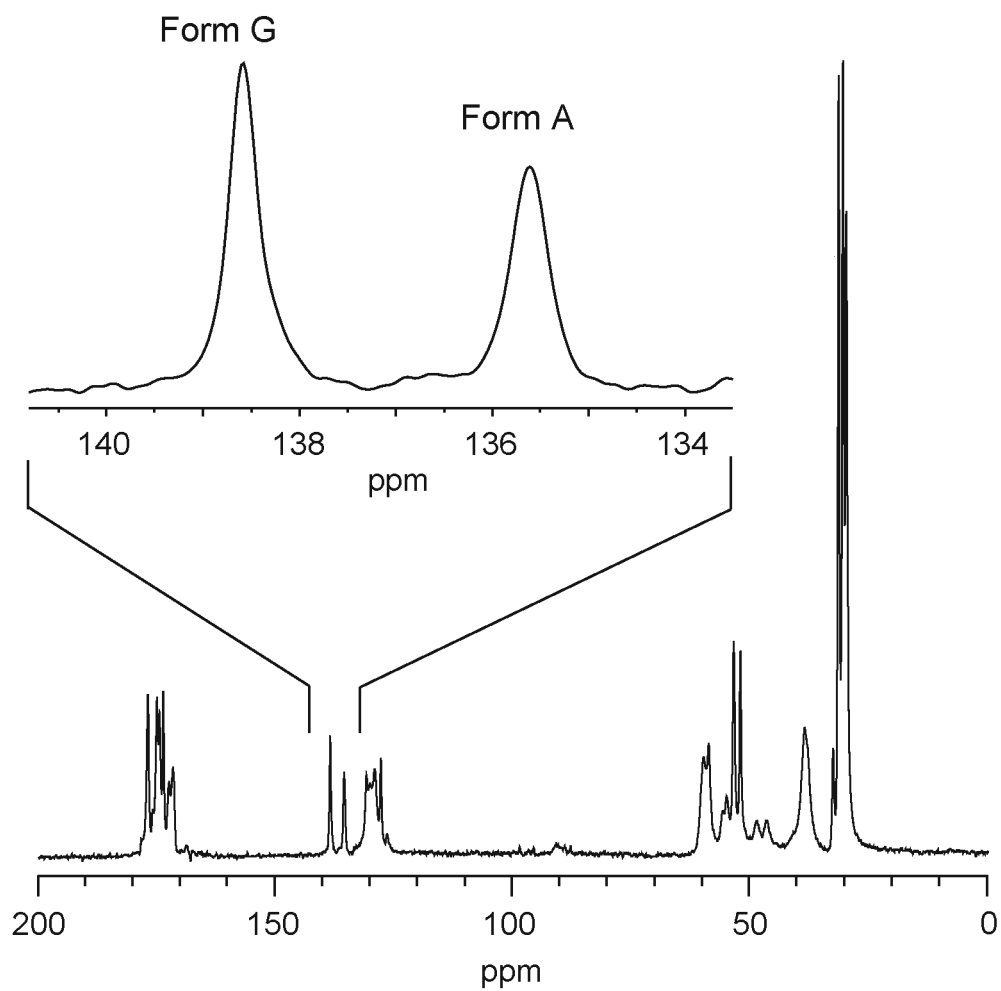
Figure 2.4. ^{13}C CP-MAS NMR spectra of a 1:1 (w/w) mixture of neotame Form A and Form G. Adapted from Offerdahl et al.[44]

Table 2.2. A table displaying the weight percentages of neotame Form A and Form G, as determined by mass and by SSNMR quantitation methods.[a]

Percent Form A	Form	Wt. % by Mass	y-intercept	Relative Area	Wt.% by SSNMR	Difference (absolute)
10	A	12.62	7.298	1478	13.7	1.0
	G	87.38	9.142	9340	86.3	
20	A	21.20	4.955	141.9	22.0	0.8
	G	78.80	6.221	503.1	78.0	
30	A	29.71	4.899	134.2	29.4	0.4
	G	70.29	5.777	322.9	70.6	
40	A	39.12	5.038	154.2	37.9	1.3
	G	60.88	5.534	253.1	62.1	
50	A	49.73	4.856	128.5	50.3	0.5
	G	50.27	4.845	127.1	49.7	
60	A	61.56	4.868	130.1	62.3	0.7
	G	38.44	4.367	78.80	37.7	
70	A	70.29	4.887	132.6	71.4	1.1
	G	29.71	3.971	53.10	28.6	
80	A	80.88	4.878	131.4	81.8	1.0
	G	19.12	3.372	29.10	18.2	
90	A	88.41	7.185	1320	89.0	0.5
	G	11.59	5.099	164.0	11.0	

[a]Adapted from Offerdahl et al.[44]
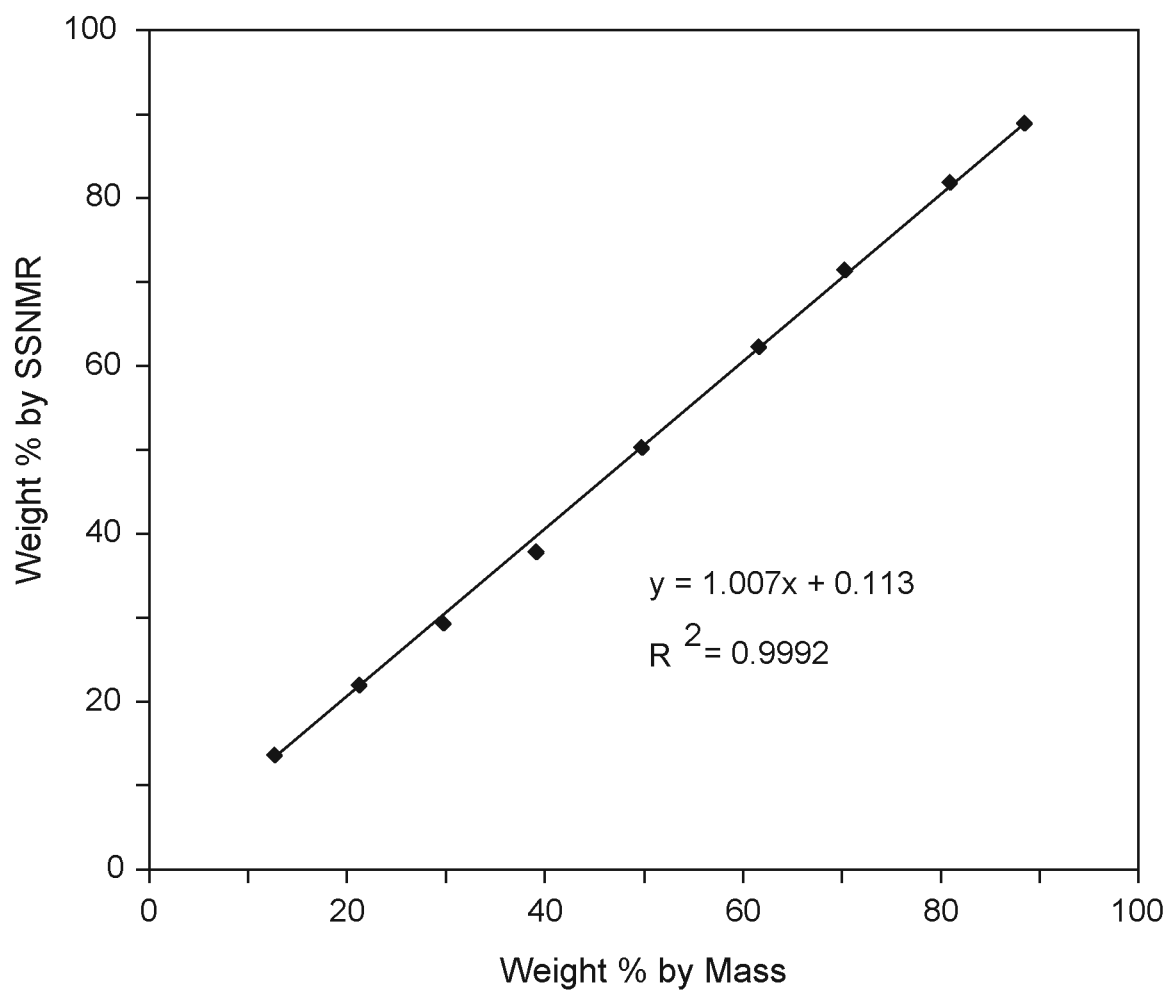
Figure 2.5. Plot of the wt% of neotame Form A as measured by mass versus SSNMR quantitation. Adapted from Offerdahl et al.[44]

2.3.5 Relaxation dynamics and molecular mobility

SSNMR is a particularly powerful technique for studying the dynamics of a system. For a crystalline system, the mobility in the lattice can be observed, but potentially more important is the ability to look at specific sites of high mobility. These highly mobile areas are often defect sites. The mobility of a solid pharmaceutical system has important role in the physical and chemical stability of the drug. Byrn and coauthors have shown that there is a relationship between molecular mobility and solid-state chemical reactivity.[48] Such mobility can easily be introduced into a sample during processing steps, such as grinding or sorption of water vapor.[49]

There are many different methods for assessing mobility in solids by SSNMR,[1,48] including measuring NMR relaxation dynamics. The most commonly cited relaxation values are the spin–lattice relaxation times T_1 and $T_{1\rho}$.

As described in § 2.2.3, T_1 spin–lattice relaxation is a calculated constant that describes the rate at which a nucleus returns to its equilibrium state after excitation by a radiofrequency pulse. Equilibrium is achieved by the release of energy from the nucleus to the surrounding lattice. For the ^{1}H nucleus, dipolar interactions are the dominant mechanism for the relaxation process.

The T_1 of the ^{1}H nucleus is often of interest due to its role in choosing the proper experimental pulse delay, but it also is a measure of molecular motions in the MHz range, such as methyl-group rotations. Theoretically, every crystallographically distinct ^{1}H nucleus should possess its own ^{1}H T_1 value. However, through the process of spin diffusion, in which the nuclei (spins) at different local sites equilibrate with one another through mutual exchange of magnetization, the relaxation rates are usually averaged for a

single solid phase.[50] Thus, a single, averaged ^{1}H T_1 value is observed when the solid consists of a single phase. However, when multiple phases are present, each phase may possess its own relaxation rate. Due to the fact that the molecular arrangement/packing among different physical forms/phases often results in differences in molecular mobility, the relaxation rates between phases usually differ as well.

Relaxation measurements are often performed with a saturation–recovery NMR experiment that includes CP, such that it is possible to measure the ^{1}H T_1 value indirectly by measuring the changes in ^{13}C signal. In this manner, it is possible to refer to ^{1}H T_1 relaxation times in reference to peaks in the corresponding ^{13}C spectrum. For instance, when looking at a ^{13}C SSNMR spectrum that contains multiple peaks for a single carbon, it is possible to measure the ^{1}H T_1 values associated with each peak. If the T_1 values for all of the peaks are different, it suggests that each peak corresponds to a different crystal phase/form, whereas a similar T_1 value suggests that a single phase exists. This means that relaxation measurements can be helpful in distinguishing phase separation and polymorphism from crystallographic inequivalence. Characterizing phase separation in this manner has predominantly been reported for determination of polymeric miscibility of solid dispersions in polymer science[50] but applications to small molecule solids are reported as well.[51-53]

Whereas T_1 values (typically measured in seconds) are associated with motions on the MHz scale, $T_{1\rho}$ values (ms) correspond to slower motions that occur at the kHz scale.[1] Aso et al. used these timescale differences to determine the domain sizes of two different phases, where very small domains (<5 nm) possessed T_1 and $T_{1\rho}$ relaxation decays that were describable by a mono-exponential equation, domains >50 nm gave rise to T_1 and

$T_{1\rho}$ relaxation decays describable by bi-exponential decays, and domain sizes of 5–50 nm

had $T_{1\rho}$ described by a bi-exponential decay and a T_1 by a mono-exponential decay.[50]

Thus, T_1 and $T_{1\rho}$ values are able to not only determine phase separation, but also estimate

the degree of miscibility that exists between multiple components in a mixture or solid

dispersion.[50,52] Measuring differences in mobility among crystalline forms can be useful

for understanding the physicochemical stability of a system, as well as for establishing

and characterizing differences in physical forms.[53]

2.3.6   Disadvantages

Despite the strengths of SSNMR, there are several reasons why it is not widely

used for the characterization of pharmaceutical solids. One reason is that considerable

expertise is needed to acquire the SSNMR spectrum and to interpret the data. Solid-state

NMR spectrometers are also about an order of magnitude more expensive than many of

the other analytical instruments available. SSNMR is also relatively insensitive, leading

to long analysis times. This is a significant drawback because it limits the number of

samples that can be run during a particular period of time. Currently, the development of

a multiple-sample NMR probe is being pursued in order to solve some of these sensitivity

issues.[54]

2.4   **Conclusion**

Solid-state NMR spectroscopy has emerged as an important technique for the characterization of pharmaceutical solids. When a new drug molecule is discovered, it is important to characterize its solid-state properties, as these properties can have a dramatic effect on dissolution rate (and therefore bioavailability) and stability (both chemical and physical). The advantage of using SSNMR experiments for characterizing pharmaceuticals stems from five areas. They are: 1) nondestructive and noninvasive analysis; 2) detection and identification of different phases/solid forms; 3) elucidation of structural information, such as conformation and arrangement of molecules within a solid; 4) quantitation of different solid forms; and 5) study of molecular dynamics. The unique information obtained by SSNMR also makes it useful for studying chiral solids, the subject of this dissertation. Although current use of SSNMR is not widespread within the pharmaceutical industry due to expense, long analysis times, and low throughput, the development of the multiple-sample probe, as well as other advancements, will increase the potential employment of SSNMR in the near future.

2.5 References

1. Byrn SR, Pfeiffer RR, Stowell JG 1999. Solid-State Chemistry of Drugs. 2nd ed., West Lafayette, Indiana: SSCI, Inc.

2. Fyfe CA 1983. Solid State NMR for Chemists. Ontario, Canada: C.F.C. Press.

3. Berendt RT, Sperger DM, Munson EJ, Isbester PK 2006. Solid-state NMR spectroscopy in pharmaceutical research and analysis. TrAC, Trends Anal Chem 25(10):977-984.

4. Fung BM, Khitrin AK, Ermolaev K 2000. An improved broadband decoupling sequence for liquid crystals and solids. J Magn Reson 142(1):97-101.

5. Andrew ER, Bradbury A, Eades RG 1959. Removal of dipolar broadening of nuclear magnetic resonance spectra of solids by specimen rotation. Nature 183:1802-1803.

6. Dixon WT, Schaefer J, Sefcik MD, Stejskal EO, McKay RA 1982. Total suppression of sidebands in CPMAS carbon-13 NMR. J Magn Reson 49(2):341-345.

7. Chakravarty P, Berendt RT, Munson EJ, Young VG, Jr., Govindarajan R, Suryanarayanan R 2010. Insights into the dehydration behavior of thiamine hydrochloride (vitamin B1) hydrates: Part II. J Pharm Sci 99(4):1882-1895.

8. Chapman RP, Bryce DL 2007. A high-field solid-state 35/37Cl NMR and quantum chemical investigation of the chlorine quadrupolar and chemical shift tensors in amino acid hydrochlorides. PCCP 9(47):6219-6230.

9. Pines A, Gibby MG, Waugh JS 1973. Proton-enhanced NMR of dilute spins in solids. J Chem Phys 59(2):569-590.

10.   Metz G, Wu X, Smith SO 1994. Ramped-amplitude cross polarization in magic-angle-spinning NMR. J Magn Reson, Ser A 110(2):219-227.

11.   Bugay DE 1993. Solid-state nuclear magnetic resonance spectroscopy: Theory and pharmaceutical applications. Pharm Res 10(3):317-327.

12.   Stejskal EO, Schaefer J, Waugh JS 1977. Magic-angle spinning and polarization transfer in proton-enhanced NMR. J Magn Reson (1969-1992) 28(1):105-112.

13.   Pines A, Gibby MG, Waugh JS 1972. Proton-enhanced nuclear induction spectroscopy. Carbon-13 chemical shielding anisotropy in some organic solids. Chem Phys Lett 15(3):373-376.

14.   Abraham RJ, Fisher J, Loftus P 1988. Introduction to NMR Spectroscopy. New York: Wiley.

15.   Opella SJ, Frey MH 1979. Selection of nonprotonated carbon resonances in solid-state nuclear magnetic resonance. J Am Chem Soc 101(19):5854-5856.

16.   Wu X, Zilm KW 1993. Complete spectral editing in CPMAS NMR. J Magn Reson, Ser A 102(2):205-213.

17.   Sudmeier JL, Anderson SE, Frye JS 1990. Calculation of nuclear spin relaxation times. Concepts Magn Reson 2(4):197-212.

18.   Alderman DW, McGeorge G, Hu JZ, Pugmire RJ, Grant DM 1998. A sensitive, high resolution magic angle turning experiment for measuring chemical shift tensor principal values. Mol Phys 95(6):1113-1126.

19.   Song Z, Antzutkin ON, Rupprecht A, Levitt MH 1996. Order-resolved sideband separation in magic-angle-spinning NMR. 31P NMR of oriented DNA fibers. Chem Phys Lett 253(3,4):349-354.

20. Frydman L, Chingas GC, Lee YK, Grandinetti PJ, Eastman MA, Barrall GA, Pines A 1992. Correlation of isotropic and anisotropic chemical shifts in solids by two-dimensional variable-angle-spinning NMR. Isr J Chem 32(2-3):161-164.

21. Harris RK 1986. Nuclear Magnetic Resonance Spectroscopy. New York, New York: Longman Scientific & Technical.

22. Tishmack PA, Bugay DE, Byrn SR 2003. Solid-state nuclear magnetic resonance spectroscopy-pharmaceutical applications. J Pharm Sci 92(3):441-474.

23. Aliev AE, Harris KDM, Champkin PH 2005. Structural and dynamic aspects of hydrogen-bonded complexes and inclusion compounds containing α,ω-dicyanoalkanes and urea, investigated by solid-state 13C and 2H NMR techniques. J Phys Chem B 109(49):23342-23350.

24. Geppi M, Guccione S, Mollica G, Pignatello R, Veracini CA 2005. Molecular properties of ibuprofen and its solid dispersions with Eudragit RL100 studied by solid-state nuclear magnetic resonance. Pharm Res 22(9):1544-1555.

25. Lubach JW, Padden BE, Winslow SL, Salsbury JS, Masters DB, Topp EM, Munson EJ 2004. Solid-state NMR studies of pharmaceutical solids in polymer matrices. Anal Bioanal Chem 378(6):1504-1510.

26. Padden BE, Zell MT, Dong Z, Schroeder SA, Grant DJW, Munson EJ 1999. Comparison of solid-state 13C NMR spectroscopy and powder X-ray diffraction for analyzing mixtures of polymorphs of neotame. Anal Chem 71(16):3325-3331.

27. Suzuki N, Kawasaki T 2005. Evaluation of solid state form of troglitazone by solid state NMR spectroscopy. J Pharm Biomed Anal 37(1):177-181.

28. Bettinetti G, Giordano F, Fronza G, Italia A, Pellegata R, Villa M, Ventura P 1990. Sobrerol enantiomers and racemates: solid-state spectroscopy, thermal behavior, and phase diagrams. J Pharm Sci 79(6):470-475.

29. Potrzebowski MJ, Tadeusiak E, Misiura K, Ciesielski W, Bujacz G, Tekely P 2002. A new method for distinguishing between enantiomers and racemates and assignment of enantiomeric purity by means of solid-state NMR. Examples from oxazaphosphorinanes. Chem Eur J 8(21):5007-5011.

30. Hill HDW, Zens AP, Jacobus J 1979. Solid-state NMR spectroscopy. Distinction of diastereomers and determination of optical purity. J Am Chem Soc 101(23):7090-7091.

31. Li ZJ 1996. Implications of chirality for the physicochemical properties and crystallization of chiral drugs. Department of Pharmaceutics, Minneapolis, Minnesota: The University of Minnesota.

32. Reutzel-Edens SM, Russell VA, Yu L 2000. Molecular basis for the stability relationships between homochiral and racemic crystals of tazofelone: a spectroscopic, crystallographic, and thermodynamic investigation. Perkin 2 (5):913-924.

33. Zell MT, Padden BE, Paterick AJ, Hillmyer MA, Munson EJ, Thakur KAM, Kean RT 1998. Characterization of poly(lactide) using solution and solid-state NMR spectroscopy. Polym Mater Sci Eng 78:137-138.

34. Jenkins R, Snyder R, Editors. 1996. Introduction to X-Ray Powder Diffractometry. New York: Wiley.

35. Song Z, Antzutkin ON, Rupprecht A, Levitt MH 1996. Order-resolved sideband separation in magic-angle-spinning NMR. 31P NMR of oriented DNA fibers. Chem Phys Lett 253(3,4):349-354.

36. Smith JR, Xu W, Raftery D 2006. Analysis of conformational polymorphism in pharmaceutical solids using solid-state NMR and electronic structure calculations. J Phys Chem B 110(15):7766-7776.

37. Heller J, Laws DD, Tomaselli M, King DS, Wemmer DE, Pines A, Havlin RH, Oldfield E 1997. Determination of dihedral angles in peptides through experimental and theoretical studies of α-carbon chemical shielding tensors. J Am Chem Soc 119(33):7827-7831.

38. Brender JR, Taylor DM, Ramamoorthy A 2001. Orientation of amide-nitrogen-15 chemical shift tensors in peptides: A quantum chemical study. J Am Chem Soc 123(5):914-922.

39. Mauri F, Pfrommer BG, Louie SG 1997. Ab initio NMR chemical shift of diamond, chemical-vapor-deposited diamond, and amorphous carbon. Phys Rev Lett 79(12):2340-2343.

40. Smith J, MacNamara E, Raftery D, Borchardt T, Byrn S 1998. Application of two-dimensional 13C solid-state NMR to the study of conformational polymorphism. J Am Chem Soc 120(45):11710-11713.

41. Harper JK, Grant DM 2000. Solid-state 13C chemical shift tensors in terpenes. 3. structural characterization of polymorphous verbenol. J Am Chem Soc 122(15):3708-3714.

42.	Barich DH, Pugmire RJ, Grant DM, Iuliucci RJ 2001. Investigation of the structural conformation of biphenyl by solid state 13C NMR and quantum chemical NMR shift calculations. J Phys Chem A 105(28):6780-6784.

43.	Harper JK, Mulgrew AE, Li JY, Barich DH, Strobel GA, Grant DM 2001. Characterization of stereochemistry and molecular conformation using solid-state NMR tensors. J Am Chem Soc 123(40):9837-9842.

44.	Offerdahl TJ, Salsbury JS, Dong Z, Grant DJW, Schroeder SA, Prakash I, Gorman EM, Barich DH, Munson EJ 2005. Quantitation of crystalline and amorphous forms of anhydrous neotame using 13C CPMAS NMR spectroscopy. J Pharm Sci 94(12):2591-2605.

45.	Gao P 1996. Determination of the composition of delavirdine mesylate polymorph and pseudopolymorph mixtures using 13C CP/MAS NMR. Pharm Res 13(7):1095-1104.

46.	Sheth AR, Lubach JW, Munson EJ, Muller FX, Grant DJW 2005. Mechanochromism of piroxicam accompanied by intermolecular proton transfer probed by spectroscopic methods and solid-phase changes. J Am Chem Soc 127(18):6641-6651.

47.	Offerdahl TJ, Munson EJ 2004. Solid state NMR spectroscopy of pharmaceutical materials. Am Pharm Rev 7(1):109-112.

48.	Byrn SR, Xu W, Newman AW 2001. Chemical reactivity in solid-state pharmaceuticals: formulation implications. Adv Drug Delivery Rev 48(1):115-136.

49. Ahlneck C, Zografi G 1990. The molecular basis of moisture effects on the physical and chemical stability of drugs in the solid state. Int J Pharm 62(2-3):87-95.

50. Aso Y, Yoshioka S, Miyazaki T, Kawanishi T, Tanaka K, Kitamura S, Takakura A, Hayashi T, Muranushi N 2007. Miscibility of nifedipine and hydrophilic polymers as measured by 1H-NMR spin–lattice relaxation. Chem Pharm Bull (Tokyo) 55(8):1227-1231.

51. Lubach JW, Xu D, Segmuller BE, Munson EJ 2007. Investigation of the effects of pharmaceutical processing upon solid-state NMR relaxation times and implications to solid-state formulation stability. J Pharm Sci 96(4):777-787.

52. Campbell GC, VanderHart DL, Feng Y, Han CC 1992. Proton NMR study of the intimacy of mixing in a hydrogen-bonded blend of polystyrene and poly(butyl methacrylate). Macromol 25(8):2107-2111.

53. Zumbulyadis N, Antalek B, Windig W, Scaringe RP, Lanzafame AM, Blanton T, Helber M 1999. Elucidation of polymorph mixtures using solid-state 13C CP/MAS NMR spectroscopy and direct exponential curve resolution algorithm. J Am Chem Soc 121(49):11554-11557.

54. Nelson BN, Schieber LJ, Barich DH, Lubach JW, Offerdahl TJ, Lewis DH, Heinrich JP, Munson EJ 2006. Multiple-sample probe for solid-state NMR studies of pharmaceuticals. Solid State Nucl Magn Reson 29(1-3):204-213.

Chapter 3

Comparison of Polymorphic Forms Produced from

Different Crystallization Techniques in Enantiomeric Systems:

Solution Crystallization and Lyophilization of Proline

3.1   Introduction

3.1.1   Chirality and crystal form

The purpose of this work was to evaluate the differences in crystal forms of proline that result from changes in enantiomeric ratio and crystallization conditions.

Most chiral drugs are marketed as single enantiomers because each enantiomeric form can possess significantly different pharmacological and toxicological activities.[1,2] Despite improvements in stereoselective synthesis and chiral separations in the past decades, crystallization mechanisms remain a common method for achieving the desired enantiopurity from a mixture of enantiomers.[3] This means that both enantiomers (the desired enantiomer as well as the undesired, enantiomeric impurity) are present during the crystallization process.

The enantiomeric impurity can crystallize in the presence of its antipode to form a) its own enantiopure crystal lattice, b) a racemic crystal (denoted as a cocrystal) by pairing with the antipode to form the crystal lattice, and/or c) a solid solution where the impurity exists as a guest (chiral defect) within the homochiral lattice of the antipode (Figure 3.1).[4]

The crystallization process can greatly affect the number and ratio of the resulting crystal forms.   For enantiomeric systems, the process may determine whether the resulting product is a pure form or a solid solution. Of particular interest in these studies was determining the effect of the overall enantiomeric ratio on the crystallization of enantiopure, cocrystal, and solid-solution forms.

77
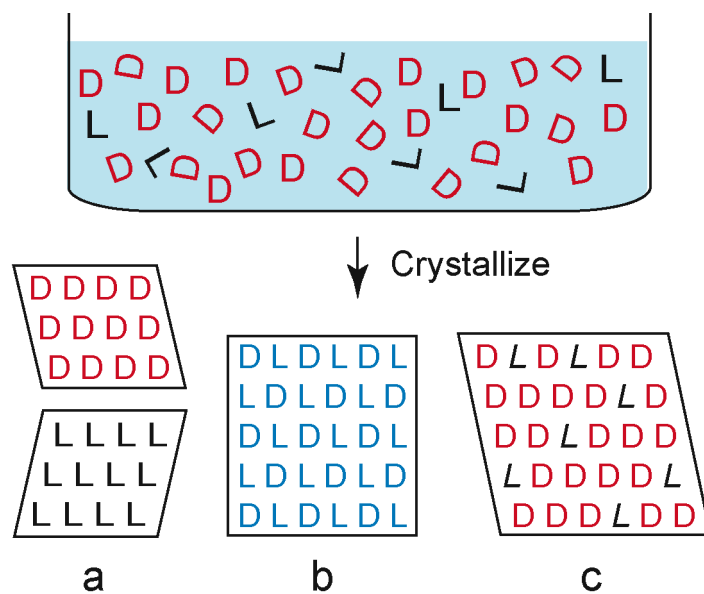
Figure 3.1. a) racemic conglomerate, consisting of physically mixed enantiopure crystals; b) racemic compound, which is a cocrystal of the enantiomers; and c) solid solution.

3.1.2   Crystallization of L- and D-proline enantiomers

We were interested in comparing two crystallization methods, specifically crystallization from a solution and crystallization by lyophilization, in order to determine the effect of each on the observed crystalline products. Crystallization from a saturated solution is a well-established method for generating crystals of a particular form. Polymorphic screens are often performed by crystallizing a drug molecule from many different solvents, at different temperatures, and at various pH values.[5] On the other hand, lyophilization is a technique often used to produce amorphous, non-crystalline materials. Despite this, we have observed that lyophilization of some small molecules (e.g., aspirin, unpublished) will produce crystalline material.

These two crystallization methods fundamentally differ in the kinetics associated with crystallization. In solution-based crystallization, the molecules possess a high degree of mobility and can diffuse relatively easily during the growth of a crystal lattice. In lyophilization, however, the drug molecules are frozen in place as the water (ice) is removed by sublimation. Thus, the lyophilization process slows the translational diffusion that occurs readily during crystallization of a drug in solution.

Proline was chosen as a model chiral compound for these studies. It has several benefits as a model compound, including: one chiral center in the molecule; readily purchasable with single or multiple ^{13}C-labeled sites; relatively low molecular weight, corresponding to a reasonable signal-to-noise ratio for a given sample mass; few known crystal forms; and a long ^{1}H T_1 relaxation time, which is helpful for observing relaxation differences between crystal forms. Other model compounds in the literature for studying chiral impurities[6-8] lacked one or more of the requirements listed above.

79

3.2   Experimental

3.2.1   *Bulk materials*

L- and DL-proline were purchased from Alfa Aesar (Ward Hill, MA), D-proline was purchased from Sigma-Aldrich (St. Louis, MO), and L-proline containing an isotopic label on the carbonyl carbon (denoted L-[1-^{13}C]proline) was purchased from Cambridge Isotope Laboratories, Inc. (Andover, MA).   All amino acids were used as received without further purification.

3.2.2   *Sample preparation*

L-proline monohydrate (MH) was formed by incubating bulk L-proline at 30ºC, 60% RH, for 16 hr.

DL-proline monohydrate (DL-MH) was prepared by exposure of lightly ground DL-proline to RH >35% at ambient temperature. TGA and DSC analysis were used to confirm the formation of both L-MH and DL-MH.

Crystallization from aqueous solution. Solutions of proline enantiomers were prepared by dissolving w/w mixtures of L- and D-proline in double-distilled water. Each solution was transferred to a 400-mL beaker, covered with a KimWipe, and heated at 75ºC in a dry bath until the water had evaporated. The solid material was periodically agitated with a spatula in order to facilitate complete drying and dehydration.

Crystallization by lyophilization. Solutions of various L-proline to D-proline ratios were prepared as above, at final concentrations of 0.6% w/v. In order to perform spectral subtractions at lower concentrations of L-proline (2–15% L-proline, vide infra), each L-/D-proline ratio was prepared twice: One solution contained natural-abundance L-

proline, and the other contained L-[1-^{13}C]proline. The solutions were then lyophilized in 10-mL aliquots (within 20-mL scintillation vials) using a bench top freeze dryer (VirTis AdVantage; VirTis; Gardiner, NY). The lyophilization cycle was 32 hr (-35, -5, 5, 15, and 25°C; for 2, 8, 6, 6, and 10 hr respectively) with an initial 2-hr freezing step (-35°C) and a vacuum set point of 90 mTorr. Upon completion of the lyophilization recipe, the vacuum was released by purging the sample chamber with ambient air. Due to their hygroscopic nature, all samples were stored in a desiccator over anhydrous calcium sulfate until analysis was performed.

3.2.3 *Solid-state NMR spectroscopy*

All ^{13}C spectra were acquired on a Chemagnetics CMX-300 spectrometer (Varian, Inc.), operating at 75 MHz for ^{13}C. All acquisitions included cross polarization (CP),[6,7] magic-angle spinning (MAS)[8] at a rate of 4 kHz (±3 Hz), two-pulse phase modulation (TPPM) or SPINAL64 decoupling[9] at a field strength of ~72 kHz, and total sideband suppression (TOSS).[10] A contact time of 2 ms was used for all samples. ^{1}H T_1 relaxation measurements were performed using a saturation–recovery pulse sequence, and T_1 values were calculated using KaleidaGraph (version 4.01, Synergy) with the equation y = amp(1-exp(-τ/T_1), where y is the integrated signal intensity, amp is the amplitude constant, τ is saturation–recovery time, and T_1 is the spin–lattice relaxation time. 3-methylglutaric acid (MGA) was used to optimize the spectrometer settings as well as to set the reference frequency.[11] All samples were packed into zirconia rotors with Teflon® or ribbed Kel-F® end caps. Experiments were performed at ambient

temperature (~20ºC) using a 7-mm double-resonance MAS probe (Revolution NMR, Inc.; Fort Collins, CO) with a 3.5-μs ^{1}H pulse duration.

3.2.4   Powder X-ray diffraction

Diffraction patterns were acquired with either a Scintag X2 Diffraction System (XGEN-4000; Scintag, Inc.; CuKα radiation, 45 kV × 35 mA) or a Scintag XDS 2000 (Scintag, Inc.; CuKα radiation, 45 kV × 40 mA) with an angular range of 8–35º 2θ, a step size of 0.02º, and a dwell time of 4 sec.   Each sample (~300 mg) was packed into a stainless-steel die.   Analyses were performed at ambient conditions.   Powder patterns were simulated from Cambridge Structural Database CIF files using Mercury (version 2.3, Build RC4; CCDC; Cambridge, UK).

3.2.5   Differential scanning calorimetry

Differential scanning calorimetry (Q100 DSC; TA Instruments; New Castle, DE) was performed on samples of 3–8 mg that were packed into standard aluminum pans under ambient conditions and lightly crimped.   Data was collected from room temperature to ~240ºC, with a temperature ramp of 10ºC/min and a 50-mL/min dry nitrogen purge.

3.2.6   Thermogravimetric analysis

Sample water content and degradation were determined by thermogravimetric analysis (Q50 TGA, TA Instruments; New Castle, DE).   Samples of 10–20 mg were

heated from room temperature to >300ºC at a rate of 10ºC/min under a 40-mL/min dry nitrogen purge.

3.2.7   Dynamic water vapor sorption and desorption

Approximately 15–30 mg of sample was placed in a round-bottom quartz sample holder of an automated symmetric vapor sorption analyzer (VT1-SGA-100; TA Instruments; New Castle, DE).   The RH (25ºC) was increased from 10% to 60%, then decreased back to 10%, in increments of 5%.   The equilibrium criteria for each step was <0.0100 wt % change in 5.0 min, with a maximum hold time of 2400 min.

3.3   Results

Our strategy for comparing traditional solution crystallization to lyophilization was to prepare mixtures of proline enantiomers using the two different methods and characterize the products using DSC, PXRD, and SSNMR.   One of the most common methods to characterize enantiomeric systems is to prepare a phase diagram.

3.3.1   Characterization of the phase diagram of proline enantiomers

The binary melting-point phase diagram for proline enantiomers was constructed and is shown in Figure 3.2a.   The samples used to create this phase diagram were crystallized from aqueous solution.   The shape of the plot shows that proline forms a racemic compound as opposed to a racemic conglomerate.[4,12]   This is consistent with published X-ray diffraction results and demonstrates the existence of a proline racemic cocrystal.[13-15]   The eutectic melting temperature is ~207ºC (dotted line in Figure 3.2a),
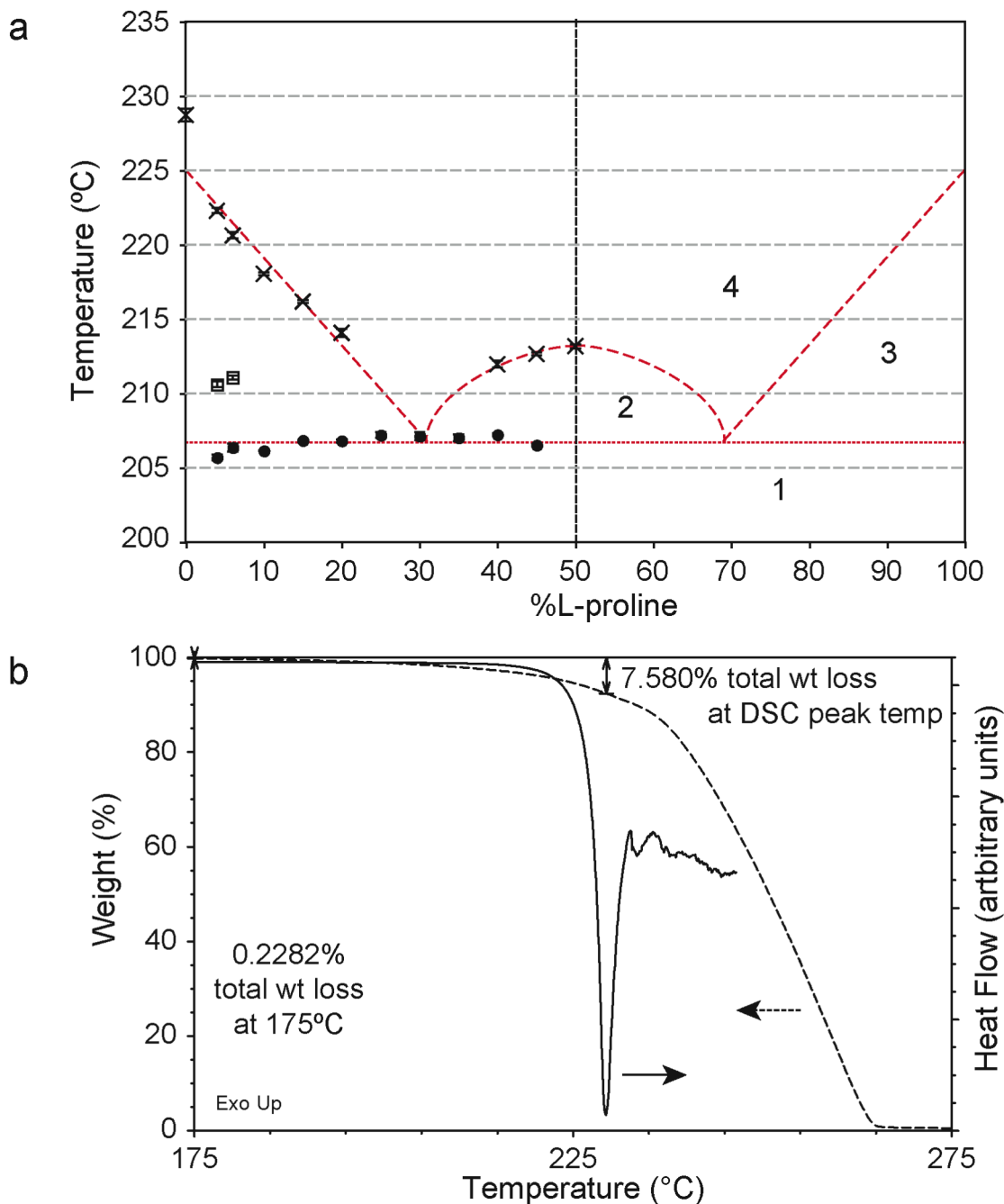
Figure 3.2. Thermal analysis of proline. a) Binary melting-point phase diagram of proline enantiomers. Melting onset (eutectic melting) and end-of-fusion peak (liquidus) temperatures are represented by circles and crosses, respectively. (n=3: averages and standard deviations plotted.) Dotted and dashed lines indicate trends in liquidus and solidus melting temperatures. Theoretical compositions of each region: 1) $DL_{sol} + L_{sol}$, 2) $DL_{sol} + D_{liq} + L_{liq}$, 3) $L_{sol} + D_{liq} + L_{liq}$, and 4) $D_{liq} + L_{liq}$.
b) Overlay of DSC and TGA thermograms for bulk L-proline. Percent total weight loss at 175ºC and the melting peak are included.

and the eutectic composition is estimated to be ~30:70. This is a typical ratio for a phase diagram, which can theoretically possess a eutectic anywhere between 0:100 and 50:50, where a eutectic at 50:50 evidences the formation of a racemic conglomerate versus a racemic cocrystal

Typically, the eutectic composition can be obtained by calculating the intersection of theoretical liquidus and solidus lines using the Schröder-Van Laar and Prigogine-Defay equations.[4] However, these calculations require accurate heat-of-fusion measurements, which were not measurable by DSC due to the sublimation/degradation of proline at high temperatures (Figure 3.2b). The estimated eutectic composition of 30:70 is consistent with results from Blackmond et al., who defined a eutectic composition of ~25:75 in the tertiary phase diagram of L- and D-proline in DMSO.[16]

During the construction of the binary phase diagram for proline, melting peaks were observed between the eutectic and liquidus melting temperatures for 4 and 6% L-proline levels. When multiple crystal forms are present, multiple eutectic melts can be observed.[4] These peaks (~211°C) may correspond to a polymorph or solvate of proline.

3.3.2   Proline crystal forms

The Cambridge Structural Database (CSD) contains single-crystal structures corresponding to four crystalline forms of proline. These consist of two enantiopure crystal forms (anhydrous L-proline[17] and L-proline monohydrate[18]) and two racemic cocrystal forms (anhydrous DL-proline[13] and DL-proline monohydrate[14,15]).

Figure 3.3 shows PXRD patterns of proline crystal forms prepared as reference materials. The identity of each form was confirmed by comparing the experimental
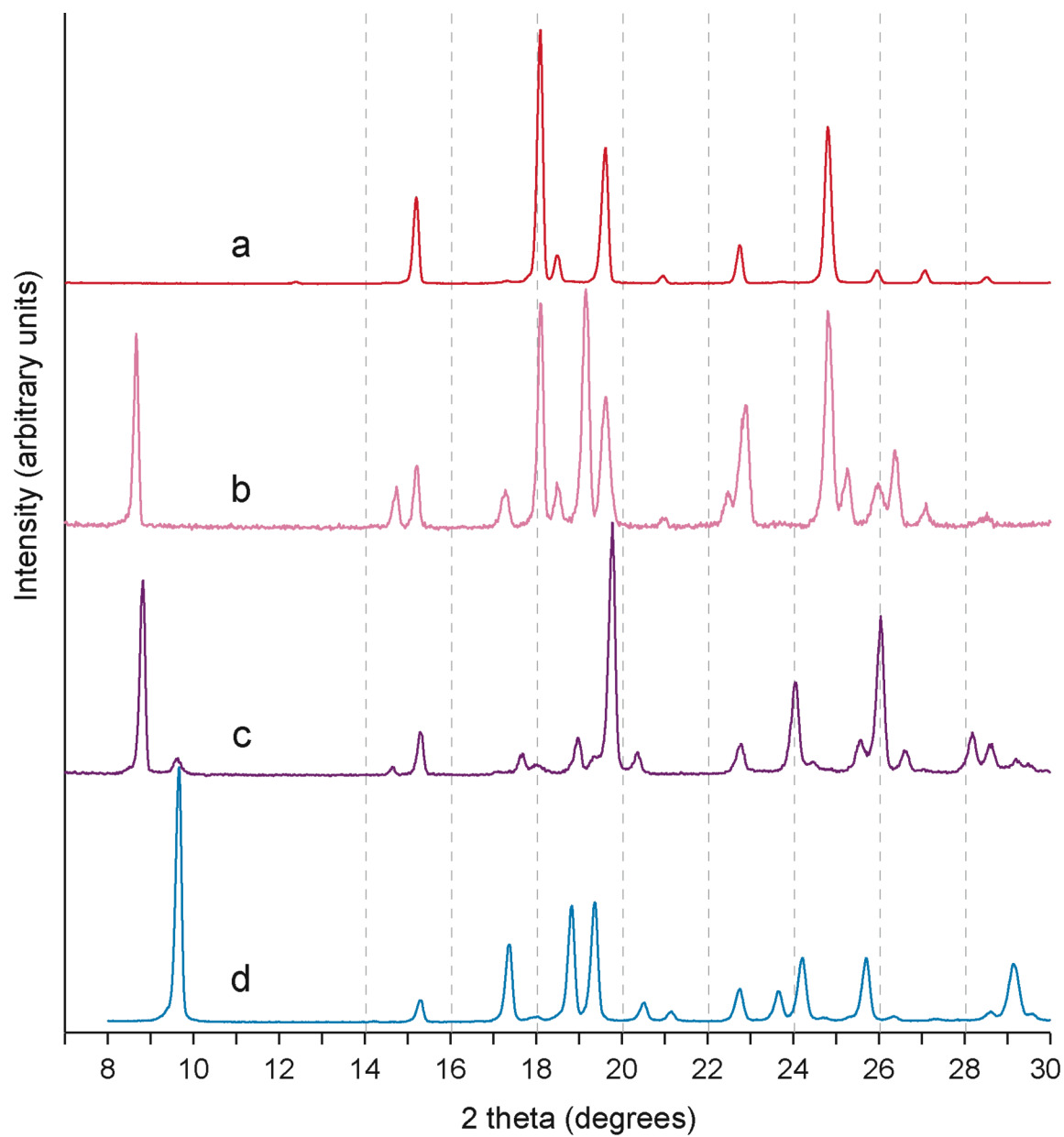
Figure 3.3. PXRD patterns of proline crystal forms: a) L, b) L-MH, c) DL-MH, and d) DL.

powder patterns from Figure 3.3 to simulated patterns from the CSD single-crystal structures. Simulated patterns for L-proline (L), L-proline monohydrate (L-MH), DL-proline monohydrate (DL-MH), and DL-proline (DL) matched the patterns shown in Figures 3.3a–d, respectively.

These reference materials were also analyzed by ^{13}C SSNMR in order to identify the carbon peak positions associated with each crystal form. Figure 3.4 shows ^{13}C CP-MAS NMR spectra of these proline crystal forms. The spectrum of enantiopure L-proline (same spectrum as D-proline) is shown in Figure 3.4a with peak assignments. There is a single peak for each carbon in the molecule, indicating the presence of one molecule per asymmetric unit. The peaks at ~62 and 46 ppm correspond to carbons 2 and 5 in the proline molecule. These peaks show splitting and are broader than the other peaks in the spectrum due to heteronuclear dipolar coupling with the neighboring quadrupolar nitrogen.

The other crystalline proline forms represented in Figure 3.4 include L-MH (Figure 3.4b, same spectrum as D-MH) and the two racemic cocrystal forms, DL-MH (Figure 3.4c) and anhydrous DL (Figure 3.4d). The ^{13}C CP-MAS NMR chemical shifts and the abbreviated name for each crystal form are shown in Table 3.1. Differences in chemical shifts are clearly observed among different proline crystalline forms, allowing for SSNMR identification of each form when present in a mixture. With reference SSNMR spectra and PXRD patterns in hand, it was possible to analyze mixtures of various enantiomeric ratios of proline that were crystallized together from aqueous solution.
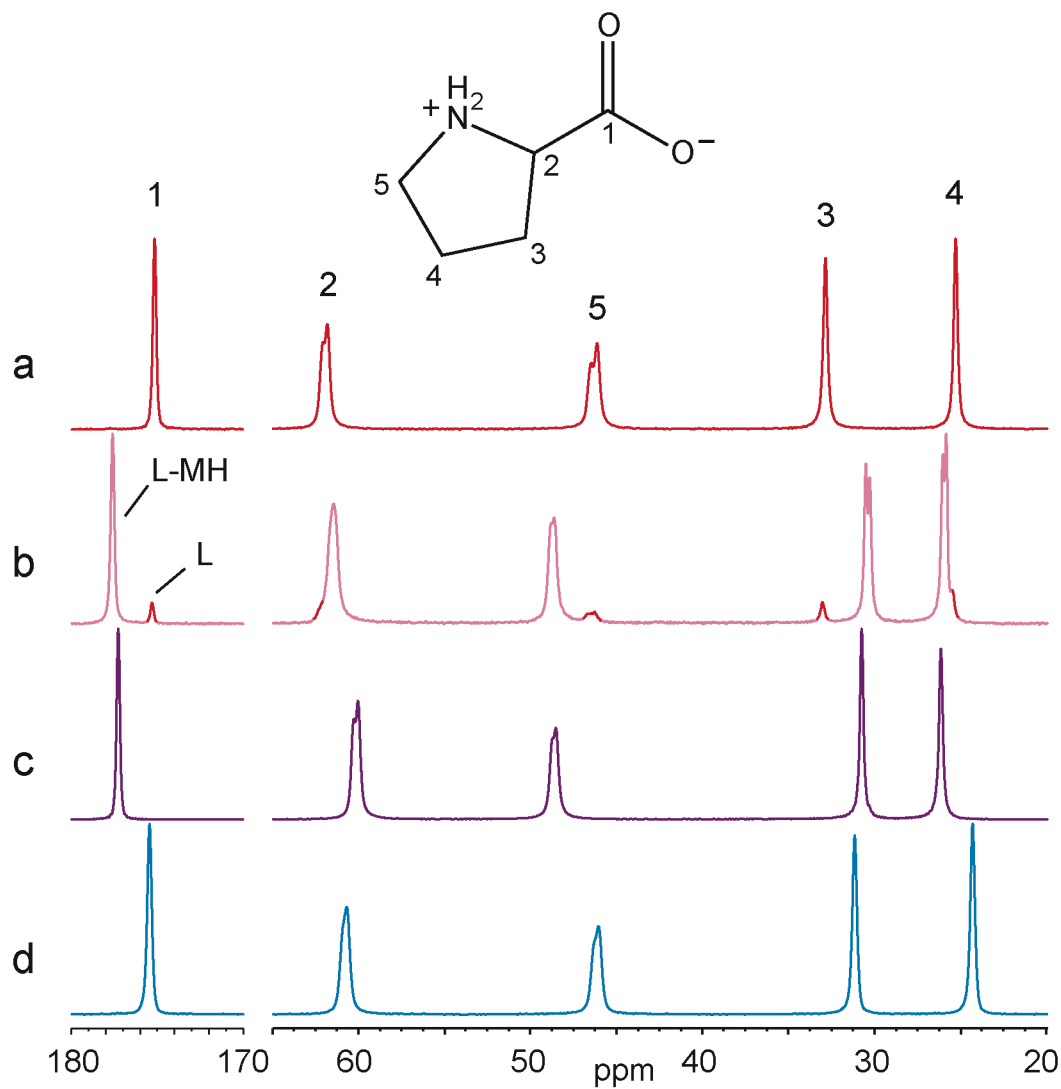
Figure 3.4. ^{13}C CP-MAS NMR spectra (top to bottom) of proline crystal forms corresponding to enantiopure a) L and b) L-MH; and racemic cocrystals c) DL-MH, and d) DL.

Table 3.1. ^{13}C CP-MAS NMR chemical shifts (ppm) for proline crystal forms

Crystal form	Abbrev.	Carbonyl peak	Aliphatic peaks			
		C1	C2	C5	C3	C4
Enantiopure[a]	L/D	175.3[b]	61.9	46.5	33.0	25.4
Enantiopure monohydrate	L-MH	177.6	61.5	48.6	30.5, 30.3	26.1, 25.9
Racemic cocrystal monohydrate	DL-MH	177.2	60.1	48.5	30.8	26.2
Racemic cocrystal	DL	175.3[b]	60.6	45.9	31.0	24.2

[a]Enantiopure D- and L-proline have the same ^{13}C SSNMR peak positions. [b]Enantiopure and DL spectra overlap at the carbonyl peak, but peak differences are observed for the aliphatic peaks.

3.3.3 *Crystallization of various enantiomeric ratios from aqueous solution*

Figure 3.5a shows the ^{13}C CP-MAS NMR spectra corresponding to samples of 25–50% L-proline. These samples were crystallized from aqueous solution, which was the same preparation method used to create samples for the binary phase diagram in Figure 3.2a. Concentrations of 25–50% L-proline were chosen in order to facilitate observation of peaks for different crystalline forms in SSNMR spectra and PXRD patterns. Peak identification was more difficult at much lower concentrations. The 25% L-proline sample showed the presence of D and DL crystal environments, indicated by the presence of peaks at 33.0 and 25.4 ppm (D-proline) and at 31.0 and 24.2 ppm (DL). There is only one peak in the carbonyl region due to overlapping peaks for these two forms in this region of the spectrum. As the amount of L-proline in the crystallization medium was increased to 50%, DL peak area increased at the expense of D, until only DL was observed. The peak areas for C-3 were used to calculate the relative amount of each crystal form, which was then plotted as a function of total L-proline concentration in Figure 3.5b.

$$\text{Relative amount of each crystal form} \; = \; \frac{\text{Individual peak area}_{\text{C-3}}}{\text{Total peak area}_{\text{C-3}}} \times 100\%$$

Table 3.2 contains the ^{1}H T_1 values corresponding to these samples. There are no apparent trends in the relaxation data, but the average values for both D and DL crystal forms are relatively high (~60 s), which is indicative of low molecular mobility in the crystal lattices.

Figure 3.6 contains PXRD patterns of 25–50% L-proline that complement the SSNMR spectra shown in Figure 3.5a. These diffraction patterns followed the same
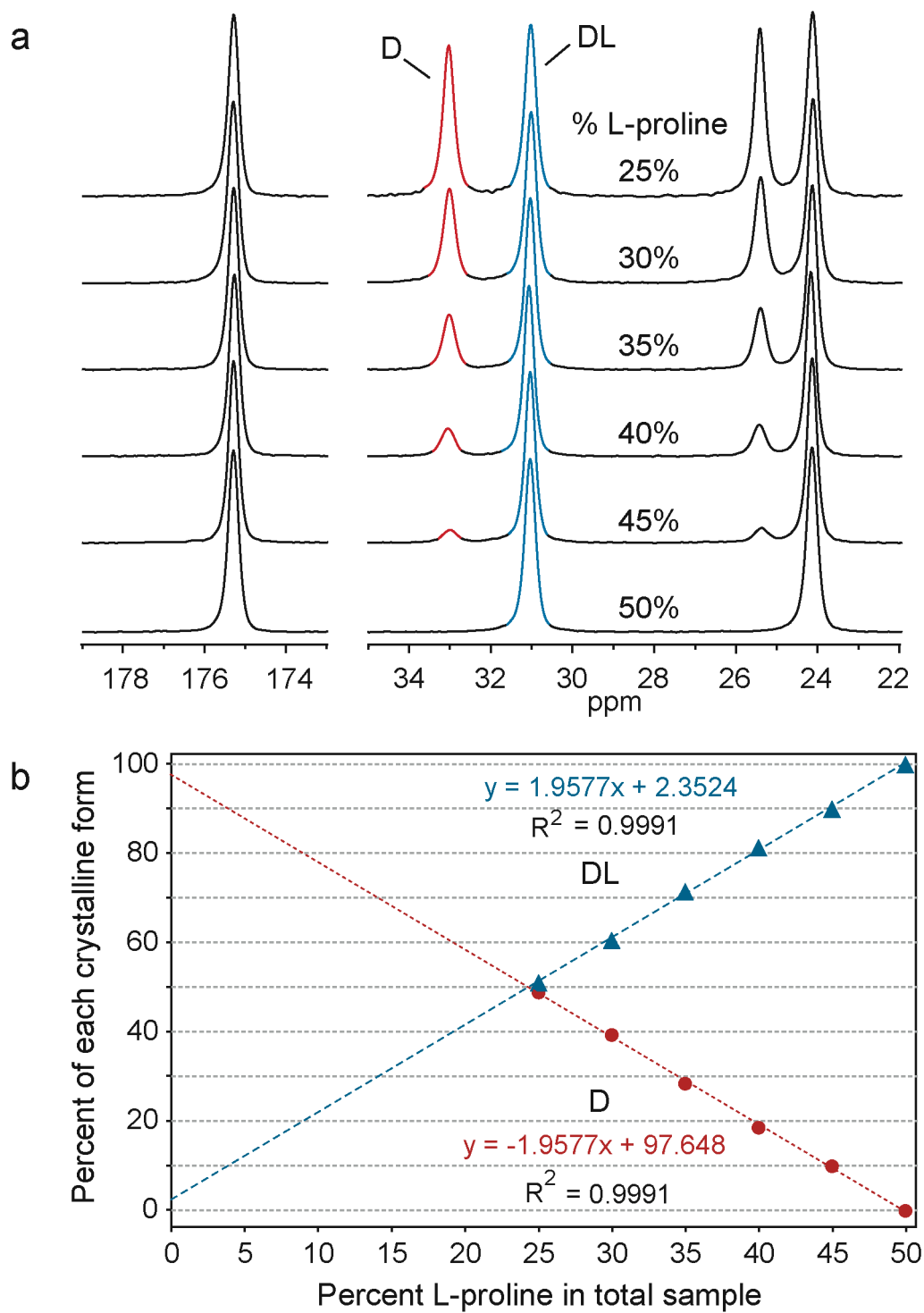
Figure 3.5. a) ^{13}C CP-MAS NMR spectra of 25–50% L-proline samples crystallized from aqueous solutions. C-1, C-3, and C-4 peaks are shown. b) Plot of C-3 relative peak areas as a function of total % L-proline in each sample.

Table 3.2. ^{1}H T_1 relaxation values (s) for proline samples[a]

Preparation method	Percent L-proline	DL-MH	DL[b]	D[b]
Solution	25	--	44.9 (0.3)	64.0 (0.4)
	30	--	66.6 (0.6)	70.2 (0.3)
	35	--	64.5 (0.2)	62.7 (0.3)
	40	--	71.6 (0.7)	63 (1)
	45	--	62.5 (0.6)	47 (2)
	50	--	56.6 (0.9)	--
	Average (st. dev.)	--	61 (9)	61 (9)

[a]Values were calculated by integrating or deconvoluting (when not resolved) peak areas of carbonyl and aliphatic peaks and averaging the resulting relaxation times. Values in parentheses indicate standard deviation. [b]Enantiopure and DL spectra completely overlap at the carbonyl peak, thus the T_1 value of this peak was not included in the averages.
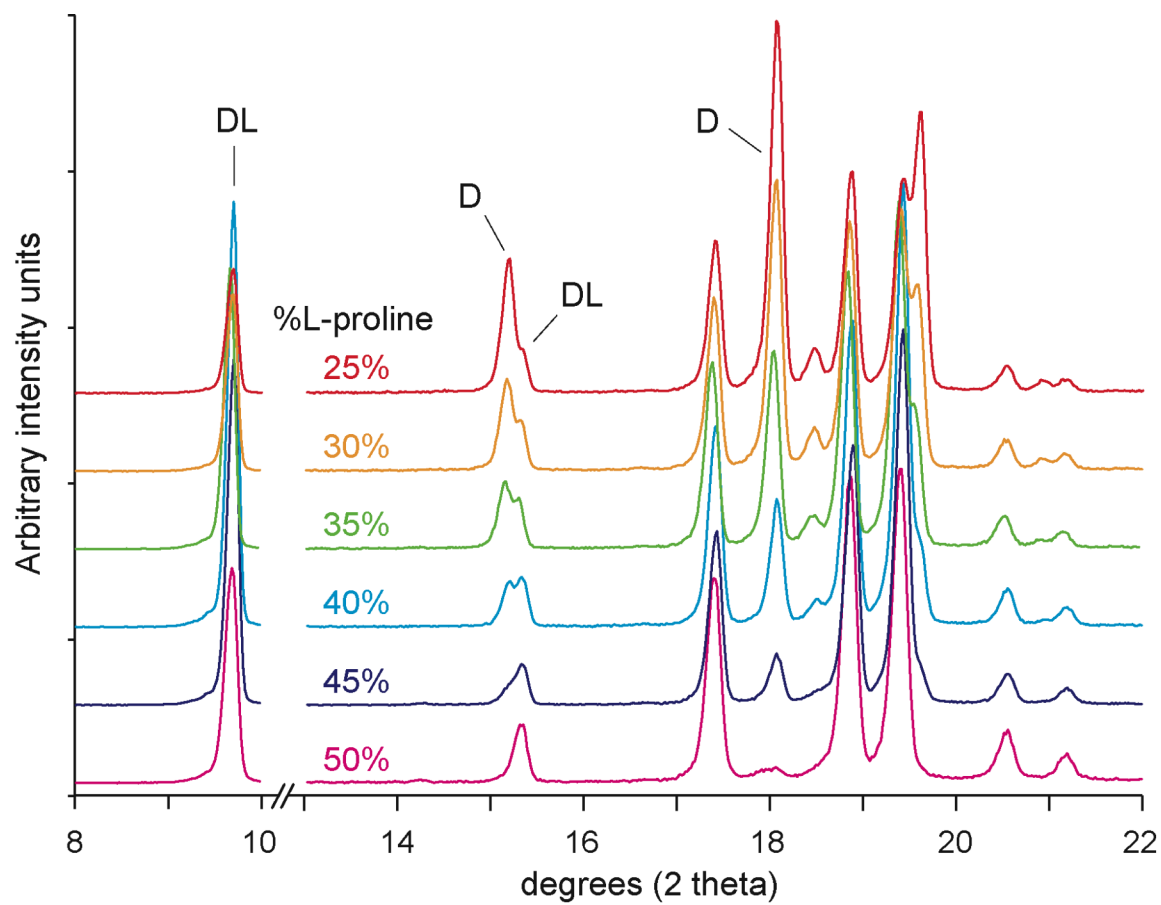
Figure 3.6. PXRD patterns of 25–50% L-proline samples crystallized from aqueous solutions.

trend as observed by SSNMR analysis, in which only forms D and DL were present, and DL was the only crystal form present at the 50% L-proline level. All of the diffraction peaks are fairly sharp, which demonstrates highly ordered crystalline material. This highly ordered nature contributes to the interpretation of the long relaxation times, as material with a high degree of crystallinity often possesses slow relaxation due to decreased molecular mobility.[19]

The SSNMR and PXRD data support the conclusion that proline is a racemic cocrystal at room temperature, not a racemic conglomerate or solid solution. It also indicates that the amount of excess enantiomer (L-proline, in this case) in a proline sample prepared by this crystallization method can be directly measured in the solid state by quantitating the relative amounts of DL and enantiopure material.[20]

3.3.4   Samples prepared by lyophilization

Figure 3.7 shows ^{13}C CP-MAS NMR spectra for samples of 25–50% L-proline prepared by lyophilization. Unlike in the solution-crystallized samples, where only DL and D crystal forms were observed, these spectra show that there were at least 4 different crystal environments present in the lyophilized samples, including D, DL, DL-MH, and an unreported form with peaks at 32.0 and 26.7 ppm in the spectrum.

This new form was determined to be a racemic cocrystal based on the relative peak areas in the ^{13}C CP-MAS spectrum. For instance, theoretically, upon crystallizing a sample containing 25% L-proline, the L molecules (25% of the total) will pair in a 1:1 ratio with D molecules (25%) to form DL. The resulting DL form(s) will compose 50% (25% L + 25% D) of the total sample. The remaining 50% of the sample will consist of

94
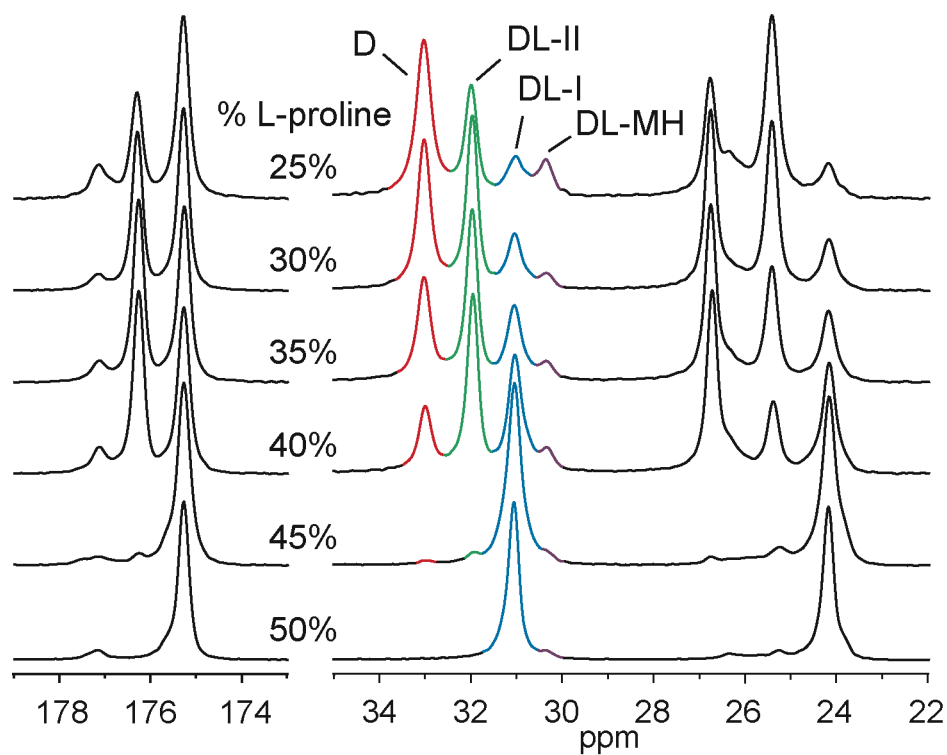
Figure 3.7. ^{13}C CP-MAS NMR spectra of 25–50% L-proline samples prepared by lyophilization. C-1, C-3, and C-4 peaks are shown.

the excess D-proline form(s). This is exactly what is observed in Figure 3.5a and b: At the 25% L-proline level, 50% of the peak intensity for C-3 corresponded to D and the other 50% corresponds to DL. If new forms of D or DL existed, changes in the relative areas of each of these peaks would decrease by an amount corresponding to the peak area of the new form(s). In Figure 3.7, at the 25% L-proline level, the relative C-3 peak area for D was ~50%. Thus, there was no polymorphism associated with D, and the other three peaks corresponded to DL (racemic cocrystal) forms.

Additionally, dynamic water vapor sorption analysis (DVS) indicated that this new racemic cocrystal form was anhydrous (Figure 3.8). It did not lose weight at 0% RH (25ºC), which would demonstrate loss of waters of hydration. However, increasing the RH resulted in a weight % gain that corresponded to the formation of a monohydrate (Figure 3.8). The behavior of this monohydrate formation is very similar to that of the previously reported racemic cocrystal form. The DVS sorption/desorption profiles for crystal forms of the new DL polymorph, as well as previously reported D and DL forms, are overlayed in Figure 3.8.

This new anhydrous racemic cocrystal will now be referred to as DL-proline form II (DL-II). The previously published form, previously abbreviated DL, is now denoted as DL-proline form I (DL-I). SSNMR spectra and PXRD pattern overlays that include the new polymorph DL-II are shown in Figures 3.9 and 3.10. The ^{13}C chemical shifts of DL-II are provided in Table 3.3.

In Figure 3.7, at the 25% L-proline level, the major components were D and DL-II, with small amounts of DL-I and DL-MH. Increasing amounts of L-proline in the crystallization medium led to decreases in D-proline as more DL-I and DL-II were
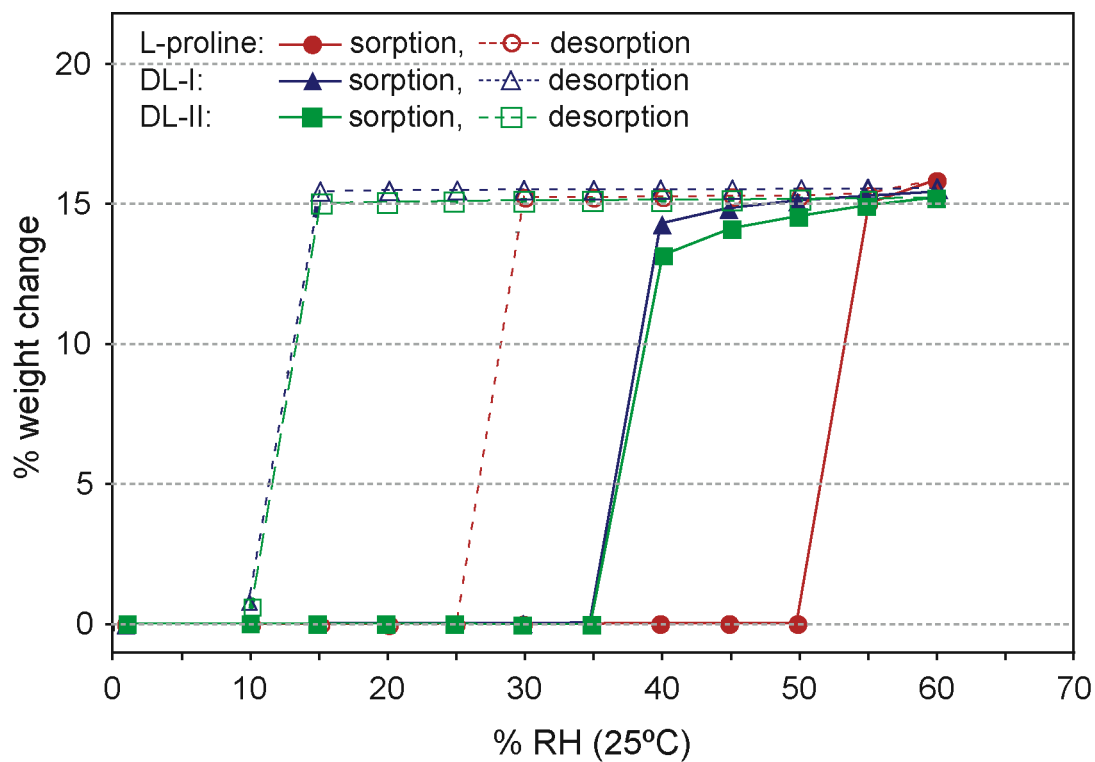
Figure 3.8. Dynamic water vapor sorption analysis of proline crystal forms L, DL-I, and DL-II. Solid icons and lines indicate sorption profiles, and dashed lines and open icons indicate the desorption profiles.
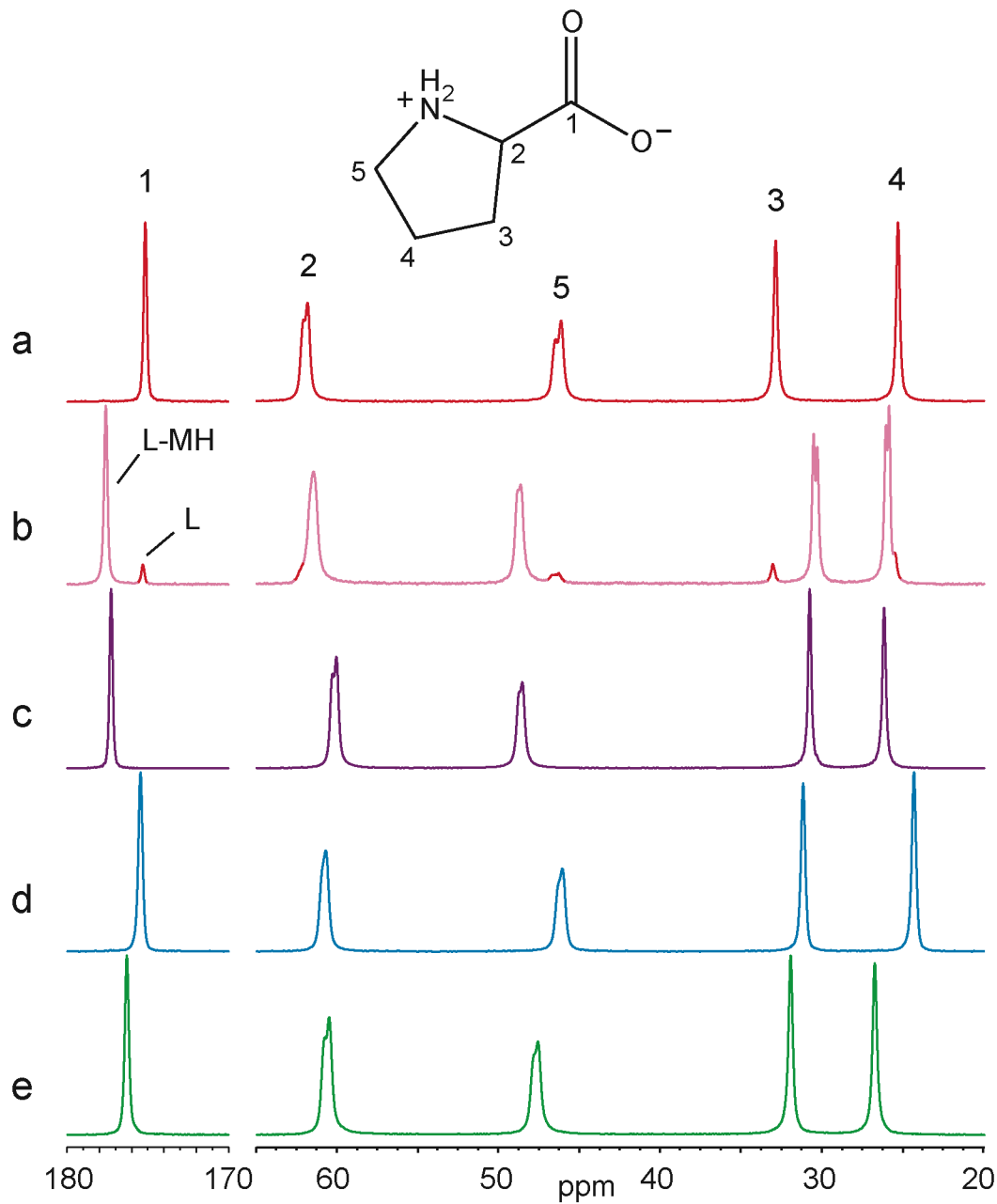
Figure 3.9. ^{13}C CP-MAS NMR spectra (top to bottom) of proline crystal forms corresponding to enantiopure a) L and b) L-MH; and racemic cocrystals c) DL-MH, d) DL-I, and e) DL-II.
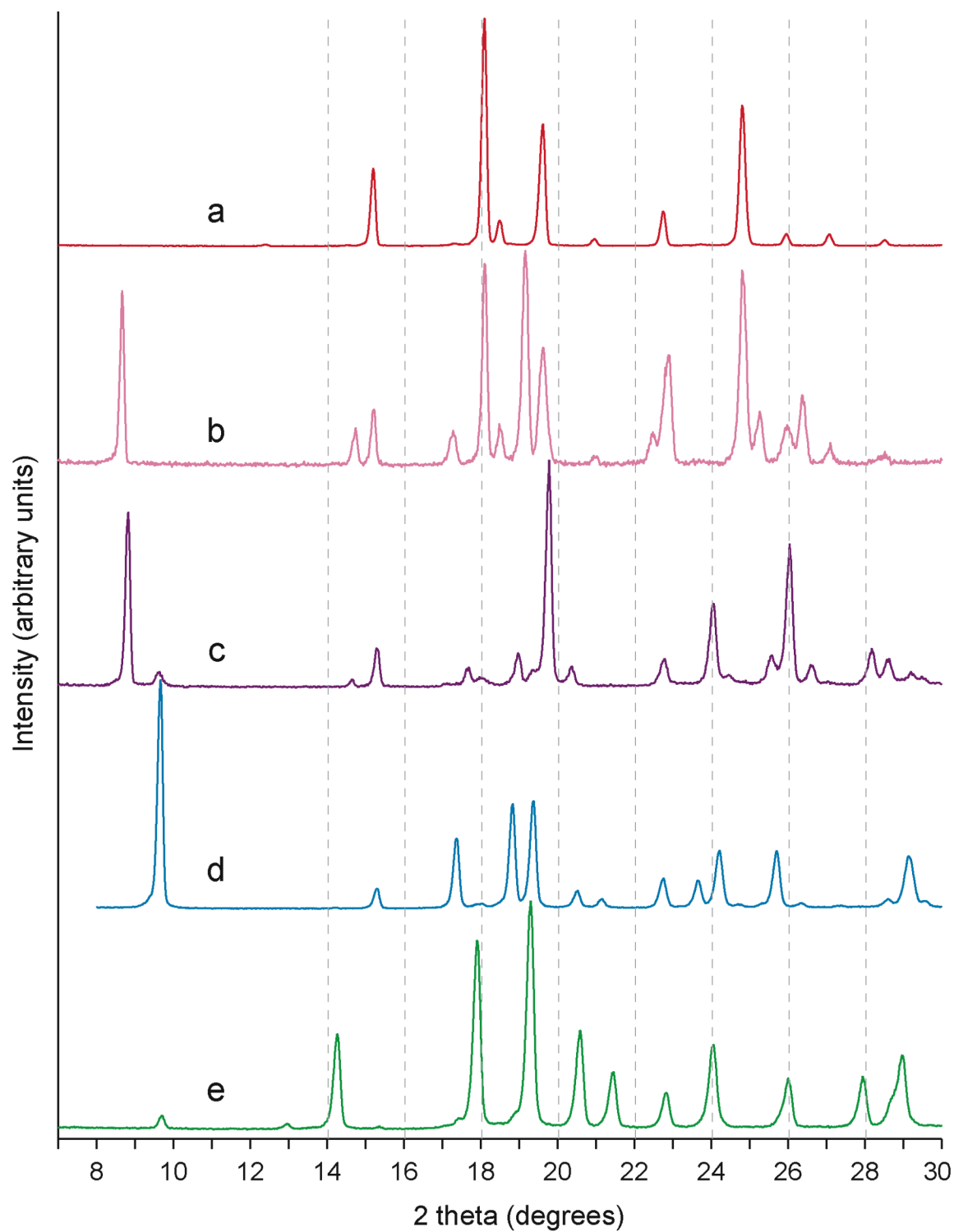
Figure 3.10. PXRD patterns of proline crystal forms: a) L, b) L-MH, c) DL-MH, d) DL-I, and e) DL-II.

Table 3.3. ^{13}C CP-MAS NMR chemical shifts (ppm) for proline crystal forms

Crystal form	Abbrev.	Carbonyl peak	Aliphatic peaks			
		C1	C2	C5	C3	C4
Enantiopure[a]	L/D	175.3[b]	61.9	46.5	33.0	25.4
Enantiopure monohydrate	L-MH	177.6	61.5	48.6	30.5, 30.3	26.1, 25.9
Racemic cocrystal monohydrate	DL-MH	177.2	60.1	48.5	30.8	26.2
Racemic cocrystal form I	DL-I	175.3[b]	60.6	45.9	31.0	24.2
Racemic cocrystal form II	DL-II	176.3	60.6	47.6	31.9	26.7

[a]Enantiopure D- and L-proline have the same ^{13}C SSNMR peak positions.
[b]Enantiopure and DL-I spectra overlap at the carbonyl peak, but peak differences are observed for the aliphatic peaks.

produced. Between 40 and 45% L-proline, the level of DL-I surpassed that of DL-II. At the 50% L-proline level, the sample consisted almost solely of DL-I.

Figure 3.11 shows the PXRD diffraction patterns for samples of lyophilized 25– 50% L-proline. Peaks corresponding to crystalline DL-MH (~8.7º 2θ), DL-I (~9.5º 2θ), DL-II (~14.2º 2θ), and D (~18.0º 2θ) were observed. Additionally, there was a peak at ~15.4º 2θ that could not be attributed to a specific form, but may correspond to a metastable form, as it was not observed in subsequent analyses. It is not surprising that there may be additional peaks in the PXRD patterns. Several other crystalline forms were observed in the SSNMR spectra of proline samples that were prepared under dry conditions (nitrogen gas). This topic is discussed in further detail in Chapter 5.

The PXRD peaks for the lyophilized samples (Figure 3.11) were broader and less resolved than the peaks for samples crystallized from solution (Figure 3.6). However, no amorphous halo is observed.   These observations indicate the absence of amorphous material but the presence of disorder within the crystal lattices of the lyophilized proline samples.   In this case, the use of the word "disorder" is based on the idea that a completely ordered crystal lattice can gradually and continuously decrease in order, becoming a completely disordered amorphous phase in the extreme case.[21-23] If such disorder exists, it should produce a decrease in SSNMR ^{1}H T_1 relaxation values due to increased molecular mobility in the crystal lattice.

Table 3.4 contains ^{1}H T_1 relaxation values corresponding to the spectra shown in Figure 3.7. The average relaxation values for all crystal forms among lyophilized samples are lower than those in the samples crystallized from solution (shown in both Tables 3.2 and 3.4). This suggests that a greater degree of molecular mobility exists
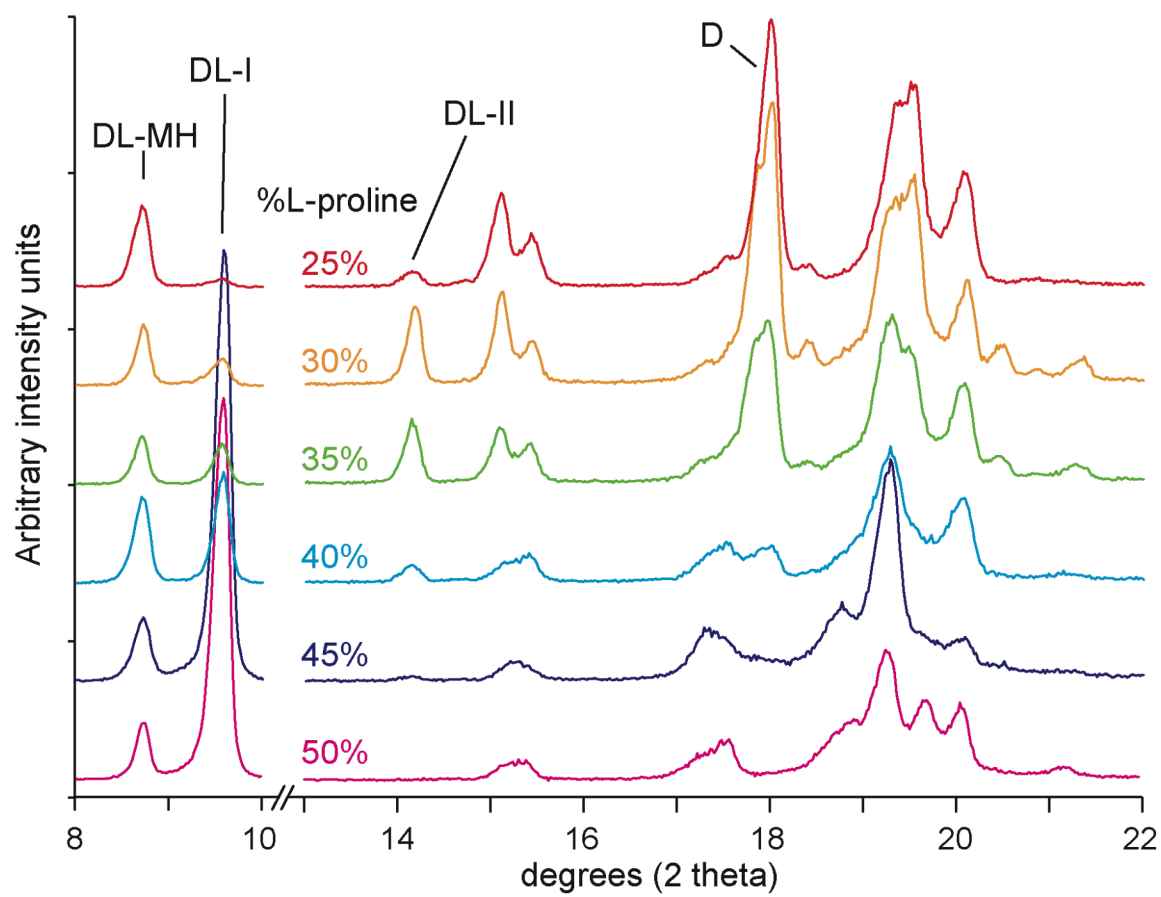
Figure 3.11. PXRD patterns of 25–50% L-proline samples prepared by lyophilization.

Table 3.4. Compiled ^{1}H T_1 relaxation values (s) for proline samples[a]

Preparation method	Percent L-proline	DL–MH	DL–II	DL–I[b]	D[b]
Solution	25	--	--	44.9 (0.3)	64.0 (0.4)
	30	--	--	66.6 (0.6)	70.2 (0.3)
	35	--	--	64.5 (0.2)	62.7 (0.3)
	40	--	--	71.6 (0.7)	63 (1)
	45	--	--	62.5 (0.6)	47 (2)
	50	--	--	56.6 (0.9)	--
	Average (st. dev.)	--	--	61 (9)	61 (9)
Lyophilized	25	17 (2)	27 (2)	25.9 (0.4)	30.8 (0.4)
	30	20 (2)	26.9 (0.3)	29.7 (0.7)	29.7 (0.1)
	35	19 (2)	24.2 (0.4)	29.3 (0.7)	25.1 (0.8)
	40	20 (1)	27.9 (0.4)	33.2 (0.9)	28 (2)
	45	18 (2)	25 (2)	27.3 (0.1)	26 (0.6)
	50	19 (2)	--	37.1 (0.2)	--
	Average (st. dev.)	19 (1)	26 (2)	30 (4)	28 (2)

[a]Values were calculated by integrating or deconvoluting (when not resolved) peak areas of carbonyl and aliphatic peaks and averaging the resulting relaxation times. Values in parentheses indicate standard deviation.
[b]Enantiopure and DL-I spectra completely overlap at the carbonyl peak, thus the T_1 value of this peak was not included in the averages.

in the crystal lattices of lyophilized samples than in solution-crystallized samples and is consistent with the differences in PXRD diffraction peaks for samples prepared by these two methods.

SSNMR and PXRD analyses both detected D, DL-I, DL-II, and DL-MH crystalline phases in the lyophilized samples, and the PXRD patterns and ^{1}H T_1 relaxation values indicated disorder within the crystal lattices. This is in contrast to samples prepared from solution, which only contained D and DL-I crystalline phases. Due to the observation of the new polymorphic form, DL-II, it was of interest to extend the range of enantiomeric ratios crystallized by lyophilization. In order to measure relative ratios of the various crystal forms at lower L-proline concentrations, it was necessary to use isotopic ^{13}C labeling.

3.3.5 *Observing low levels of impurities in lyophilized proline products*

The methodology used to study low levels of L-proline was the same as used by Zell et al. to study the location of chiral defects in polylactide.[24,25] Figure 3.12 illustrates the spectral-subtraction method used in this study. At each concentration of L-proline, two samples were prepared: one containing L-[1-^{13}C]proline (Figure 3.12a) and the other containing natural-abundance (NA) L-proline (Figure 3.12b). The spectrum of the NA sample was subtracted from that of the ^{13}C-labeled sample, and the resulting spectral subtraction (Figure 3.12c) shows only the carbonyl peaks that arise from the ^{13}C-labeled L-proline. By performing spectral subtractions and comparing the remaining carbonyl peaks to known forms (Table 3.3), it was possible to selectively determine the crystal environments in which L-proline molecules were incorporated. The subtraction in Figure
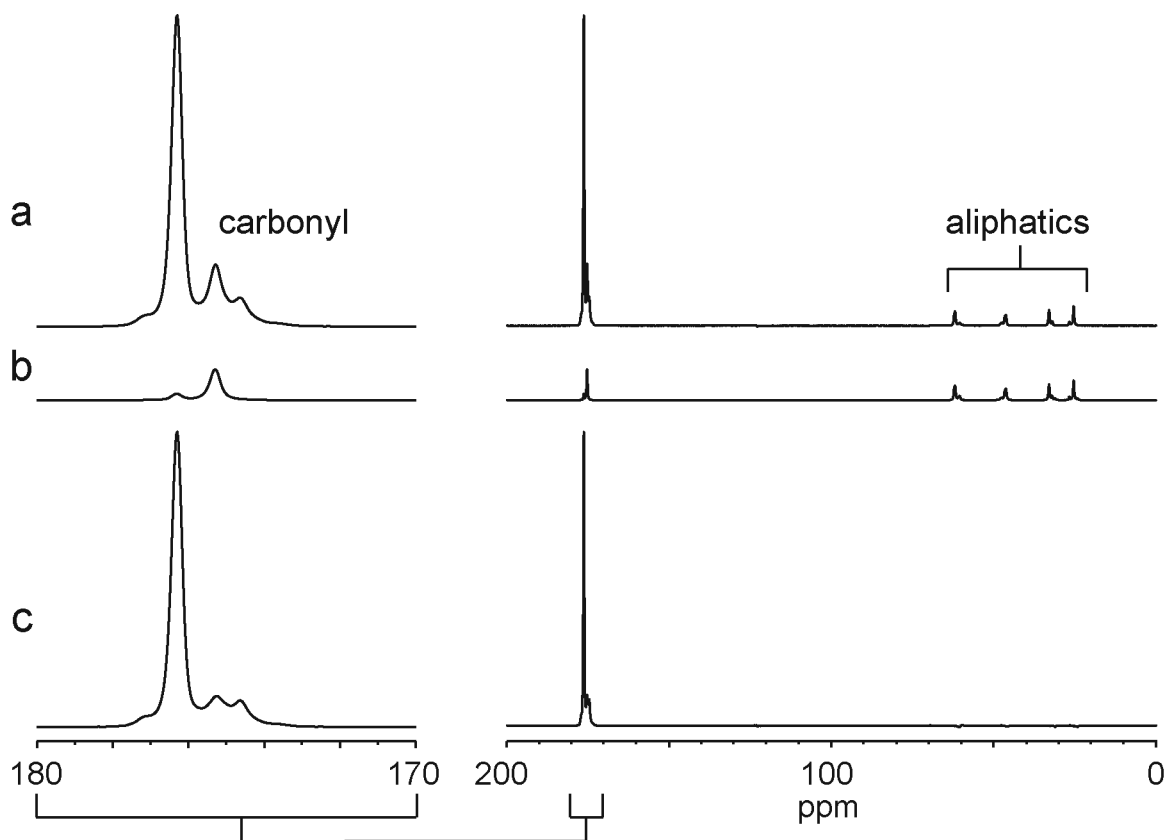
Figure 3.12. Spectral-subtraction method for lyophilized 12% L-proline in D-proline. a) ^{13}C CP-MAS NMR spectrum of 12% L-[1-^{13}C]proline and 88% D-proline; b) ^{13}C CP-MAS NMR spectrum of 12% L-proline and 88% D-proline; and c) difference spectrum that selectively shows peaks of only the ^{13}C-labeled L-proline.

105

3.12 corresponds to lyophilized samples of 12% L-proline with 88% D-proline. In this subtraction, there are four carbonyl peaks. The peaks located at 177.2, 176.3, and 175.3 ppm correspond to the carbonyl carbon of racemic cocrystals DL-MH, DL-II, and DL-I, respectively. A fourth peak at 174.7 ppm that does not correspond to any known form of proline has been assigned to L-proline molecules incorporated as substitutional chiral defects (L-CD) in the D-proline host crystal matrix. Evidence for the assignment of the 174.7-ppm SSNMR peak to L-CD is the basis of Chapter 4.

Figure 3.13 shows a series of ^{13}C CP-MAS NMR spectral subtractions that were performed with lyophilized samples containing 2–15% L-proline. Again, because these are spectral subtractions, the peaks arise from only the carbonyl carbon of the L-proline molecules. All spectra are normalized to the same maximum intensity in this figure. At the 2% L-proline level (Figure 3.13), predominantly DL-MH, some DL-I, and L-CD are observed. Higher levels of L-proline resulted in large increases in DL-II, moderate increases in DL-I and L-CD, and a decrease in DL-MH. At 15% L-proline, DL-II dominates the spectrum, but peaks for DL-MH, DL-I, and L-CD are still visible.

3.3.6   *Quantitating crystal forms in lyophilized samples*

Deconvoluted peak areas were used to calculate the relative amounts of each crystal form. Strict quantitation methods were not used, but all samples were acquired with a pulse delay greater than five times the longest [1]H T_1 to avoid saturation effects.[26] As in the Figure 3.5b plot, the peak areas for C-3 were used to calculate the relative amount of each crystal form in lyophilized 20–50% L-proline samples:
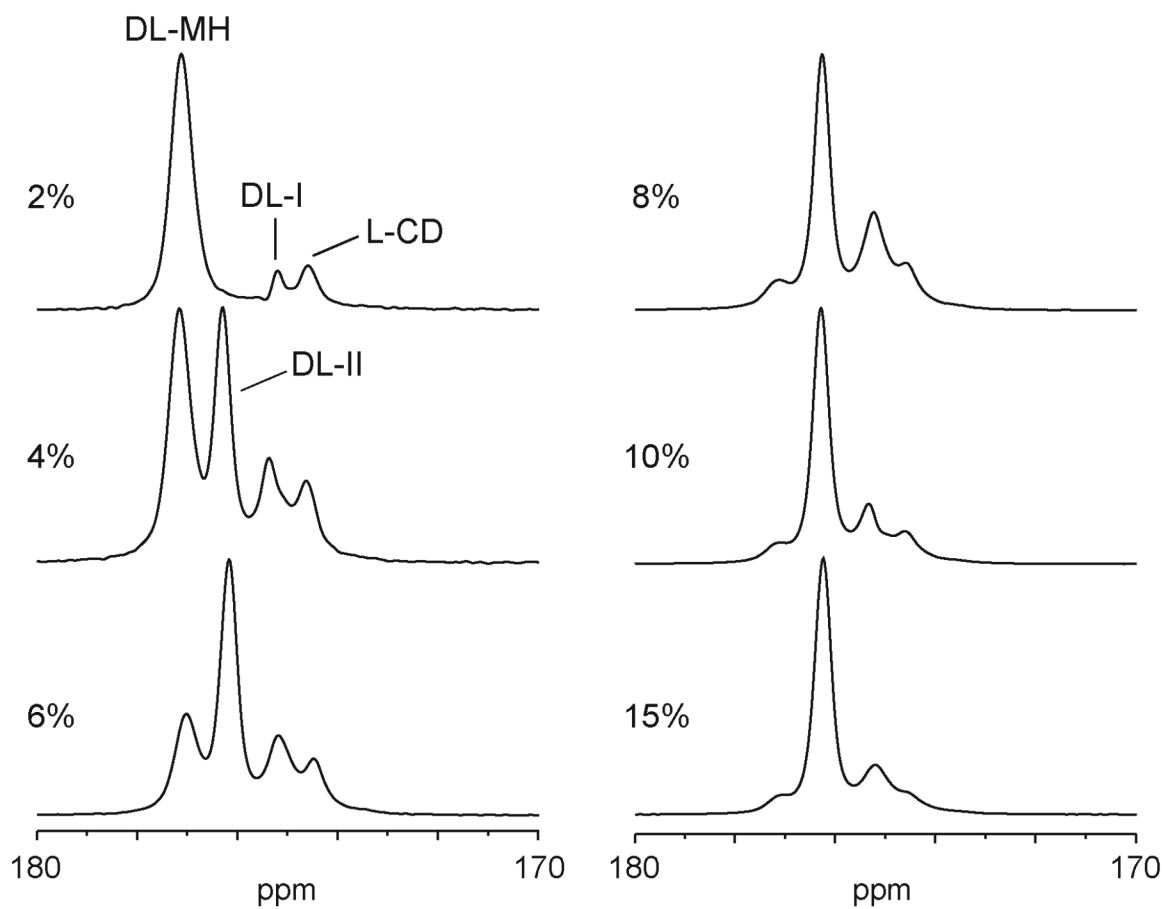
Figure 3.13. ^{13}C CP-MAS NMR spectral subtractions for increasing amounts of L-proline in D-proline prepared by lyophilization.

$$\text{Relative amount of crystal form} \ = \ \frac{\text{Individual peak area}_{C\text{-}3}}{\text{Total peak area}_{C\text{-}3}} \times 100\%$$

Due to the use of isotopic labeling for 2–15% L-proline samples, the method for calculating the amount of each crystal form differed slightly from unlabeled samples. The relative amount of each crystal form in labeled samples was calculated based on carbonyl peak area using the equation:

$$\text{Rel. amt. of crystal form} \ = \ \left(\frac{\text{Individual peak area}_{C\text{-}1}}{\text{Total peak area}_{C\text{-}1}} \times 100\% \right) \times (\text{Total \% L - proline}) \times 2$$

The factor of two is required for calculating the amounts of racemic cocrystal forms because the subtracted spectra correspond only to the ^{13}C-labeled L-proline. Thus, only half of the signal due to the presence of a racemic cocrystal, which is composed of equimolar amounts of both L- and D-proline molecules, is represented in the observed spectrum. The measured signal must be doubled to account for the "missing" D-proline.

The relative amounts of each crystal form, calculated as just described, are plotted in Figure 3.14. Dashed lines were added to the plot in order to highlight trends. This plot qualitatively and quantitatively demonstrates sample differences resulting from lyophilization (Figure 3.14) versus solution-crystallization (Figure 3.5b) preparation methods. Qualitatively, the most apparent difference was the presence of DL-II and DL-MH, which were not observed in the solution-crystallized samples. Quantitatively, trends show that DL-II was the predominant racemic cocrystal form at low concentrations of L-proline. Slightly above the eutectic composition, DL-II reached a maximum level, and there was a dramatic increase in the amount of DL-I with increasing L-proline concentration. At the 50% L-proline concentration, DL-I was the main product.
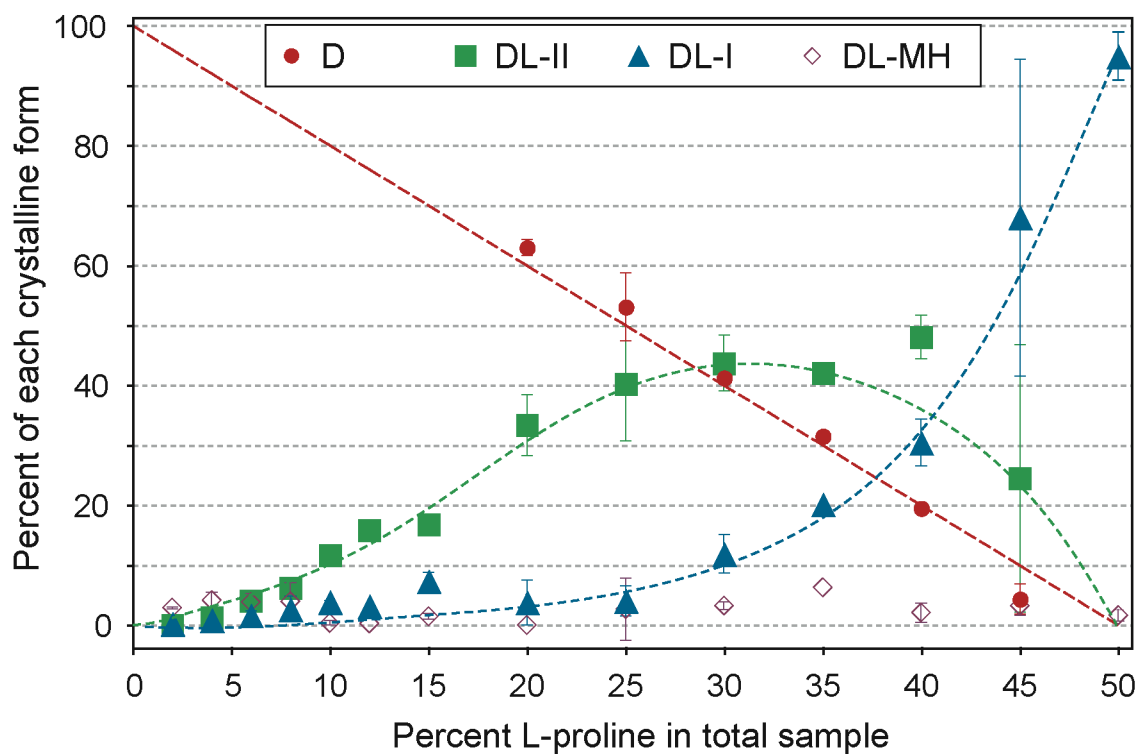
Figure 3.14. Plot of C-3 (20–50% L) and C-1 (2–15% L, subtracted spectra) relative peak areas as a function of total % L-proline in each sample. (n=1: 12 and 35% L; n=2: 2–10, 15, 20, 30, 45% L; n=3: 40, 50% L; n=5: 25% L; average and either range or standard deviation plotted; n represents analyses of different samples, not repeated analyses.)

In order to better understand the trends observed in Figure 3.5b versus Figure 3.14, including the presence/absence of the previously unreported DL-II polymorph, the energy relationship between DL-I and II was studied.

3.3.7   Energy relationship between DL-I and II

Energetic relationships between polymorphic forms are defined as either monotropic (one form is more stable at all temperatures) or enantiotropic (the relative stability of the two polymorphs switches at a defined transition temperature). Enantiotropic versus monotropic relationships are usually assigned by Burger–Ramberger rules.[27,28]   In the proline system, these rules could not be applied because it was not possible to accurately measure the enthalpy of fusion, and no endotherm/exotherm transitions were observed in the DSC prior to melting. However, defining the relative stability of the polymorphs at two different temperatures allows one to define the energy relationship that exists between those two temperatures.   The observation of a spontaneous polymorphic transformation during SSNMR analysis demonstrated the relative stability of DL-I and DL-II at room temperature. An example of this observed transformation is shown in Figure 3.15.

Figure 3.15a shows ^{13}C CP-MAS NMR spectra of a lyophilized 40% L-proline sample analyzed as a function of time at room temperature, starting immediately after the lyophilization method was completed. The initial spectrum (45 min) contains peaks for D, DL-II, and DL-I, but changes in the peaks were observed over time. The changes in the relative peak area of C-3 as a function of time are plotted in Figure 3.15b. The plot demonstrates a rapid initial transformation from DL-I to DL-II, with a plateau ~16 hr
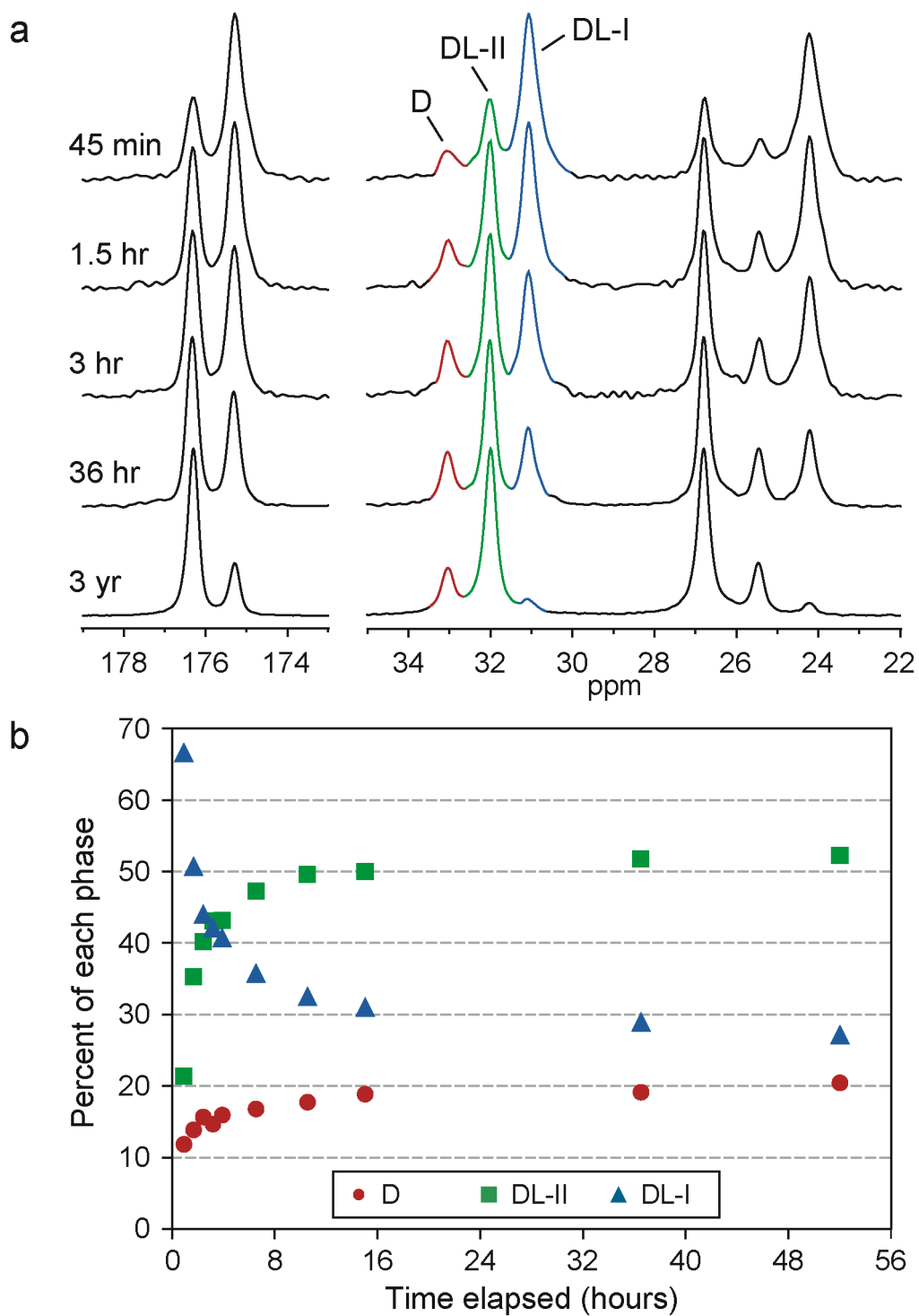
Figure 3.15. A 40% L-proline sample prepared by lyophilization. a) ^{13}C CP-MAS NMR spectra as a function of time elapsed since the end of the lyophilization cycle. Peaks for C-1, C-3, and C-4 are shown. b) Plot of C-3 relative peak areas for D (circles), DL-II (squares), and DL-I (triangles) as a function of elapsed time.

111

after the sample was removed from the lyophilizer. This spontaneous polymorphic transformation indicates that DL-II is more thermodynamically stable at room temperature than DL-I. It is important to note that, due to these observations, SSNMR analyses (spectra in Figure 3.7, relaxation measurements in Table 3.4) were not performed until after the initial rapid transformation had occurred.

In addition to the polymorphic transformation of DL-I to DL-II, Figure 3.15b also indicates a potential transformation involving D. The plot shows a relative increase in the amount of D at the apparent expense of DL-I. There are two potential causes for these relative changes: 1) the presence of an unidentified D polymorph that possesses a peak located underneath the DL-I C-3 peak (31.0 ppm), the area under which was used to calculate the relative amounts of each crystal form, or 2) a relative change in the relaxation times between the two forms occurred, in which case the observed relative increase in D is not real, but simply reflective of changes in relaxation dynamics within the sample. Due to the rapid changes in the sample, it was not possible to measure the initial relaxation times of the sample. Thus, it is not possible to determine whether the changes in this peak area are due to relative changes in the relaxation of D and DL-I, or if they demonstrate a real growth of the D phase. This potential D polymorphism might be of interest for future study.

In order to assess the relative stability of DL-I and II at high temperatures, a sample of bulk DL-proline was heated to 200ºC (located below the eutectic melting temperature) and held for various periods of time. Figure 3.16 shows SSNMR and DSC analyses performed on this sample as it was held at 200ºC for increasing amounts of time (t). The initial bulk DL-proline sample (t_0) was composed predominantly of DL-I, but a

small amount of DL-II existed, as noted by the small peak at 176.3 ppm in the ^{13}C CP-MAS NMR spectrum (Figure 3.16a, t_0). The DSC thermogram of this same sample (Figure 3.16b, t_0) contained two endotherms, with peak temperatures at ~214 and 217ºC. At this point, it was not clear which endotherm corresponded to DL-I and which to DL-II. Upon exposing this sample to 200ºC for 5 min (t_5), SSNMR showed a large increase in the DL-II peak, and there was a relative increase in the intensity of the DSC endotherm at 217ºC. Further exposure of this DL-proline sample to 200ºC for an additional 30 min (t_{35}), and then another 60 min (t_{95}), resulted in additional increases in the DL-II SSNMR peak and the 217ºC DSC melting peak. These complementary SSNMR and DSC results demonstrate that: 1) DL-II is the thermodynamically favorable form at 200ºC, since SSNMR showed a transformation from DL-I to DL-II at this temperature, and 2) the DSC-observed melting at 214ºC corresponds to the melting of DL-I, whereas the 217ºC peak, which increased in intensity during the course of the 200ºC hold, corresponds to DL-II. Because DL-II is more stable than DL-I at room temperature and at 200ºC, it can be stated that DL-II is more stable than DL-I over this entire temperature range. In other words, DL-I and DL-II are monotropically related, and DL-II is thermodynamically more stable over the temperature range of ~25–200ºC,.

As noted previously in Figure 3.2b, degradation of proline occurs upon melting. Degradation was also observed during the thermal treatment experiments shown in Figure 3.16. After heating the bulk DL-proline at 200ºC for 5 min, a slight discoloration of the sample (from white to off-white) was observed, and it progressively browned as thermal treatment continued. The presence of thermal degradants in the sample was also

113
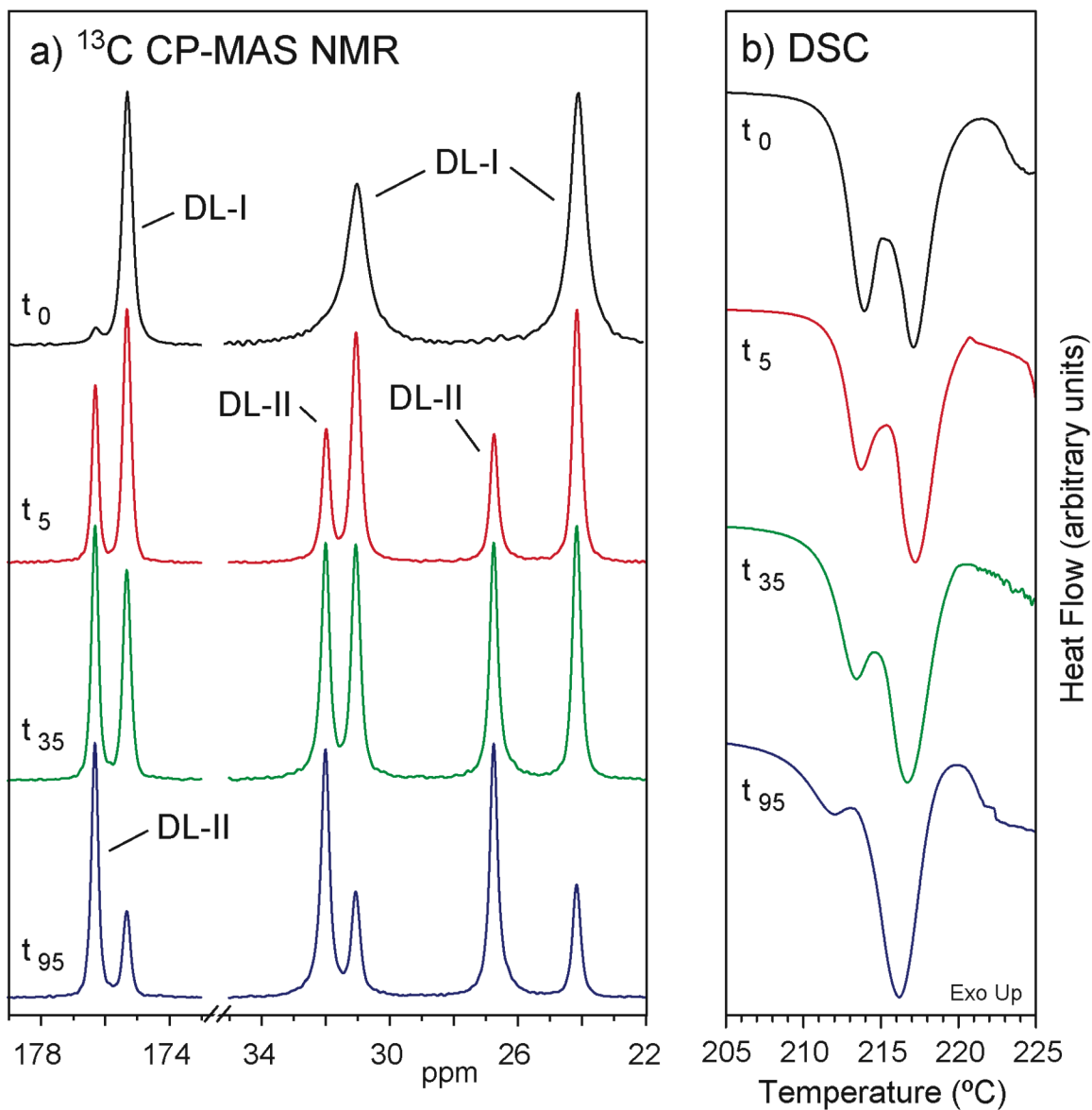
Figure 3.16. Bulk DL-proline heated at 200ºC for increasing amounts of time (t$_0$ = untreated sample). a) ^{13}C CP-MAS NMR spectra collected at 20ºC and b) corresponding DSC analysis (10ºC/min ramp) for each time point. SSNMR peaks for C-1, C-3, and C-4 are shown.

observed in DSC by progressive lowering of the endotherm peak temperatures (Figure 3.16) and by decreases in the SSNMR ^{1}H T_1 relaxation values (Table 3.5).

Because DL-II is the more stable form, the eutectic melt observed in the binary melting phase diagram in Figure 3.2a likely corresponds to DL-I. The additional peaks observed at ~211ºC for the melting of samples of 4 and 6% L-proline likely correspond to the eutectic melt associated with DL-II.

3.3.8   Kinetic stability of DL-I

The fact that the bulk DL-proline material was composed primarily of DL-I with just a trace amount of DL-II (Figure 3.16a, t_0) indicates that the DL-I crystals in this product were kinetically stable. Similarly, no transformations of DL-I to DL-II were observed among samples prepared from solution. This contrasts with the spontaneous polymorphic conversions that were observed among lyophilized samples (Figure 3.15). The previously described (§ 3.3.4) differences in crystal lattice disorder/mobility among samples are the most likely explanation for the decreased physical stability of DL-I in the lyophilized samples. The samples crystallized from solution possessed relatively long relaxation times compared to relaxation within the lyophilized samples (Table 3.4), suggesting more mobility/disorder within the crystal lattices of lyophilized samples. The presence of such disorder translates into a lower energy barrier for polymorphic transformations,[29,30] therein decreasing the kinetic stability of the metastable DL-I. Thus, the differences in the kinetic stability of DL-I among solution-crystallized and lyophilized samples is likely due to a lack of disorder within the solution-crystallized samples.

Table 3.5. ^{1}H T_1 relaxation values (s) for DL-proline heated at 200°C^a

Total time (min) at 200°C	DL-II	DL-I
0	63 (5)	75 (2)
5	43 (3)	68 (1)
35	--	--
95	35.4 (0.4)	61 (1)

^{a}Calculated using carbonyl peak area. Values in parentheses indicate error of fit.

3.4   Discussion

In characterizing the effect of enantiomeric composition on the crystallization of proline, an unreported polymorphic form of the racemic cocrystal was observed. This form possessed a higher melting point than the previously reported form (herein termed DL-proline form I), and it also was more stable at room temperature than DL-I, as observed through a spontaneous polymorphic transformation from DL-I to DL-II. These observations demonstrated that DL-II is thermodynamically more stable than DL-I above room temperature.

It is not surprising that DL-I is observed as the initial product upon crystallization of DL-proline from solution. Ostwald's Rule of Stages[31] states that a metastable form (kinetic product) is often observed prior to formation of the most stable form (thermodynamic product) upon crystallization. Additionally, new polymorphic forms are frequently identified, so the discovery of DL-II is not altogether surprising. However, what is interesting about this observed polymorphism is the method by which it was produced.

As demonstrated by Figures 3.5b and 3.14, the crystallization method, as well as the enantiomeric ratio, had a very large effect on the crystallization products that were observed. Upon crystallization from solution, a typical preparation method, only forms D and DL-I were produced. In contrast, crystallization by lyophilization produced samples that included D, DL-I, and the more thermodynamically stable DL-II. Of additional interest in the lyophilized samples were the observed trends between the DL-I/DL-II polymorphic ratio and the total amount of L-proline present, where no DL-II is produced at the 50% L-proline level. These observations lead to two main questions: 1) Why is

DL-II formed by the lyophilization method but not by crystallization from solution; and 2) why is DL-I the only form present at the 50% L-proline concentration, regardless of preparation method?

The answer to both of these questions likely can be answered by looking at the differences in crystallization kinetics associated with crystallizing from solution versus lyophilization. On–off movement in solution allows for formation of pairs of D and L molecules to be produced, which then all come together to form the crystal lattice as the kinetic product, in accordance with Ostwald's Rule of Stages.[31] On the other hand, in the lyophilization method, the molecules are "frozen" in the ice lattice. As the water molecules are removed by sublimation, the proline molecules, now in the solid state, are left behind. Molecular mobility is greatly restricted in a solid as compared to in solution, resulting in a large reduction in the translational motion associated with pairing of D and L molecules.

At the 50% L-proline level, assuming that D and L molecules are homogeneously distributed throughout the solution prior to freezing, the probability of finding a D and an L molecule neighboring each other is quite high. This means that forming the hetero-enantiomeric pair (and others around it) to create the racemic cocrystal requires little translational motion. In contrast, at lower concentrations of L-proline (e.g., 25% L-proline), the translational movement necessary to form a DL crystal lattice becomes much greater.

At the 25% L-proline level, a homogeneous distribution of D and L molecules means that every L molecule is likely very close to a D molecule. As a result, upon solidification, the formation of DL pairs does not require much translational motion.

That said, these DL pairs are physically separated from each other by the presence of the excess D molecules, and translational motion is necessary for DL pairs to pack together to form the crystal lattice. Growth of the crystal lattice is therefore inhibited. By slowing down the crystallization process, it is possible to form the thermodynamically stable crystal form (DL-II), not just the kinetically favorable form (DL-I).

The ability for an impurity to inhibit crystal growth of one form, allowing for growth of a different form, has been reported previously for solution-based crystallizations.[5,32] In these cases, the impurity molecule preferentially adsorbs to the surface of a specific type of crystal, therein preventing further growth, while still allowing growth of a different crystalline phase. The studies reported in this chapter are distinguished from these previous studies in that, in this case, selective production of the thermodynamically stable phase is produced by inhibiting the translation of molecules in the solid state, not the solution state.

The restricted motion of proline molecules in the lyophilized materials is supported by additional lyophilization experiments that are reported in Chapter 5. In these cases, many metastable crystalline forms were observed, and the samples were highly disordered, but not amorphous. The presence of so many forms indicates many different molecular conformations and packing arrangements. However, as soon as solid-state mobility is introduced to the system, either through the presence of water[33] or by increasing the temperature, these various crystal forms quickly convert into previously observed proline crystal forms. Traditionally, lyophilization has been considered a solution-based preparation method. However, these results suggest that this broad

categorization should be reconsidered, since this terminology suggests the presence of molecular mobility that does not exist in the solid state.

Cryogrinding the enantiomers together (Chapter 6) in order to produce molecular dispersions of proline enantiomers was also performed in order to probe the manner in which crystallization of the enantiomers occurs in the complete absence of water molecules.

These results are highly relevant to polymorphic screening assays. By controlling the crystallization kinetics in the solid state, the formation of a unique crystal form might occur. Additionally, due to increased chemical stability in the solid state arising from decreased molecular mobility, such crystallization mechanisms may be favorable for systems with solution-state–chemical-stability issues.

3.5   Conclusion

A new polymorphic form of the racemic cocrystal of proline is reported here. The energy relationship between this new form (DL-form II) and the previously observed form (DL-form I) was determined to be monotropic, where DL-form II is the thermodynamically stable form above room temperature.

DL-form II was observed upon crystallization of D- and L-proline by lyophilization when the enantiomeric excess was greater than zero. This observed behavior is hypothesized to occur due to inhibition of the solid-state crystallization process by the excess enantiomer. When crystallized from solution, or at ratios nearing 1:1 of D- to L-proline, the major product was the kinetically favored product, DL-form I.

Solid-state NMR spectroscopy was highly suited for investigating this chiral system in the solid state. Different crystal forms, including chiral defects, gave rise to different peaks in SSNMR spectra. Isotopic labeling, combined with spectral subtraction at low levels of L-proline, allowed for identification and relative quantitation of the various forms under a wide range of enantiomeric ratios. Future studies will include further analysis of the formation of chiral defects, as well as the solid-state crystallization process for proline enantiomers.

3.6   References

1.   Thayer A 2005. Trial separations. Chem Eng News 83(36):49-53.

2.   Murakami H 2007. From racemates to single enantiomers - chiral synthetic drugs over the last 20 years. Top Curr Chem 269:273-299.

3.   Li ZJ, Zell MT, Munson EJ, Grant DJW 1999. Characterization of racemic species of chiral drugs using thermal analysis, thermodynamic calculation, and structural studies. J Pharm Sci 88(3):337-346.

4.   Jacques J, Collet A, Wilen SH 1981. Enantiomers, Racemates, and Resolutions. New York: Wiley.

5.   Byrn SR, Pfeiffer RR, Stowell JG 1999. Solid-State Chemistry of Drugs. 2nd ed., West Lafayette, Indiana: SSCI, Inc.

6.   Pines A, Gibby MG, Waugh JS 1973. Proton-enhanced NMR of dilute spins in solids. J Chem Phys 59(2):569-590.

7.   Metz G, Wu X, Smith SO 1994. Ramped-amplitude cross polarization in magic-angle-spinning NMR. J Magn Reson, Ser A 110(2):219-227.

8.   Andrew ER, Bradbury A, Eades RG 1959. Removal of dipolar broadening of nuclear magnetic resonance spectra of solids by specimen rotation. Nature 183:1802-1803.

9.   Fung BM, Khitrin AK, Ermolaev K 2000. An improved broadband decoupling sequence for liquid crystals and solids. J Magn Reson 142(1):97-101.

10.   Dixon WT, Schaefer J, Sefcik MD, Stejskal EO, McKay RA 1982. Total suppression of sidebands in CPMAS carbon-13 NMR. J Magn Reson 49(2):341-345.

11.   Barich DH, Gorman EM, Zell MT, Munson EJ 2006. 3-Methylglutaric acid as a 13C solid-state NMR standard. Solid State Nucl Magn Reson 30(3-4):125-129.

12.   Roozeboom HWB 1899. Solubility and melting point as criteria for racemic compounds, pseudoracemic mixed crystals and inactive conglomerates. [machine translation]. Z Phys Chem 28:494-517.

13.   Myung S, Pink M, Baik M-H, Clemmer DE 2005. DL-proline. Acta Cryst, Sec C Cryst Structure Commun C61(8):506-508.

14.   Padmanabhan S, Suresh S, Vijayan M 1995. DL-Proline monohydrate. Acta Cryst, Sec C Cryst Structure Commun C51(10):2098-2100.

15.   Flaig R, Koritsanszky T, Dittrich B, Wagner A, Luger P 2002. Intra- and intermolecular topological properties of amino acids: A comparative study of experimental and theoretical results. J Am Chem Soc 124(13):3407-3417.

16.   Klussmann M, Iwamura H, Mathew SP, Wells DH, Jr., Pandya U, Armstrong A, Blackmond DG 2006. Thermodynamic control of asymmetric amplification in amino acid catalysis. Nature 441(7093):621-623.

17. Kayushina RL, Vainshtein BK 1965. Structure determination of L-proline by x-ray diffraction. Kristallografiya 10(6):834-844.

18. Janczak J, Luger P 1997. L-Proline monohydrate at 100 K. Acta Cryst, Sec C Cryst Structure Commun C53(12):1954-1956.

19. Lubach JW, Xu D, Segmuller BE, Munson EJ 2007. Investigation of the effects of pharmaceutical processing upon solid-state NMR relaxation times and implications to solid-state formulation stability. J Pharm Sci 96(4):777-787.

20. Stahly GP, McKenzie AT, Andres MC, Russell CA, Byrn SR, Johnson P 1997. Determination of the optical purity of ibuprofen using X-ray powder diffraction. J Pharm Sci 86(8):970-971.

21. Suryanarayanan R, Mitchell AG 1985. Evaluation of two concepts of crystallinity using calcium gluceptate as a model compound. Int J Pharm 24(1):1-17.

22. Huettenrauch R 1978. Molecular galenics as the basis of modern drug formation. Acta Pharm Technol, Suppl 6:55-127.

23. Coquerel G 2006. The 'structural purity' of molecular solids - elusive concept? Chem Eng Process 45(10):857-862.

24. Zell MT, Padden BE, Paterick AJ, Hillmyer MA, Kean RT, Thakur KAM, Munson EJ 1998. Direct observation of stereodefect sites in semicrystalline poly(lactide) using 13C solid-state NMR. J Am Chem Soc 120(48):12672-12673.

25. Munson EJ, Carlson LK, Jorvig JE, Zell MT, Abbott J, Hillmyer MA 2003. Determining stereodefect locations in polylactide using solid-state NMR spectroscopy. Polym Prepr 44(1):325-326.

26. Offerdahl TJ, Salsbury JS, Dong Z, Grant DJW, Schroeder SA, Prakash I, Gorman EM, Barich DH, Munson EJ 2005. Quantitation of crystalline and amorphous forms of anhydrous neotame using 13C CPMAS NMR spectroscopy. J Pharm Sci 94(12):2591-2605.

27. Burger A, Ramberger R 1979. On the polymorphism of pharmaceuticals and other molecular crystals. II. Applicability of thermodynamic rules. Mikrochim Acta 2(3-4):273-316.

28. Burger A, Ramberger R 1979. On the polymorphism of pharmaceuticals and other molecular crystals. I. Theory of thermodynamic rules. Mikrochim Acta 2(3-4):259-271.

29. Brittain HG 2002. Effects of mechanical processing on phase composition. J Pharm Sci 91(7):1573-1580.

30. Pirttimaki J, Laine E, Ketolainen J, Paronen P 1993. Effects of grinding and compression on crystal structure of anhydrous caffeine. Int J Pharm 95(1-3):93-99.

31. Ostwald W 1897. Studies on the formation and inversion of solids. First paper: supersaturation and supercooling. Z Phys Chem, Stoechiom Verwandtschaftsl 22:289.

32. Poornachary SK, Chow PS, Tan RBH 2008. Influence of solution speciation of impurities on polymorphic nucleation in glycine. Cryst Growth Des 8(1):179-185.

33. Andronis V, Yoshioka M, Zografi, George 1997. Effects of sorbed water on the crystallization of indomethacin from the amorphous state. J Pharm Sci 86(3):346-351.

Chapter 4

Detection of L-Proline Chiral Defects in the D-Proline Homochiral Lattice

Using Solid-State NMR Spectroscopy

4.1   Introduction

The previous chapter investigated the influence of enantiomeric ratio and crystallization method on the crystal forms of proline. During those studies, a peak in the solid-state NMR spectrum was attributed to the presence of chiral defects. This chapter focuses on the additional studies that were performed in order to identify and characterize the presence of L-proline chiral defects within the D-proline crystal lattice.

4.1.1   Previous investigations of chiral impurities

The incorporation of impurity molecules (often referred to as "guest" molecules) into a host crystal lattice has been researched extensively by Grant and coworkers.[1-4] Earlier studies by Go et al. investigated the incorporation of oleic acid impurities into adipic acid crystals.[1] It was acknowledged that there are two possible environments for the oleic acid upon crystallization from solution with adipic acid: 1) incorporation as a guest into the adipic acid (host) crystals, and 2) adsorption to the exterior of the adipic acid crystals.   In order to distinguish between these two possible environments, a continuous-flow–dissolution HPLC method measured the concentration of oleic acid in solution as the adipic acid particles were progressively dissolved. The results showed a high initial concentration of oleic acid (attributed to adsorbed material), followed by a decrease and eventual plateau in oleic acid concentration (attributed to oleic acid within the host crystals). The concentration of oleic acid within the adipic acid crystals was then

used to interpret changes in physicochemical properties (heat of fusion, dissolution rate, etc.) of the adipic acid crystals.

Further studies of the inclusion of molecular impurities upon crystallization from solution included chiral systems. Duddu et al. characterized the incorporation of (+)-ephedrinium 2-naphthalenesulfonate [(+)-EN] into its opposite enantiomer [(−)-EN],[2] as well as the incorporation of (−)-pseudoephedrinium salicylate into its (+)-enantiomer.[3] Li et al. continued studying the ephedrinium 2-naphthalenesulfonate system by investigating the effects of excess (+)-EN or (−)-EN enantiomer on the crystallization of the racemic (±)-EN.[4] In all cases, the concentration of guest molecules (chiral defects) within the host crystals was measured by an HPLC method adapted from the original studies by Go et al.[1] As mentioned previously, the original studies by Go et al. assumed that the oleic acid impurity molecules were either incorporated into the adipic acid crystal lattice as guests/defects or adsorbed on the surface of the adipic acid crystals. However, a third option exists: The impurity might form additional, distinct crystalline phases. For enantiomers, there are three types of crystal forms that must be considered, as previously shown in Figure 3.1 and outlined below.

A chiral impurity can crystallize in the presence of its antipode to form a) its own enantiopure crystal lattice, b) a racemic crystal (denoted as a cocrystal) by pairing with the antipode to form the crystal lattice, and/or c) a solid solution where the impurity exists as a guest (chiral defect) within the homochiral lattice of the antipode (Figure 3.1).[5] Technically, a true solid-solution phase is a thermodynamic product, whereas a chiral defect is an enantiomer that has been kinetically trapped within its antipode. Published work from the lab of Grant did not discriminate between thermodynamic and kinetic

127

products when applying the term chiral defects. We continue its prior usage herein, where "chiral defect" refers simply to an enantiomer that is present in the crystal lattice of its antipode.

In the studies of chiral systems by the Grant lab, changes in melting point, heat of fusion, entropy of fusion, and intrinsic dissolution were attributed solely to the presence of chiral defects measured by the HPLC method. However, Li acknowledged that excess chiral impurity on the surface may form a separate phase and may considerably influence the thermodynamic properties of the crystals depending on both the nature and location of the separate phase.[4]

4.1.2 Selective detection of chiral impurities

Detection of all solid forms (e.g., cocrystals, chiral defects, polymorphic forms, etc.) is essential to understanding the physicochemical properties of a system, as each form will contribute to the overall observed properties.[6,7] Although the aforementioned studies reported that low levels of chiral impurity can alter the dissolution/stability of a pharmaceutical product, it was not possible to fully characterize the crystallographic location and local environment of chiral impurities themselves.[2-4,8] Thus, it is unclear whether these observed changes in physicochemical properties are due solely to the presence of chiral defects or also to the presence of some other crystal form within the material.[9]

Solid-state NMR spectroscopy (SSNMR) was chosen to study the chiral impurities in crystals because it can selectively identify the enantiomer in the crystalline lattice. ^{13}C-labeling of the L-enantiomer differentiated it from the D-enantiomer, and

SSNMR was used to determine the location of the ^{13}C label. [13]C is only 1.1% naturally abundant, so a 100% ^{13}C-labeled enantiomer possesses ~90 times greater signal than its corresponding natural-abundance enantiomer. This means that signal from a 1% ^{13}C-labeled chiral impurity will have signal roughly equivalent to that of 99% of the opposite enantiomer. This technique was previously used to selectively observe the location of chiral defects in polymers.[10,11] In general, SSNMR is particularly useful for the identification of different crystalline forms.[12]

4.1.3   Crystallization of D- and L-proline enantiomers

The kinetics associated with a particular crystallization method influence the incorporation of impurity molecules.[13] In order to study the effect of crystallization method on the incorporation of L-proline chiral impurities into the D-proline crystal lattice, proline samples were crystallized from aqueous solution, and by spray drying, lyophilization, and cryogrinding. The resulting samples were characterized by ^{13}C SSNMR, PXRD, and thermal analysis.

4.2   Experimental

4.2.1   Materials

L- and DL-proline were purchased from Alfa Aesar (Ward Hill, MA), D-proline was purchased from Sigma-Aldrich (St. Louis, MO), and L-proline containing an isotopic label on the carbonyl carbon (denoted L-[1-^{13}C]proline) was purchased from Cambridge Isotope Laboratories, Inc. (Andover, MA). All were used as received. DL-proline monohydrate was prepared by slow evaporation of a 98% ethanol solution at room

temperature. Thermogravimetric analysis (Q50 TGA, TA Instruments) and Karl Fischer titrimetry (DL36 KF Coulometer, Mettler Toledo) were used to confirm the formation of the monohydrate.

4.2.2   *Sample preparation*

Lyophilization.   Solutions of various (2–15%) L-proline to D-proline ratios were prepared by creating w/w mixtures of the two enantiopure compounds, followed by dissolving these mixtures in double-distilled water at a concentration of 0.6% w/v. In order to perform spectral subtractions (vide infra), each L-/D-proline ratio was prepared twice: One solution contained natural-abundance L-proline, and the other contained L-[1-^{13}C]proline. The solutions were then lyophilized in 10-mL aliquots (within 20-mL scintillation vials) using a bench top freeze dryer (VirTis AdVantage; VirTis; Gardiner, NY). The lyophilization cycle was 32 hr (-35, -5, 5, 15, and 25°C; for 2, 8, 6, 6, and 10 hr respectively) with an initial 2-hr freezing step (-35ºC) and a vacuum set point of 90 mTorr. The vacuum was released by purging the sample chamber with ambient air. Due to their hygroscopic nature, all samples were stored in a desiccator over anhydrous calcium sulfate until analyses were performed.

Crystallization from aqueous solution.   Solutions of proline enantiomers were prepared as described above. Each solution was transferred to a 400-mL beaker, covered with a KimWipe, and heated at 75ºC in a dry bath until the water had evaporated. The solid material was periodically agitated with a spatula to facilitate complete drying.

Spray drying.   Aqueous solutions of 7.5% w/v proline were spray-dried using a Büchi 190 mini spray dryer (BÜCHI Labortechnik AG, Switzerland) with an inlet

temperature of 180°C, an outlet temperature of 100°C, a pump speed of approximately 5 mL/min, a spray flow of 600 L/hr, and the maximum aspirator setting.

Cryogrinding. Mixtures of bulk L- and D-proline were weighed directly into a polycarbonate cryovial containing a stainless-steel impactor bar. Each mixture was then ground in a Freezer/Mill (SPEX 6750; SPEX Certi-Prep; Metuchen, NJ) for a total of 30 min, performed in 15 cycles (2 min of grinding followed by a 2-min rest interval), preceded by 5 min of pre-cooling. All sample handling before and after grinding was performed within a dry nitrogen glove box.

Thermal and elevated-RH treatment. Vials of freshly lyophilized 6% L-[1-^{13}C]proline were split into two groups and analyzed by SSNMR following exposure to various conditions:

1) a) The freshly lyophilized material was immediately packed into a zirconia rotor for SSNMR analysis.

   b) After SSNMR analysis of the initial material, spectra were acquired as the sample was progressively heated in the instrument to a maximum of 180ºC

2) a) The remaining "virgin" material (stored over desiccant during steps 1a–b) was placed in a 45% RH, 30ºC stability chamber for 2 hr, then quickly packed into a zirconia rotor under ambient conditions and analyzed by SSNMR.

   b) The sample was unpacked from the rotor into a scintillation vial and placed in a 60% RH, 30ºC stability chamber for 1 hr, after which SSNMR analysis was performed again.

c) The rotor was removed from the magnet but not unpacked.

The "closed" end cap was replaced with an end cap containing a

pinhole to allow water vapor to escape. The rotor was put back

into the magnet and heated to 30ºC to partially dehydrate the

sample, after which a spectrum was acquired.

4.2.3 Solid-state NMR spectroscopy

All ^{13}C spectra were acquired on a Chemagnetics CMX-300 spectrometer

(Varian, Inc.; Palo Alto, CA), operating at 75 MHz for [13]C. All CP-MAS acquisitions

included cross polarization (CP),[14,15] magic-angle spinning (MAS)[16] at a rate of 4 kHz

(±3 Hz), two-pulse phase modulation (TPPM) or SPINAL64 decoupling[17] at a field

strength of ~62–72 kHz, and total sideband suppression (TOSS)[18]. A contact time of 2 ms

was used for all samples. Spectra used for spectral subtractions were acquired using

pulse delays of at least five times the ^{1}H relaxation time (obtained by a [1]H T_1 saturation–

recovery sequence) of each corresponding sample. Peak areas were calculated using

Chemagnetics Spinsight™ software, and [1]H T_1 and $T_{1\rho}$ values were calculated using

KaleidaGraph (Synergy, version 4.01).   3-methylglutaric acid (MGA) was used to

optimize the spectrometer settings as well as to set the reference frequency.[19]   All

samples were packed into zirconia rotors with Teflon® or ribbed Kel-F® end caps.

Ambient-temperature (~20ºC) experiments were performed using a 7-mm double-

resonance MAS probe (Revolution NMR, Inc.; Fort Collins, CO), and variable-

temperature experiments were performed with a 7.5-mm double-resonance MAS probe

(Varian; Palo Alto, CA), with 3.5-μs and 4.0-μs ^{1}H pulse durations, respectively. Lead nitrate was used for temperature calibration.[20] During variable-temperature experiments, samples were equilibrated at each temperature for at least 15 min prior to tuning and data acquisition.

4.2.4 Differential scanning calorimetry

Differential scanning calorimetry (Q100 DSC; TA Instruments; New Castle, DE) was performed on samples of 3–8 mg that were packed into standard aluminum pans under ambient conditions and lightly crimped. Data was collected from room temperature to ~240ºC, with a temperature ramp of 10ºC/min and a 50-mL/min dry nitrogen purge. Samples were analyzed in triplicate.

4.2.5 Thermogravimetric analysis

Water content of samples was determined by thermogravimetric analysis (Q50 TGA, TA Instruments; New Castle, DE). Samples of 10–20 mg were heated from room temperature to >300ºC at a rate of 10ºC/min under a 40-mL/min dry nitrogen purge.

4.2.6 Powder X-ray diffraction

Diffraction patterns were acquired with a Scintag X2 Diffraction System (XGEN-4000; Scintag, Inc.) using CuKα radiation (45 kV, 35 mA), an angular range of 8–35º 2θ, a step size of 0.02º, and a dwell time of 4 sec. Each sample (~300 mg) was packed into a stainless-steel die. All analyses were performed at ambient conditions.

4.3   Results

4.3.1   *Observing impurities in proline*

In the previous chapter, the effect of various amounts of L-proline chiral impurity on the crystallization of D-proline was investigated. During those studies, a peak in the solid-state NMR spectrum was identified as the presence of L-proline chiral defects in the D-proline crystal lattice (Table 4.1). The spectral-subtraction method that allowed for the observation of these L-proline defects is reiterated here.

Figure 4.1 illustrates the spectral-subtraction method used in this study.[10,11] At each concentration of L-proline, two samples were prepared: one containing L-[1-^{13}C]proline (Figure 4.1a) and the other containing natural-abundance (NA) L-proline (Figure 4.1b). The spectrum of the NA sample was subtracted from that of the ^{13}C-labeled sample, and the resulting spectral subtraction (Figure 4.1c) shows only the carbonyl peaks that arise from the ^{13}C-labeled L-proline chiral impurity. By performing spectral subtractions and comparing the remaining carbonyl peaks to known forms (Table 4.1), it was possible to selectively determine the crystal environments in which L-proline chiral impurities were incorporated. The subtraction in Figure 4.1 corresponds to lyophilized samples of 12% L-proline with 88% D-proline. In this subtraction, there are four carbonyl peaks. The peaks located at 177.2, 176.3, and 175.3 ppm correspond to the carbonyl carbon of racemic cocrystals DL-MH, DL-II, and DL-I. A fourth peak at 174.7 ppm that does not correspond to any known form of proline was assigned to L-proline molecules incorporated as substitutional chiral defects (L-CD) in the D-proline host crystal matrix. Evidence for the assignment of the 174.7-ppm SSNMR peak to L-CD is demonstrated throughout the remainder of this chapter.

134

Table 4.1. ^{13}C CP-MAS NMR chemical shifts (ppm) of proline crystal forms

Crystal form	Abbrev.	Carbonyl peak	Aliphatic peaks			
		C1	C2	C5	C3	C4
Enantiopure[a]	L-/D-	175.3[b]	61.9	46.5	33.0	25.4
Racemic cocrystal form I	DL-I	175.3[b]	60.6	45.9	31.0	24.2
Racemic cocrystal form II	DL-II	176.3	60.6	47.6	31.9	26.7
Racemic cocrystal monohydrate	DL-MH	177.2	60.1	48.5	30.8	26.2
L-chiral defect[c]	L-CD	174.7	NA	NA	NA	NA

[a]Enantiopure D- and L-proline have the same ^{13}C peak positions.
[b]Enantiopure and DL-I spectra overlap at the carbonyl peak, but peak differences are observed for the aliphatic peaks.
[c]Due to the low concentrations of defect sites present in samples, ^{13}C labeling at these carbons would be necessary to determine their chemical shifts in the ^{13}C spectrum.
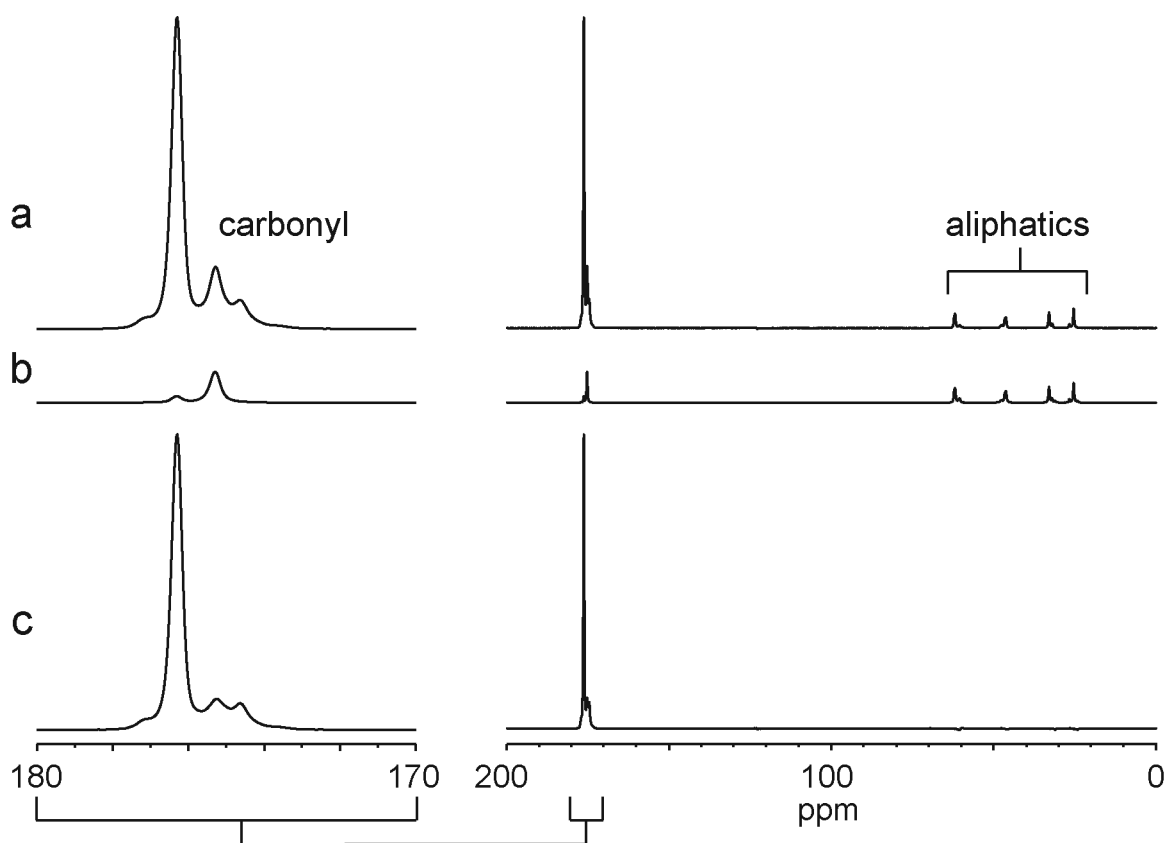
Figure 4.1. Spectral-subtraction method for lyophilized 12% L-proline in D-proline. a) ^{13}C CP-MAS NMR spectrum of 12% L-[1-^{13}C]proline and 88% D-proline; b) ^{13}C CP-MAS NMR spectrum of 12% L-proline and 88% D-proline; and c) difference spectrum that selectively shows peaks of only the ^{13}C-labeled L-proline (chiral impurity).

The effects of crystallization kinetics on the incorporation of chiral defects were studied by analyzing samples of 6% L-proline that were prepared using four crystallization methods. In order to detect the presence of chiral defects within the samples, the previously described (§ 4.3.1) spectral-subtraction method was applied.

Figure 4.2 shows the ^{13}C CP-MAS NMR spectral subtractions of 6% L-proline samples crystallized from aqueous solution, by lyophilization, and by spray drying. As a result of the subtraction, the observed carbonyl peaks correspond to only the L-proline impurity molecules in the sample. For comparison, the non-subtracted spectrum of a 6% L-[1-^{13}C]proline cryoground sample also is included. In the case of the solution-crystallized sample, L-proline was incorporated primarily into the racemic cocrystal DL-I, and also formed small amounts of DL-II and DL-MH. On the other hand, crystallizing by lyophilization and spray-drying methods caused L-proline to be incorporated to a greater extent as DL-II, as well as L-CD (peak at 174.7 ppm). Cryogrinding resulted in very broad peaks, indicative of disorder in the system, but the spectrum did not contain the L-CD peak at 174.7 ppm. The fact that L-CD incorporation was not observed when solutions of proline enantiomers were crystallized gradually from aqueous solution (dry bath, 75ºC), but were observed upon kinetically-hindered/rapid crystallization processes (lyophilization and spray-drying), supports the assignment of the 174.7-ppm peak to the presence of substitutional chiral defects. It also indicates that these chiral defects exist as kinetically trapped molecules, not as part of a true solid solution, which occur when thermodynamics dictate miscibility of the components and would have been observed in
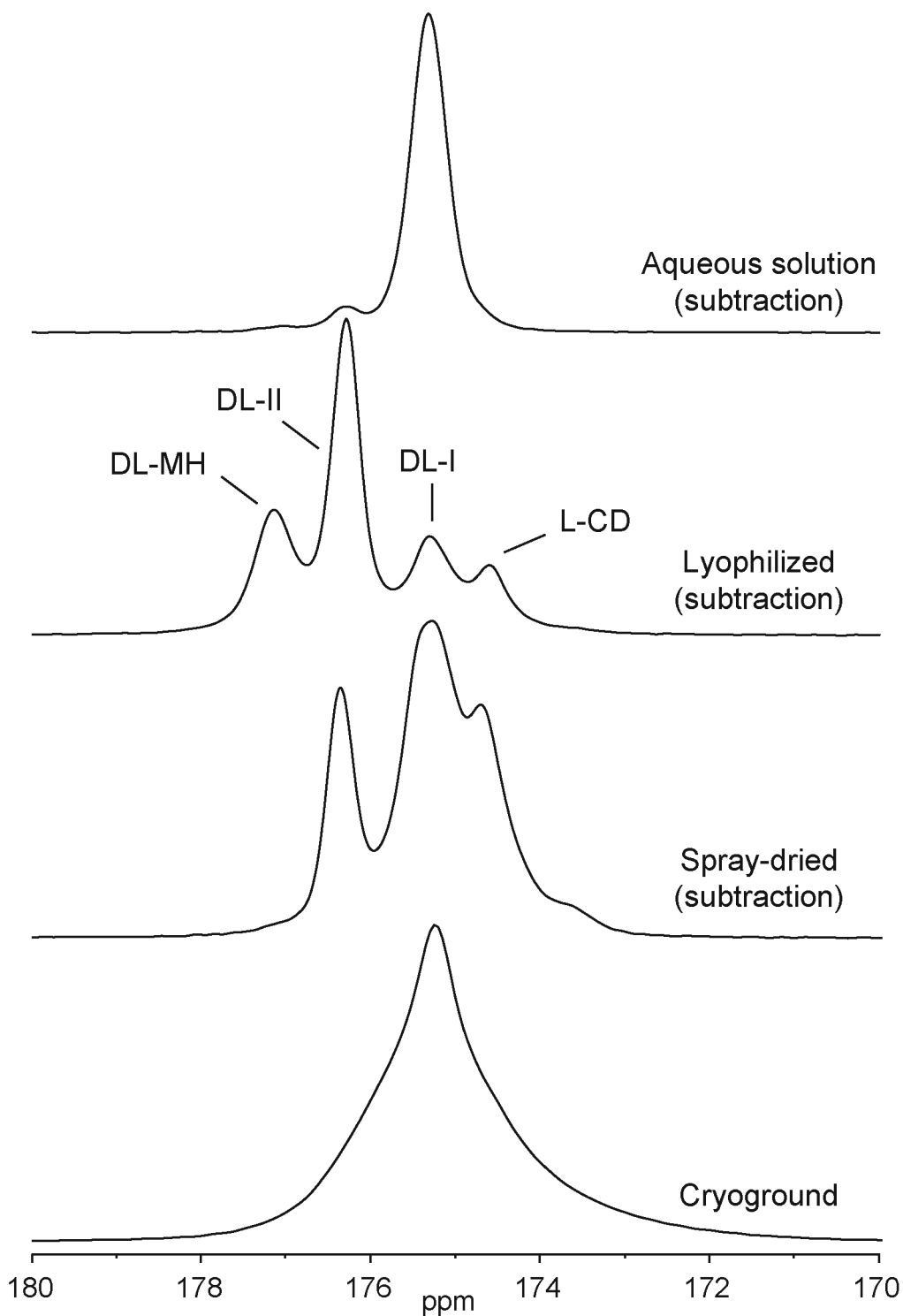
Figure 4.2. ^{13}C CP-MAS NMR spectral subtractions for 6% L-proline prepared from aqueous solution, by lyophilization, and by spray drying; and the non-subtracted spectrum of cryoground 6% L-proline.

the solution-crystallized sample as well. Additionally, the absence of the 174.7-ppm peak in the spectrum of the cryoground material suggests that the L-CD exists as part of a structured crystalline phase, not as a component within a disordered/amorphous phase. In order to further study L-proline chiral defects, additional samples were crystallized by lyophilization.

4.3.3 Effect of enantiomeric ratio

Figure 4.3 shows an overlay of ^{13}C CP-MAS NMR spectral subtractions of lyophilized samples containing 2–15% L-proline. Again, because these are spectral subtractions, the peaks arise only from only the carbonyl carbon of the L-proline molecules. These spectra were previously shown in Figure 3.13, in which all spectra were normalized to the same maximum intensity. Here, Figure 4.3 highlights relative changes between samples by overlaying the spectra. At the 2% L-proline level (Figure 4.3), predominantly DL-MH, some DL-I, and L-CD are observed. Higher levels of L-proline resulted in large increases in DL-II, moderate increases in DL-I and L-CD, and a decrease in DL-MH. At 15% L-proline, DL-II dominates the spectrum, but peaks for DL-MH, DL-I, and L-CD are still visible. Because NMR is an inherently quantitative technique,[21] it was possible to calculate the amount of L-CD present in each solid sample.

Figure 4.4 is a plot of the amount of chiral defects in each sample as determined from ^{13}C CP-MAS NMR spectra in Figure 4.3. Deconvoluted carbonyl peak areas from subtracted spectra were used to calculate the relative amounts of each crystal form. Strict quantitation methods were not used, but all samples were acquired with a pulse delay greater than five times the longest [1]H T_1 to avoid saturation effects.[21] Because the total
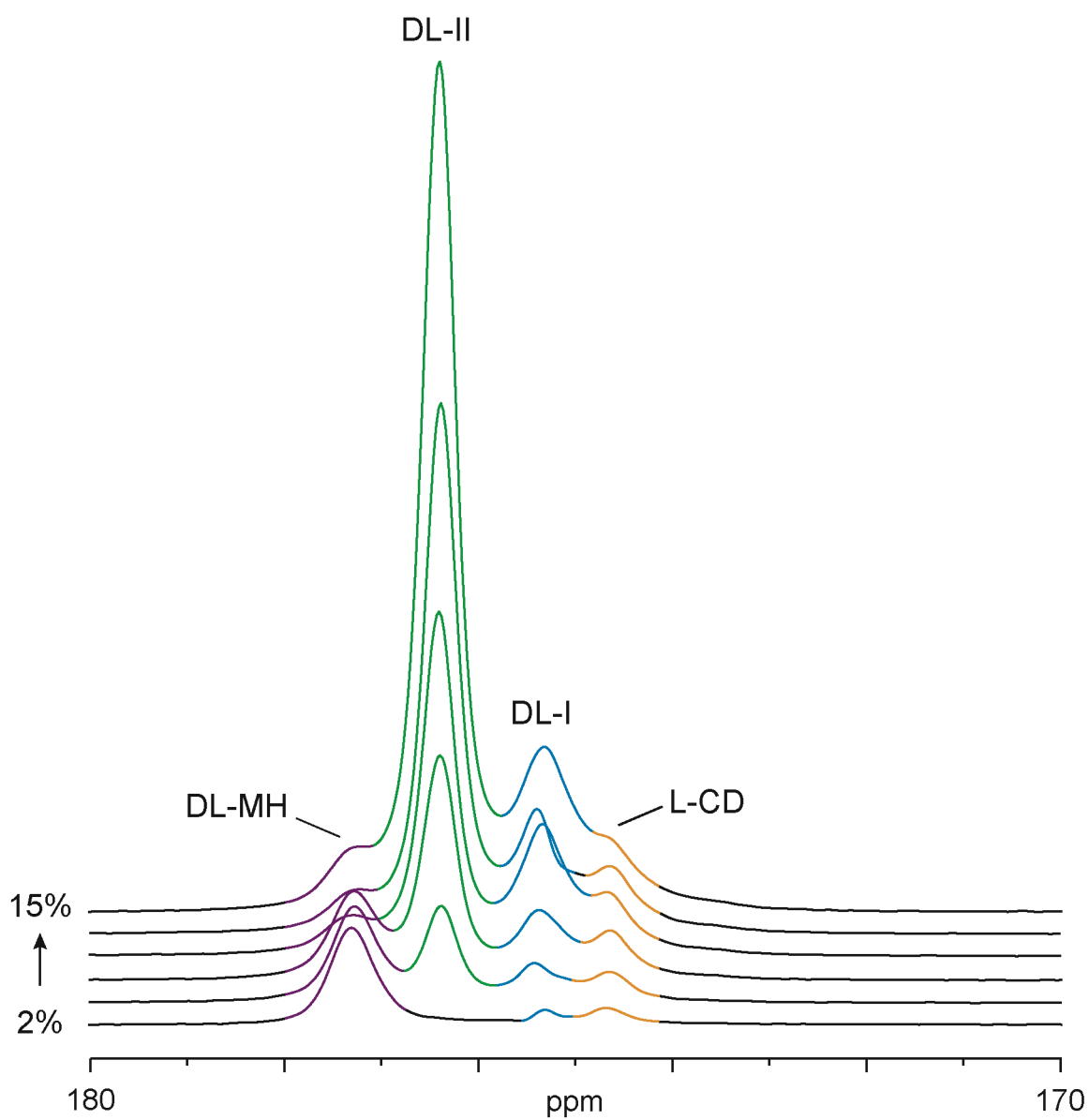
Figure 4.3. ^{13}C CP-MAS NMR spectral subtractions for increasing amounts of L-proline in D-proline prepared by lyophilization.
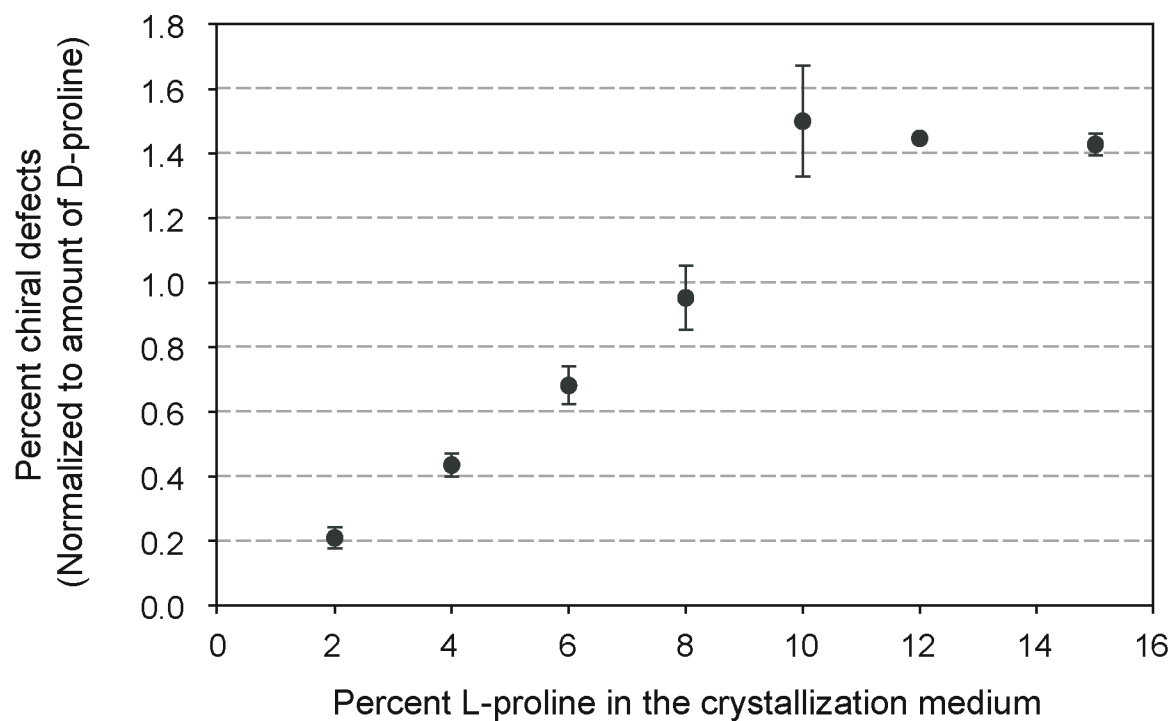
Figure 4.4. A plot of the concentration of chiral defects as a function of the total amount of L-proline. A maximum of ~1.4% L-proline in D-proline is observed. (n=2 for all values except the 12% L-proline level, where n=1. Error bars represent the range.)

amount of crystalline D-proline decreased as the L-proline concentration increased due to the formation of racemic compound, the "concentration" of L-CD present in the D-proline host crystals was calculated using the equation:

$$[L-CD] = \frac{L\text{-}CD_{peak\,area\,\%} \times total\,\%\,\,L\text{-}proline}{D\text{-}proline_{peak\,area\,\%}} = \frac{L\text{-}CD_{peak\,area\,\%} \times total\,\%\,\,L\text{-}proline}{[1-(racemic_{peak\,area\,\%} \times total\,\%\,\,L\text{-}proline)]}$$

The concentration of L-CD increased almost linearly with the total level of L-proline until approximately 10% L-proline, above which higher L-proline levels produced no further increase in the concentration of defect sites. This plateau, or "saturation," of L-CD, indicates the maximum concentration of L-proline that can be incorporated into the D-proline crystal lattice when crystallized using this lyophilization method. This saturation also seems to support assigning the 174.7-ppm peak to the presence of chiral defects, as a similar effect was observed in previous studies.[1-4]

Interestingly, the L-CD peak is fairly narrow at all concentrations, which indicates that the L-CD molecules are all in the same electronic environment and not disordered or in an amorphous-like phase.[22] This single, sharp peak also supports that the L-CD is homogeneously distributed; if some L-proline molecules were closer to each other than others, the inhomogeneous distribution would produce broader or multiple peaks due to differences in electronic environments. However, another possibility is that this peak corresponds to a completely different crystal form, in which case it likely exists as its own distinct phase.

4.3.4   Relaxation-time determination of the L-CD peak

In order to determine if the 174.7-ppm peak corresponded to a completely different crystal form, and not a chiral defect, proton spin–lattice (^{1}H T_1) relaxation measurements were performed. The manner in which molecules are arranged and packed into the crystal lattice affects the rate at which relaxation occurs. Thus, different crystal forms typically possess different relaxation values: If two peaks within the CP-MAS NMR spectrum possess different ^{1}H T_1 values, the peaks represent two different, phase-separated forms, and a shared ^{1}H T_1 value often indicates an intimate mixture.[23,24]

Table 4.2 contains the spin–lattice ^{1}H T_1 relaxation times corresponding to the lyophilized ^{13}C-labeled samples from Figures 4.1 and 4.3. The average relaxation times for each crystal phase across all L-proline concentrations are also shown. Due to overlapping peaks at 175.3 ppm for D and DL-I, the D-proline relaxation was determined from peaks in the aliphatic region of the spectra. The relaxation times of DL-MH, DL-II, and D/DL-I components are significantly different from one another, indicating phase separation. On the other hand, ^{1}H T_1 values for the D and L-CD peaks are the same within error. The similarity of the relaxation times provides evidence for an intimate mixture, as expected for a true chiral defect,[23,24] where the L-molecules are surrounded by the homochiral D lattice. Surprisingly, there was no correlation between relaxation time and the concentration of L-proline impurity. Thus, it appears that the presence of L-CD did not increase or decrease lattice mobility as measured by ^{1}H T_1 values.

Mixing-intimacy within the samples was further probed by measuring ^{1}H $T_{1\rho}$ relaxation values. Whereas ^{1}H T_1 values (s) are indicative of mobility at the MHz

Table 4.2. ^{1}H T_1 relaxation times (s) of 2–15% L-[1-^{13}C]proline samples[a]

Preparation method	Percent L-[1-^{13}C] proline	177.2 ppm (DL-MH)	176.3 ppm (DL-II)	175.3 ppm (D/DL-I)[b]	174.7 ppm (L-CD)	D aliph, Avg. (st. dev.)[b]
Lyophilized	2	8.6 (0.5)	--	29.9 (0.7)	30 (1)	30.6 (0.4)
	4	11.0 (0.8)	21 (1)	31 (1)	34 (2)	38.4 (0.3)
	6	11 (1)	21.4 (0.9)	28 (1)	37 (1)	38.1 (0.3)
	8	12.7 (0.7)	22.8 (0.5)	27.4 (0.8)	36.3 (0.6)	35.6 (0.3)
	10	10 (1)	20.5 (0.5)	24 (1)	33 (1)	32.6 (0.3)
	12	10 (1)	20.5 (0.5)	26.1 (0.9)	36.4 (0.8)	34.4 (0.2)
	15	9.9 (0.5)	19.6 (0.4)	22.2 (0.6)	29.5 (0.3)	27.8 (0.4)
	Average (st. dev.)	10 (1)	21 (1)	27 (3)	34 (3)	34 (4)
Solution	6	--	21.2 (0.9)	62 (2)	--	87 (2)
Spray-dried	6	--	13.1 (0.5)	16.4 (0.6)	20.1 (0.5)	20.48 (0.08)
Cryoground[c]	6	--	37 (1)	46 (1)	49.2 (0.5)	48.2 (0.3)

[a]Values in parentheses indicate error of fit.
[b]Enantiopure and DL-I spectra overlap at the carbonyl peak, thus this value represents an average of the T_1 for both forms. The T_1 values of the D-proline aliphatic peaks selectively represent the relaxation of the D-proline phase.
[c]Corresponds to the bottom spectrum in Figure 4.8.

frequency, ^{1}H $T_{1\rho}$ values (ms) represent mobility in the kHz frequency range and are much more indicative of local mobility.[25] Measured ^{1}H $T_{1\rho}$ relaxation values are reported in Table 4.3. As with the T_1 measurements, $T_{1\rho}$ values for the enantiopure and L-CD peaks are very similar, which supports the assignment of the 174.7-ppm peak to L-proline molecules (L-CD) trapped within the D-proline crystal lattice.

In addition to SSNMR analysis, samples were characterized by DSC and PXRD, as both of these methods are frequently used to analyze chiral molecules in the solid state.

4.3.5 Analysis of lyophilized samples by orthogonal techniques

Figure 4.5 is an overlay of differential scanning calorimetry (DSC) thermograms corresponding to lyophilized proline samples that were reclaimed following SSNMR analysis. The loss of water from the DL-MH phase was observed as an endothermic peak at ~70ºC (data not shown). No additional thermal event was observed until melting at temperatures greater than 200ºC. The overlay includes the thermogram of lyophilized enantiopure D-proline, which has a peak melting temperature at ~227ºC. Thermal degradation occurred immediately following melting, preventing calculation of heats of fusion for the various crystalline forms of proline. The overlay in Figure 4.5 shows the decrease in melting point of D-proline as the concentration of L-proline increased, along with the appearance and growth of an endotherm at ~208ºC, corresponding to the racemic cocrystal eutectic melt. These trends are consistent with the formation of a racemic cocrystal upon melting a binary mixture of enantiomers.[5] This correlates well with the SSNMR spectra (Figure 4.3), which show that increasing levels of L-proline

Table 4.3. ^{1}H $T_{1\rho}$ relaxation times (ms) of 2–15% L-[1-^{13}C]proline samples[a]

Preparation method	Percent L-[1-^{13}C] proline	177.2 ppm (DL-MH)	176.3 ppm (DL-II)	175.6 ppm (DL-III)[c]	175.3 ppm (D/DL-I)[b]	174.7 ppm (L-CD)	D aliph, Avg. (st. dev.)[b]
Lyophilized	2	14.6 (0.9)	--	12.4 (0.7)	24 (2)	45 (5)	37 (2)
	4	--	53 (3)	38 (4)	54 (3)	61 (7)	64 (1)
	6	16.1 (0.4)	59 (2)	--	63 (3)	73 (2)	68 (1)
	8	--	43 (2)	--	43 (3)	49 (2)	52 (1)
	10[d]	--	--	--	--	--	--
	12	8.0 (0.2)	24 (1)		26 (1)	30 (1)	29.1 (0.9)
	15	9.9 (0.3)	30 (2)	--	37.0 (0.7)	41 (2)	39.1 (0.8)
Cryoground	6	10.7 (0.4)	30 (2)	--	33 (2)	38 (2)	36.2 (0.7)

[a]Values in parentheses indicate error of fit.
[b]Enantiopure and DL-I spectra overlap at the carbonyl peak, thus this value represents an average of the $T_{1\rho}$ for both forms. The $T_{1\rho}$ values of the D-proline aliphatic peaks selectively represent the relaxation of the D-proline phase.
[c]Some sample changes were observed during long-term storage, including dehydration of DL-MH, resulting in the formation of DL-III (refer to § 5.3.5).
[d]Due to exposure to high relative humidity during long-term storage, this sample became completely hydrated, which led to complete disappearance of 175.6-, 175.3-, and 174.7-ppm peaks.
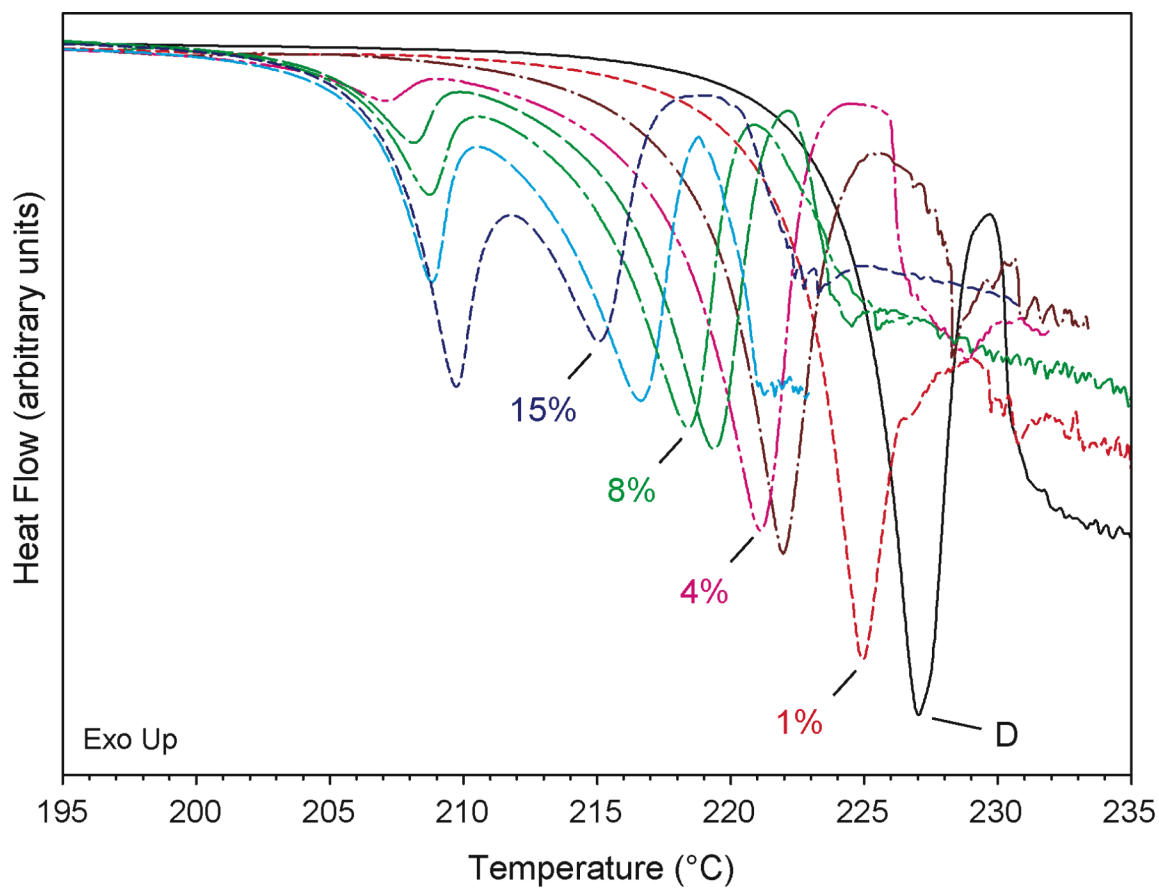
Figure 4.5. Overlay of DSC thermograms for lyophilized samples of enantiopure D-proline and 1, 2, 4, 6, 8, 10, and 15% L-proline.

produce correspondingly increased amounts of racemic cocrystals. However, due to overlapping thermal events in these DSC thermograms, it is not possible to observe the presence of both DL-I (mp ~213ºC) and DL-II (mp ~216ºC) forms in the samples. The observed eutectic melt is likely associated with DL-I, and a higher melting eutectic would be observed if only DL-II were present.

Powder X-ray diffraction (PXRD) patterns for the lyophilized samples (Figure 4.6) also supported the formation of racemic compound with increasing levels of L-proline. However, the diffraction patterns did not indicate the presence of L-CD. This was not unexpected, as distinguishing between enantiopure crystals and solid-solutions by PXRD is typically not possible.[26,27] Thus, SSNMR was the only method that was able to selectively detect the presence of L-CD.

In order to further explore the possibility that the 174.7-ppm peak corresponded to the presence of a thermal degradant or polymorph/hydrate, a sample that contained the 174.7-ppm peak in its ^{13}C CP-MAS NMR spectrum was exposed to elevated temperature and relative-humidity (RH) conditions.

4.3.6   Stability of chiral defects

Figure 4.7 shows ^{13}C CP-MAS NMR spectra of a 6% L-[1-^{13}C]proline sample prepared by lyophilization. The spectra in this figure are not subtracted spectra, so the carbonyl region contains signals from both the ^{13}C-labeled L-proline and the natural-abundance D-proline. The aliphatic peaks show the correct relative amount of each crystal form because the aliphatic carbons are natural abundance in both D- and L-proline molecules. In contrast, the carbonyl signal is due predominantly to the isotopic ^{13}C label
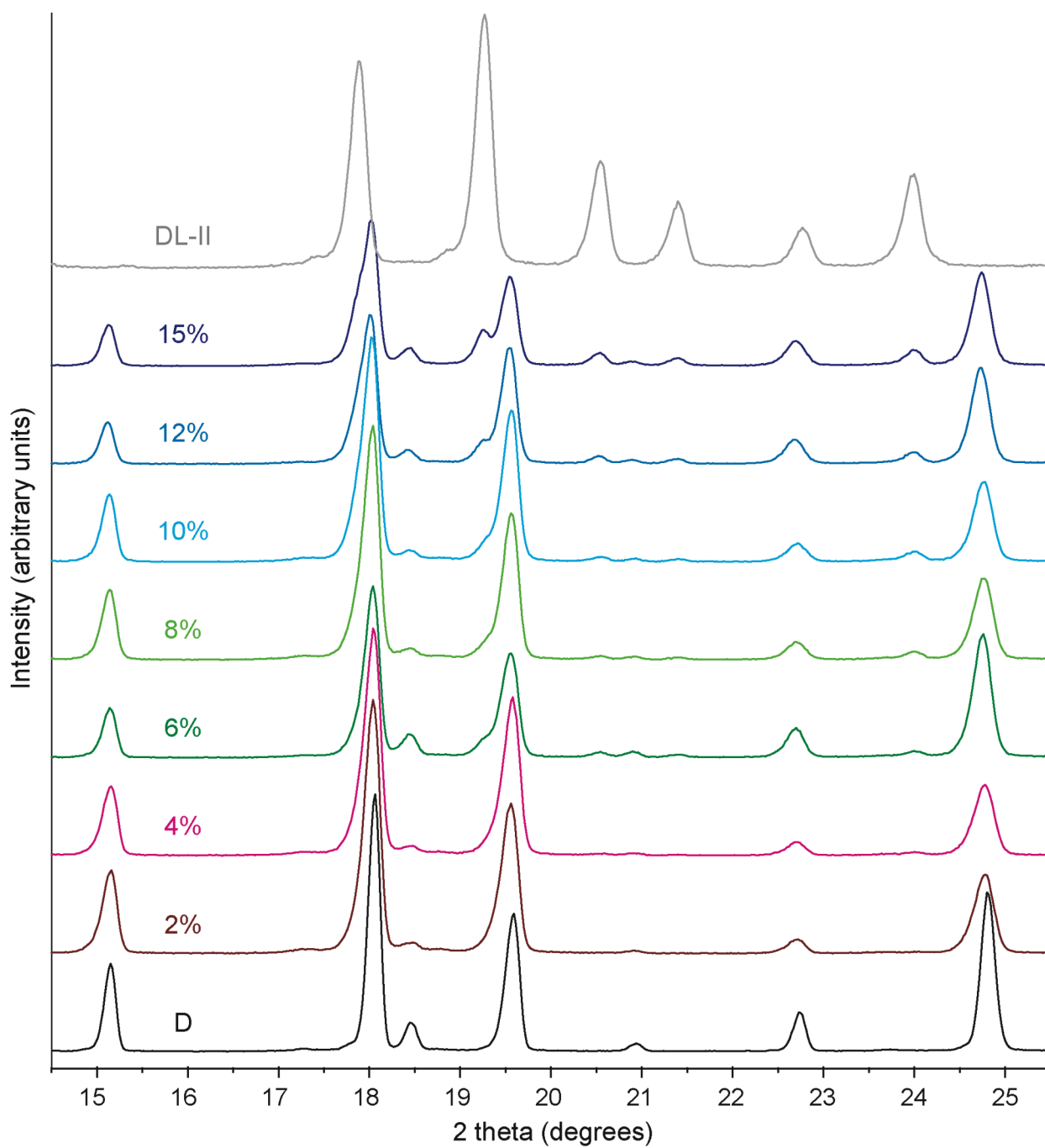
Figure 4.6. Overlay of PXRD patterns for lyophilized samples of D-proline (D) and 2–15% L-proline, along with the reference pattern of DL-proline form II (DL-II).
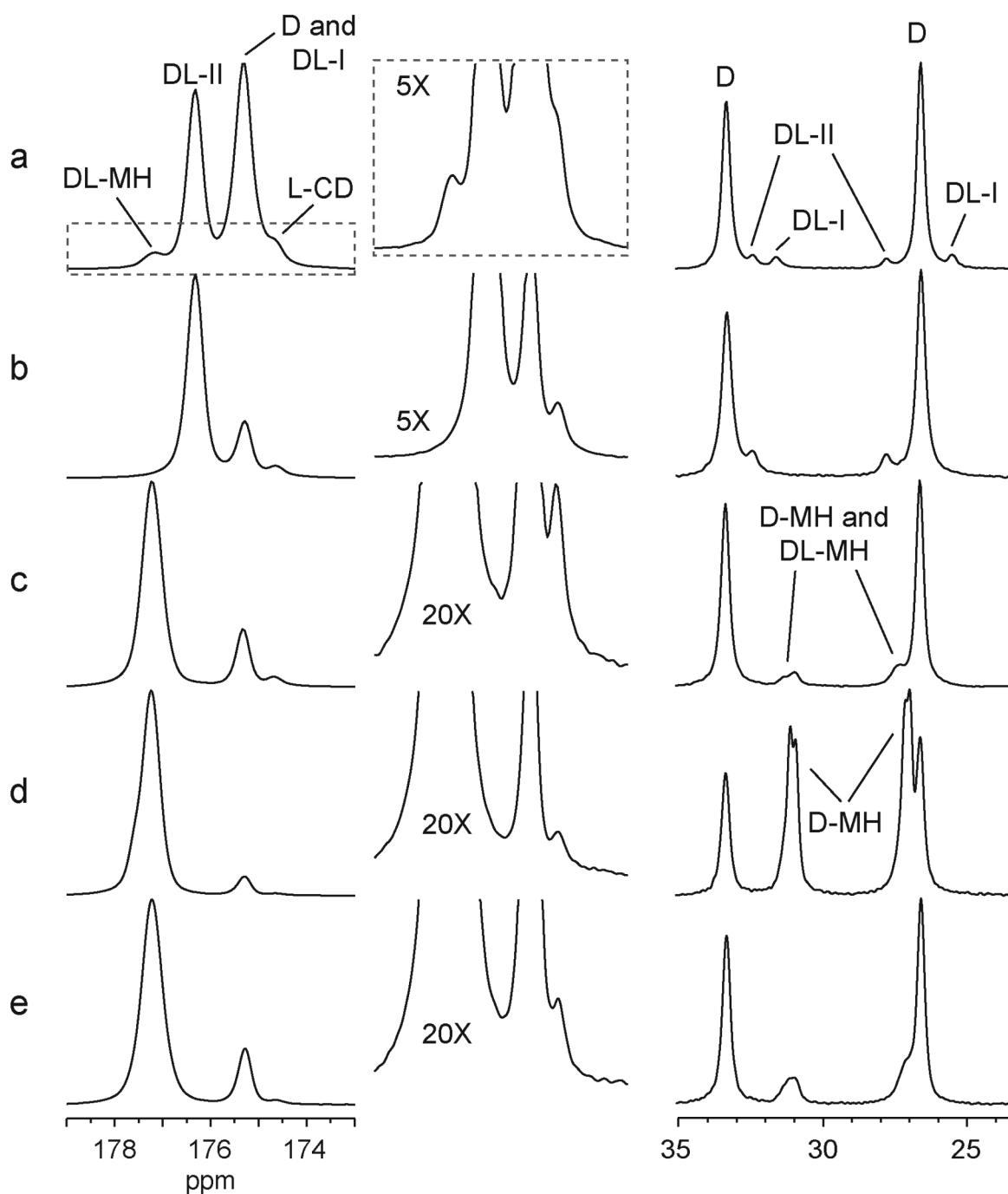
Figure 4.7. Carbonyl and aliphatic regions of ^{13}C CP-MAS NMR spectra of lyophilized 6% L-[1-^{13}C]proline in D-proline a) immediately after lyophilization; b) upon exposure of (a) to elevated temperature (max: 180ºC, 45 min); and c)–e) progressive exposure of (a) to 45% RH, 30ºC, 2 hr; then 60% RH, 30ºC, 1 hr; and lastly ambient RH, 30ºC, 3 hr. The carbonyl region is vertically expanded to better observe changes in the L-CD peak (174.7 ppm), which decreases upon hydration of D to D-MH (d).

of the L-proline impurity, and the enhanced signal due to this label must be taken into account when calculating the relative amounts of each form.

In the freshly prepared sample (Figure 4.7a) the 174.7-ppm peak is present, along with racemic compounds DL-I, II, and MH. This sample was separated into two groups, and each was exposed to different conditions:

1) Elevated temperature (Figure 4.7b) via variable-temperature SSNMR. This was done in order to assess the thermal stability of the 174.7-ppm peak, as well as to determine if this peak corresponded to the presence of a thermal degradant of proline.

2) Increased relative humidity (Figures 4.7c–e) to explore the effect of sample hydration on the presence of the 174.7-ppm peak.

The spectrum in Figure 4.7b corresponds to a sample treated to a stepwise increase in temperature, up to a maximum of 180ºC for 45 min. Spectra were acquired during the course of this thermal treatment (not shown), during which DL-MH and DL-I transformed completely to DL-II, as observed by the decrease in the 177.2- and 175.3-ppm peaks and the disappearance of the DL-I aliphatic peaks at 31.0 and 24.2 ppm. However, the 174.7-ppm peak decreased only slightly from ~4.3% to 3.2% of the total area in the carbonyl region.   More extensive heating of the sample resulted in degradation, as observed by a broad peak at 166.5 ppm in the SSNMR spectrum (not shown), as well as visible browning of the sample. The relative thermal stability of the 174.7-ppm peak suggests that it does not represent an unstable polymorphic phase. The lack of growth also indicates that it cannot be attributed to a thermal degradant.

Analyses of the sample upon exposure to elevated RH are shown in Figure 4.7c–e. Differences in water vapor sorption rates among crystal forms permitted selective hydration of the racemic versus enantiopure phases. Exposure of the sample to 45% RH, 30°C, for 2 hr (Figure 4.7c) resulted in complete conversion of the racemic cocrystal forms DL-I and II to the monohydrate form, DL-MH, while only a small amount of the D-proline converted to D-MH, as evidenced by changes in both carbonyl and aliphatic peaks in Figure 4.7c relative to the initial sample (Figure 4.7a). Deconvolution of the peak areas in the carbonyl region showed that the 174.7-ppm peak remained relatively unchanged. This supports the conclusion that the 174.7-ppm peak does not correspond to an environment within either DL-I or II, as it would be expected to change/disappear if it were associated with these racemic cocrystal phases. Upon exposing the sample to 60% RH, 30°C (Figure 4.7d), the D-proline began to hydrate to D-MH, and a significant decrease in the 174.7-ppm peak was observed. This supports the hypothesis that the 174.7-ppm peak corresponds to L-proline molecules trapped within the D-proline matrix, as a change in this peak would be expected as the D-proline goes through a form conversion. The sample was partially dried to convert D-MH back to the anhydrous D form while maintaining hydration of the racemic forms (Figure 4.7e). Although the anhydrous D-proline peak increased, the 174.7-ppm peak did not return to the pre-hydrated level but remained at the same level as was observed in Figure 4.7d. This data suggests that increased mobility during the hydration of the D-proline host lattice allows L-CD molecules to be essentially pushed out. It is important to note that the 174.7-ppm peak is present within Figure 4.7d, although at a lower level than in the initial sample.

This means that "seeds" of this environment existed and could have facilitated growth of this peak during dehydration if it corresponded to a distinct polymorphic form.

4.3.7 *Formation of chiral defects via grinding*

All of the aforementioned preparation methods involved crystallizing mixtures of the two proline enantiomers from aqueous solution. Theoretically, though, it should be possible to produce chiral defects in the absence of water by grinding the enantiomers together to form a molecular dispersion. In order to further investigate the potential role of water in the formation of the 174.7-ppm L-CD peak, a sample of 6% L-proline was prepared by cryogrinding.

Figure 4.8 shows variable-temperature ^{13}C CP-MAS NMR spectra of a cryoground physical mixture of 6% L-[1-^{13}C]proline and 94% D-proline. As in Figure 4.7, these are not subtracted spectra, so the aliphatic peaks are indicative of the true relative amounts of each form, and the carbonyl signal is "biased" toward the L-[1-^{13}C]proline impurity. Immediately following cryogrinding (Figure 4.8, 20ºC, top spectrum), the carbonyl region contained a broad, amorphous-like peak that overlapped a crystalline peak located at the chemical shift of enantiopure proline (175.3 ppm), which suggested the presence of both amorphous and residual crystalline material. Progressively raising the temperature resulted in the growth of two additional crystalline peaks at 174.7 ppm (L-CD) and 176.3 ppm (DL-II). At even higher temperatures, the DL-II peak continued to grow, eventually resulting in a spectrum very similar to that of a lyophilized sample (Figure 4.3). These crystallization events likely mirror a proline enantiomer eutectic phase diagram, where the dominant D-enantiomer initially

153
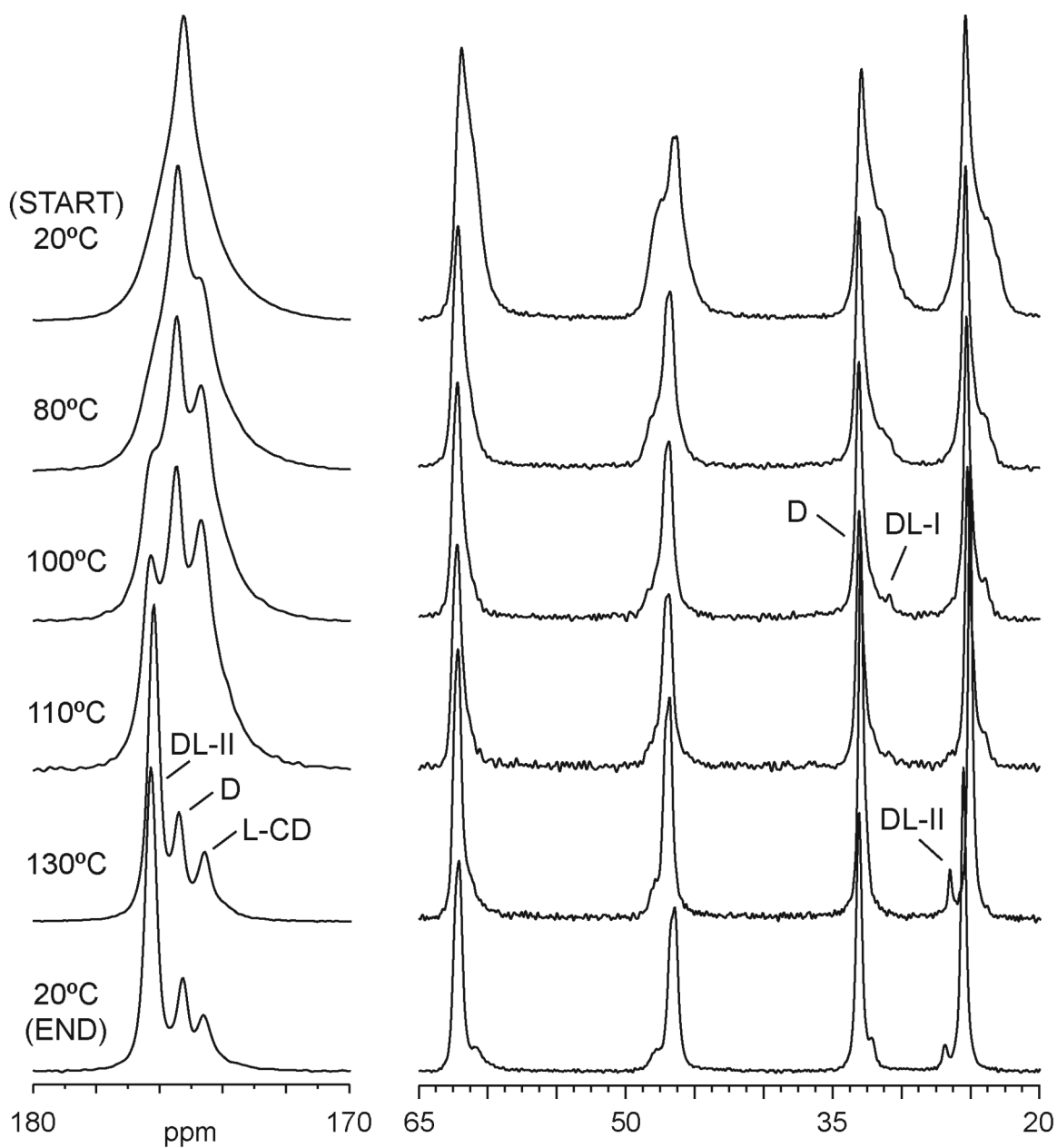
Figure 4.8. Variable-temperature ^{13}C CP-MAS NMR spectra of cryoground 6% L-[1-^{13}C]proline in D-proline collected at 10ºC intervals (representative spectra shown).

154

crystallizes to form the enantiopure lattice, therein "concentrating" the L-proline impurity until the system reaches its eutectic, which crystallizes to form DL-II (176.3-ppm peak). Due to restricted mobility within the solid state, not all of the L-proline molecules are excluded from the D-proline crystal lattice, resulting in the formation of chiral defects (174.7-ppm peak), followed by crystallization of the remaining L-proline impurity into the racemic cocrystal.

4.3.8   Variable-temperature SSNMR

In an effort to further characterize the L-CD peak, variable-temperature SSNMR was performed.   It is well established that crystals contract and expand upon cooling/heating.[28]   The magnitude and direction of these contractions/expansions depend on the molecular packing and conformation within the crystal lattice, and this can be observed in the CP-MAS NMR spectrum.   While one crystal form may exhibit a downfield peak shift upon increasing temperature, another crystal form may exhibit the opposite shift.   Thus, varying the temperature in SSNMR can be used to improve resolution between peaks, as well as to identify different phases: Two different crystal forms may have a peak at the same location, but they may differ in their temperature-dependent peak shifts.   Investigations of proline polymorphism showed linear correlations between temperature and peak position for all known crystalline forms, and the slopes of the correlations were different for each form (§ 6.3.1).

The plot in Figure 4.9 illustrates the temperature dependence of peak shifts for the L-CD peak of lyophilized and cryoground samples.   While peaks corresponding to D-proline (and all other known crystal forms) undergo peak shifts linearly as the

155
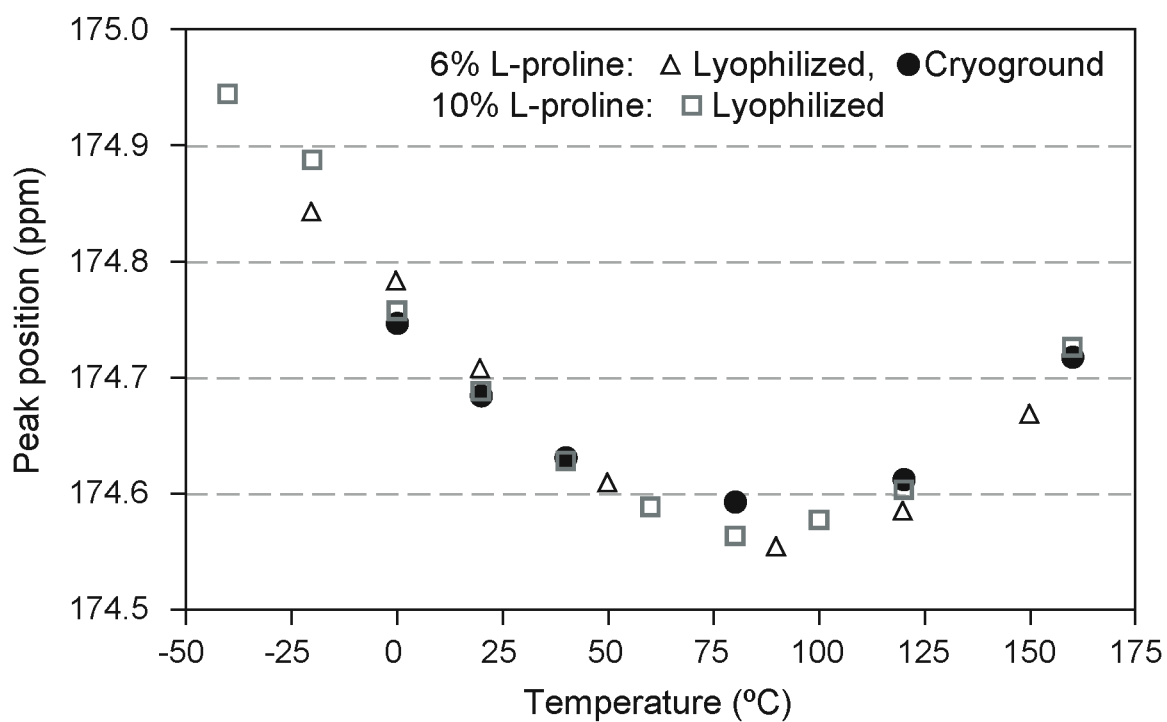
Figure 4.9. A plot of the ^{13}C CP-MAS NMR peak position of the L-CD peak as a function of temperature. The plot is a compilation of data corresponding to three different samples: lyophilized 6 and 10% L-proline, and cryoground 6% L-proline.

temperature increases, the L-CD peak initially shifts to lower ppm values, reaches a minimum at ~80ºC, then begins to shift to higher ppm values. Although this strange temperature dependence does not necessarily support the assignment of this peak to a chiral defect, it demonstrates a distinct crystallographic environment that differs substantially from other crystalline forms of proline.

4.4   Discussion

4.4.1   *Identification of chiral defects*

Identifying and characterizing chiral defects is extremely difficult due to their low concentrations and multiple crystalline forms that potentially mask the defects themselves.[2,3] Currently, there is no single experiment that can be performed in order to prove that the 174.7-ppm peak observed in ^{13}C CP-MAS NMR spectra corresponds to L-proline chiral defects in the D-proline crystal lattice. However, support for this assignment includes:

Crystallization kinetics. Faster crystallization resulted in higher levels of this peak, whereas it was not observed when crystallization occurred slowly (Figure 4.2).[13]

Concentration. This crystalline environment was present at such a low level that it was only observed when L-proline was isotopically labeled. Additionally, as the overall amount of impurity increased, the level of this environment reached a plateau, indicating "saturation" (Figure 4.4).[1-4]

Relaxation measurements. Both [1]H T_1 and $T_{1\rho}$ measurements for D-proline and the 174.7-ppm peak are the same, regardless of L-proline concentration or the crystallization method, indicating that the forms are possibly intimately mixed, not phase

separated.[23,24] Although it is possible for two different phases to coincidentally have the same relaxation values, all other observed proline crystal forms have relaxation values that differ from each other.

Thermal stability. No significant change in the level of this peak occurred as the temperature was increased to the point of observable thermal decomposition. However, polymorphic transformation of DL-I to DL-II was observed (Figure 4.7a–b). This suggests that the 174.7-ppm peak does not correspond to a metastable polymorphic form.

Stability against hydration. The 174.7-ppm peak did not appreciably decrease until hydration of the D-proline phase began, which occurred after the racemic cocrystal phases had transformed to the monohydrate form (Figure 4.7a, c–e). This is consistent with L-proline defects in the D-proline lattice, since such defects should not be affected until the surrounding D-proline host lattice undergoes hydration-related changes.

Formed in absence of water/solvent. The 174.7-ppm peak was observed in samples prepared by cryogrinding the enantiomers (under dry nitrogen gas) to the point of forming amorphous material, followed by crystallization (Figure 4.8). The ability to create this environment in the absence of water/solvent suggests that this peak does not correspond to the presence of a hydrate or molecules interacting with trapped pockets of water. Although these results indicate that the 174.7-ppm peak does not correspond to a hydrate, there are no water content measurements to support this. Water content measurements were performed by TGA. If the hydrate corresponded to a thermally stable form, in which dehydration did not occur until melting or degradation, weight loss due to waters of hydration would be obscured by weight loss from the sublimation/degradation of proline.

Disappearance but no growth. In all samples, growth of the 174.7-ppm peak was never observed, despite exposure to a wide range of temperatures (-40–160ºC) and various relative-humidity environments. However, reduction in the peak was observed upon exposure to high relative humidity. These results indicate that the peak does not correspond to a degradation product or a more thermodynamically favorable polymorph.

4.4.2   *Local environment of chiral defects*

It is interesting that the L-CD peak is a distinct, narrow crystalline peak. One might expect more disorder around a defect site due to the presence of multiple molecular conformations or the presence of void space within the crystal lattice. Such disorder is typified as producing a broader, amorphous-like SSNMR peak. Observing this single crystalline peak indicates that L-proline defects exist in one specific conformation within the D-proline lattice. This conformation, and its relationship to the conformation of D-proline molecules within the same lattice, likely mirror the packing of the enantiomers in a racemic cocrystal. Structural elucidation of the defect site was attempted using the SSNMR FIREMAT experiment.[29-31] Unfortunately, the relatively low level of the L-CD peak and the proximity of much larger peaks proved to be too limiting. Interestingly, another very small peak is observed in the spray-dried sample (Figure 4.2). This additional peak at ~173.7 ppm may correspond to the presence of neighboring L-proline defects in the D-proline crystal lattice. The L-CD peak is very large in this sample, likely a result of the very rapid crystallization process. With such a large amount of chiral defects in the sample, it seems logical that some of the defects will be located near each other in the crystal lattice.

4.4.3   Effect of chiral defects on pharmaceutically relevant properties

The proline system demonstrates the potential complexity associated with the analysis of a solid chiral product.   The possibility of multiple phases, including cocrystals, hydrates, polymorphs, and defects, makes identification and characterization of each individual component very difficult.   This is particularly true for chiral defects, which could not be produced without forming additional phases, and the properties of which could easily be masked by or improperly attributed to the presence of these other components.

In these studies, several attempts were made to simplify the system in order to facilitate selective analysis of chiral defects.   Ideally, it would be possible to physically separate the chiral-defect–containing crystals from all other phases for further analysis, such as water vapor sorption measurements[32] or dissolution testing.   Selective hydration of the racemic compounds (Figure 4.7) proved helpful for improving resolution in SSNMR spectra, and selective sublimation[33] of the racemic form was attempted, but unsuccessful due to negligible differences between lyophilized DL- and D-proline sublimation rates.   Thus, it was not possible to selectively determine the effect of L-proline chiral defects on the physicochemical properties of D-proline.   The selection of future compounds for the study of chiral defects might include large differences in sublimation/dissolution rate or density[34] between cocrystal and enantiopure forms.   This would provide the possibility for physically separating the chiral-defect–containing phase without destroying the solid-state information that gives rise to the pharmaceutically relevant physicochemical properties of interest.

4.5   Conclusions

In this chapter, we provided evidence for the identification and quantitation of the crystallographic locations of small amounts of one enantiomer (L) in the presence of predominantly the opposite (D) enantiomer upon concurrent. Results show that L-proline was incorporated in up to four different crystalline forms, which potentially included kinetically trapped substitutional chiral defects within the D-proline crystal lattice. The amount of this L-proline chiral defect was quantitated in lyophilized samples and found to exist up to a 1.4% level in the D-proline host crystal upon concurrent lyophilization of both enantiomers. This is the first solid-state observation and quantitation of chiral defects incorporated into a three-dimensional crystal lattice of an enantiopure system.[35,36]

Solid-state NMR spectroscopy (SSNMR) was highly suited for investigating this chiral system in the solid state. Different crystal forms, including chiral defects, gave rise to different peaks in SSNMR spectra. Isotopic labeling, combined with spectral subtraction, allowed for identification and relative quantitation of the various forms, and relaxation measurements were able to confirm phase separation.

4.6 References

1. Go J, Grant DJW 1987. Locating the impurity in doped crystals using isotopic double labeling and a column "flow-through" dissolution cell: adipic acid doped with oleic acid. Int J Pharm 36(1):17-28.

2. Duddu SP, Fung FKY, Grant DJW 1993. Effect of the opposite enantiomer on the physicochemical properties of (-)-ephedrinium 2-naphthalenesulfonate crystals. Int J Pharm 94(1-3):171-179.

3. Duddu SP, Fung FKY, Grant DJW 1996. Effects of crystallization in the presence of the opposite enantiomer on the crystal properties of (SS)-(+)-pseudoephedrinium salicylate. Int J Pharm 127(1):53-63.

4. Li ZJ, Grant DJW 1996. Effects of excess enantiomer on the crystal properties of a racemic compound: ephedrinium 2-naphthalenesulfonate. Int J Pharm 137(1):21-31.

5. Jacques J, Collet A, Wilen SH 1981. Enantiomers, Racemates, and Resolutions. ed., New York: Wiley.

6. Wang Y, Chen AM 2008. Enantioenrichment by crystallization. Org Process Res Dev 12(2):282-290.

7. Coquerel G 2006. The 'structural purity' of molecular solids - elusive concept? Chem Eng Process 45(10):857-862.

8. Ahuja S 2007. Assuring quality of drugs by monitoring impurities. Adv Drug Delivery Rev 59(1):3-11.

9. Byrn SR, Pfeiffer RR, Stephenson G, Grant DJW, Gleason WB 1994. Solid-state pharmaceutical chemistry. Chem Mater 6(8):1148-1158.

10. Zell MT, Padden BE, Paterick AJ, Hillmyer MA, Kean RT, Thakur KAM, Munson EJ 1998. Direct observation of stereodefect sites in semicrystalline poly(lactide) using 13C solid-state NMR. J Am Chem Soc 120(48):12672-12673.

11. Munson EJ, Carlson LK, Jorvig JE, Zell MT, Abbott J, Hillmyer MA 2003. Determining stereodefect locations in polylactide using solid-state NMR spectroscopy. Polym Prepr 44(1):325-326.

12. Lubach JW, Munson EJ 2006. Solid-state NMR spectroscopy. In Hilfiker R, editor, Polymorphism. Weinheim: Wiley-VCH. p 81-93.

13. Gu C-H, Grant DJW 2002. Relationship between particle size and impurity incorporation during crystallization of (+)-pseudoephedrine hydrochloride, acetaminophen, and adipic acid from aqueous solution. Pharm Res 19(7):1068-1070.

14. Pines A, Gibby MG, Waugh JS 1973. Proton-enhanced NMR of dilute spins in solids. J Chem Phys 59(2):569-590.

15. Metz G, Wu X, Smith SO 1994. Ramped-amplitude cross polarization in magic-angle-spinning NMR. J Magn Reson, Ser A 110(2):219-227.

16. Andrew ER, Bradbury A, Eades RG 1959. Removal of dipolar broadening of nuclear magnetic resonance spectra of solids by specimen rotation. Nature 183:1802-1803.

17. Fung BM, Khitrin AK, Ermolaev K 2000. An improved broadband decoupling sequence for liquid crystals and solids. J Magn Reson 142(1):97-101.

18. Dixon WT, Schaefer J, Sefcik MD, Stejskal EO, McKay RA 1982. Total suppression of sidebands in CPMAS carbon-13 NMR. J Magn Reson 49(2):341-345.

19. Barich DH, Gorman EM, Zell MT, Munson EJ 2006. 3-Methylglutaric acid as a 13C solid-state NMR standard. Solid State Nucl Magn Reson 30(3-4):125-129.

20. Bielecki A, Burum DP 1995. Temperature dependence of 207Pb MAS spectra of solid lead nitrate. An accurate, sensitive thermometer for variable-temperature MAS. J Magn Reson, Ser A 116(2):215-220.

21. Offerdahl TJ, Salsbury JS, Dong Z, Grant DJW, Schroeder SA, Prakash I, Gorman EM, Barich DH, Munson EJ 2005. Quantitation of crystalline and amorphous forms of anhydrous neotame using 13C CPMAS NMR spectroscopy. J Pharm Sci 94(12):2591-2605.

22. McBride JM 1989. Symmetry reduction in solid solutions: a new method for materials design. Angew Chem 101(3):391-393.

23. Campbell GC, VanderHart DL, Feng Y, Han CC 1992. Proton NMR study of the intimacy of mixing in a hydrogen-bonded blend of polystyrene and poly(butyl methacrylate). Macromol 25(8):2107-2111.

24. Zumbulyadis N, Antalek B, Windig W, Scaringe RP, Lanzafame AM, Blanton T, Helber M 1999. Elucidation of polymorph mixtures using solid-state 13C CP/MAS NMR spectroscopy and direct exponential curve resolution algorithm. J Am Chem Soc 121(49):11554-11557.

25. Aso Y, Yoshioka S, Miyazaki T, Kawanishi T, Tanaka K, Kitamura S, Takakura A, Hayashi T, Muranushi N 2007. Miscibility of nifedipine and hydrophilic

polymers as measured by 1H-NMR spin-lattice relaxation. Chem Pharm Bull (Tokyo) 55(8):1227-1231.

26. Stahly GP, McKenzie AT, Andres MC, Russell CA, Byrn SR, Johnson P 1997. Determination of the optical purity of ibuprofen using X-ray powder diffraction. J Pharm Sci 86(8):970-971.

27. Zhang GGZ, Paspal SYL, Suryanarayanan R, Grant DJW 2003. Racemic species of sodium ibuprofen: Characterization and polymorphic relationships. J Pharm Sci 92(7):1356-1366.

28. Lee EH, Smith DT, Fanwick PE, Byrn SR 2010. Characterization and anisotropic lattice expansion/contraction of polymorphs of tenofovir disoproxil fumarate. Cryst Growth Des 10(5):2314-2322.

29. Harper JK, Mulgrew AE, Li JY, Barich DH, Strobel GA, Grant DM 2001. Characterization of stereochemistry and molecular conformation using solid-state NMR tensors. J Am Chem Soc 123(40):9837-9842.

30. Song Z, Antzutkin ON, Rupprecht A, Levitt MH 1996. Order-resolved sideband separation in magic-angle-spinning NMR. 31P NMR of oriented DNA fibers. Chem Phys Lett 253(3,4):349-354.

31. Alderman DW, McGeorge G, Hu JZ, Pugmire RJ, Grant DM 1998. A sensitive, high resolution magic angle turning experiment for measuring chemical shift tensor principal values. Mol Phys 95(6):1113-1126.

32. Guerrieri P, Salameh AK, Taylor LS 2007. Effect of small levels of impurities on the water vapor sorption behavior of ranitidine HCl. Pharm Res 24(1):147-156.

33. Soloshonok VA, Ueki H, Yasumoto M, Mekala S, Hirschi JS, Singleton DA 2007. Phenomenon of optical self-purification of chiral non-racemic compounds. J Am Chem Soc 129(40):12112-12113.

34. Mastai Y, Voelkel A, Coelfen H 2008. Separation of racemate from excess enantiomer of chiral nonracemic compounds via density gradient ultracentrifugation. J Am Chem Soc 130(8):2426-2427.

35. Fasel R, Parschau M, Ernst K-H 2006. Amplification of chirality in two-dimensional enantiomorphous lattices. Nature 439(7075):449-452.

36. Weissbuch I, Lahav M, Leiserowitz L, Meredith GR, Vanherzeele H 1989. Centrosymmetric crystals as host matrices for second-order optical nonlinear effects. Chem Mater 1(1):114-118.

Chapter 5

Production and Stabilization of Frustrated Chiral Crystals:

Lyophilizing Enantiomers of Proline and Maintaining Dry Conditions

5.1   Introduction

In this chapter, we report further characterization of the solid-state crystallization of proline enantiomers by lyophilization. Specifically, the purpose of these additional studies is to elucidate the mechanism of DL-proline form I versus form II crystallization, which was previously shown to depend upon both the crystallization method and the ratio of L- and D-proline in the system.

5.1.1   Lyophilization of proline enantiomers

Chapter 3 showed that lyophilization of solutions that contained non-racemic ratios of proline enantiomers resulted in the formation of a more thermodynamically stable form of the racemic cocrystal, DL-proline form II (DL-II). This was only observed upon crystallization by lyophilization; crystallization from solution only produced the metastable form, DL-proline form I (DL-I). The hypothesized explanation for these observations is that crystallization of the racemic cocrystal in the solid-state lyophilization process is slowed by the presence of enantiomeric excess, which acts as a physical barrier between DL-proline pairs during the crystallization process. This slowed the crystallization and allowed formation of the thermodynamic product (DL-II) instead of the kinetic product (DL-I).

If this hypothesis were true, then we should be able to observe the "frustrated" state, in which the racemic cocrystal DL-pairs and D-proline molecules cannot

168

completely separate from one another in order to form their own thermodynamically stable crystal lattices. However, no such amorphous or disordered state was observed. The purpose of the work in this chapter was to determine whether or not an amorphous/disordered state existed in the lyophilized proline samples.

5.1.2 *Role of water in sample mobility and crystallization*

The process of lyophilization often results in the formation of amorphous materials. However, among lyophilized proline samples, no amorphous phase was observed. The absence of an amorphous phase may have resulted from crystallization of the samples prior to analysis.

It has been well established that the presence of water can assist the crystallization of amorphous/disordered materials due to plasticization or increased lattice mobility.[1,2] Among previous lyophilized proline samples, DL-proline monohydrate (DL-MH) was often observed (Figure 3.7), demonstrating the presence and involvement of water. This water could have facilitated crystallization of an amorphous proline phase and produced the observed DL-MH form in the process. Therefore, it is possible that the lyophilization of proline produced amorphous material that was not observed during analysis because water-assisted crystallization had already taken place.

The previous method for lyophilizing samples (outlined in Chapter 3) included purging the vacuum of the lyophilizer chamber with ambient air following completion of the recipe. The samples were then removed from the lyophilizer and packed into SSNMR and PXRD sample holders at ambient laboratory conditions. Exposure of these samples to ambient conditions could have allowed the samples to sorb water vapor,

therein facilitating crystallization of various forms, including the observed DL-MH phase.

Rapid water vapor sorption is feasible for these lyophilized proline samples. Previous water vapor sorption analysis (Figure 3.8) shows formation of DL-MH at a relatively low RH (<35% RH, 25ºC), indicating that DL-proline is innately hygroscopic. Additionally, Zografi and coworkers have shown that disordered and amorphous crystalline materials have an increased tendency to sorb water vapor.[3] Lyophilized proline samples possessed crystal-lattice disorder, observed as increased peak width in PXRD analyses (Figure 3.11), perhaps resulting in an even greater tendency to absorb water vapor.

In order to prevent the possible sorption of water vapor following the lyophilization process, and potentially observe an amorphous proline phase, samples of 25–50% L-proline were prepared as before, but the vacuum was purged with nitrogen gas instead of ambient air. Additionally, the samples were promptly moved to a dry nitrogen glove box, where they were packed into sample holders for SSNMR, PXRD, and DSC analysis. By preventing water-assisted crystallization of lyophilized proline, we hoped to gain further insight into the solid-state crystallization process of proline enantiomers by lyophilization and the role that water vapor might play.

5.2   Experimental

5.2.1   Bulk materials

L- and DL-proline were purchased from Alfa Aesar (Ward Hill, MA), D-proline was purchased from Sigma-Aldrich (St. Louis, MO), and uniformly ^{13}C labeled L-proline was

purchased from Cambridge Isotope Laboratories, Inc. (Andover, MA). All amino acids were used as received.

5.2.2 Sample preparation

N₂-Lyophilization. Solutions of various L-proline to D-proline ratios were prepared as above, at final concentrations of 0.6% w/v. The solutions were then lyophilized in 10-mL aliquots (within 20-mL scintillation vials) using a bench top freeze dryer (VirTis AdVantage; VirTis; Gardiner, NY). The lyophilization cycle was 32 hr (-35, -5, 5, 15, and 25°C; for 2, 8, 6, 6, and 10 hr, respectively) with an initial 2-hr freezing step (-35ºC) and a vacuum set point of 90 mTorr. Upon completion of the lyophilization recipe, the vacuum was released by purging the sample chamber with compressed nitrogen gas. Following the lyophilization cycle, samples were immediately transferred to a dry nitrogen glove box for all subsequent storage, preparation, and packing of sample holders/DSC pans.

5.2.3 Solid-state NMR spectroscopy

All ^{13}C spectra were acquired on a Chemagnetics CMX-300 spectrometer (Varian, Inc.), operating at 75 MHz for [13]C. All acquisitions included cross polarization (CP),[4,5] magic-angle spinning (MAS)[6] at a rate of 4 kHz (±3 Hz), two-pulse phase modulation (TPPM) or SPINAL64 decoupling[7] at a field strength of ~62–72 kHz, and total sideband suppression (TOSS).[8] A contact time of 2 ms was used for all samples. [1]H T_1 relaxation measurements were performed using a saturation–recovery pulse sequence, and T_1 values were calculated using KaleidaGraph (version 4.01, Synergy) with the equation y =

amp(1-exp(-τ/T_1), where y is the integrated signal intensity, amp is the amplitude constant, τ is saturation–recovery time, and T_1 is the spin–lattice relaxation time. 3-methylglutaric acid (MGA) was used to optimize the spectrometer settings as well as to set the reference frequency.[9] All samples were packed into zirconia rotors with Teflon® or ribbed Kel-F® end caps. Ambient-temperature (~20ºC) experiments were performed using a 7-mm double-resonance MAS probe (Revolution NMR, Inc.; Fort Collins, CO), and variable-temperature experiments were performed with a 7.5-mm double-resonance MAS probe (Varian; Palo Alto, CA), with 3.5-μs and 4.0-μs ^{1}H pulse durations, respectively. Lead nitrate was used for temperature calibration.[10] During variable-temperature experiments, samples were equilibrated at each temperature for at least 15 minutes prior to tuning and data acquisition. The two-dimensional experiment consisted of exchange via spin diffusion and a mixing time of 1 s in order to observe longer-range couplings. The initial t_1 time was 1 μs, and 750 points were collected in each dimension with a sweep width of 15 kHz. Processing included 10 Hz of exponential line broadening in both dimensions.

5.2.4 *Powder X-ray diffraction*

Diffraction patterns were acquired with a Scintag XDS 2000 (Scintag, Inc.; CuKα radiation, 45 kV × 40 mA) with an angular range of 8–40º 2θ, a step size of 0.02º, and a dwell time of 4 sec. Each sample (~100 mg) was quickly packed at ambient conditions into a stainless-steel die. To maintain low relative humidity during analysis, the sample environment was purged with dry air using a previously described assembly.[11]

5.2.5 Differential scanning calorimetry

Differential scanning calorimetry (Q100 DSC; TA Instruments; New Castle, DE) was performed on samples of 3–8 mg that were packed into standard aluminum pans and lightly crimped. Data was collected from room temperature to ~240ºC, with a temperature ramp of 10ºC/min and a 50-mL/min dry nitrogen purge. All samples were analyzed in triplicate.

5.2.6 Thermogravimetric analysis

Sample water content was determined by thermogravimetric analysis (Q50 TGA, TA Instruments; New Castle, DE). Samples of 10–20 mg were heated from room temperature to >300ºC at a rate of 10ºC/min under a 40-mL/min dry nitrogen purge.

5.3 Results

5.3.1 "Dry" lyophilization of various enantiomeric ratios of proline

As described in the introduction, previous preparations of lyophilized proline contained DL-MH, indicating the presence of water within the samples. This water may have been sorbed by the sample after the lyophilization process, during subsequent preparation and sample packing for analysis by SSNMR and PXRD. In order to avoid the potential for such water vapor sorption, proline samples containing a range of enantiomeric ratios were lyophilized in the same manner as previously reported; however, these samples were not exposed to ambient conditions following lyophilization and were kept in a glove box under dry nitrogen gas until analysis by SSNMR and PXRD.

Figure 5.1 shows ^{13}C CP-MAS NMR spectra for samples of 25–50% L-proline prepared by lyophilization and subsequently kept under dry conditions by purging the lyophilizer with nitrogen gas and performing all additional sample preparation/packing within a dry nitrogen glove box. In the 25% L-proline spectrum, the number of peaks and the peak locations are quite different from previous samples (Figure 3.7). Although the peaks in this 25% L-proline sample spectrum appear to be broad, they did not correspond to amorphous proline peaks (Figure 6.8). The apparent breadth in the peaks is likely due to the presence of several overlapping peaks. Interestingly, the carbonyl region contains only two main peaks while there are many (unresolved) peaks for C-3 and C-4. This suggests that the presence of such a large number of crystal forms is largely due to differences in the conformation and packing of the proline ring, while the bonding of the carboxylic acid group is similar among all forms. Whereas it was previously possible to deconvolute peaks based on the peak positions of known crystal forms, in these spectra, there are multiple unknown crystal forms that overlap to such an extent as to prohibit reliable deconvolution. In the 25% L-proline sample, qualitative assessment indicates peaks corresponding to D (33.0 ppm) and DL-I (31.0 ppm). Note that there is a peak located at 32.0 ppm, which typically is characteristic of DL-II; however, DL-II also gives rise to a peak at 26.7 ppm, which is absent in this spectrum. Thus, DL-II is not present in this sample. Peaks for C-2 and C-5 are not shown because these peaks are extremely broad and unresolved due to dipolar coupling with the directly bonded quadrupolar nitrogen.

From a quantitative aspect, Figure 5.1 shows very little signal from enantiopure D-proline (33.0 ppm), regardless of the overall level of L-proline in the sample.
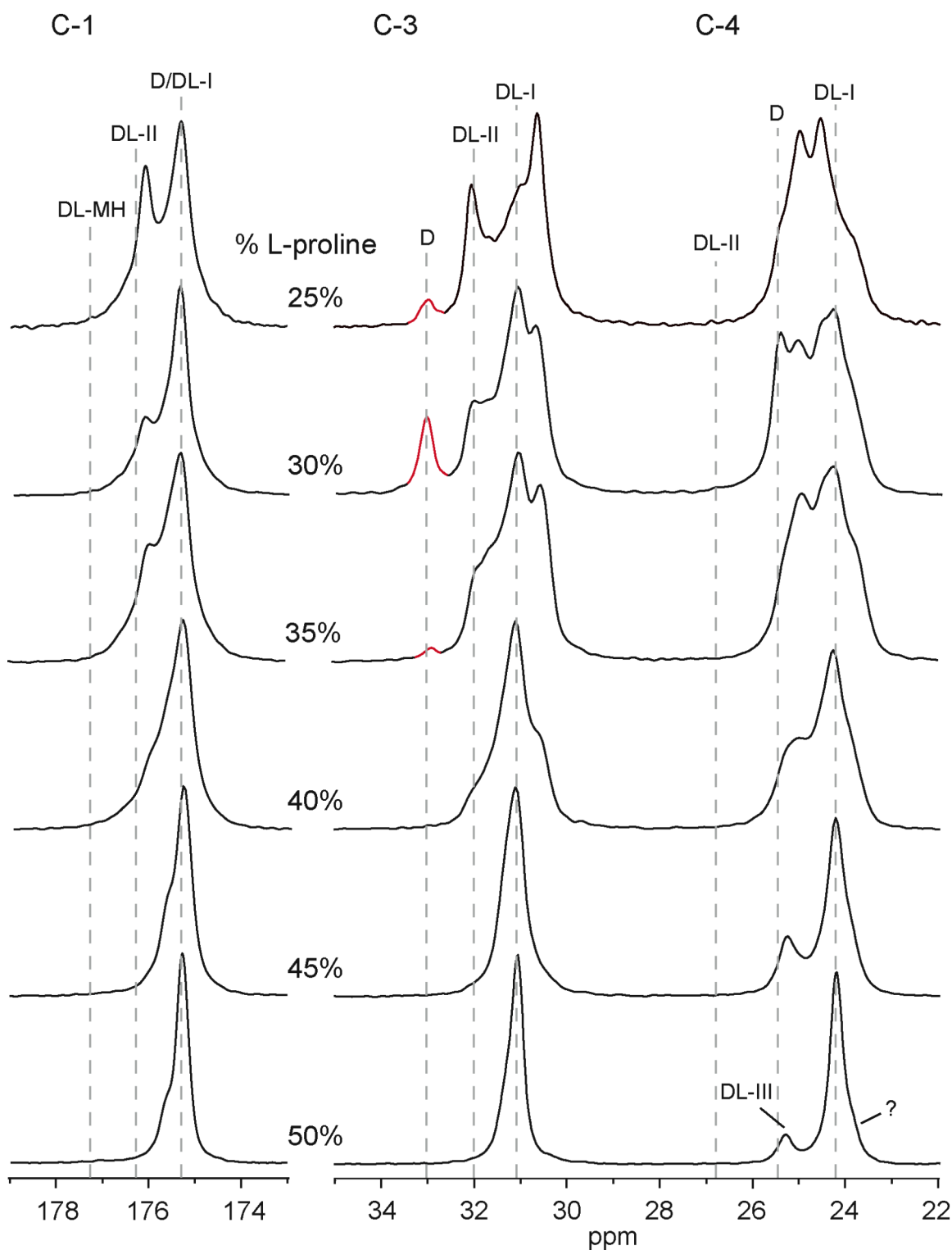
Figure 5.1. ^{13}C CP-MAS NMR spectra of 25–50% L-proline samples prepared by N$_2$-lyophilization. C-1, C3, and C-4 peaks are shown.

Theoretically, at the 25% L-proline level, 50% of the total solid sample should exist in an enantiopure crystal form: the 25% L-proline will pair with 25% D-proline to produce DL-proline, and the excess 50% D-proline will remain. Yet in the spectrum for 25% L-proline in Figure 5.1, the D-proline peak at 33.0 ppm constitutes <10% of the total signal for C-3, suggesting that very little D-proline exists in this sample. In all previous sample preparations (crystallizing from solution and by lyophilization, Chapter 3), the relative peak area of the 33.0-ppm peak was consistent with the theoretical amount of the enantiopure D-proline material. The lack of signal at 33.0 ppm among the spectra of N_2-lyophilized samples suggests that D-proline molecules possess conformations and/or are located within packing environments that differ substantially from those that exist within the known crystal form of enantiopure proline.

As the concentration of L-proline increased (Figure 5.1), fewer overlapping peaks were observed, but resolution among these peaks did not improve. Again, the presence of the D-proline peak at 33.0 ppm was noticeably absent from the spectra at 40 and 45% L-proline. At the 45 and 50% L-proline level, a distinct peak at 25.3 ppm was observed. This peak is attributed to another racemic cocrystal form of DL-proline, denoted DL-proline form III (DL-III), and will be discussed later in this chapter. Additionally, the presence of another unknown form was observed as a shoulder on the DL-I peak at 24.2 ppm. DL-proline monohydrate (characteristic peak at 177.2 ppm) was not detected in any of these samples.

Figures 5.2 and 5.3 show PXRD patterns corresponding to the same samples analyzed by SSNMR in Figure 5.1. The overlay of diffraction patterns in Figure 5.2 was plotted with an expanded y-axis scale in order to look for an amorphous halo. For all N_2-

176
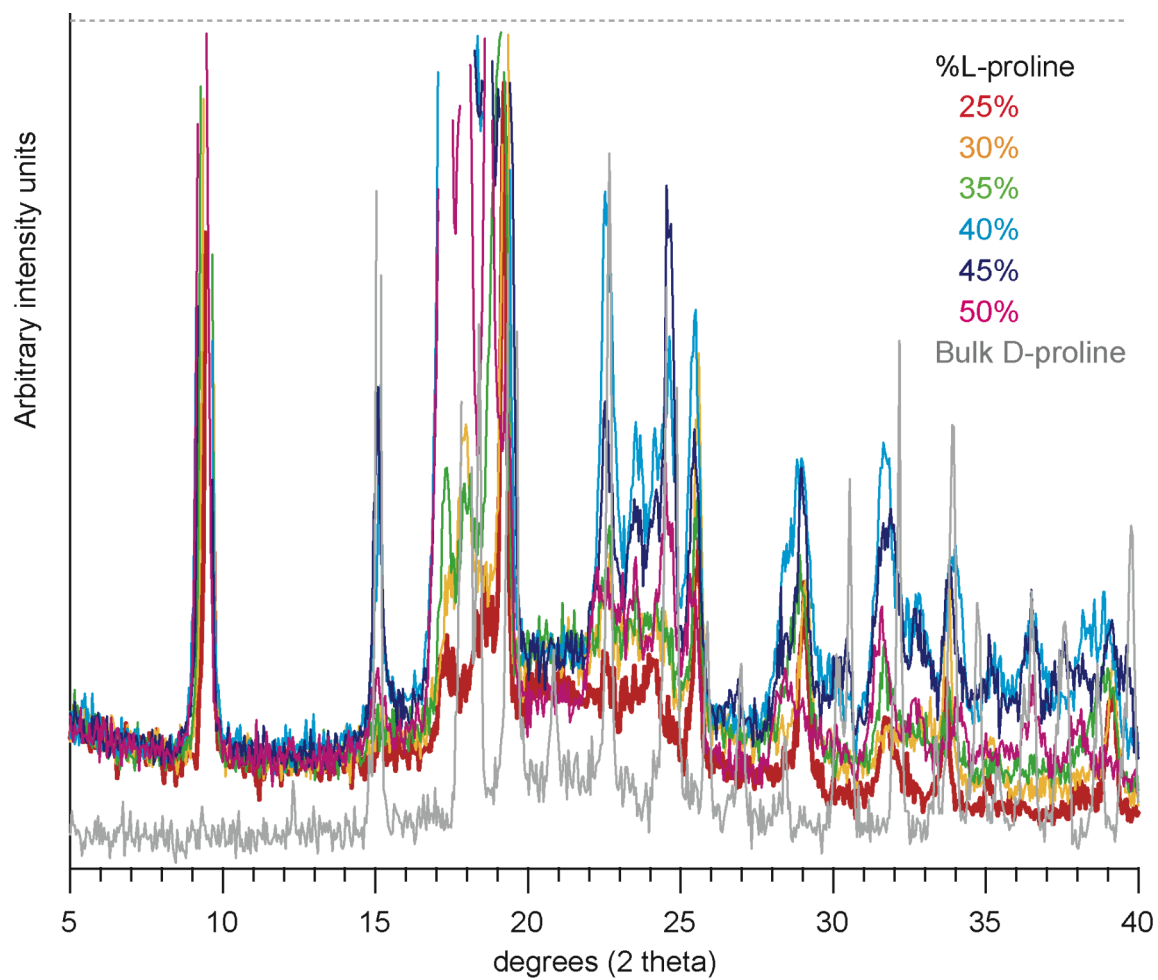
Figure 5.2. PXRD patterns of bulk D-proline and 25–50% L-proline samples prepared by N_2-lyophilization. The tops of diffraction peaks are truncated due to y-axis expansion.
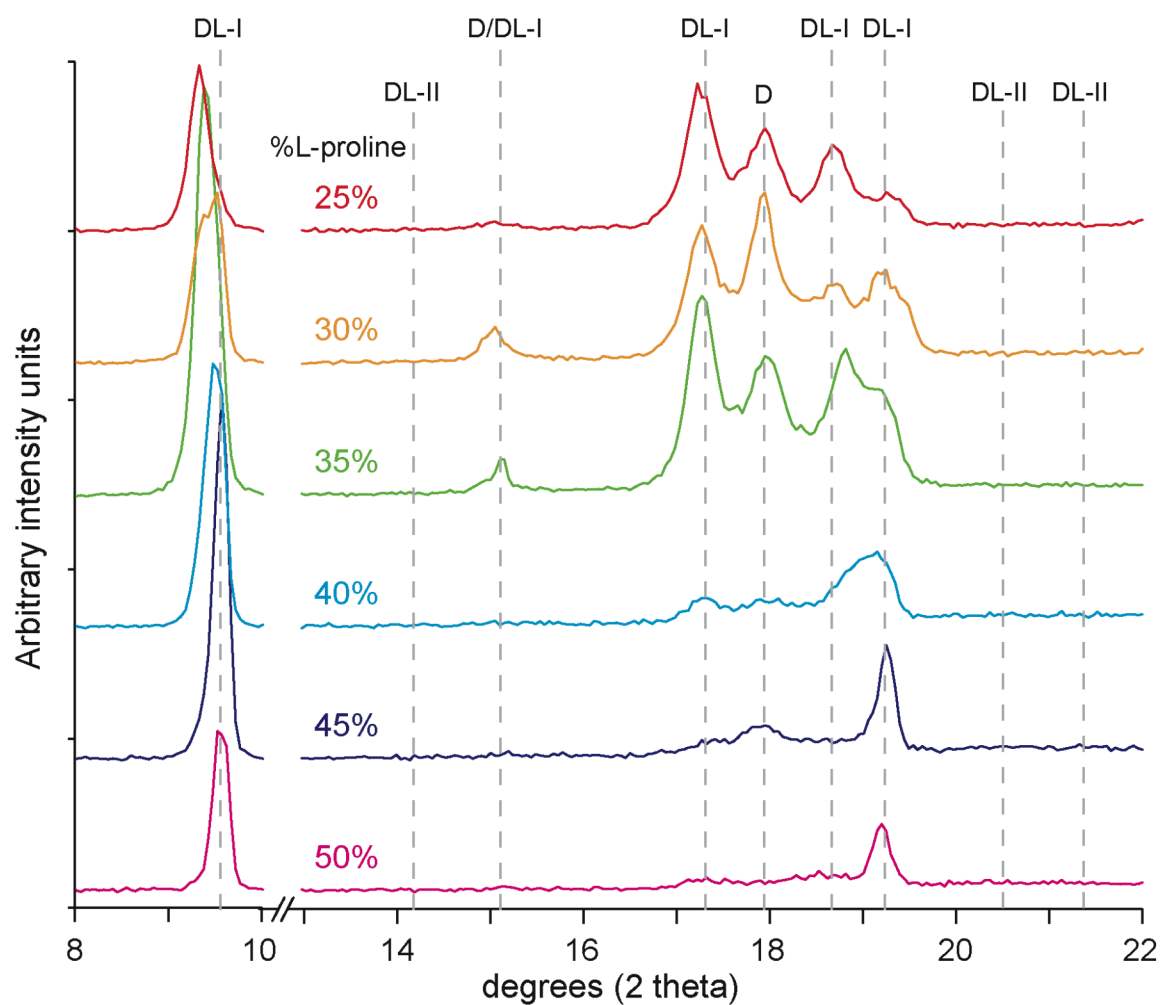
Figure 5.3. PXRD patterns of 25–50% L-proline samples prepared by N$_2$-lyophilization.

lyophilized samples, there is a broad hump centered at ~22° 2θ, which could correspond to an amorphous halo. However, the diffraction pattern of bulk D-proline (bottom pattern, gray) also contains a similar hump at the same location. Due to the fact that PXRD is sensitive to loss of long-range order in the crystal lattice, the hump observed in all of these samples is likely a result of lattice disorder and not the presence of an amorphous phase.[12]

In Figure 5.3, the diffraction patterns from Figure 5.2 are expanded along the x-axis in order to better observe individual peaks. Compared to diffraction patterns of samples prepared from solution (Figure 3.6), the diffraction patterns of N_2-lyophilized proline samples contain broad peaks, which further indicate the presence of lattice disorder in these samples. Samples of 45 and 50% L-proline have diffraction patterns with relatively sharp DL-I peaks at ~9.5 and 19.2° 2θ, but most other peaks are broad, unresolved, and of low intensity. Unlike in the previously lyophilized (ambient purge) samples (Figure 3.11), the usually intense peak at 18° 2θ that corresponds to D-proline was missing or of greatly reduced intensity, consistent with the low levels of D-proline observed in SSNMR spectra. As with SSNMR, PXRD did not indicate the presence of DL-MH (characteristic peak at ~8.7° 2θ).

Both SSNMR and PXRD results suggest the absence of an amorphous phase in any of the N_2-lyophilized proline samples. However, the multiplicity of peaks within the SSNMR spectra indicates the presence of multiple molecular conformations/packing environments within these samples. It is not clear if each peak corresponds to a distinct, phase-separated crystal form, or if they represent a single phase with crystallographic-inequivalence–like disorder. The broad, unresolved peaks in the PXRD patterns could be

consistent with either situation. Typically, ^{1}H T_1 measurements could be used to differentiate between these two possibilities, since differences in T_1 values indicate the presence of multiple phases. However, due to the large degree of overlap among peaks in the SSNMR spectra, it was not possible to accurately and specifically determine the relaxation values for each SSNMR peak. In order to determine whether the multiple peaks in the SSNMR spectra correspond to different crystal forms or to a discrete set of molecular conformations that coexist within a single, disordered phase, a 2D-exchange SSNMR experiment was performed.

5.3.2 *Identifying peaks with 2D-exchange SSNMR*

In a ^{13}C CP-MAS NMR spectrum, the presence of multiple peaks for a particular carbon can indicate the presence of multiple, phase-separated crystal forms, or the presence of crystallographic inequivalence. In a complex spectrum that contains unknown components, such as the N_2-lyophilized proline samples, determining which peaks correspond to distinct (phase-separated) crystal forms versus crystallographic inequivalence may not be possible if there are many overlapping peaks. However, the use of 2D-exchange NMR experiments can provide insight into the intra- and intermolecular connectivity for a molecule within a crystal lattice. This information can be helpful in assigning individual peaks to their respective nuclei in the molecule, or in identifying the number of crystallographically inequivalent sites in the unit cell, as demonstrated by Zell et al. in the characterization of crystallographic inequivalence among polymorphs of aspartame.[13]

For the proline 2D-exchange NMR experiment, a special, isotopically labeled sample of 25% L-proline was prepared by the N_2-lyophilization method. The purpose of a ^{13}C 2D-exchange NMR experiment is to observe the connectivity among carbon nuclei, which provides important information for identifying peaks in the spectrum (e.g., the C-3 peak at 33.4 ppm corresponds to the same crystal form as the C-2 peak at 23.4 ppm.) In order to observe these interactions, which are observed through transfer of magnetization between neighboring nuclei,[14] it is necessary for the molecules to possess neighboring ^{13}C nuclei. Due to the low natural abundance of ^{13}C nuclei (1.1%), the probability of finding neighboring ^{13}C nuclei is very low. Thus, isotopic labeling is necessary for a 2D-exchange experiment. L-proline was purchased uniformly labeled, meaning that all carbon nuclei in the material were ^{13}C (versus the more abundant ^{12}C) nuclei. This type of label is denoted [U-^{13}C] for Uniformly ^{13}C labeled. Of the 25% L-proline present within the N_2-lyophilized sample, 10% was L-[U-^{13}C]proline, and the other 90% was natural-abundance L-proline. Thus, the L-[U-^{13}C]proline composed 2.5% of the total sample. This "dilution" of the U-^{13}C material with natural-abundance proline was necessary to avoid excessive ^{13}C–^{13}C dipolar coupling, which would lead to extremely broad peaks within the SSNMR spectrum.

One of the important parameters of a 2D-exchange NMR experiment is the mixing time. This is the amount of time that nuclei are allowed to "talk" to each other, and it is directly related to the distance between nuclei, where longer mixing times allow for longer-range interactions (couplings). This experiment was performed with a mixing time of 1 s. This was chosen in order to observe couplings of several carbon bond lengths.

Figure 5.4 shows the two-dimensional exchange spectrum (contour plot) for the N$_2$-lyophilized 25% L-proline sample that contained 2.5% L-[U-^{13}C]proline, diluted in a matrix of unlabeled 22.5% L-proline and 75% D-proline. The aliphatic region is expanded in this figure in order to better observe cross peaks, which indicate the presence of coupling between the ^{13}C nuclei. The one-dimensional spectrum of the sample is shown directly above the 2D contour plot, and a spectrum of a fully unlabeled 25% L-proline sample prepared by the same method is shown at the very top. Upon comparing the one-dimensional spectra at the top of the figure, line broadening due to the ^{13}C–^{13}C dipolar coupling in the labeled sample is readily apparent. This line broadening, along with the fact that the ^{13}C spectrum already suffered from poor resolution due to the presence of multiple overlapping peaks, led to the presence of unresolved cross peaks in the 2D spectrum. Thus, although cross peaks were observed, it was not possible to make any peak assignments. Higher spin speeds and decoupling power[13] would be necessary to achieve better resolution of the peaks in the spectrum.

5.3.3   *Thermal analysis*

Figures 5.5 and 5.6 contain DSC thermograms for samples of 25–50% L-proline prepared by the N$_2$-lyophilization method. Figure 5.5 shows the temperature range of 60–210ºC, and the y-axis is expanded to observe very small thermal events. There were no thermal events <70ºC that are characteristic for dehydration of DL-MH or loss of sorbed water. A small exotherm at ~96ºC was observed in all thermograms. This is attributed to a chemical impurity within the DSC cell, as it was also observed in thermograms of ibuprofen samples analyzed immediately prior to these proline samples.
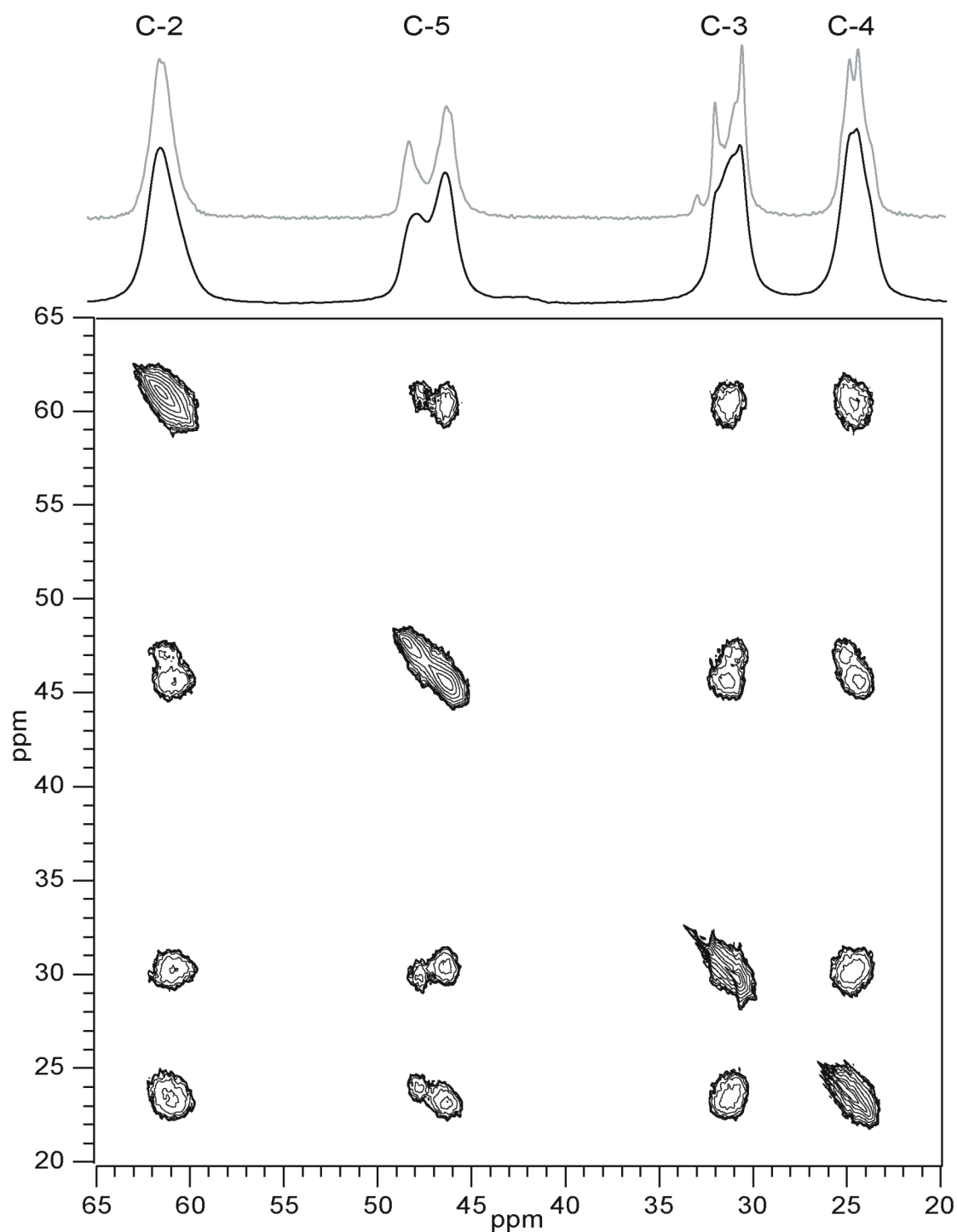
Figure 5.4. Two-dimensional–exchange contour plot of N_2-lyophilized 25% L-proline (2.5% L-[U-^{13}C]proline) acquired with a mixing time of 1 s. The ^{13}C CP-MAS NMR spectra shown at the top of the 2D plot correspond to samples of N_2-lyophilized 25% L-proline that were U-^{13}C labeled (black, used for the 2D-exchange experiment) and unlabeled (gray).
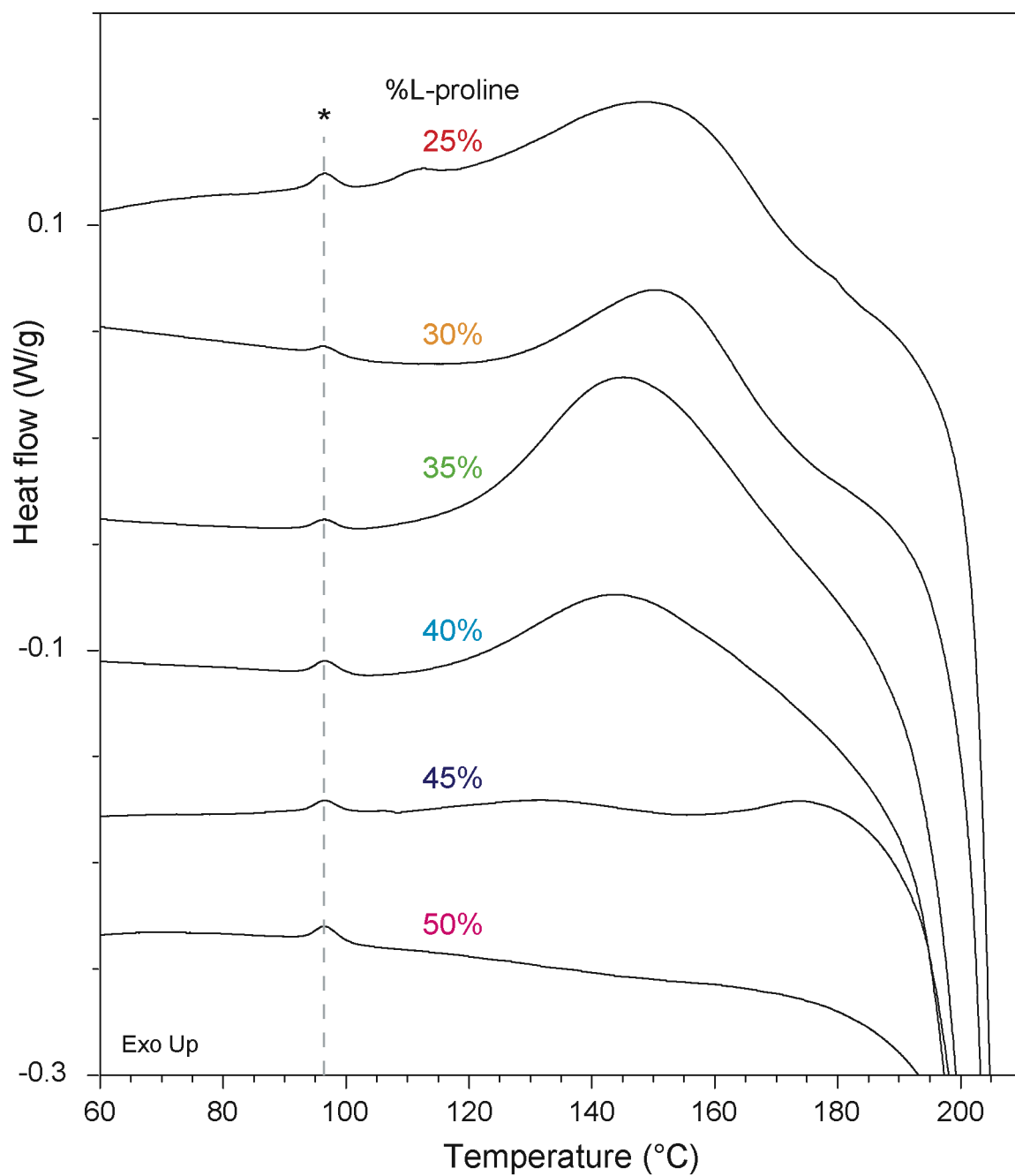
Figure 5.5. DSC thermograms of N_2-lyophilized proline samples containing 25–50% L-proline. Asterisk and dashed line indicate impurity in the DSC thermal cell.

184
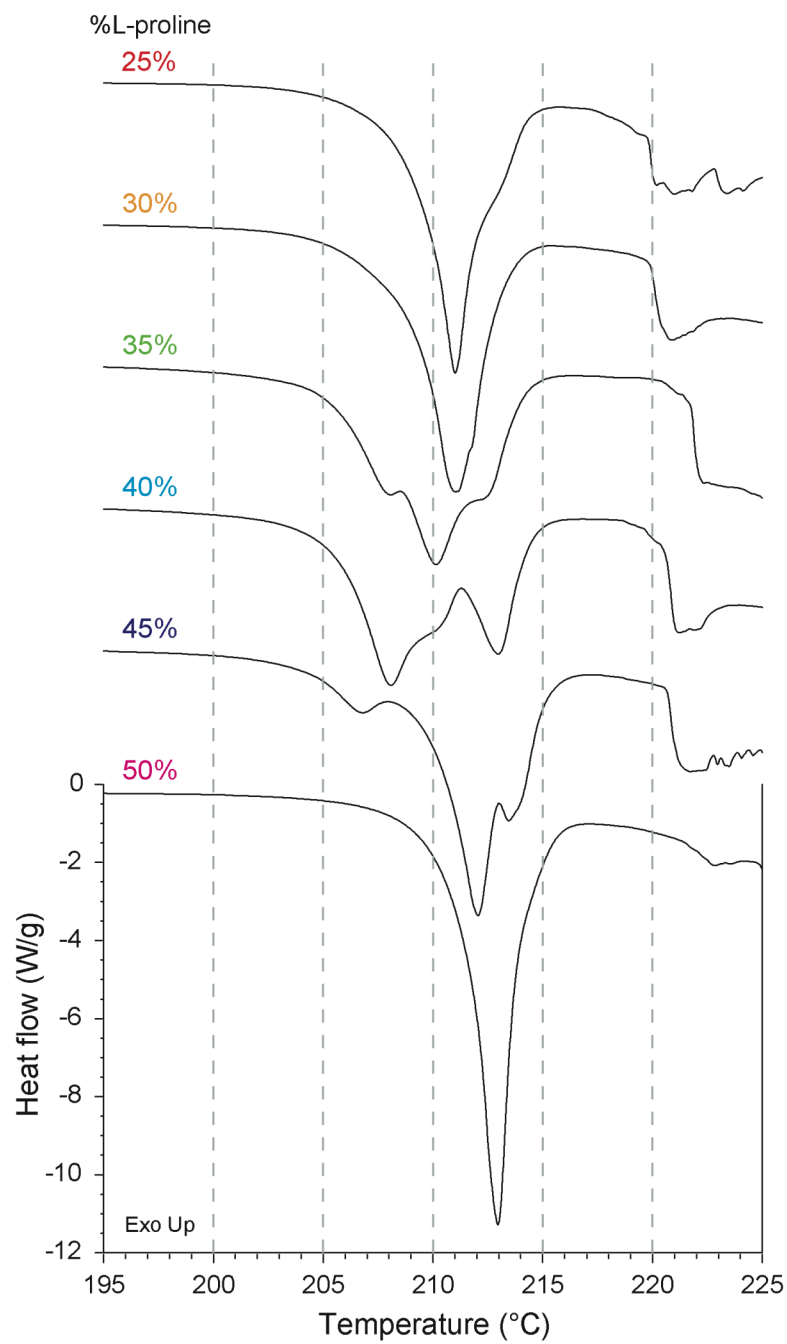
Figure 5.6. DSC thermograms of N$_2$-lyophilized proline samples containing 25–50% L-proline. All thermograms are on the same y-scale.

In 25–40% L-proline samples, there was a broad exotherm (centered at ~150ºC) with an onset temperature of ~110ºC. This peak was not observed in the thermograms of 45 and 50% L-proline samples. Exothermic transitions in a polymorphic system can often indicate a transformation between crystal forms that are monotropically related,[15] but such transformations typically exhibit narrower peaks within a DSC thermogram. Exothermic events also are associated with the crystallization of amorphous materials, but SSNMR and PXRD indicated the absence of such a phase. Another possible explanation for the broad exothermic peaks is the recrystallization of crystal defects.[16] Although it is not possible to identify the exact nature (monotropic polymorphic transformation or "healing" of defects within the crystal lattice) of the exothermic event at ~150ºC, its presence appears to coincide with the broad overlapping SSNMR peaks (Figure 5.1).

Figure 5.6 shows the DSC thermograms from 195–225ºC. The scale of the y-axis is the same for all thermograms. Multiple, overlapping melting endotherms were observed for the samples, followed by degradation at ~220ºC. Although it is not possible to identify these endotherms, they likely correspond to melting of various crystalline forms of D- and DL-proline and their corresponding eutectics. Interestingly, the same peaks were present in DSC thermograms of samples prepared under ambient conditions, even though the SSNMR demonstrated significant differences in these samples at room temperature. This suggests that the overlapping peaks in the SSNMR spectra of N_2-lyophilized samples correspond to forms that transform prior to melting.

In order to understand the thermally induced transformations of the overlapping peaks observed in the SSNMR spectra of N_2-lyophilized samples, as well as observe the

effect of water vapor on recrystallization, samples were exposed to either elevated temperature or water vapor. The purpose of exposing these samples to various conditions was two-fold: 1) to simplify the system by selectively transforming some of the overlapping peaks, therein providing greater resolution of the remaining peaks and 2) to determine whether the overlapping peaks would transform differently upon introducing either water-induced or elevated-temperature–induced molecular mobility.

5.3.4   *Increasing mobility of the sample via temperature and water*

Transformations of the N_2-lyophilized proline samples were probed by exposing several of these samples to elevated temperatures or ambient conditions. Figure 5.7 demonstrates the thermal stability of a 35% L-proline sample prepared by the N_2-lyophilization method. Figure 5.7a shows the ^{13}C CP-MAS NMR spectrum of the freshly prepared sample, and Figure 5.7b shows the spectrum of the sample after dry-N_2 storage for 8 months. Some changes were observed during the dry storage, including a small amount of D crystallization (peak at 33.0 ppm). However, the multiplicity of peaks remained. Immediately after collecting the spectrum in Figure 5.7b, the sample was heated in the spectrometer at 60ºC for 3 hr, cooled and equilibrated at 20ºC, and analyzed again (Figure 5.7c). This thermal treatment did not result in any significant spectral changes. The sample was then heated at 100ºC for 2 hr, equilibrated at 20ºC, and then analyzed again (Figure 5.7d). Broad peaks corresponding to D, DL-II, and DL-I were observed, but there still appeared to be other overlapping peaks present. The sample was again heated to 100ºC, held for 3 additional hr, and cooled to 20ºC for analysis (Figure 5.7e). At this point, the spectrum contained peaks corresponding to D, DL-II,

Figure 5.7. ^{13}C CP-MAS NMR spectra of N_2-lyophilized 35% L-proline collected at 20ºC a) immediately after lyophilization; b) after 8 months of storage under dry nitrogen, room temperature; c) heated at 60ºC, 3 hr; d) sample (c), heated again at 100ºC, 2 hr; and e) sample (d), after an additional 3 hr at 100ºC. Dashed vertical lines show the characteristic peak locations of D, DL-I, and DL-II.

and DL-I, but the peaks were still broad relative to peaks in the spectra of ambient-lyophilized samples (Figure 3.7). At the end of the thermal treatment (Figure 5.7e) DL-II was the predominant component of the spectrum, and DL-I was present at a much lower relative amount. Again, this supports that DL-II and DL-I are thermodynamic and kinetic products, respectively. No further heating of this sample was performed, but it would be interesting to determine if additional heating would completely transform DL-I to DL-II. Although the kinetics associated with thermal transformations by DSC versus the heat-hold-cool method shown in Figure 5.7 are very different, it is possible to draw parallels between the two. Of particular interest is that the overlapping peaks in the SSNMR spectra slowly disappeared while held at 100ºC. This temperature is ~100ºC away from the DSC-observed melt, but very close to the onset of the broad exothermic peak observed in the DSC (Figure 5.5), suggesting that the DSC-observed exotherm corresponds to molecular rearrangement to crystal forms of D, DL-I, and DL-II (Figure 5.7e). Similar to observing sample transformation due to thermal treatment, another sample was exposed to ambient conditions in order to determine the possible effect of water vapor on the transformation process.

Figure 5.8a shows ^{13}C CP-MAS NMR spectra of 25% L-proline prepared by the N_2-lyophilization method (same spectrum as in Figure 5.1). Following analysis, the sample was stored under dry nitrogen for ~1 month before analyzing again by SSNMR (Figure 5.8b). Slight changes in the peaks were observed, including growth of the D peak at 33.0 ppm and a relative decrease in the intensity of the peak at ~176 ppm, but the sample appeared to be relatively stable under these dry, room-temperature conditions. The sample was then exposed to ambient (room-temperature and RH) conditions. Figure
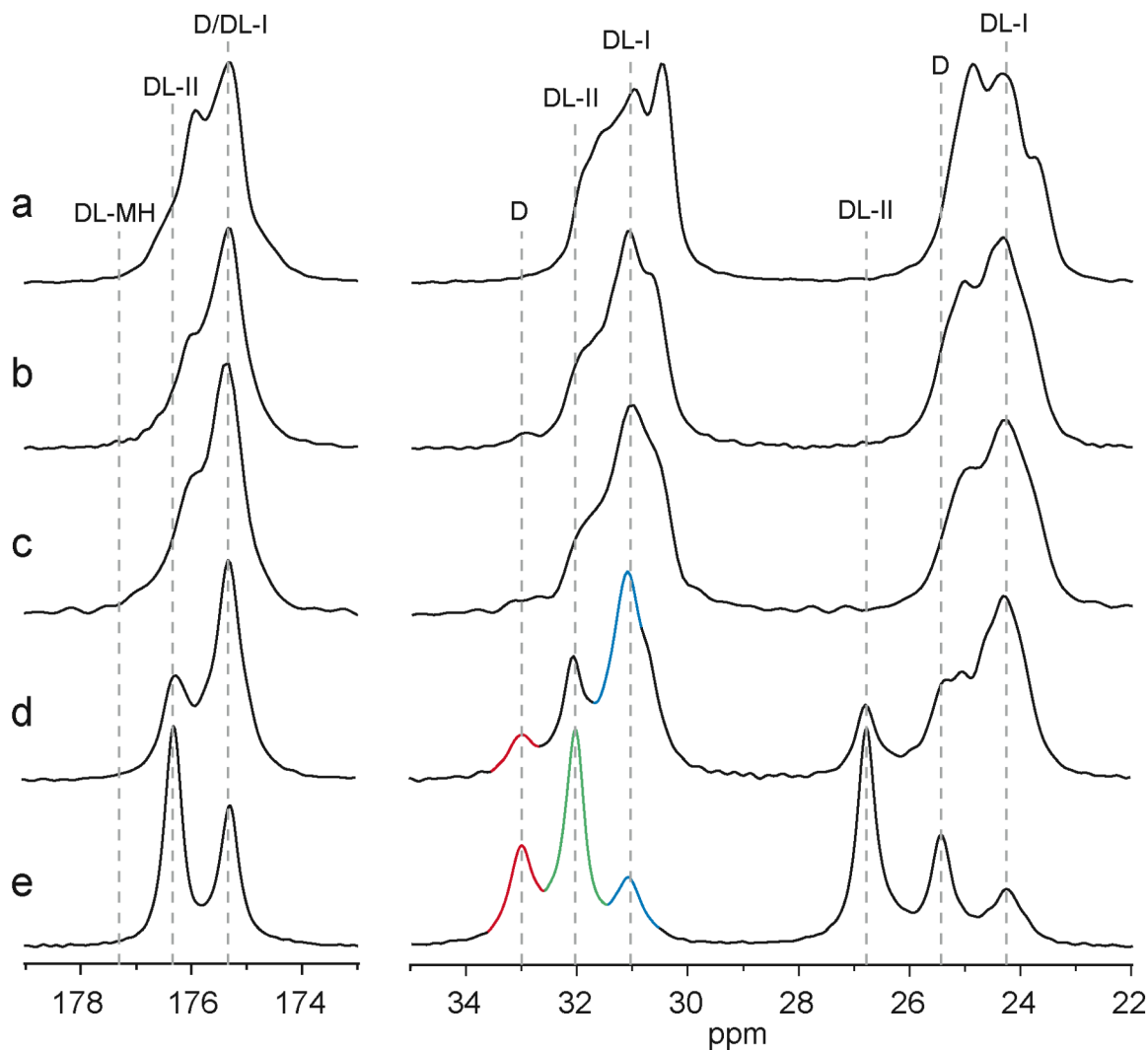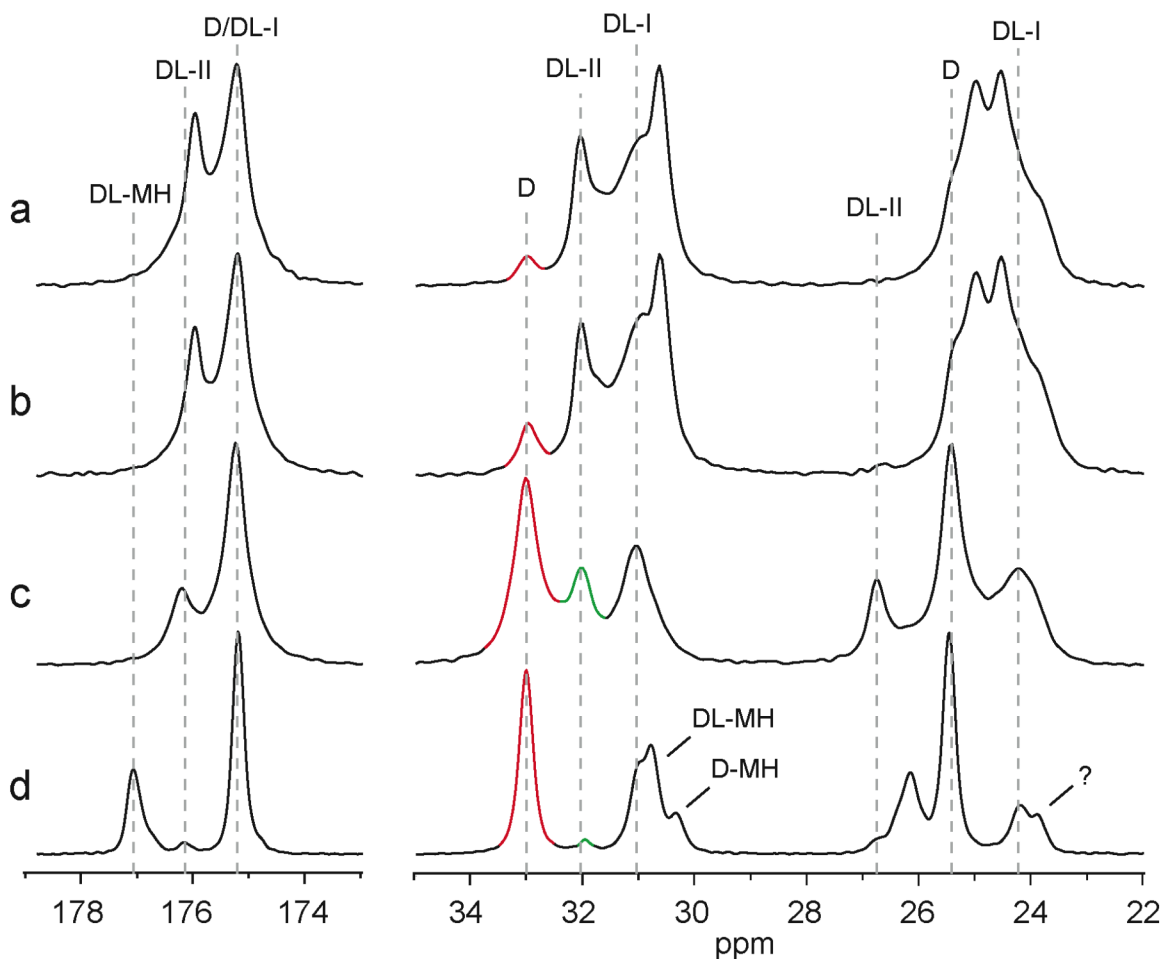
Figure 5.8. ^{13}C CP-MAS NMR spectra of N$_2$-lyophilized 25% L-proline a) immediately after lyophilization; b) after 1 month of storage under dry nitrogen, room temperature; c) after 1 day of exposure to ambient laboratory conditions; and d) sample (c), after an additional week at ambient conditions. Dashed vertical lines show the characteristic peak locations of D, DL-I, and DL-II.

5.8c shows the spectrum of the sample after 1 day of exposure to ambient laboratory conditions. Crystalline D, DL-I, and DL-II peaks were clearly visible following exposure to these conditions, although the peaks were somewhat broad. After an additional week of exposure to ambient conditions (Figure 5.8d), the peaks had narrowed, and the hydrate forms DL-MH and D-MH were observed, along with D, some DL-I, DL-II, and an unknown peak (~23.9 ppm). This demonstrates the ability for water vapor to assist the crystallization of proline. The observed peak narrowing upon lengthy exposure to ambient conditions also suggests that the presence of water allows for crystal perfection to take place, likely due to increased lattice mobility in the presence of water.[2] Although T_1 relaxation measurements are often used to probe the mobility of a solid system,[17] it is not clear if it would be helpful in elucidating this mechanism. The increased mobility due to the presence of water could be counteracted by the decrease in mobility that is achieved upon lattice perfection.

Exposure of the disordered N_2-lyophilized samples to either ambient water vapor or elevated temperature resulted in crystalline peaks for D, DL-I, and DL-II. However, due to the large degree of peak overlap, it was not possible to selectively observe and assign the decrease in one peak to the appearance of another. Therefore, it was not possible to determine the order of transformation of the various forms, i.e., direct transformation of "unstable" crystal phase(s) to DL-II, or transformation first to DL-I, then to DL-II.

Up until this point, it was assumed that the lyophilization method itself produced the SSNMR-observed metastable crystal forms, and the lack of water vapor increased the stability of these forms. However, an alternative explanation for the observed disorder is that DL-MH was present upon completion of the lyophilization cycle, but exposure to the dry nitrogen gas rapidly dehydrated it, resulting in partial lattice collapse and the observed disorder/multiple unstable forms. In order to address this second possibility, DL-MH was dehydrated under various conditions and characterized by SSNMR.

In order to determine the products resulting from DL-MH dehydration, a sample of DL-MH was dried at 80ºC under vacuum and then packed into a SSNMR rotor within a dry nitrogen glove box. The resulting ^{13}C CP-MAS NMR spectrum (Figure 5.9f) showed sharp crystalline peaks, not the broad peaks associated with a disordered material. The crystalline peaks corresponded to DL-I and another crystal form that had not been previously observed (DL-III). Additional DL-MH samples were dehydrated under a variety of conditions, including at lower temperatures (20, 35, 45ºC) and over desiccant (room temperature). In all cases, SSNMR analysis showed crystalline peaks that corresponded to various levels of DL-I and the new crystalline form. Although dehydration of some crystalline hydrates can result in collapse of the crystal lattice, and therefore the formation of amorphous material, there were no indications of disorder or amorphous material in any of the dehydrated DL-MH samples. Thus, under a variety of dehydration conditions, DL-MH dehydration always produced crystalline material, and the presence of the overlapping peaks in the N_2-lyophilized samples (SSNMR, Figure 5.1) cannot be attributed to the dehydration of DL-MH upon exposure to nitrogen gas
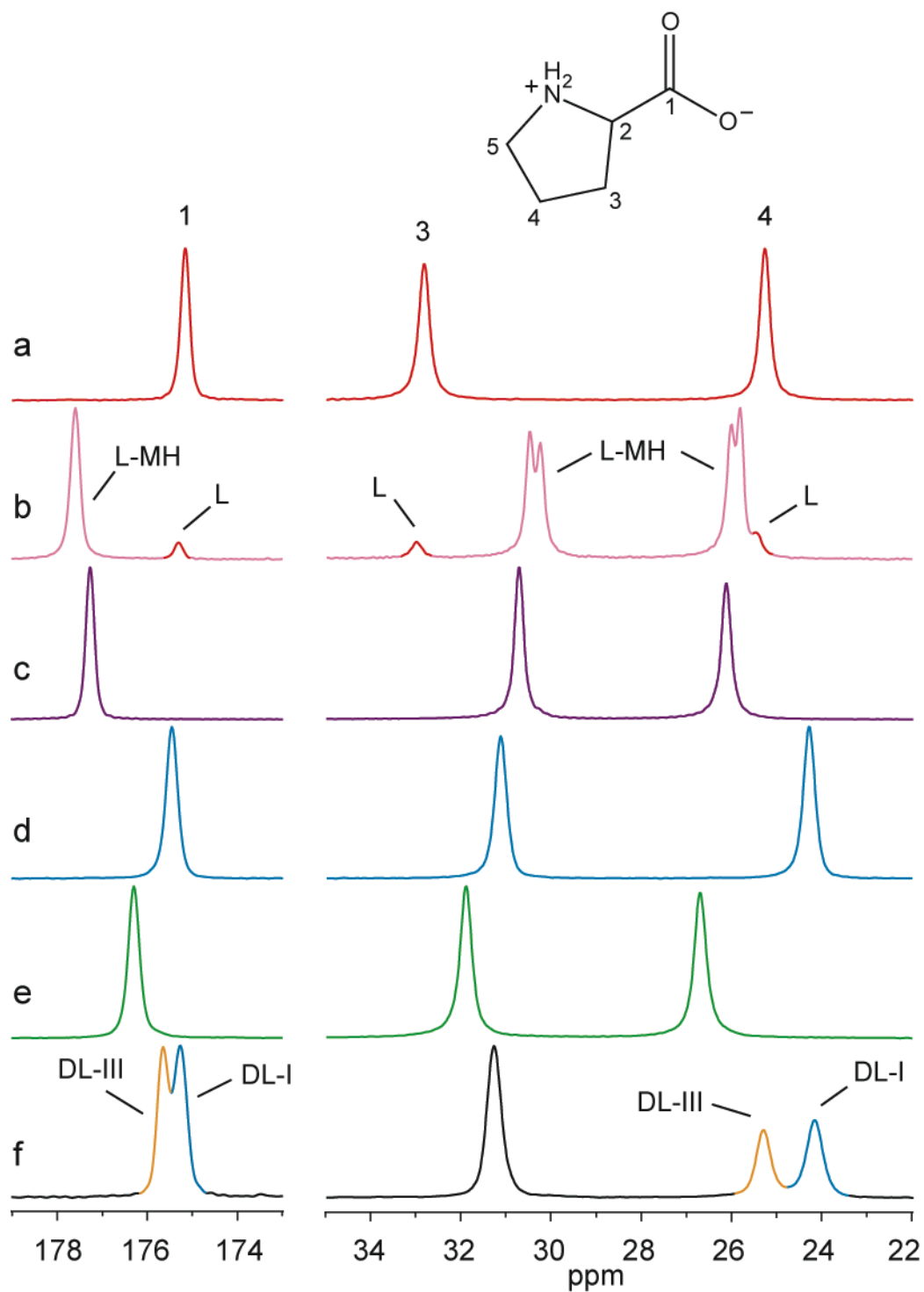
Figure 5.9. ^{13}C CP-MAS NMR spectra of proline crystal forms: a) enantiopure proline, b) enantiopure monohydrate, c) DL-monohydrate, d) DL-form I, e) DL-form II, and f) a mixture of DL-forms I and III.

after the lyophilization process. This means that the SSNMR-observed, overlapping peaks are the result of the lyophilization process itself.

Although the new crystal form was repeatedly observed upon dehydration of DL-MH, it was not possible to isolate it. This form was always observed in the presence of DL-I, and the ^{13}C SSNMR peaks corresponding to this unknown form slowly decreased in intensity over time, eventually resulting in a sample composed solely of DL-I. This behavior suggests that this unknown form corresponds to a metastable racemic cocrystal, which slowly transforms into DL-I. It is referred to as DL-proline form III (DL-III) from here forward. The overall dehydration behavior of DL-MH is outlined below:

$$(DL\text{-}MH)_{solid} \xrightarrow{\text{dehydration}} (DL\text{-}I)_{solid} + (DL\text{-}III)_{solid} \xrightarrow{\text{solid-state transformation}} (DL\text{-}I)_{solid}$$
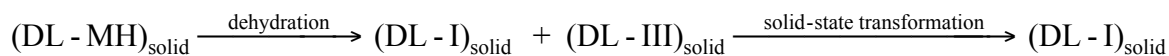
5.4 Discussion

In Chapter 3, we reported a new polymorphic form of the proline racemic cocrystal. This form, DL-II, was only observed upon lyophilizing solutions that contained an enantiomeric excess of D-proline. When crystallized from solution and/or with an equimolar ratio of the D- and L-proline enantiomers, only the kinetic product, DL-I, was observed. The observed DL-II versus DL-I formation was hypothesized to arise from the combination of reduced molecular motion associated with crystallizing by lyophilization and the presence of excess D-enantiomer, which acted as a physical barrier to slow formation of the DL-proline crystal lattice. According to the hypothesis, both of these conditions were necessary to allow the thermodynamic product (DL-II) to form as opposed to the kinetic product (DL-I).

194

If this hypothesis were true, then the following should be observed: 1) We should be able to observe the "frustrated" state, in which the racemic cocrystal DL-pairs and D-proline molecules cannot completely separate from one another in order to form their own respective crystal lattices; and 2) Not only should the formation of the racemic cocrystal lattice be inhibited due to the presence of intervening D-proline, but to an extent, the reverse must also be true: Formation of the D-proline crystal lattice must also be slowed by the presence of the L-proline. The purpose of the work in this chapter was to determine whether or not an amorphous/disordered state existed in the lyophilized proline samples.

5.4.1 *Observation of disordered crystalline material*

Due to the ability of water to induce crystallization of amorphous materials,[1-3] we prevented exposure of the samples to ambient water vapor following the lyophilization process. The resulting samples demonstrated differences in SSNMR spectra and PXRD patterns relative to lyophilized samples that were exposed to ambient conditions. The SSNMR spectra contained a number of overlapping, unresolvable peaks that had not previously been observed, and the PXRD patterns contained broad, unresolved peaks located at/near the peak locations associated with DL-I. The results from both techniques suggested the presence of disorder but the absence of an amorphous phase. Upon introducing mobility into the system, either through increasing temperature or by exposure to water, the material transformed into known crystal forms D, DL-I, and DL-II. These results demonstrate that, by preventing sample exposure to ambient water vapor, it

was possible to stabilize and detect the presence of thermodynamically unstable crystal forms that may correspond to the hypothesized "frustrated" state.

5.4.2 "Missing" D and DL-II peaks

In the ^{13}C CP-MAS NMR spectra of N_2-lyophilized samples (Figure 5.1), the characteristic D-proline peak located at 33.0 ppm was noticeably missing or reduced relative to the amount that was theoretically anticipated in most samples. This was particularly true at higher concentrations (35–45%) of L-proline, where almost no peak was observed for D-proline at 33.0 ppm. Also, DL-II (characteristic peak located at 26.7 ppm, Figure 5.1) was never present in the absence of the D-proline (33.0-ppm peak). These observations suggest the presence of the aforementioned "mutual" frustration of the DL and D lattice packing. If this is indeed the case, and both D and DL-proline prevented each other from forming their thermodynamically favorable crystal lattices, it would follow that, when the system becomes mobile, both forms should recrystallize/transform at the same time. This concurrent crystallization of D- and DL-II was observed upon increasing the mobility in the system by thermal- or water-induced mechanisms (Figures 5.7 and 5.8), supporting the hypothesis of "mutual frustration."

Also supporting this is the fact that the "frustrated" state was not observed when samples of 50% L-proline (Figure 5.1) or 100% L-proline (not shown) were prepared by the same N_2-lyophilization method. At these concentrations, where enantiomeric excess is either 0 or 100%, there are no molecules to act as defects to frustrate formation of the D or DL lattice structure. Thus, as in Chapter 3, it is observed that "frustration" occurred only in the case of non-equimolar ratios of proline enantiomers.

5.4.3   Characterization of the "frustrated" crystalline material

SSNMR peaks and PXRD patterns indicated the absence of amorphous material within the N_2-lyophilized samples, indicating that the material was crystalline. However, the presence of new peaks in the SSNMR spectrum demonstrated that the proline molecular conformations/packing arrangements were different from those previously observed for D, DL-I, and DL-II crystal forms.

The presence of multiple peaks for each carbon within the ^{13}C CP-MAS NMR spectrum could have arisen from either the presence of multiple, phase-separated polymorphic forms, or from the presence of crystallographic inequivalence within a single phase, or both.[13] A 2D-exchange NMR experiment and spin–lattice relaxation measurements were unable to differentiate between these possibilities due to a high degree of peak overlap in the spectra of N_2-lyophilized samples.

PXRD patterns (Figure 5.3) showed broad peaks corresponding to the presence of disordered lattice structures. The peaks corresponded to the characteristic diffraction peak locations for D and DL-I. This suggests that the crystal lattice structures that exist within the N_2-lyophilized samples are similar to the lattice packing within D and DL-I.

It is interesting to note that the ^{13}C CP-MAS NMR peaks in the carbonyl region of the N_2-lyophilized samples (Figure 5.1) were not dramatically different from the corresponding peaks for samples exposed to ambient conditions (Figure 3.7). This suggests that the intermolecular bonding of the carbonyls did not differ greatly. In contrast, many different peaks were present in SSNMR spectra for carbons C-3 and C-4, indicating that the observed disorder is largely due to conformational flexibility in the 5-membered ring.

197

Although it was not possible to determine whether or not a single phase or multiple crystalline phases existed within the N_2-lyophilized samples, the combined SSNMR and PXRD results suggest that DL-pairs and D-proline molecules potentially existed together in a single phase that possessed an overall lattice structure similar to that of DL-I and D, as well as intermolecular carbonyl-bonding patterns that were similar to those within DL-I and D lattice structures. The observed differences among the SSNMR peaks for C-3 and C-4 peaks likely arose from ring puckering that took place to minimize unfavorable interactions, while preserving the carboxyl–ammonium intermolecular bonding observed among proline crystal structures.[18] Similar to crystallographic inequivalence, these ring puckering conformations could exist in a set of discrete (versus a broad range of) conformations, leading to the non-amorphous peaks observed in the SSNMR spectra for C-3 and C-4 carbons.

Additional studies would be necessary to fully characterize the observed "frustrated" crystalline material. It would be of interest to determine whether or not phase separation exists between D and DL chiral crystal structures, as well as to identify the conformations of the proline enantiomers within the solid. In addition, it would be very interesting to study and compare the effect of a polymer on the crystallization of proline enantiomers by lyophilization.

5.4.4 DL-proline form III

In order to demonstrate that the observed disordered phase was formed by the lyophilization method itself, and not dehydration of DL-MH upon exposure to dry nitrogen gas, DL-MH was dehydrated under a variety of conditions. Analysis of the

198

resulting materials by SSNMR always showed the formation of crystalline materials, predominantly DL-I and a variable amount of another new polymorphic form, DL-III. The relative amounts of DL-I and DL-III in the sample always contained DL-I $\geq$ DL-III, and the DL-III gradually decreased over time to form DL-I. This behavior indicates that DL-III is metastable to DL-I at room temperature. Further studies would be necessary to define a monotropic or enantiotropic relationship between the two polymorphic forms.

5.5   Conclusion

Lyophilizing enantiomeric ratios of proline and maintaining the samples in low-RH conditions through the use of dry nitrogen resulted in a multiplicity of peaks in the ^{13}C CP-MAS NMR spectrum and the presence of crystal-lattice disorder, as observed by PXRD. This material was relatively stable at room temperature when kept dry, but exposure to ambient water vapor or increased temperature resulted in transformation of the material to known crystal forms. These transformations were likely the result of increased solid-state molecular mobility due to the presence of water molecules and the kinetic energy associated with increased temperature. The combination of SSNMR and PXRD results suggests that the N_2-lyophilized material likely corresponded to "frustrated" structures that arose from the inability for D and L molecules to translate into proper configurations for the formation of separate racemic cocrystal and enantiopure crystal lattices. These observations support the hypothesized mechanism by which DL-II (thermodynamic product) is formed over DL-I (kinetic product) in the presence of enantiomeric excess under solid-state crystallization conditions.

5.6   References

1.   Brittain HG 2002. Effects of mechanical processing on phase composition. J Pharm Sci 91(7):1573-1580.

2.   Andronis V, Yoshioka M, Zografi, George 1997. Effects of sorbed water on the crystallization of indomethacin from the amorphous state. J Pharm Sci 86(3):346-351.

3.   Ahlneck C, Zografi G 1990. The molecular basis of moisture effects on the physical and chemical stability of drugs in the solid state. Int J Pharm 62(2-3):87-95.

4.   Pines A, Gibby MG, Waugh JS 1973. Proton-enhanced NMR of dilute spins in solids. J Chem Phys 59(2):569-590.

5.   Metz G, Wu X, Smith SO 1994. Ramped-amplitude cross polarization in magic-angle-spinning NMR. J Magn Reson, Ser A 110(2):219-227.

6.   Andrew ER, Bradbury A, Eades RG 1959. Removal of dipolar broadening of nuclear magnetic resonance spectra of solids by specimen rotation. Nature 183:1802-1803.

7.   Fung BM, Khitrin AK, Ermolaev K 2000. An improved broadband decoupling sequence for liquid crystals and solids. J Magn Reson 142(1):97-101.

8.   Dixon WT, Schaefer J, Sefcik MD, Stejskal EO, McKay RA 1982. Total suppression of sidebands in CPMAS carbon-13 NMR. J Magn Reson 49(2):341-345.

9.   Barich DH, Gorman EM, Zell MT, Munson EJ 2006. 3-Methylglutaric acid as a 13C solid-state NMR standard. Solid State Nucl Magn Reson 30(3-4):125-129.

10. Bielecki A, Burum DP 1995. Temperature dependence of 207Pb MAS spectra of solid lead nitrate. An accurate, sensitive thermometer for variable-temperature MAS. J Magn Reson, Ser A 116(2):215-220.

11. Han J, Suryanarayanan R 1999. A method for the rapid evaluation of the physical stability of pharmaceutical hydrates. Thermochim Acta 329(2):163-170.

12. Suryanarayanan R, Mitchell AG 1985. Evaluation of two concepts of crystallinity using calcium gluceptate as a model compound. Int J Pharm 24(1):1-17.

13. Zell MT, Padden BE, Grant DJW, Chapeau M-C, Prakash I, Munson EJ 1999. Two-dimensional high-speed CP/MAS NMR spectroscopy of polymorphs. 1. uniformly 13C-labeled aspartame. J Am Chem Soc 121(6):1372-1378.

14. Szeverenyi NM, Sullivan MJ, Maciel GE 1982. Observation of spin exchange by two-dimensional Fourier transform carbon-13 cross polarization-magic angle spinning. J Magn Reson (1969-1992) 47(3):462-475.

15. Burger A, Ramberger R 1979. On the polymorphism of pharmaceuticals and other molecular crystals. I. Theory of thermodynamic rules. Mikrochim Acta 2(3-4):259-271.

16. Feng T, Pinal R, Carvajal MT 2008. Process induced disorder in crystalline materials: differentiating defective crystals from the amorphous form of griseofulvin. J Pharm Sci 97(8):3207-3221.

17. Lubach JW, Xu D, Segmuller BE, Munson EJ 2007. Investigation of the effects of pharmaceutical processing upon solid-state NMR relaxation times and implications to solid-state formulation stability. J Pharm Sci 96(4):777-787.

18.   Myung S, Pink M, Baik M-H, Clemmer DE 2005. DL-proline. Acta Crystallographica, Section C Cryst Structure Commun C61(8):506-508.

Chapter 6

Solid-State Crystallization of Proline Racemic Cocrystals from

Amorphous Cryoground Material

6.1 Introduction

In this chapter, we report the crystallization behavior of proline enantiomers from an amorphous phase produced by cryogrinding. By comparing the solid-state crystallization behavior of cryoground proline enantiomers to lyophilized proline enantiomers, we expect to gain insight into the previously observed preferential crystallization of DL-I versus DL-II (Chapters 3–5).

6.1.1 Grinding to produce cocrystals

Pharmaceutical cocrystals have gained attention due to desirable physicochemical properties, including enhanced dissolution rates and stability.[1] Cocrystals are multiple-component crystalline materials that are composed of stoichiometric ratios of the active pharmaceutical ingredient (API) and a "co-former" molecule, which typically possesses hydrogen-bonding potential that complements that of the API. Most often, cocrystals are produced by solvent-evaporation of a solution containing both the drug molecule and a co-former. More recently, solid-state grinding has been shown to be a feasible and potentially more efficient process for producing and screening potential pharmaceutical cocrystals.[2]

The mechanism by which cocrystals are formed during the grinding process is an active area of research.[3,4] Of particular interest is the formation of an intermediate

amorphous phase, which then crystallizes during or after the grinding process to produce the cocrystal.[5,6] Studies have indicated that the amorphous phase is indeed a possible intermediate, and its formation is facilitated by grinding at low temperatures.[1,7,8]

6.1.2   Amorphization by cryogrinding

Grinding organic crystalline material produces defects within the crystal lattice.[9] After sufficient grinding, these defects reach a critical concentration, at which point the crystal lattices collapse, resulting in an amorphous phase.   However, this trituration process competes with recrystallization.   If the kinetics associated with recrystallization are greater than the formation of defects, an amorphous phase will not be observed.[7]

Cryogrinding is performed at liquid nitrogen temperatures (77 K).   These low temperatures reduce molecular mobility within the system, therein slowing the crystallization process.   This creates the potential to stabilize the formation of amorphous and metastable crystalline states that might exist transiently when grinding at room temperature.[5,7]

6.1.3   Cryogrinding proline

We have shown in Chapters 3–5 that the crystallization of proline enantiomers in the solid state (lyophilization) versus solution state had a large effect on the resulting product.   Of particular focus has been the preferential formation of DL-proline form I versus form II.   Whereas DL-I formed when solid-state crystallization proceeded readily, DL-II was the major product when the crystallization process was impeded by the presence of enantiomeric excess.

Due to our interest in better understanding the formation of DL-I versus DL-II, we explored the possibility of producing the proline racemic cocrystals by grinding.[10] Of particular interest was the potential observation of an amorphous phase. Previous proline-sample preparation methods included lyophilization and spray drying, both of which are conventional methods for producing amorphous solids.[7] However, these preparation methods only produced non-amorphous, crystalline forms of proline. Thus, cryogrinding was used in an attempt to achieve amorphous material, from which the crystallization of DL-I and/or DL-II could be observed.

6.2   Experimental

6.2.1   Materials

L- and DL-proline were purchased from Alfa Aesar (Ward Hill, MA), D-proline was purchased from Sigma-Aldrich (St. Louis, MO). DL-proline form I was crystallized from aqueous solution. All amino acids were used as received.

6.2.2   Cryogrinding.

Bulk D-proline, DL-proline form I, or equimolar mixtures of bulk L- and D-proline were weighed directly into a polycarbonate cryovial containing a stainless-steel impactor bar. The material (~1 g total) was then ground in a Freezer/Mill (SPEX 6750; SPEX Certi-Prep; Metuchen, NJ) for a total of either 30 or 60 min, performed in 15 or 30 cycles (2 min of grinding followed by a 2-min rest interval), preceded by 5 min of pre-cooling. All sample handling before and after grinding was performed within a dry nitrogen glove box.

6.2.3 Solid-state NMR spectroscopy

All ^{13}C spectra were acquired on a Chemagnetics CMX-300 spectrometer (Varian, Inc.), operating at 75 MHz for [13]C. All acquisitions included cross polarization (CP),[11,12] magic-angle spinning (MAS)[13] at a rate of 4 kHz (±3 Hz), SPINAL64 decoupling[14] at a field strength of ~64 kHz, and total sideband suppression (TOSS).[15] A contact time of 2 ms was used for all samples. [1]H T_1 relaxation measurements were performed using a saturation–recovery pulse sequence, and T_1 values were calculated using KaleidaGraph (version 4.01, Synergy) with the equation y = amp(1-exp(-τ/T_1)), where y is the integrated signal intensity, amp is the amplitude constant, τ is saturation–recovery time, and T_1 is the spin–lattice relaxation time. 3-methylglutaric acid (MGA) was used to optimize the spectrometer settings as well as to set the reference frequency.[16] All samples were packed into zirconia rotors with ribbed Kel-F® end caps. Variable-temperature experiments were performed with a 7.5-mm double-resonance MAS probe (Varian; Palo Alto, CA) with a 3.9-μs ^{1}H pulse duration. Lead nitrate was used for temperature calibration.[17] During variable-temperature experiments, samples were equilibrated at each temperature for at least 15 min prior to tuning and data acquisition.

6.2.4 Powder X-ray diffraction

Diffraction patterns were acquired with a Scintag X2 Diffraction System (XGEN-4000; Scintag, Inc.) using CuKα radiation (45 kV, 35 mA), an angular range between 5 and 40º 2θ, a step size of 0.02º, and a dwell time of either 0.3 or 4 s. Each sample (~300 mg) was packed into a stainless-steel die. All analyses were performed at ambient conditions.

6.2.5 Differential scanning calorimetry

Differential scanning calorimetry (Q100 DSC; TA Instruments; New Castle, DE) was performed on samples of 3–8 mg that were packed into either standard or hermetic aluminum pans and crimped. Data was collected from room temperature to ~240ºC, with a temperature ramp of 10 or 20ºC/min and a 50-mL/min dry nitrogen purge. The MDSC method included a 1ºC/min ramp with a modulation of ±0.40ºC/60 s and a temperature range of -20 to 200ºC.

6.2.6 Thermogravimetric analysis

Water content of samples was determined by thermogravimetric analysis (Q50 TGA, TA Instruments; New Castle, DE). Samples of 10–20 mg were heated from room temperature to >300ºC at a rate of 10ºC/min under a 40-mL/min dry nitrogen purge.

6.3   Results

6.3.1 Stabilizing physical forms in cryoground proline: Variable-temperature SSNMR

Before cryogrinding mixtures of proline enantiomers, it was of interest to obtain a spectrum of amorphous enantiopure material. Bulk D-proline was cryoground for a total of 60 min, then analyzed by SSNMR at 20ºC. The initial ^{13}C CP-MAS NMR spectrum (Figure 6.1, bold red line) possessed several crystalline peaks but no broad amorphous peaks. The crystalline peaks indicated the presence of the previously observed D-proline crystal form, as well as new crystal forms (Table 6.1). As SSNMR analysis continued, the intensity of these new peaks decreased, with corresponding increases in the intensity of the known D-proline peaks. After 18 hr, the spectrum contained only peaks of the
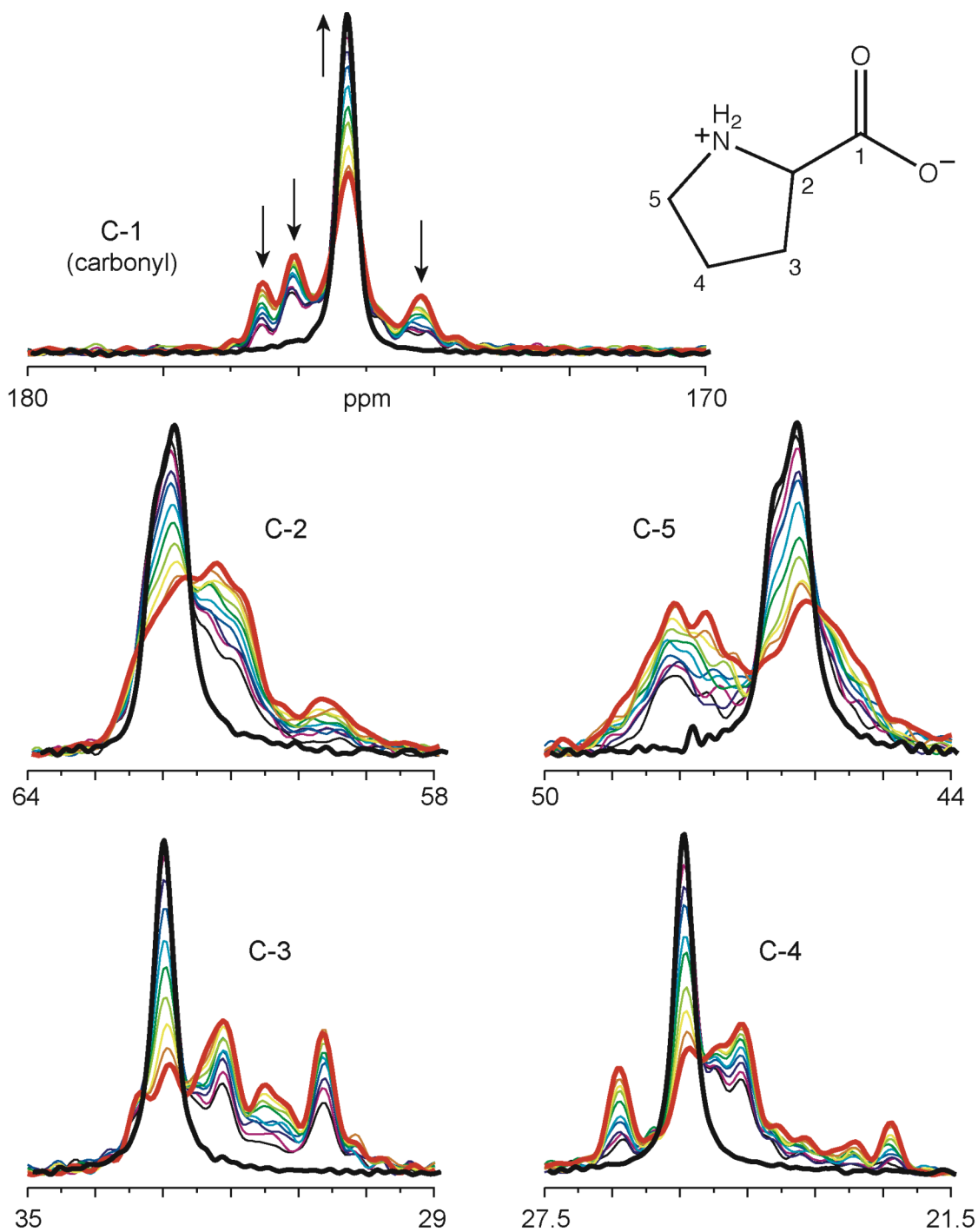
Figure 6.1. ^{13}C CP-MAS NMR spectra of cryoground (60 min) D-proline over time at 20ºC. The spectral region of each carbon in the proline molecule has been plotted separately. Spectra were collected consecutively every 8 min starting at t=0, and then after 18 hr (bold black line). The initial spectrum is denoted as a bold red line. Arrows indicate relative changes in C-1 peak intensities.

Table 6.1. ^{13}C CP-MAS NMR chemical shifts (ppm) of proline crystal forms

Crystal form	Abbrev.	Carbonyl peak	Aliphatic peaks			
		C1	C2	C5	C3	C4
Enantiopure[a]	L/D	175.3[b]	61.9	46.5	33.0	25.4
Enantiopure monohydrate	L-MH	177.6	61.5	48.6	30.5, 30.3	26.1, 25.9
Racemic cocrystal monohydrate	DL-MH	177.2	60.1	48.5	30.8	26.2
Racemic cocrystal form I	DL-I	175.3[b]	60.6	45.9	31.0	24.2
Racemic cocrystal form II	DL-II	176.3	60.6	47.6	31.9	26.7
Racemic cocrystal form III	DL-III	175.6	59.6	47.0	31.3	25.3

[a]Enantiopure D- and L-proline have the same ^{13}C SSNMR peak positions.
[b]Enantiopure and DL-I spectra overlap at the carbonyl peak, but peak differences are observed for the aliphatic peaks.

known crystal form of enantiopure D-proline (Figure 6.1, bold black line).

This sample transformation was rapid relative to the time necessary to obtain a quality SSNMR spectrum and/or relaxation measurements. To slow the progression of the transformation, the samples were cooled to below room temperature. This was accomplished by coupling a variable-temperature (VT) stack to the NMR probe. The VT system was calibrated using lead nitrate,[17] and the resulting calibration curve (i.e., temperature dependence of the ^{207}Pb chemical shift) is shown in Figure 6.2. The slope of this plot is 0.7347 ppm/degree, which is slightly less than the value of 0.753 ppm/degree previously published.[17] Therefore, slight temperature corrections were necessary (e.g., to achieve a temperature of -60 or 200ºC using this VT stack, the instrument temperature setting had to be at -62.2 or 204.2ºC, respectively).

In addition to calibrating the VT SSNMR system with lead nitrate, it was necessary to characterize the possible temperature-dependence of proline chemical shifts. The cause for temperature-dependent peak changes in the ^{13}C CP-MAS NMR spectrum of a molecular crystal is the expansion/contraction of the crystal lattice that occurs as the temperature changes.[18] ^{13}C CP-MAS NMR spectra of proline crystal forms (D, DL-I, and DL-II) were acquired as a function of temperature (-20–200ºC). There was noticeable temperature dependence for the peak positions of these proline crystal forms. The peak shifts were linear, and the direction and magnitudes of the shifts differed among the different crystal forms, as demonstrated by Figure 6.3. Figures 6.4a–c are plots of the temperature dependence for each carbon peak of proline crystal forms D, DL-I, and DL-II. These shifts were accounted for when assigning peaks in VT ^{13}C CP-MAS NMR spectra.

$$y = 0.7347x - 14.512$$
$$R^2 = 0.9996$$
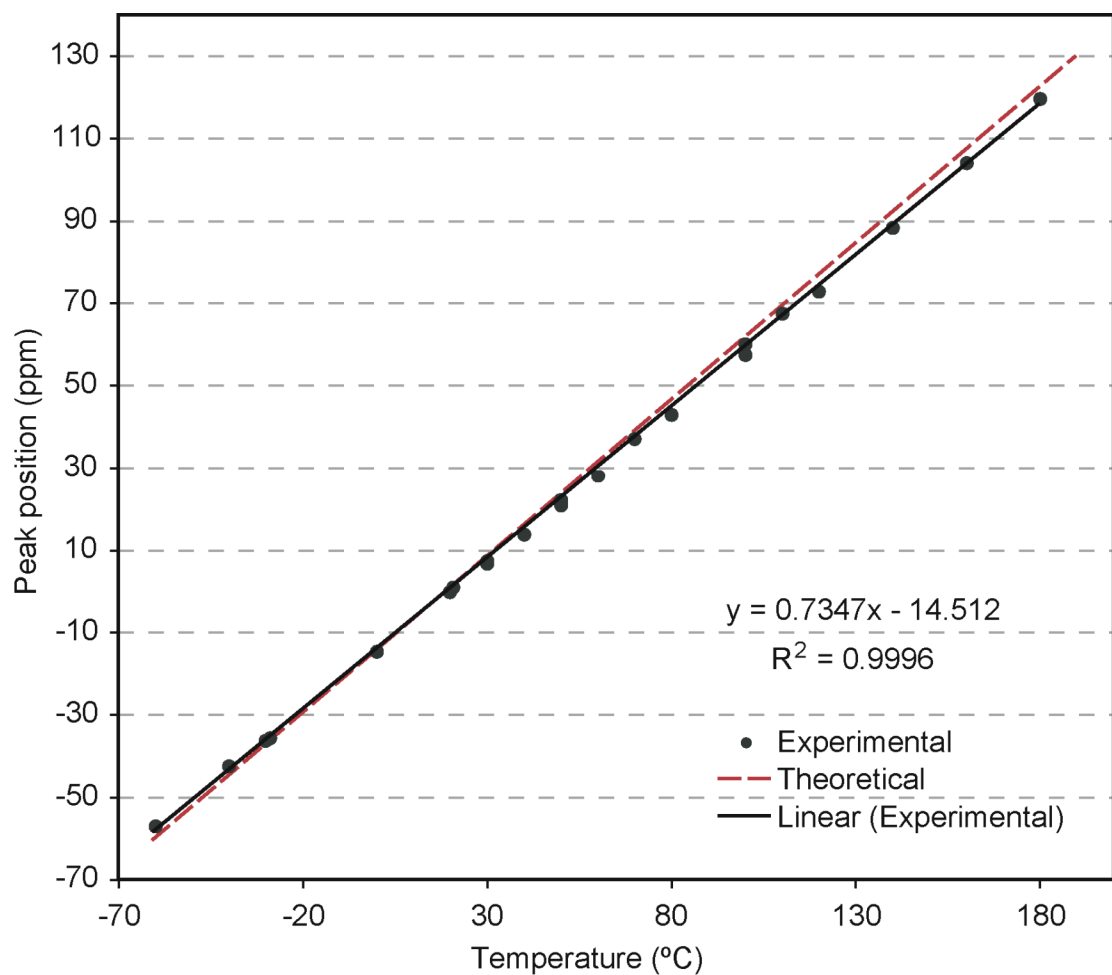
Figure 6.2. Lead nitrate temperature calibration plot. Solid black line represents the linear regression of the experimental data (equation shown). Dashed red line indicates the theoretical temperature dependence of ^{207}Pb peak shift.[17]
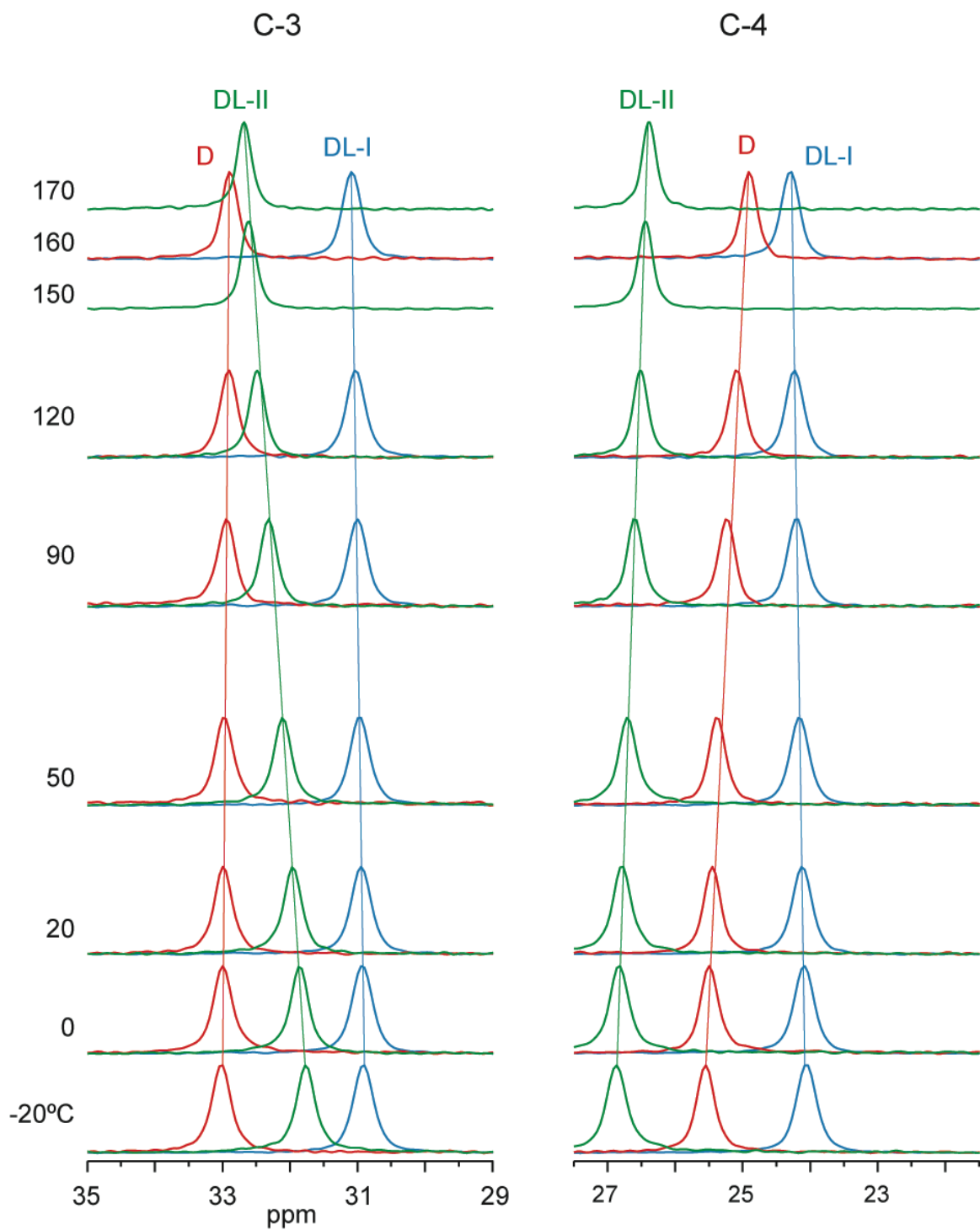
Figure 6.3. ^{13}C CP-MAS NMR temperature dependence of C-3 and C-4 carbons of proline crystal forms D, DL-I, and DL-II. Lines highlight the linearity of chemical shift as a function of temperature.
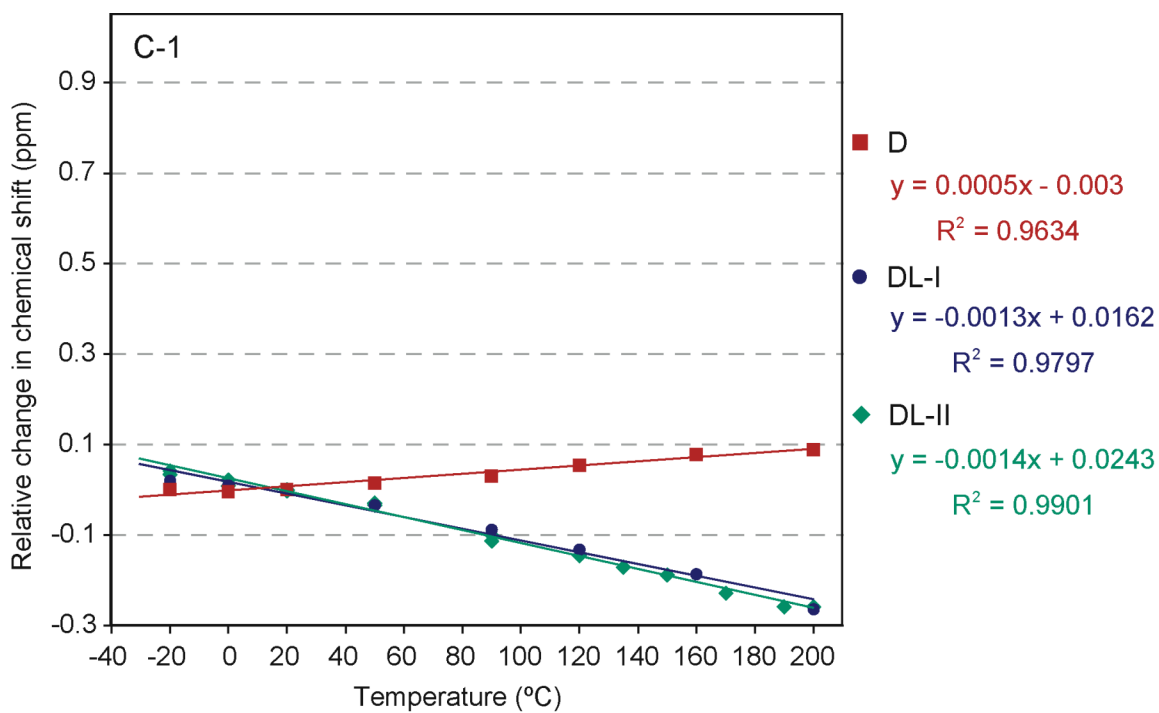
Figure 6.4a. ^{13}C CP-MAS NMR temperature dependence of the C-1 (carbonyl) carbon of proline crystal forms D, DL-I, and DL-II. Peak shifts are plotted as the change in chemical shift relative to the position at 20ºC.
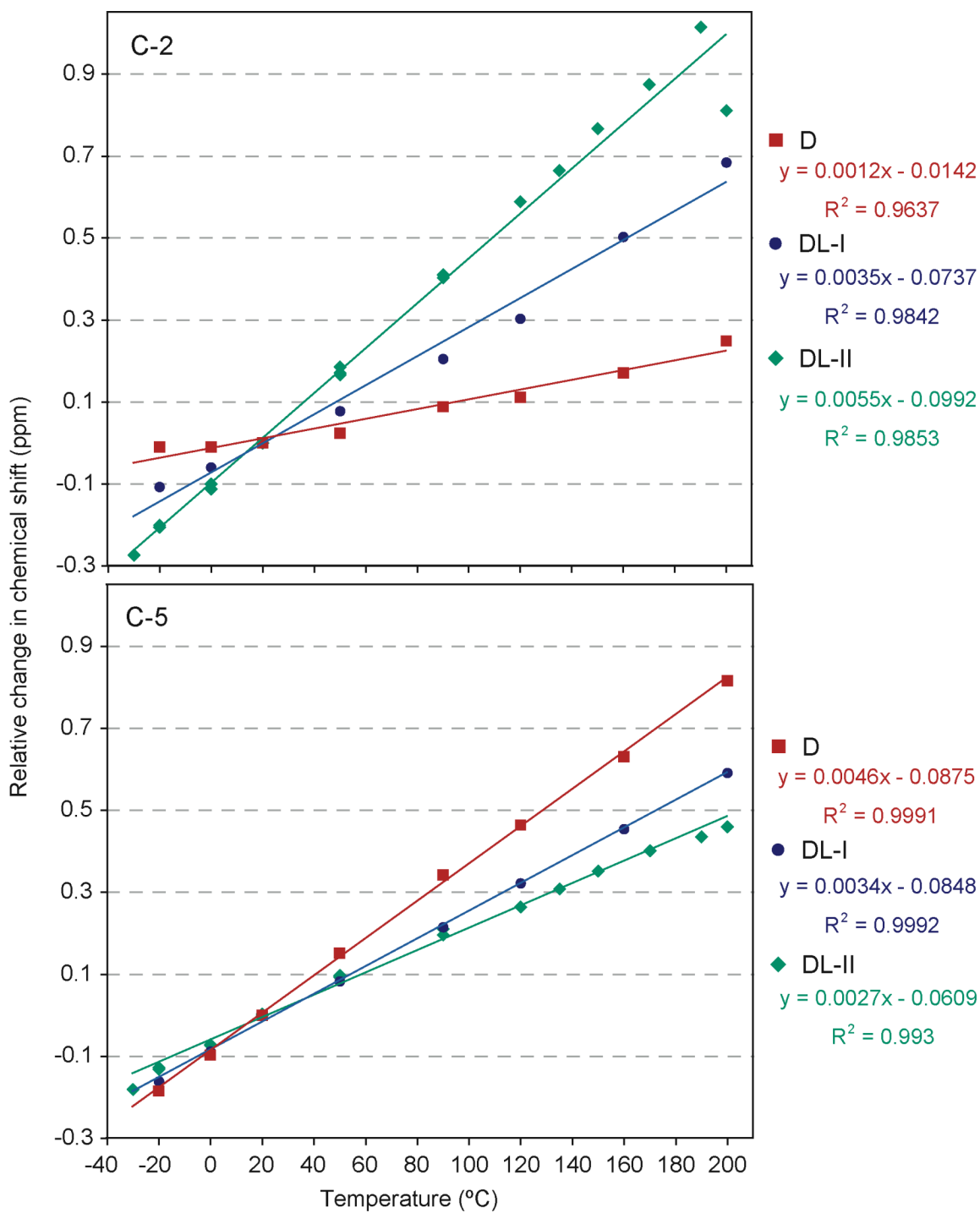
Figure 6.4b. ^{13}C CP-MAS NMR temperature dependence of C-2 and C-5 carbons of proline crystal forms D, DL-I, and DL-II. Peak shifts are plotted as the change in chemical shift relative to the position at 20ºC.

215

Figure 6.4c. ^{13}C CP-MAS NMR temperature dependence of C-3 and C-4 carbons of proline crystal forms D, DL-I, and DL-II. Peak shifts are plotted as the change in chemical shift relative to the position at 20ºC.

216

For all additional analyses of cryoground proline samples, the SSNMR probe was pre-cooled to -20ºC in attempt to stabilize any metastable physical forms that might be present. Ad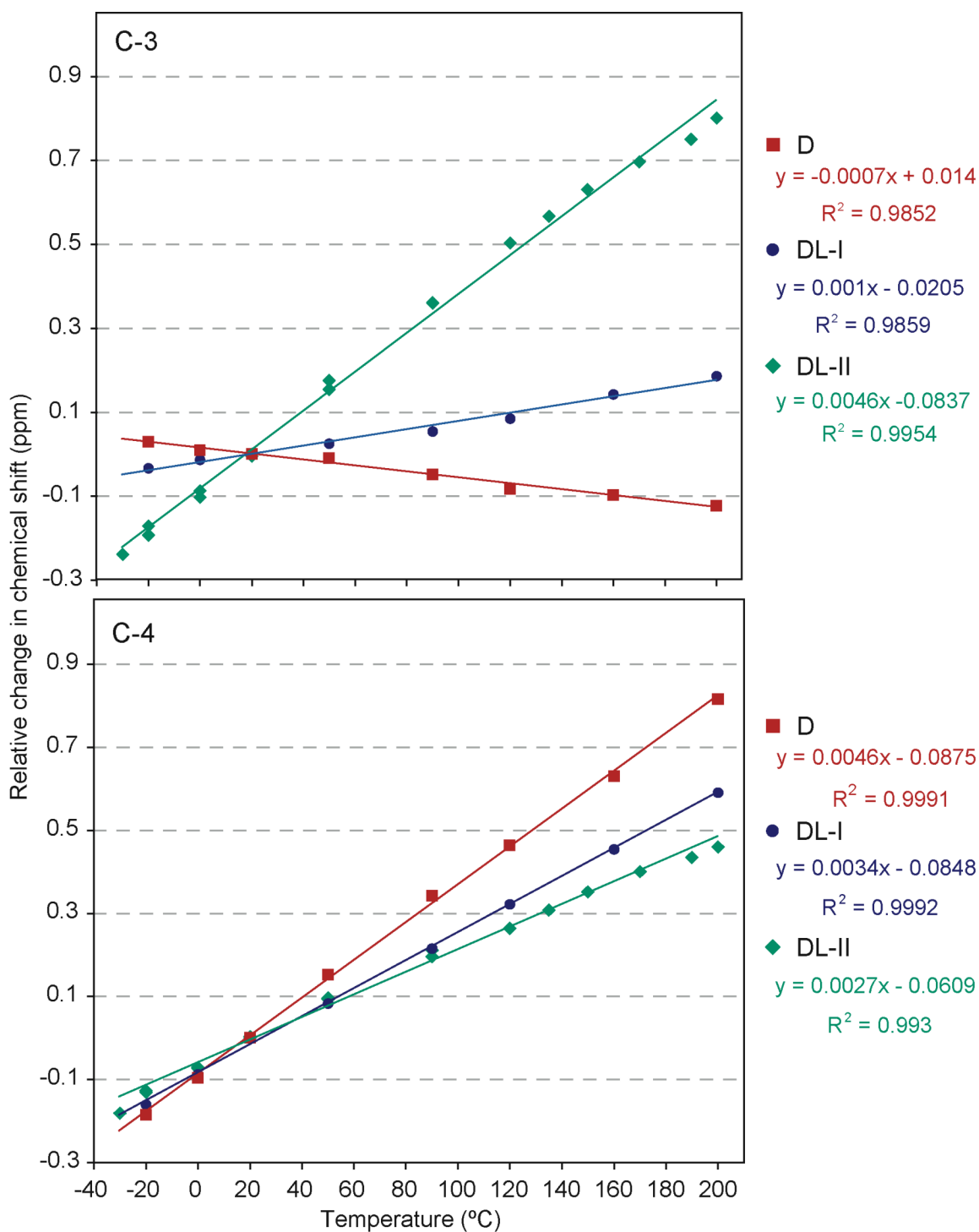ditionally, steps were taken to keep the samples dry, since the presence of water has been shown to reduce the stability of amorphous and disordered forms.[19-21] Cryovials were sealed in a dry nitrogen glove box prior to cryogrinding and moved back to the glove box after the grinding process, at which time samples were quickly packed into SSNMR rotors, PXRD sample holders, and DSC pans for analysis.

Following initial SSNMR characterization at -20ºC, spectra were acquired as the temperature was increased step-wise, typically in 10ºC increments, with a 15-min temperature-equilibration period at each step. SSNMR is a powerful identification method, and by adding the variable-temperature component, it potentially allows for identification of thermal transitions observed by DSC, which is not considered an identification method.[22] Whereas SSNMR provides valuable identification information, DSC provides information about energetic changes associated with physical and chemical transformations. Comparison of DSC results (thermal information) to VT SSNMR analysis (spectroscopic identification) can potentially be very helpful in characterizing temperature-dependent physical transformations of a system. However, although VT SSNMR and DSC are complementary techniques, the large difference in heating kinetics associated with these two methods (minutes for DSC, hours/days for VT SSNMR) means that direct comparisons of the results are not always possible.

6.3.2   Cryogrinding D-proline

Another sample of bulk D-proline was cryoground for 30 min and quickly transferred to the pre-cooled SSNMR probe. The ^{13}C CP-MAS NMR spectrum of this freshly cryoground material at -20ºC is shown in Figure 6.5. As with the previous sample of cryoground D-proline (Figure 6.1), multiple peaks were observed for each carbon in the spectrum. By maintaining the sample temperature below 20ºC, transformation of the forms within the sample was minimized, allowing high–signal-to-noise spectra to be collected. The widths of the peaks in the spectra indicate that these are crystalline, not amorphous materials.

In both iterations of cryogrinding D-proline, amorphous material was not observed by SSNMR analysis. It may not be possible to completely disorder/amorphize the D-proline crystal lattice. This type of resistance to mechanical disordering has been reported for other small molecules, including acetaminophen and aspirin.[23]   Although amorphous material was not observed, the presence of metastable crystalline forms was evidenced by "disappearing" peaks in the ^{13}C CP-MAS NMR spectra of cryoground D-proline. It is not clear if each peak corresponded to a distinct crystalline phase, or if they indicated crystallographic inequivalence. Relaxation measurements were not able to distinguish between these two possibilities.

Figure 6.6 shows the PXRD pattern of the cryoground D-proline material. No environmental control during analysis was possible, but the sample holder was packed within a dry nitrogen glove box and analyzed with a short dwell time (0.3 s/step, ~7 min total) immediately after preparation. No new peaks were observed in the pattern of this
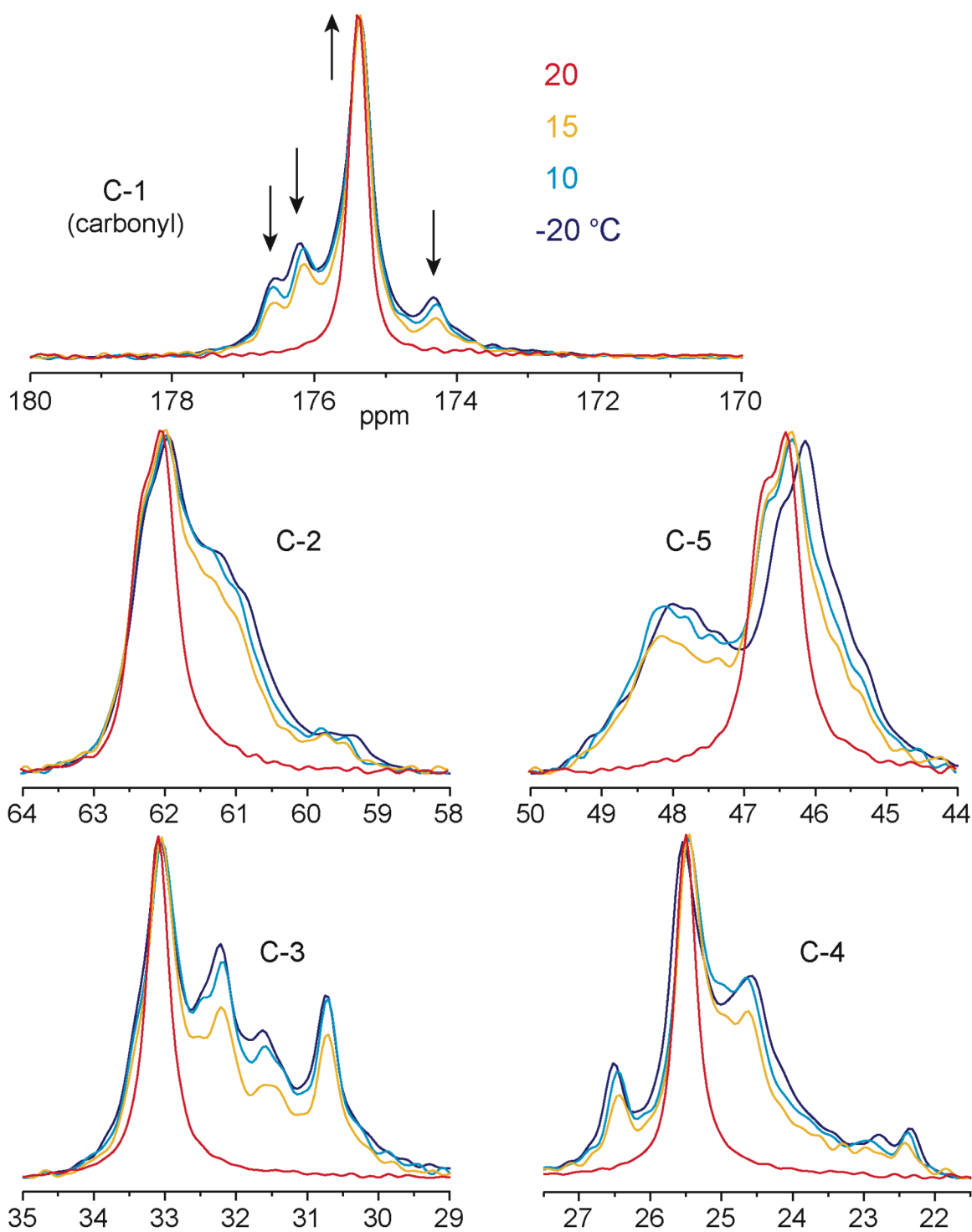
Figure 6.5. ^{13}C CP-MAS NMR spectra of cryoground (30 min) D-proline. Spectra were acquired at -20, 10, 15, and then 20ºC. The spectral region of each carbon in the proline molecule has been plotted separately and normalized to the same maximum intensity.

219
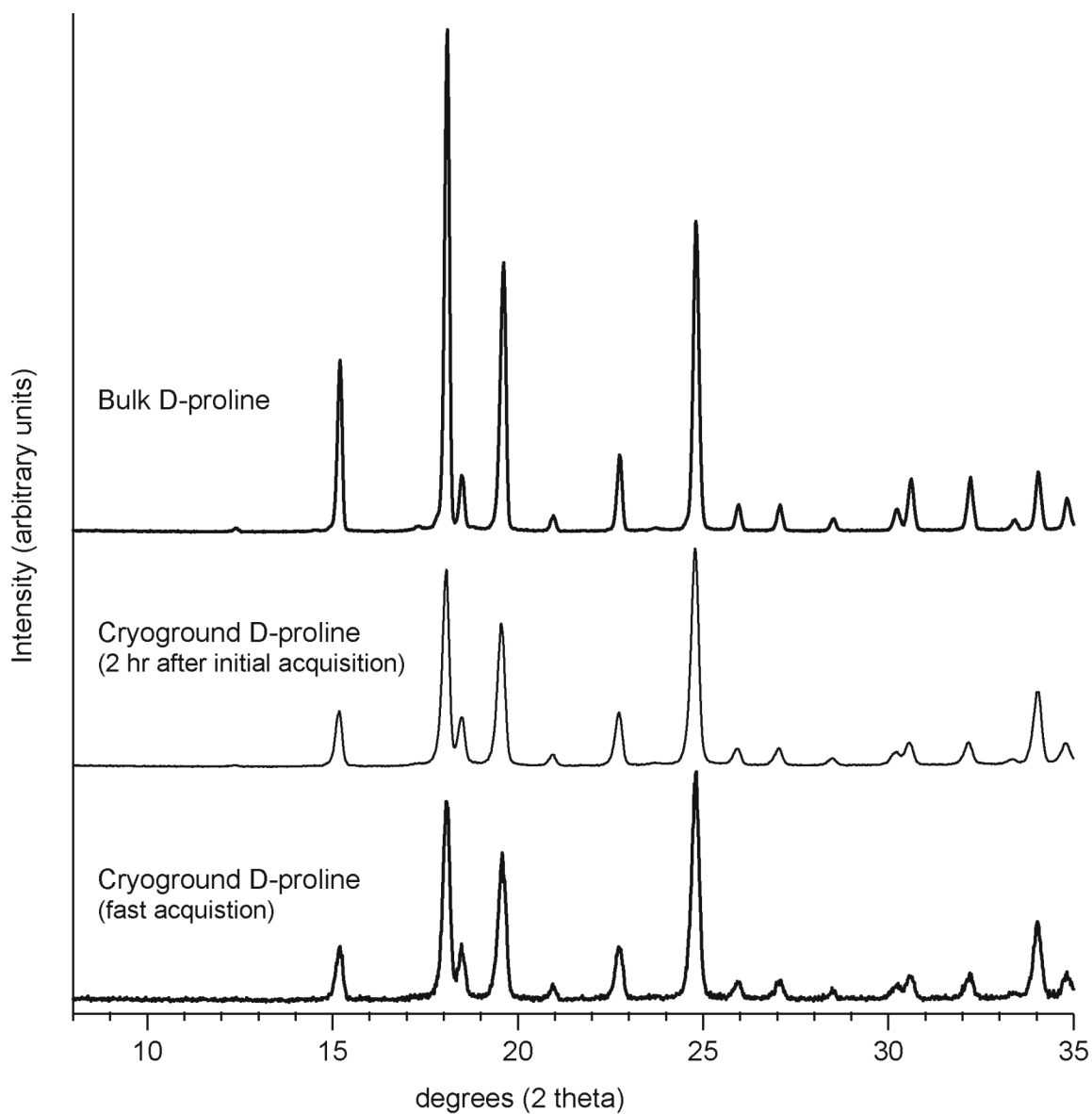
Figure 6.6. PXRD patterns for cryoground (30 min) D-proline immediately after preparation (fast acquisition) and again after 2 hr at ambient conditions. The diffraction pattern for the bulk D-proline material is shown for reference.

cryoground material, and peak widths did not appear to be significantly different from those of the bulk material. Additionally, no amorphous halo was observed. This supports the observations of SSNMR in that cryogrinding bulk D-proline did not produce amorphous material. Although amorphous/disordered materials have an increased tendency to sorb ambient water vapor,[19] which can induce crystallization,[20] diffraction peaks corresponding to the hydrated form were not observed.

Figure 6.7 shows DSC thermograms of the bulk D-proline material and the freshly cryoground sample. In the cryoground material, there is an exothermic transition with an onset of ~26ºC. This temperature corresponds well with the observed transformation by SSNMR, in which the additional peaks disappeared quite quickly after the sample temperature was increased to 20ºC. Thus, this exothermic transition might correspond to the monotropic[24] transformation of the metastable crystalline D-proline to the known crystal form of D. At higher temperatures, the DSC thermogram contains two melting peaks: a eutectic, indicating the presence of the opposite L-enantiomer in the bulk material, and the liquidus melt. The melting temperature of the cryoground material was lower than the bulk, possibly due to differences in particle size.[25]

Two attempts to produce amorphous D-proline by cryogrinding were unsuccessful. This is not altogether surprising, as lyophilization of L-proline, even under N_2-lyophilization conditions, also did not result in an observable amorphous phase (Chapter 5). As noted previously, some materials are unable to be fully amorphized by grinding, even at low temperature.[23] In order to determine if the racemic cocrystal also was resistant to amorphization, DL-I was cryoground for 30 min and analyzed.
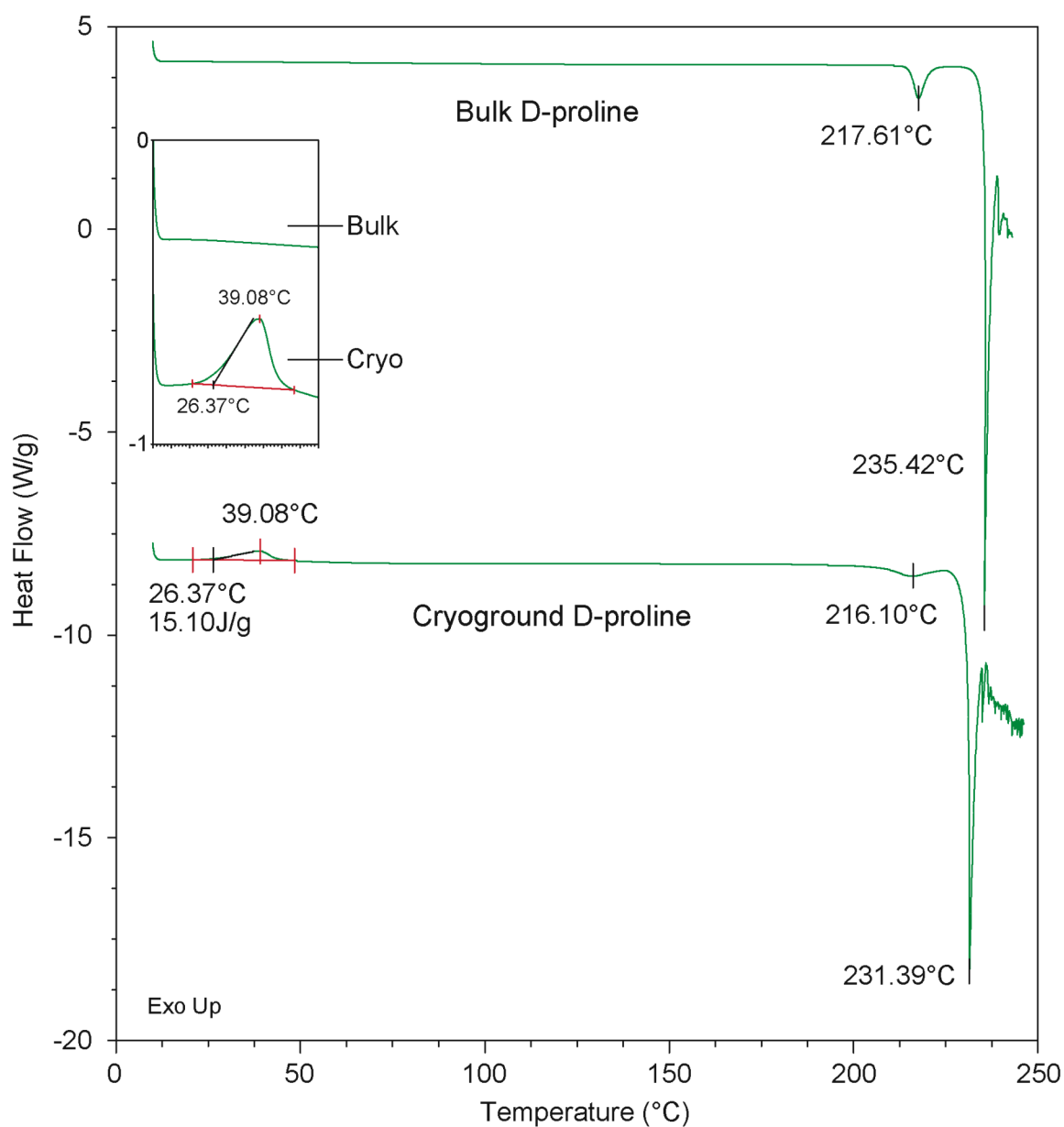
Figure 6.7. DSC thermograms of bulk and cryoground D-proline. Inset shows a y-axis expansion from 10–55ºC.

6.3.3   Cryogrinding DL-proline form I

Figure 6.8 shows VT ^{13}C CP-MAS NMR of cryoground DL-I (30 min) from -20 to 50ºC. In the initial spectrum, collected at -20ºC (bold purple line), broad amorphous peaks are clearly observed. These amorphous peaks overlap with small crystalline peaks (denoted by arrows) that correspond to DL-I. This suggests that 30 min of cryogrinding successfully amorphized part, but not all, of the DL-I starting material. As the sample temperature was increased, two transformations were observed in the SSNMR spectra. First, between 20 and 30ºC, a large reduction in peak width and change in chemical shift occurred (Figure 6.8a), but the peaks remained quite broad and did not appear to correspond to a crystallization event. The second transformation was crystallization to DL-I between 40 and 50ºC (Figure 6.8b).

PXRD diffraction patterns of the cryoground DL-I are shown in Figure 6.9. An initial acquisition with a short dwell time (0.3 s) indicated the presence of both DL-I and DL-II crystal forms. After 4 hr at ambient laboratory conditions, changes in the sample were observed, including the appearance of the characteristic peak of DL-MH (~8.8º 2θ) and relative increases in the intensity of DL-II peaks (characteristic peak at 14.2º 2θ) and corresponding decreases in DL-I (characteristic peak at 9.8º 2θ). All of these changes can possibly be explained by the absorption of water, as this could have led to the formation of the monohydrate crystal and increased the mobility within the system, therein allowing the transformation of the kinetically stable DL-I to DL-II.[19]

Figure 6.10 shows DSC thermograms of the bulk and cryoground DL-I. The thermogram for cryoground material contained a large exothermic transition after 50ºC. This is attributed to the crystallization event observed between 40 and 50ºC by
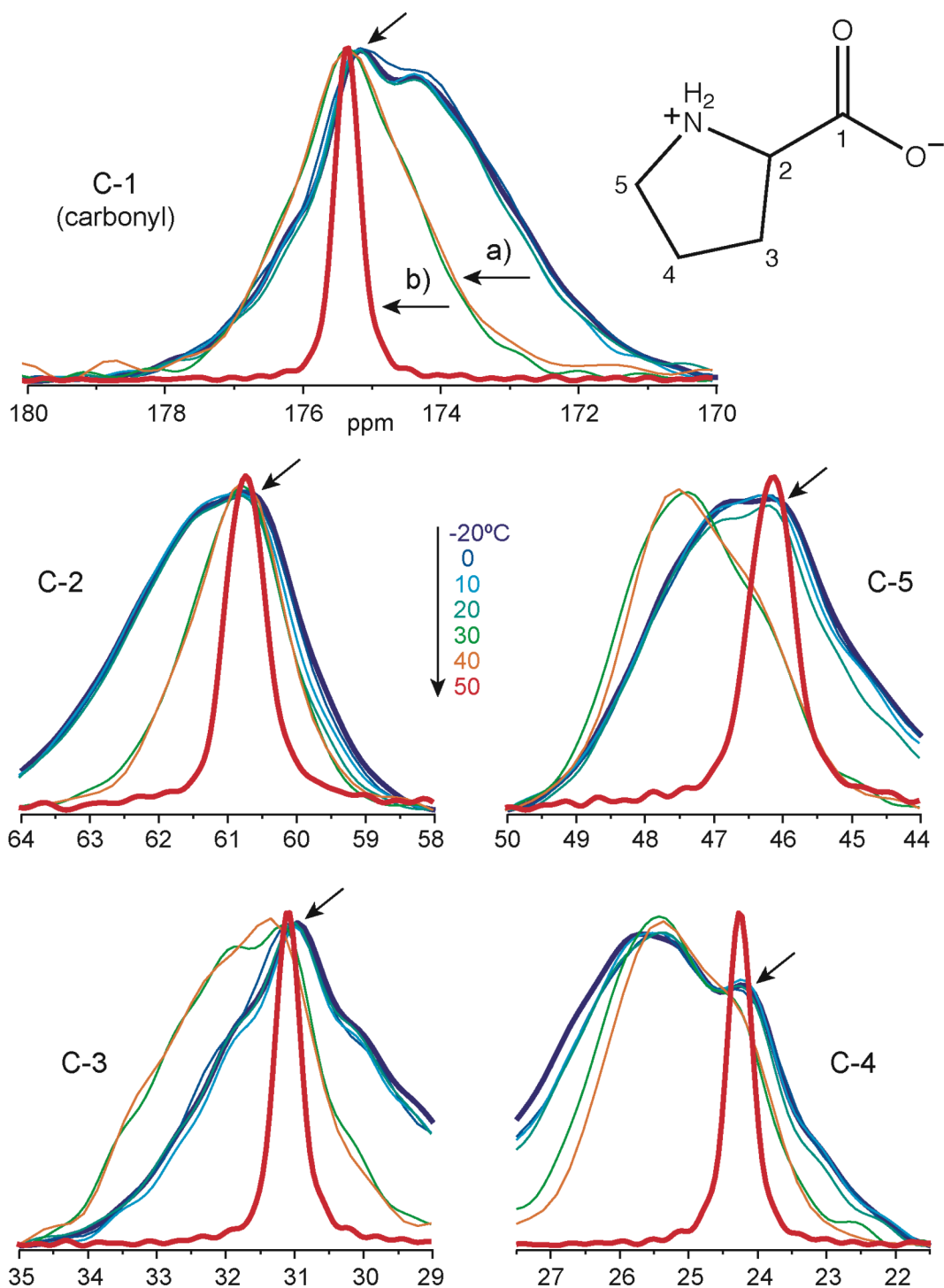
Figure 6.8. ^{13}C CP-MAS NMR spectra of cryoground (30 min) DL-I. Spectra were acquired at -20 to 50ºC in 10ºC increments. The spectral region of each carbon in the proline molecule has been plotted separately. a) Transition between 20 and 30ºC. b) Crystallization transition between 40 and 50ºC. Arrows denote crystalline peaks. Bold lines indicate initial (-20ºC) and final (50ºC) spectra.
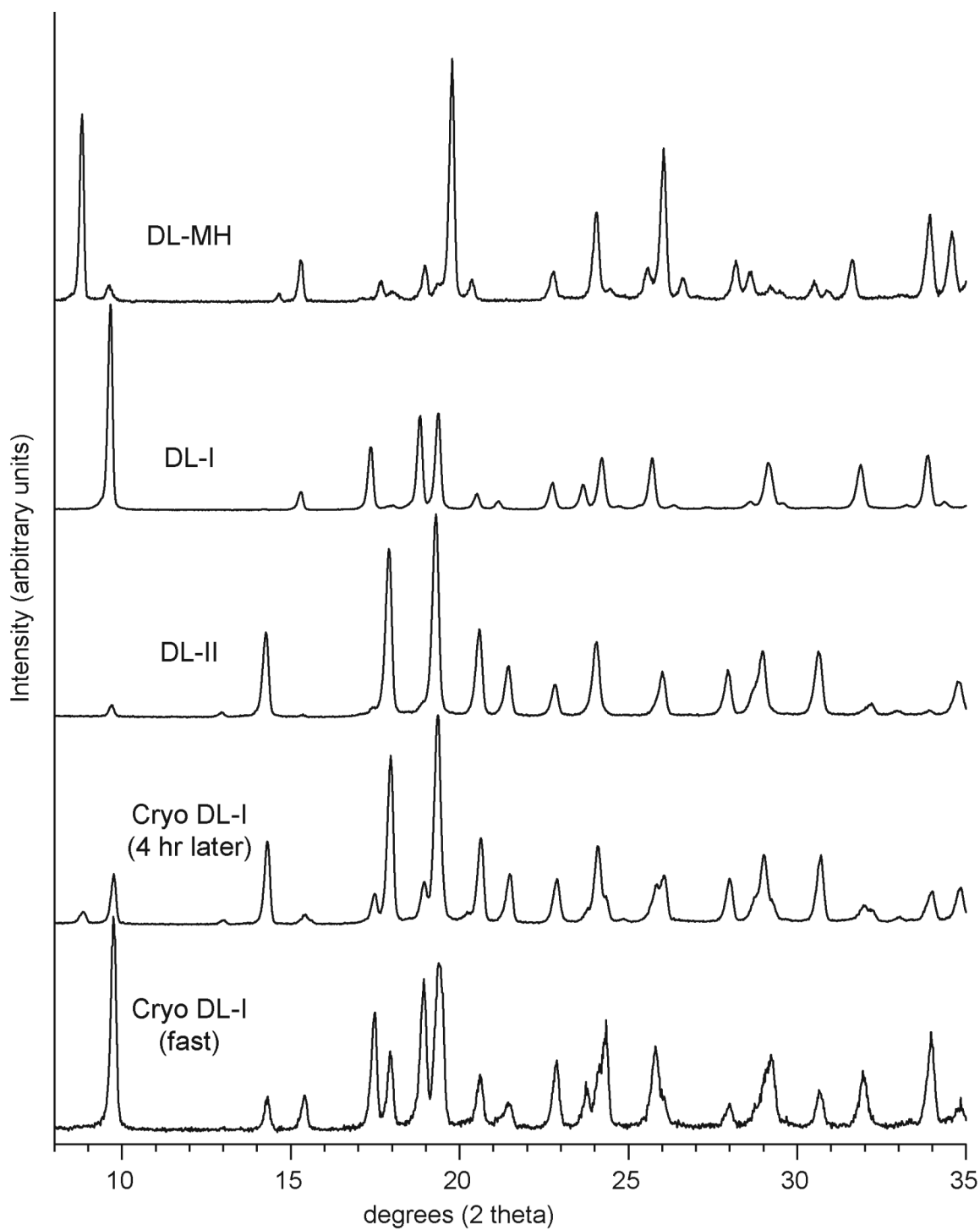
Figure 6.9. PXRD patterns of cryoground (30 min) DL-I acquired with a fast (0.3 s) dwell time and again after 4 hr with a 4 s dwell time. PXRD patterns for D, DL-I, and DL-II proline crystal forms are shown for reference.
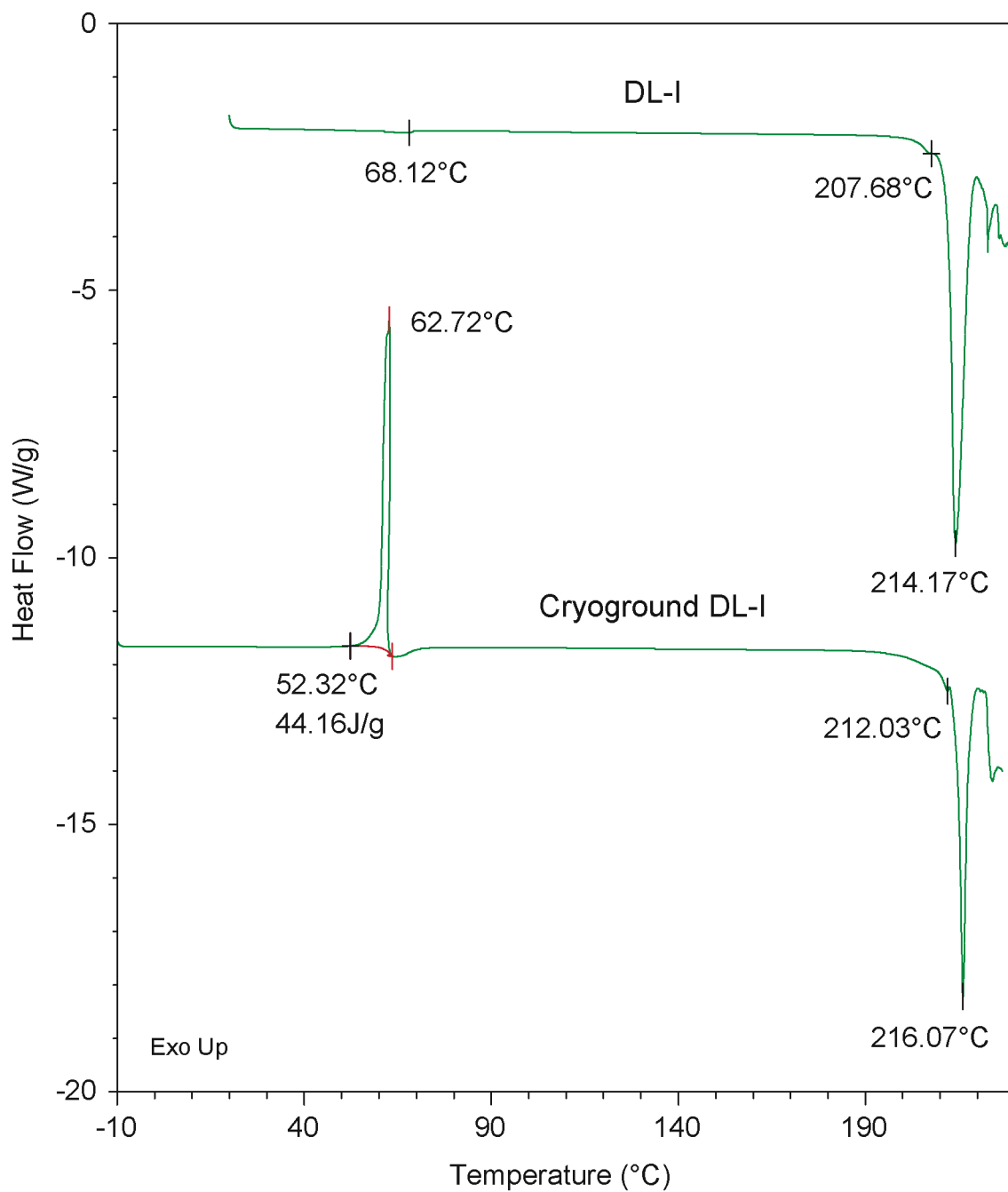
Figure 6.10. DSC thermograms of bulk and cryoground (30 min) DL-I.

SSNMR. The melting endotherm for the cryoground DL-I was located at ~216ºC, which suggests the melting of DL-II (mp ~217ºC) versus DL-I (mp ~213ºC). However, as mentioned previously, the use of DSC for polymorph identification can be ambiguous.[22] Despite the observation of amorphous material by SSNMR and a crystallization peak by DSC, a T_g transition was not observed by DSC or MDSC of the cryoground material (not shown).

It is important to reiterate that the heating rate for analysis by SSNMR versus DSC was very different in these studies. Whereas DSC samples were analyzed while heating at a constant rate of 10ºC/min, the SSNMR samples were heated step-wise (from -20 to 50ºC for the cryoground DL-I sample) over the course of hours, and ^{13}C CP-MAS NMR spectral acquisitions occurred under isothermal holds. Previous studies have demonstrated that the heating rate and thermal history can have a dramatic effect on the crystallization product and the observation of intermediate forms.[6] The potential for such differences in transformations needs to be kept in mind when directly comparing DSC and VT-SSNMR results.

For the cryoground DL-I sample, broad peaks characteristic of an amorphous phase were observed in the ^{13}C CP-MAS NMR spectrum, but the presence of amorphous material was not necessarily supported by PXRD or DSC analyses. Of particular interest in the SSNMR spectra was the transition from one set of broad peaks to another between 20 and 30ºC. There were no transitions in the DSC thermogram that could be assigned to this SSNMR-observed transition, possibly due to conversion prior to the DSC run or due to differences in the kinetics of the two thermal analyses. The breadth of the SSNMR peaks before and after this transition is typically associated with the presence of an

amorphous phase, which suggests that this peak shift might be associated with the amorphous phase transition from the rubbery to the glassy state. This transition (glass transition, T_g) is a reversible process. In order to better understand this transition, and determine its potential reversibility, the VT-SSNMR analysis of cryoground DL-I was repeated with the addition of a heat-cool-heat cycle during the course of the experiment.

6.3.4   Reversibility of broad–broad peak transition

A sample of DL-I was cryoground for 30 min, quickly packed into a rotor within the glove box, and transferred to the pre-cooled SSNMR probe. VT ^{13}C CP-MAS NMR spectra were collected in 3 phases (heat-cool-heat: -20→30→10→50) as shown in Figure 6.11. These results showed the same transition previously observed between 20 and 30ºC. After increasing the temperature through this transition, the temperature was lowered back to 20ºC, then 10ºC, with no apparent change at either temperature. Sample temperature was then increased again, and no significant spectral changes were observed until crystallization to DL-I between 40 and 50ºC. The irreversibility of the transformation between 20 and 30ºC indicates that this event is not related to the glass transition, which is a reversible transition.

Figure 6.12 shows the PXRD diffraction pattern of the cryoground DL-I material corresponding to the SSNMR of Figure 6.11. The diffraction pattern of previously cryoground DL-I material (from Figure 6.9) is also shown. In the first preparation, PXRD indicated the presence of predominantly DL-II, but the peaks for the second preparation demonstrate a composition predominantly of DL-I.
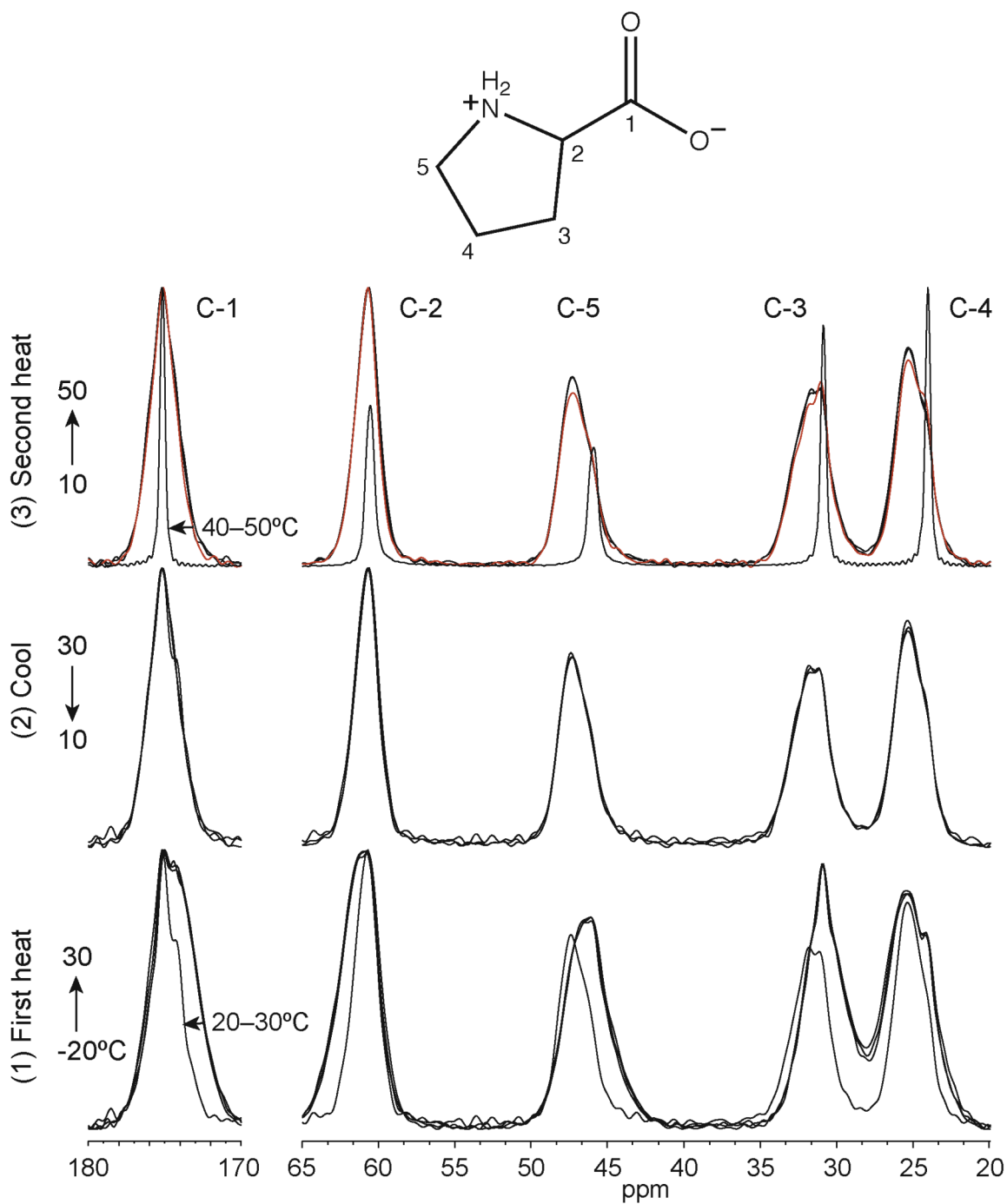
Figure 6.11. VT ^{13}C CP-MAS NMR spectra of cryoground (30 min) DL-I. The VT experiment consisted of 1) heat: -20–30ºC, 2) cool: 30–10ºC, and 3) heat: 10–50ºC phases.
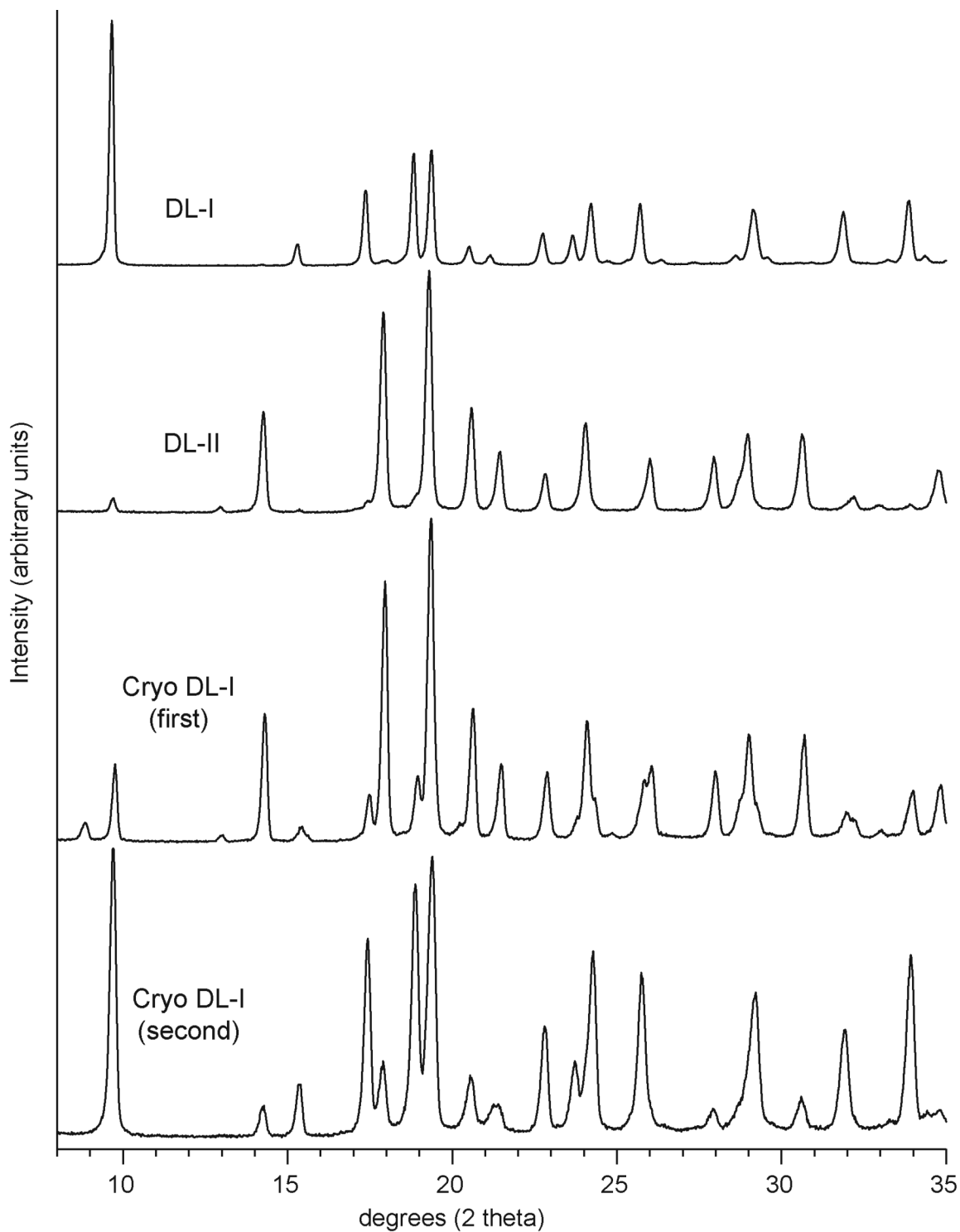
Figure 6.12. PXRD pattern of cryoground (30 min) DL-I (bottom, "second"). For reference, the patterns of the previously cryoground DL-I sample ("first"), DL-II, and DL-I are included.

Differences between the two iterations of cryogrinding were also observed by DSC. Figure 6.13 shows the DSC thermogram of the second preparation of cryoground DL-I. A small exotherm at ~35ºC and a large exotherm at ~65ºC were observed. The large exotherm, which had been observed previously (Figure 6.10), likely corresponded to the SSNMR-observed crystallization at ~50ºC. The smaller exotherm ~35ºC was not present in the thermogram shown in Figure 6.10. This event might correspond to the SSNMR-observed transition between 20 and 30ºC. The melting endotherms above 200ºC suggest the melting of both DL-I and DL-II crystal forms.

The exact nature of the 20–30ºC transition observed by SSNMR is still unclear. However, the VT SSNMR heat-cool-heat experiment indicates that it is nonreversible, and DSC suggests that it might be an exothermic transformation.

According to SSNMR, the final crystalline product upon cryogrinding DL-I was solely DL-I. The most likely explanation for this observation is that residual seed crystals of DL-I nucleated the crystallization of the amorphous phase. This is especially plausible because SSNMR indicated the presence of crystalline DL-I material following the cryogrinding process.[26] To test this, an equimolar physical mixture of enantiopure D- and L-proline bulk material were cryoground together. In this sample, even in the absence of complete amorphization, there should be no seed crystals of DL-I.

6.3.5 Cryogrinding D- and L-proline

Figure 6.14 shows ^{13}C CP-MAS NMR spectra of a cryoground (30 min) equimolar mixture of D- and L-proline (D+L). The initial material (-20ºC) contained the same broad amorphous peaks as the cryoground DL-I, but instead of the crystalline peaks
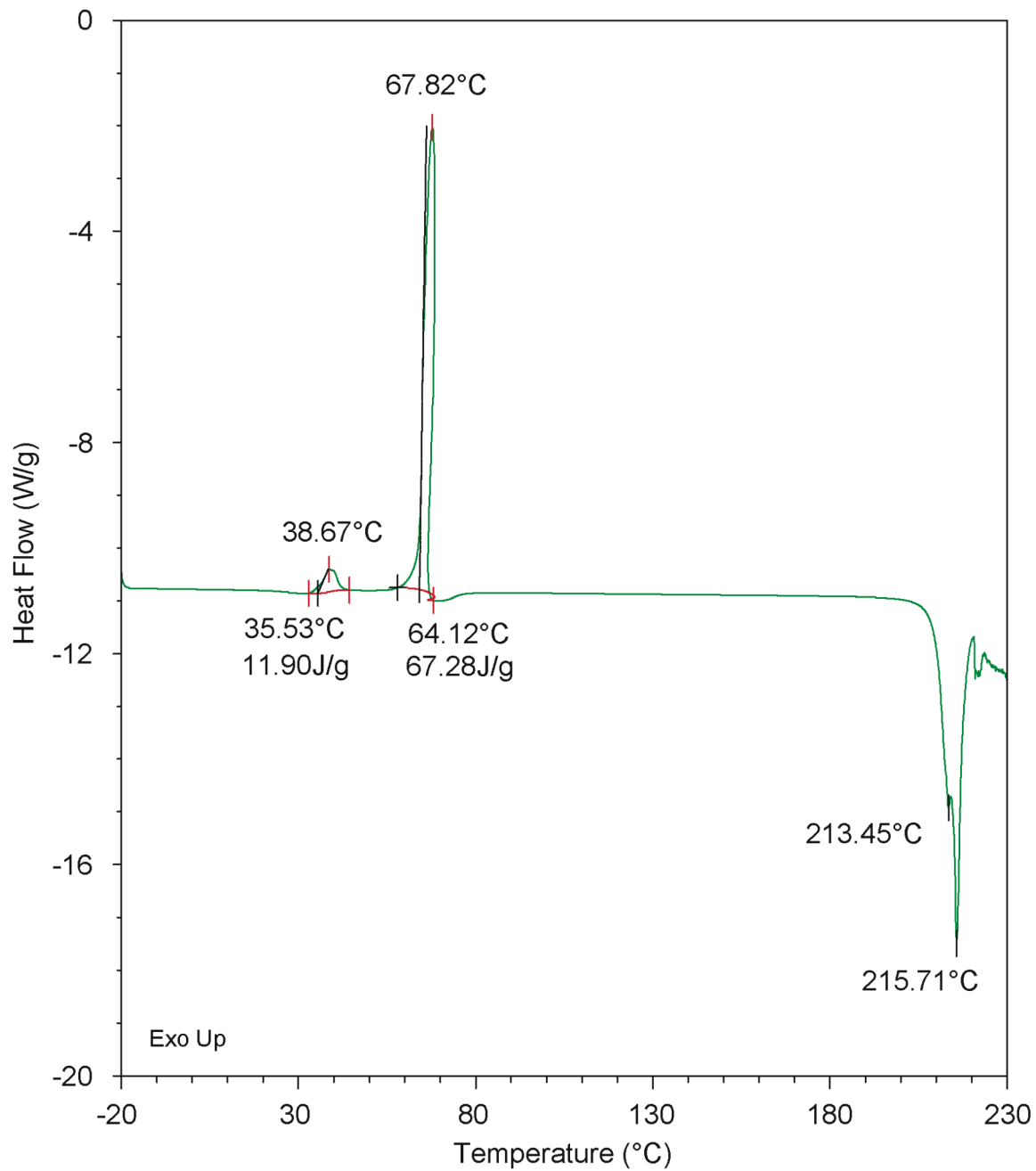
Figure 6.13. DSC thermogram for cryoground (30 min) DL-I.
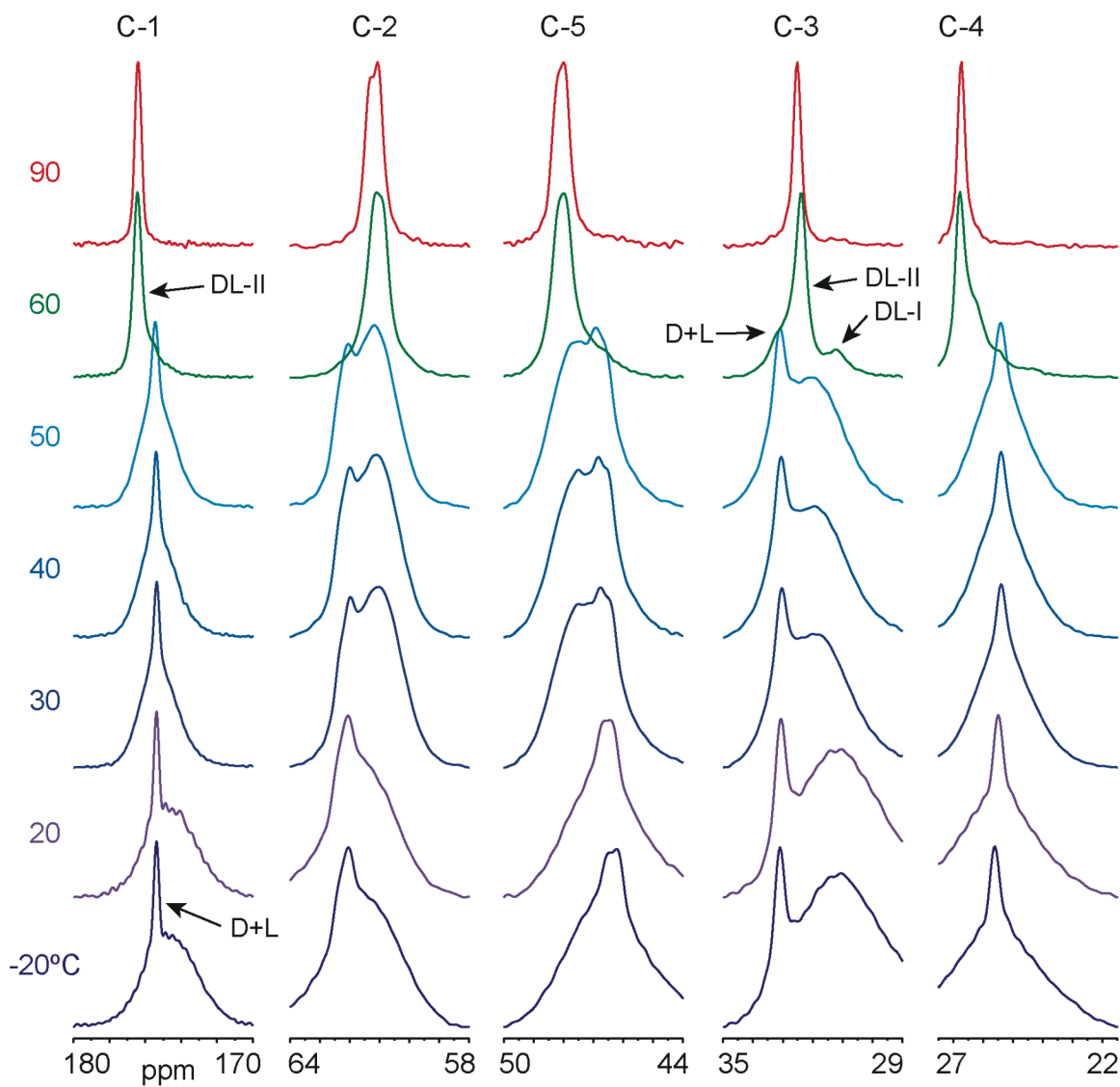
Figure 6.14. VT ^{13}C CP-MAS NMR spectra of a cryoground (30 min) equimolar mixture of D- and L-proline. Spectra were collected (from bottom to top) at -20, 20–60, and 90ºC.

of DL-I, crystalline peaks of enantiopure proline were observed. This demonstrates that the presence of crystalline material in both cryoground DL-I and cryoground D+L are due to incomplete mechanical disordering. Several notable transformations took place upon performing VT SSNMR. This analysis was performed over the course of two days, in the temperature sequence -20, 20–60 in 10ºC increments, and ending at 90ºC. First, the broad–broad peak transition was again observed between 20 and 30ºC. Comparing these broad D+L peaks to those of cryoground DL-I indicates no significant differences in peak position or shape. However, unlike in the cryoground DL-I samples, which crystallized by 50ºC, crystallization of this cryoground D+L sample did not occur until 60ºC. Additionally, this crystallization at 60ºC took place slowly enough to observe multiple phases in the ^{13}C CP-MAS NMR spectrum: The amorphous phase crystallized to DL-II relatively rapidly, but the aliphatic region, in particular at the C-3 peak (35–29 ppm), shows the presence of both enantiopure crystalline material and DL-I. By 90ºC, all of the observed peaks correspond solely to DL-II.

The presence of peaks corresponding to crystalline D- and L-proline in the initial SSNMR spectra demonstrates that the cryogrinding process did not create a completely homogeneous molecular dispersion of the enantiomers. Interestingly, the temperature at which crystallization of the amorphous phase took place (~60ºC) was higher than the crystallization of cryoground DL-I (<50ºC). This higher temperature requirement is potentially indicative of the additional energy necessary for molecular translation to form the DL lattice in the absence of seed crystals.

Although it is expected that the amorphous material would crystallize to a racemic cocrystal, it was interesting that the residual enantiopure crystalline material also

234

converted into the racemic cocrystal at the same temperature (~60ºC). This enantiopure → cocrystal solid-state transformation is possibly explained by the relatively high-energy state and small particle size typically associated with cryoground materials. The ability for cryogrinding to affect molecular mobility, and therefore the physical stability, of solid materials has been demonstrated previously.[21,27]

PXRD analysis (not shown) of the freshly cryoground D+L sample indicated the presence of DL-II with small peaks of DL-I. All peaks were narrow and well resolved, indicative of ordered lattice structures for the DL-I and II crystal forms. Peaks for enantiopure proline and DL-MH were not observed. Because analysis took place under ambient conditions, it is possible that the combination of uncontrolled temperature and ambient water vapor allowed crystallization of both amorphous and residual enantiopure crystalline material into the racemic cocrystal forms prior to analysis.

Figure 6.15 shows a DSC thermogram of the material, which gave rise to multiple exothermic peaks (~45ºC, 83ºC and 91ºC, peak temps) and a possible endothermic peak overlapping with the first exotherm. The presence of multiple exotherms in the DSC (~83 and 91ºC) near the temperature of SSNMR-observed crystallization (~60ºC) suggests that one exotherm might correspond to the crystallization of the amorphous phase, and the other might correspond to the enantiopure → racemic cocrystal transformation. Also, these crystallization temperatures are higher than the crystallization temperature observed for cryoground DL-I (~65ºC). As noted previously, this higher temperature might reflect the greater molecular mobility necessary for arranging D- and L-proline molecules into the DL crystal lattice (i.e., to nucleate) in the absence of seed crystals. Once again, MDSC did not show the presence of a T_g or
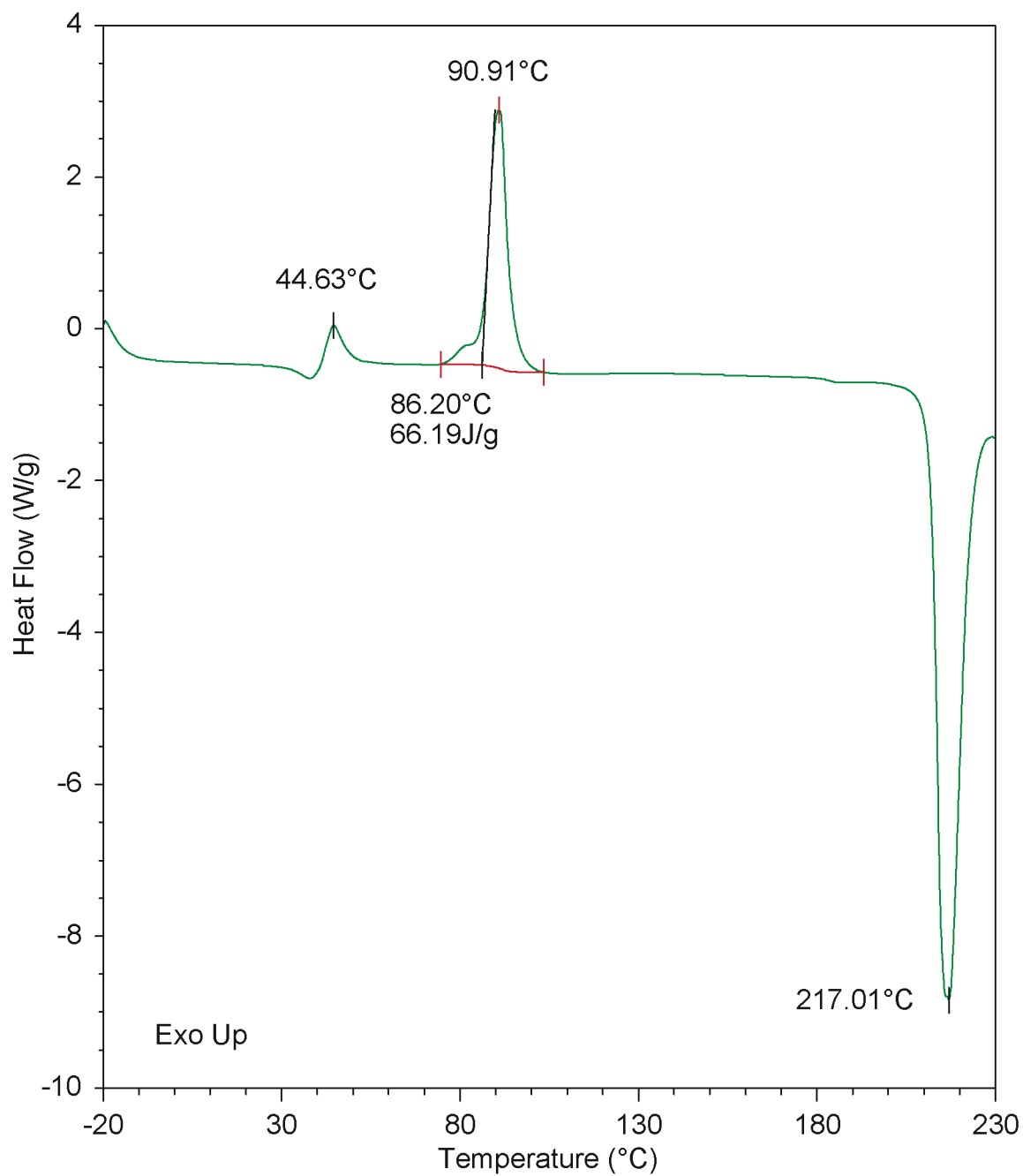
Figure 6.15. DSC thermogram of a cryoground (30 min) equimolar mixture of D- and L-proline.

any other reversible event within the sample. The melting endotherm at 217ºC demonstrates DL-II melting.

Overall, the results from the analysis of cryoground D+L are consistent with the idea that seed crystals strongly influence the formation of DL-I or DL-II. In the presence of DL-I seeds, DL-I forms. In the absence of such seeds, DL-II forms. It is possible that enantiopure material could act as seeds for DL-II, since the ^{13}C CP-MAS NMR spectra in Figure 6.14 indicated that a relatively large amount of enantiopure crystalline material (sharp peaks in the spectrum) remained after the 30 min of grinding. To attempt complete amorphization of the sample, and possibly achieve a complete molecular dispersion of the two enantiomers, an additional equimolar D+L sample was prepared by cryogrinding for 60 min.

Figure 6.16 shows the VT ^{13}C CP-MAS NMR spectra of the cryoground (60 min) D+L material. As before, spectra were collected step-wise as the sample temperature was increased: -20, 20, 30, 60, 90–120 in 10ºC increments, 150, 200 (briefly), and ending with 20ºC. The initial material (-20ºC) contained peaks for an amorphous phase and for crystalline enantiopure material, similar to the previously cryoground sample. However, in this sample, the relative intensities of the crystalline peaks are much smaller. This is attributed to the increased grinding time (30 versus 60 min), which led to a greater degree of amorphization of the material. Upon increasing the sample temperature, notable spectral changes occurred between 20 and 30ºC (Figure 6.16a), at which point the broad amorphous peaks appeared to shift, and between 50 and 60ºC (Figure 6.16b), where complete crystallization of the amorphous phase to DL-II occurred. Very small peaks that correspond to the presence of DL-I were detected in the spectra from 60ºC to 200ºC.

237
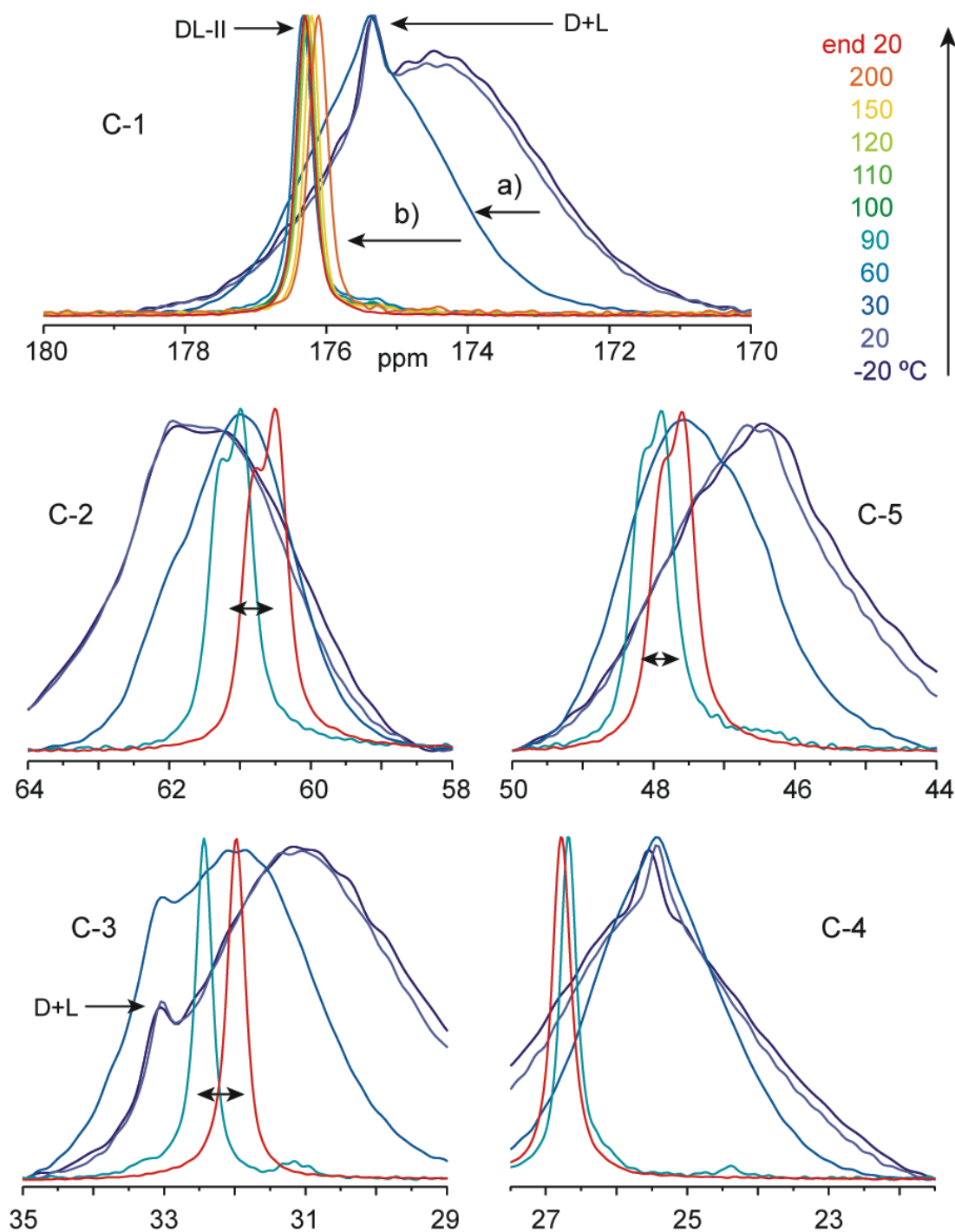
Figure 6.16. ^{13}C CP-MAS NMR spectra of a cryoground (60 min) equimolar mixture of D- and L-proline. Spectra were acquired from -20 to 200ºC and then at 20ºC. The spectral region of each carbon in the proline molecule is plotted separately. a) Transition between 20 and 30ºC. b) Crystallization transition (to DL-II) between 50 and 60ºC. Double-headed arrows highlight temperature-dependent peak shifts for DL-II between 90 and 20ºC.

Upon lowering the temperature back to 20ºC, the spectrum contained only peaks corresponding to DL-II.

Previous PXRD analyses of cryoground proline samples did not detect an amorphous/disordered phase, but only the sharp diffraction peaks of crystalline material. In order to potentially mitigate thermal instability of the cryoground sample, the stainless-steel sample holder for PXRD analysis was pre-cooled at -40ºC. Upon completion of the cryogrinding process, the sample holder was packed under dry nitrogen and promptly transferred to the PXRD instrument. Figure 6.17 (bottom pattern) shows a diffraction pattern that was quickly collected with a 0.3-s dwell time, a step size of 0.06º, and a range of 5–35º 2θ (total analysis time of 2.5 min). Diffraction peaks at ~14.3 and 14.8º 2θ indicated the coexistence of DL-II and enantiopure crystalline proline forms. An additional peak at ~24.6º 2θ (1.6 min from the beginning of the data collection) also demonstrated the presence of the enantiopure crystal form. Consecutive analysis with a longer dwell time indicated that the enantiopure crystal form was no longer present in the sample, as all diffraction peaks of the enantiopure lattice were absent, and only peaks of DL-II remained. This means that complete transformation of the enantiopure crystal lattices → DL-II took place in <3 min when exposed to ambient conditions. The pattern did not significantly change after a full day at ambient conditions, or after heating at 60ºC, 100ºC, or 160ºC (not shown). This demonstrates that the cryoground proline samples are very unstable at ambient conditions and transform rapidly into stable forms. It also indicates that the PXRD analyses performed on cryoground proline samples are probably not representative of the material observed by VT SSNMR, and direct comparisons between results from the two methods are not possible.
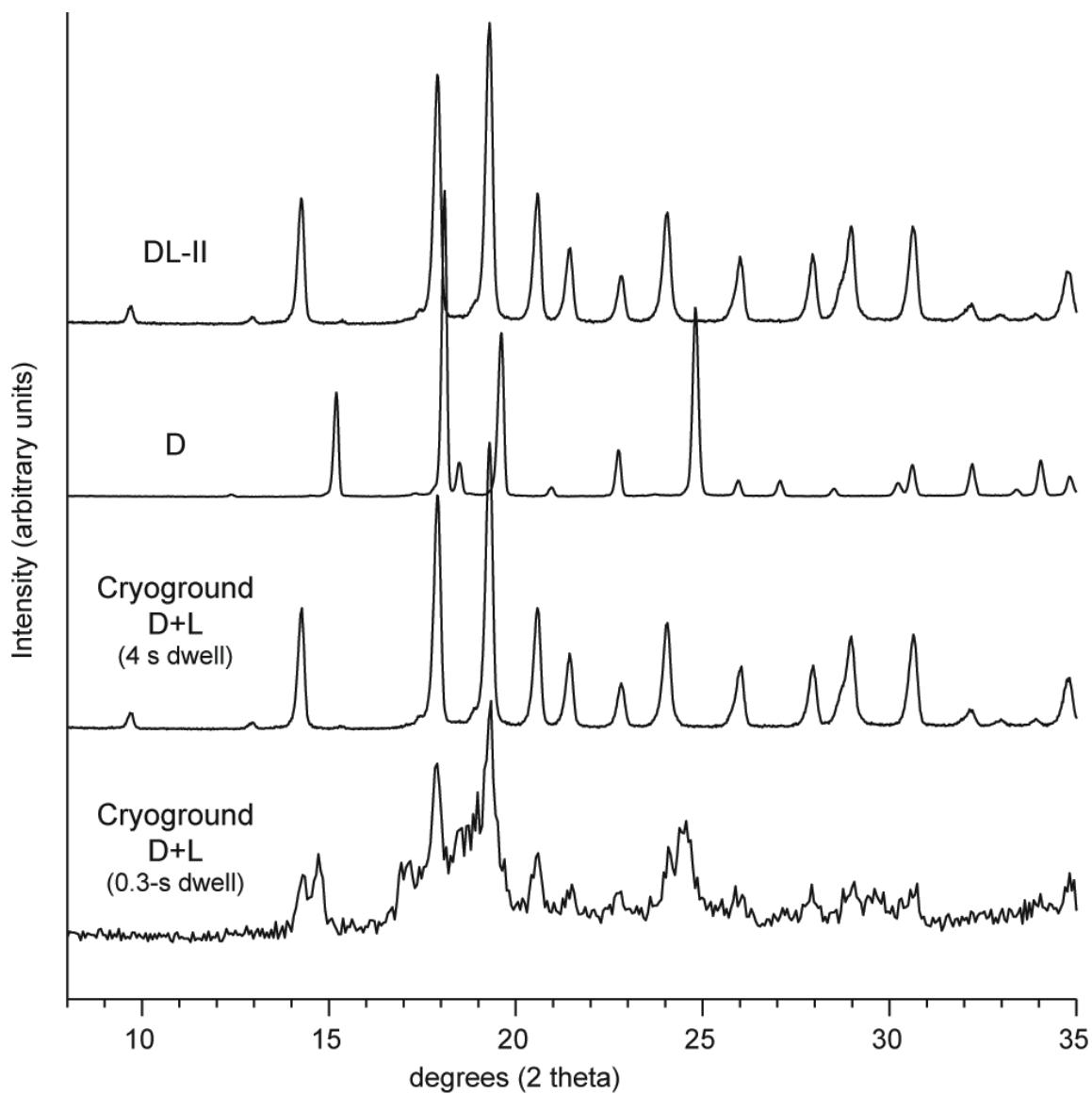
Figure 6.17. PXRD patterns of a cryoground (60 min) equimolar mixture of D- and L-proline acquired with a fast dwell time (0.3 s, bottom) and immediately repeated (4-s dwell, second from bottom). Patterns of D and DL-II are included for reference.

Figure 6.18 shows DSC analysis of the freshly ground material. The thermogram for this sample (cryoground 60 min) was very similar to the sample cryoground for 30 min. Both possessed the same exotherms between 30 and 100ºC, and a single melting endotherm. Unlike previous samples, these pans were packed into hermetic pans and sealed within the glove box (versus standard pans packed under nitrogen but crimped at ambient conditions). These preparation conditions did not noticeably affect the thermal transitions. Heat-cool-heat and MDSC methods demonstrated that the observed exothermic transitions were nonreversible, and no T_g was observed by MDSC.

The SSNMR and DSC results were similar for D+L samples cryoground for 30 and 60 min. In both cases, SSNMR demonstrated the presence of residual crystalline enantiopure material, which indicated that the cryoground material was not a fully amorphized, homogeneous molecular dispersion of enantiomers. Both SSNMR and DSC indicated that crystallization occurred at a higher temperature than crystallization of cryoground DL-I materials, and SSNMR showed that crystallization of the cryoground D+L material produced DL-II as the initial crystalline phase. These results support the effect of seeding in the cryoground DL-I samples.

6.4   Discussion

6.4.1   Cryogrinding enantiopure proline

During the course of these experiments, proline samples of three different compositions were cryoground: enantiopure D-proline, DL-proline form I, and an equimolar physical mixture of D- and L-proline. D-proline could not be amorphized, even after 60 min of cryogrinding. The ability for a material to be resistant to complete
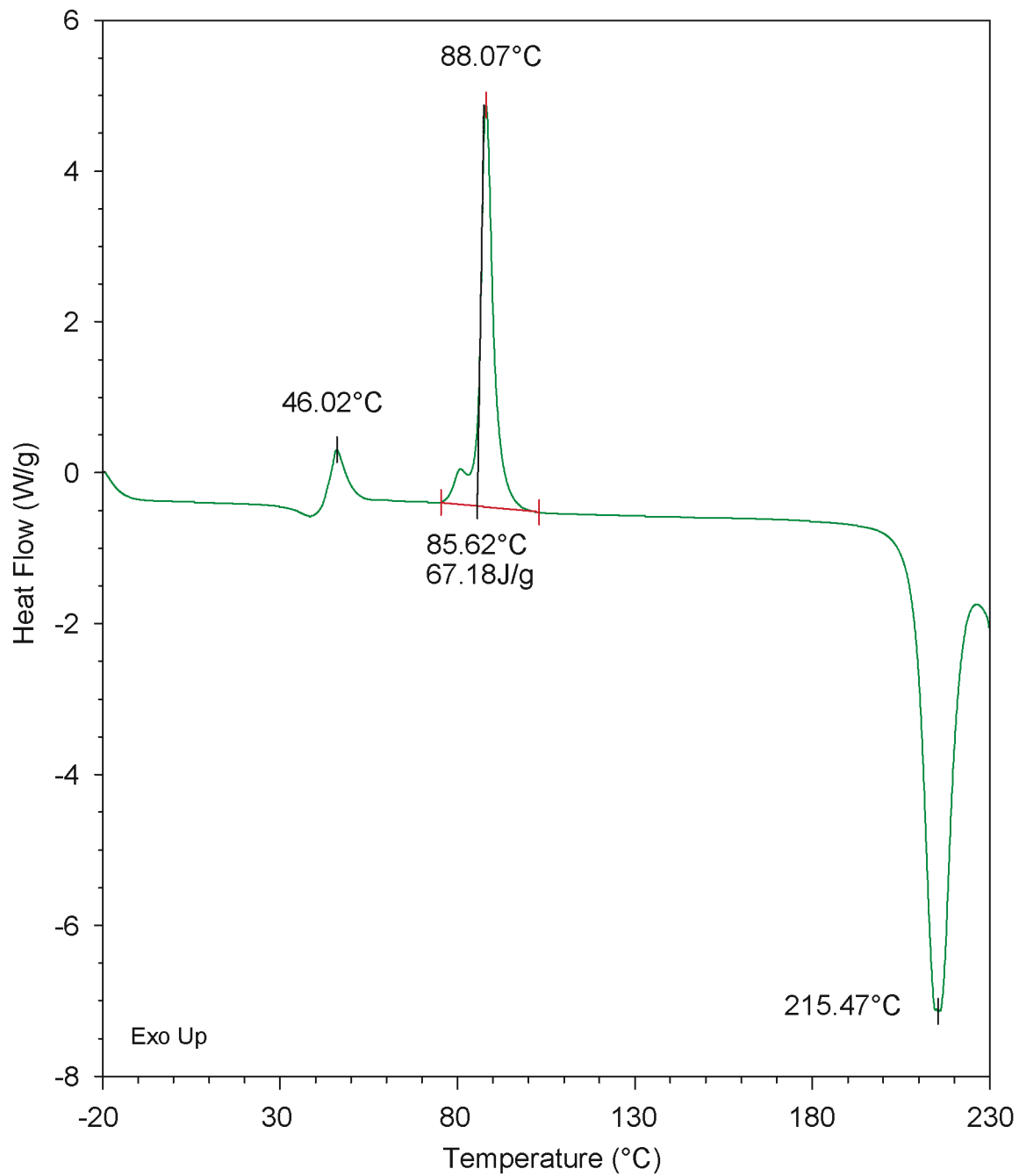
Figure 6.18. DSC thermogram of a cryoground (60 min) equimolar mixture of D- and L-proline.

mechanical disordering has been observed previously.[23] Although amorphous material was not observed following cryogrinding, new peaks in the ^{13}C CP-MAS NMR spectra were observed, and a small exothermic transition was observed near room temperature by DSC.

Carvajal et al. investigated the disorder that arose from cryogrinding griseofulvin and compared it to the disorder observed in amorphous griseofulvin prepared by a melt–quench method.[9] These studies indicated that cryogrinding griseofulvin reduced crystallinity by inducing crystal defects within the material, and the differences between defective crystals (produced by milling) and the amorphous form (produced from melt–quench) gave rise to significant differences in bulk thermal properties. Specifically, the authors noted a recrystallization event of the grinding-induced crystal defects (a small exothermic transition) that was independent of the amorphous-associated crystallization event. Because a similar exothermic event was observed for the cryoground proline sample (Figure 6.7), it is possible that the multiple peaks in the cryoground D-proline spectrum (Figures 6.1 and 6.5) correspond to D-proline crystal defects.

Another possible explanation for the observed SSNMR peaks and exothermic transition for cryoground D-proline is the presence of multiple polymorphic forms. There are many studies that have demonstrated that sample grinding can produce a change in crystal form, typically to a metastable crystal form,[21] but production of a more stable form also has been reported.[28] However, these studies typically involved room-temperature grinding. The molecular mobility, and thus the kinetics of crystallization, at room temperature versus at liquid-nitrogen temperature (77 K) can have a large effect on the product that is produced by a grinding process.[8]

The slower crystallization rate at liquid-nitrogen temperature potentially allows the production and observation of amorphous or defective crystalline material, as reported by Carvajal et al.[8,9] However, the production of a metastable crystalline state is also a possibility.[21] In the case of cryoground D-proline, additional studies would be necessary to determine whether the DSC-observed exotherm and multiple peaks in the SSNMR spectra correspond to the presence of crystal defects or metastable crystalline polymorphs. Such studies might include 2D–exchange experiments, which could be used to determine possible phase separation.

6.4.2 Co-cryogrinding L- and D-proline enantiomers

Whereas it was not possible to produce an amorphous phase by cryogrinding D-proline alone, SSNMR indicated the production of amorphous material upon co-cryogrinding both D- and L- enantiomers. The ability for the two-component system to become amorphized is likely due in part to entropic differences between the single enantiomer and the two-component racemic cocrystal, where the mixing of both enantiomers produces a favorable increase in entropy that offsets the increase in enthalpy.[29,30] This argument has been used to explain the amorphous solid-dispersion formation between polymers and small molecules.[29]

Amorphous material was produced when either DL-I or a mixture of D- and L-enantiomers (D+L) were cryoground, but the amount of grinding time required to produce the same relative amount of amorphous material differed. When DL-I was cryoground for 30 min, ^{13}C CP-MAS NMR spectra indicated only a small amount of residual DL-I (Figures 6.8 and 6.11). However, when D+L was cryoground for the same

amount of time (30 min), a large crystalline peak was observed in the ^{13}C CP-MAS NMR spectrum (Figure 6.14). This observation likely is a reflection of the relative stability of the enantiopure crystals (DSC melting point at ~230ºC) versus the cocrystal DL-I (mp ~214ºC).[10] This difference in relative stability likely contributed to the amorphization potential of enantiopure crystals versus racemic cocrystals.

6.4.3 SSNMR-observed transformation between 20 and 30ºC

In all samples of cryoground DL-I and D+L, VT ^{13}C CP-MAS NMR indicated a significant change in peak width and chemical shift between 20 and 30ºC. The breadth of the peaks before and after this transition is typically associated with the presence of an amorphous phase. The first thought was that this peak shift might be associated with the amorphous phase transition from the glassy to the rubbery state. However, movement through a glass transition (T_g) is a reversible process, and a heat-cool-heat VT SSNMR experiment (Figure 6.11) showed that the observed spectral changes were not reversible. Thus, this transition cannot be attributed to movement through the T_g.

The SSNMR results were compared to those obtained by DSC. DSC thermograms contained an exothermic peak near the 20–30ºC temperature range. Both heat-cool-heat and MDSC measurements showed that this exothermic event was nonreversible, suggesting that this exothermic peak might correspond to the nonreversible transition observed by VT SSNMR. Exotherms are often indicative of recrystallization events. The apparent decrease in SSNMR peak width, as well as the observed exotherm in the DSC thermogram, could potentially be explained by recrystallization of defective crystals.[9] Carvajal and coworkers have demonstrated that

recrystallization of griseofulvin crystal defects are independent of amorphous crystallization events, so the initial breadth of the SSNMR peaks (<20ºC) could arise from the presence of defects and amorphous material, while the broad peaks above the 20ºC transition might be attributed solely to an amorphous phase. However, if recrystallization of defects is the cause for the observed decrease in SSNMR peak width, a corresponding increase in the peak intensities of crystalline components should be observed. No such changes were observed in the SSNMR spectra following the 20–30ºC transition. Thus, it is unlikely that this event corresponds to crystallization of defective crystals.

The exact nature of this peak shift is unclear, as this type of observation has not been reported previously. It is possible that multiple phases of amorphous material (i.e., an enantiopure amorphous phase and a separate amorphous phase containing both enantiomers) existed below 20ºC and transformed into a single phase above this temperature. However, this is unlikely due to the fact that the transition was observed in both cryoground DL-I and mixtures of D- and L-proline. Although amorphous phase separation might be anticipated upon co-grinding a mixture of D- and L-proline, it would not be anticipated for cryoground DL-I, which exists as a single crystalline phase even prior to grinding. Yet in both samples of cryoground DL-I and cryoground D+L, the same broad–broad peak transition was observed during VT SSNMR. Perhaps a more feasible explanation is that, below 20ºC, the enantiomers are mixed together somewhat randomly. However, above 20º, the opposite enantiomers acquire sufficient mobility to pair with each other to form DL-proline dimers. This dimerization would be expected to reduce the distribution of molecular conformations, which would produce a decrease in

SSNMR peak width. However, the dimers would potentially still be disordered relative to one another, causing the SSNMR peaks to remain relatively broad.

This broad–broad peak transition highlights the need to understand the nature of the material that gives rise to broad peaks within the SSNMR spectrum. Unlike diffraction methods, by which decreases in material crystallinity give rise to progressively broader and less intense peaks, the peaks in the SSNMR spectrum are not greatly affected by such changes. A material may appear completely amorphous by PXRD (termed PXRD-amorphous), but crystalline by SSNMR. Although the SSNMR peaks become very broad upon amorphization of a material, the exact "degree of crystallinity" at which the broad amorphous peaks are observed in SSNMR is still unclear. This is an area of current research in the Munson Lab.

6.4.4   DL-I versus DL-II

Cryogrinding DL-I or D+L resulted in SSNMR-observed amorphous material. Regardless of the starting material, the ^{13}C CP-MAS NMR peaks associated with the amorphous materials were located at the same chemical shift and possessed the same shape. However, upon heating the samples, the crystallization products differed. When DL-I was amorphized, DL-I was the crystalline product (Figures 6.8 and 6.11), which is not surprising due to the presence of DL-I seed crystals.[26] On the other hand, when D+L mixtures were cryoground, DL-II was the crystalline product (Figures 6.14 and 6.16). Because residual enantiopure D- and L-proline crystals were always observed following the cryogrinding of D+L, these crystals could have acted as seeds for crystallization of the amorphous phase into DL-II (i.e., heteronucleation). To better understand the

potential role of seeding in this system, the grinding time should be increased to completely amorphize both DL-I and D+L materials, and the effect of cross seeding the amorphous-phase–containing materials using both DL-I and DL-II crystals should be studied.

An alternative explanation to the observed crystallization of DL-I versus DL-II involves mixing homogeneity in the cryoground samples. In previous chapters, it was noted that DL-I formed whenever an equimolar amount of D- and L-proline molecules were homogeneously distributed and able to crystallize rapidly in the solid state. This is the same type of situation observed for cryogrinding DL-I. Upon amorphizing a DL cocrystal, the resulting amorphous phase is expected to contain a homogeneous distribution of both enantiomers within the amorphous phase. This allows 1) DL pairs to form and 2) DL pairs to pack together to form the DL crystal lattice with relatively little translational movement. The overall crystallization process could therefore take place quickly, resulting in the kinetic product DL-I, as observed by VT SSNMR. On the other hand, the presence of an inhomogeneous distribution of D- and L-proline enantiomers within the amorphous material would slow the crystallization of the DL lattice and preferentially produce the thermodynamic product (DL-II) over the kinetic product (DL-I). Based on this reasoning, it is expected that cryogrinding an equimolar physical mixture of enantiopure D- and L-proline could produce either DL-I or DL-II, depending on the degree of mixing that is achieved by the cryogrinding process. A short cryogrinding method would produce inhomogeneous distributions of the enantiomers, leading to DL-II formation, whereas longer grinding periods would produce a homogeneous distribution of enantiomers, leading to DL-I formation. This mechanism of

DL-I versus DL-II crystallization among cryoground samples requires support from additional studies.

6.4.5 SSNMR versus PXRD and DSC analyses

During these studies, cryoground materials were analyzed by VT SSNMR, PXRD, and DSC. It became apparent that the environmental conditions and the kinetics associated with variable-temperature analyses had a significant effect on the results.

It was demonstrated in Chapter 5 that the presence of ambient water vapor had a strong effect on the crystallization of lyophilized proline. In those studies, environmental control during PXRD analysis was possible. In contrast, PXRD analysis of cryoground materials was limited to ambient conditions. Although extra steps were taken to minimize exposure of the cryoground material to ambient conditions, the material changed relatively rapidly under these conditions (i.e. from a combination of enantiopure crystals and an amorphous phase to highly crystalline DL-II in <3 min, Figure 6.17). Due to the potential effect of both uncontrolled sample temperature and water content on the crystallization process of the PXRD samples, a direct comparison between PXRD- and SSNMR-observed results is not possible. However, the PXRD results are helpful in that they demonstrate the instability of the cryoground proline material and that the crystallization products under ambient conditions can differ substantially from those observed by DSC and VT SSNMR.

Unlike SSNMR and PXRD, DSC analysis is not considered an identification method.[22] However, it does provide information about energetic changes associated with physical and chemical transformations. Comparison of DSC results (thermal

information) to VT SSNMR analysis (spectroscopic identification) can potentially be very helpful in characterizing temperature-dependent physical transformations of a system. However, the kinetics associated with data collection by these two methods is very different. The literature contains many examples of systems in which the pathways of crystallization or the final crystallization product differed greatly when heated at different rates.[6,22] This means that the heating rate can affect the temperature at which transitions occur, or even whether or not a particular transition is observed. The standard DSC method employed in these studies consisted of a 10ºC/min ramp, and the total analysis time was <30 min for each sample. In contrast, ^{13}C CP-MAS NMR spectral acquisitions took over an hour at each temperature step, and the total analysis often took place over multiple days. Although VT SSNMR and DSC are very complementary techniques, the large difference in heating kinetics associated with these two methods means that care should be taken when comparing the thermal and spectroscopic data.

6.4.6   Temperature dependence of chemical shifts

VT SSNMR has been used to study changes in physical form as a function of temperature,[31] as well as to study the mobility of a solid system,[32,33] but taking advantage of this temperature dependence as a method for resolving peaks in a spectrum or for identifying polymorphs has not been reported. As shown in Figures 6.3 and 6.4, the ^{13}C CP-MAS NMR peaks for proline varied significantly (by as much as 1 ppm) over the temperature range of -20 to 200ºC. In cases where peak overlap or poor resolution is an issue, varying the temperature may be a feasible option for mitigating the problem. Of course, this method is only practical for thermally stable samples.[31] Additionally, the

observation that different shifts were observed for different crystal structures suggests that this could be another method for identifying polymorphic forms. Although two similar crystal forms may possess similar peaks, they might not possess the exact same thermal expansion/contraction behavior.

It is also important to note that the use of NMR to elucidate crystal structures has been of great interest.[34] However, whereas most X-ray–determined crystal structures are acquired at very low temperatures, NMR experiments and PXRD diffraction patterns are typically performed at room temperature.[18] These temperature discrepancies may make direct comparisons problematic. The temperature dependence of SSNMR chemical shifts has implications for current NMR crystallography studies, including the ability to calculate chemical shifts for solid materials.[34]

6.5   Conclusion

Proline samples of three different compositions were cryoground: enantiopure D-proline, DL-proline form I, and an equimolar physical mixture of D- and L-proline (D+L). Use of a variable temperature ^{13}C CP-MAS NMR system at low temperatures allowed stabilization and analysis of metastable forms, including an amorphous phase, that were produced upon cryogrinding the proline samples. Sample temperatures were varied step-wise during analysis in order to identify thermal transitions within the samples, and these were compared to corresponding DSC analyses.

D-proline could not be amorphized, even after 60 min of cryogrinding. However, cryogrinding either DL-I or an equimolar mixture of both enantiomers together (D+L) for 30 min did produce an amorphous phase that was observable by SSNMR. The

crystallization of cryoground DL-I and cryoground D+L produced DL-I and DL-II respectively. These results suggest the nucleation of amorphous material by seeding. However, another possible explanation involves the potential influence of mixing homogeneity on the crystallization process, where the metastable DL-I is the major crystal product when both enantiomers are homogeneously distributed, allowing for rapid crystallization of the cocrystal. This is in contrast to an inhomogeneous distribution of the enantiomers, which results in slower crystallization kinetics, therein allowing the thermodynamically stable form, DL-II, to crystallize as the major product.

6.6   References

1.   Rodríguez-Hornedo N, Nehm SJ, Jayasankar A 2007. Cocrystals: design, properties, and formation mechanisms.   Encyclopedia of Pharmaceutical Technology. Informa Healthcare USA, Inc. p 615-635.

2.   Lu E, Rodriguez-Hornedo N, Suryanarayanan R 2008. A rapid thermal method for cocrystal screening. CrystEngComm 10(6):665-668.

3.   Friscic T, Jones W 2009. Recent advances in understanding the mechanism of cocrystal formation via grinding. Cryst Growth Des 9(3):1621-1637.

4.   Nguyen KL, Friscic T, Day GM, Gladden LF, Jones W 2007. Terahertz time-domain spectroscopy and the quantitative monitoring of mechanochemical cocrystal formation. Nat Mater 6(3):206-209.

5.   Jayasankar A, Somwangthanaroj A, Shao ZJ, Rodriguez-Hornedo N 2006. Cocrystal formation during cogrinding and storage is mediated by amorphous phase. Pharm Res 23(10):2381-2392.

6.   Seefeldt K, Miller J, Alvarez-Nunez F, Rodriguez-Hornedo N 2007. Crystallization pathways and kinetics of carbamazepine-nicotinamide cocrystals from the amorphous state by in situ thermomicroscopy, spectroscopy and calorimetry studies. J Pharm Sci 96(5):1147-1158.

7.   Willart JF, Descamps M 2008. Solid state amorphization of pharmaceuticals. Mol Pharm 5(6):905-920.

8.   Descamps M, Willart JF, Dudognon E, Caron V 2007. Transformation of pharmaceutical compounds upon milling and comilling: the role of Tg. J Pharm Sci 96(5):1398-1407.

9. Feng T, Pinal R, Carvajal MT 2008. Process induced disorder in crystalline materials: differentiating defective crystals from the amorphous form of griseofulvin. J Pharm Sci 97(8):3207-3221.

10. Piyarom S, Yonemochi E, Oguchi T, Yamamoto K 1997. Effects of grinding and humidification on the transformation of conglomerate to racemic compound in optically active drugs. J Pharm Pharmacol 49(4):384-389.

11. Pines A, Gibby MG, Waugh JS 1973. Proton-enhanced NMR of dilute spins in solids. J Chem Phys 59(2):569-590.

12. Metz G, Wu X, Smith SO 1994. Ramped-amplitude cross polarization in magic-angle-spinning NMR. J Magn Reson, Ser A 110(2):219-227.

13. Andrew ER, Bradbury A, Eades RG 1959. Removal of dipolar broadening of nuclear magnetic resonance spectra of solids by specimen rotation. Nature 183:1802-1803.

14. Fung BM, Khitrin AK, Ermolaev K 2000. An improved broadband decoupling sequence for liquid crystals and solids. J Magn Reson 142(1):97-101.

15. Dixon WT, Schaefer J, Sefcik MD, Stejskal EO, McKay RA 1982. Total suppression of sidebands in CPMAS carbon-13 NMR. J Magn Reson 49(2):341-345.

16. Barich DH, Gorman EM, Zell MT, Munson EJ 2006. 3-Methylglutaric acid as a 13C solid-state NMR standard. Solid State Nucl Magn Reson 30(3-4):125-129.

17. Bielecki A, Burum DP 1995. Temperature dependence of 207Pb MAS spectra of solid lead nitrate. An accurate, sensitive thermometer for variable-temperature MAS. J Magn Reson, Ser A 116(2):215-220.

18.   Lee EH, Smith DT, Fanwick PE, Byrn SR 2010. Characterization and anisotropic lattice expansion/contraction of polymorphs of tenofovir disoproxil fumarate. Cryst Growth Des 10(5):2314-2322.

19.   Ahlneck C, Zografi G 1990. The molecular basis of moisture effects on the physical and chemical stability of drugs in the solid state. Int J Pharm 62(2-3):87-95.

20.   Andronis V, Yoshioka M, Zografi, George 1997. Effects of sorbed water on the crystallization of indomethacin from the amorphous state. J Pharm Sci 86(3):346-351.

21.   Brittain HG 2002. Effects of mechanical processing on phase composition. J Pharm Sci 91(7):1573-1580.

22.   Craig D 2007. Pharmaceutical applications of DSC. Therm Anal Pharm:53-99.

23.   Wildfong PLD, Hancock BC, Moore MD, Morris KR 2006. Towards an understanding of the structurally based potential for mechanically activated disordering of small molecule organic crystals. J Pharm Sci 95(12):2645-2656.

24.   Burger A, Ramberger R 1979. On the polymorphism of pharmaceuticals and other molecular crystals. I. Theory of thermodynamic rules. Mikrochim Acta 2(3-4):259-271.

25.   Jiang Q, Shi HX, Zhao M 1999. Melting thermodynamics of organic nanocrystals. J Chem Phys 111(5):2176-2180.

26.   Yoshioka M, Hancock BC, Zografi G 1994. Crystallization of indomethacin from the amorphous state below and above its glass transition temperature. J Pharm Sci 83(12):1700-1705.

27.   Lubach JW, Xu D, Segmuller BE, Munson EJ 2007. Investigation of the effects of pharmaceutical processing upon solid-state NMR relaxation times and implications to solid-state formulation stability. J Pharm Sci 96(4):777-787.

28.   Pirttimaki J, Laine E, Ketolainen J, Paronen P 1993. Effects of grinding and compression on crystal structure of anhydrous caffeine. Int J Pharm 95(1-3):93-99.

29.   Taylor LS, Zografi G 1998. Sugar-polymer hydrogen bond interactions in lyophilized amorphous mixtures. J Pharm Sci 87(12):1615-1621.

30.   Patterson D, Robard A 1978. Thermodynamics of polymer compatibility. Macromol 11(4):690-695.

31.   Min KH, Kurosu H, Ando I, Yamamoto T, Kanbara T 1991. Structural characterization of polyallene in the solid state as studied by variable-temperature high-resolution carbon-13 NMR spectroscopy. Macromol 24(8):2011-2014.

32.   Byrn SR, Xu W, Newman AW 2001. Chemical reactivity in solid-state pharmaceuticals: formulation implications. Adv Drug Delivery Rev 48(1):115-136.

33.   Byrn SR, Pfeiffer RR, Stowell JG 1999. Solid-State Chemistry of Drugs. 2nd ed., West Lafayette, Indiana: SSCI, Inc.

34.   Dumez J-N, Pickard CJ 2009. Calculation of NMR chemical shifts in organic solids: Accounting for motional effects. J Chem Phys 130(10):104701-104708.

Chapter 7

Summary and Suggestions for Future Work

7.1 Summary

Chiral molecules are prevalent among currently marketed pharmaceutical products, many of which are solid formulations. The challenges associated with producing and characterizing chiral small molecules in the solid state are not trivial. Understanding the solid forms that exist for a chiral (or nonchiral) drug molecule is critical to ensure product performance and safety, as the solid-state form of a drug can have a dramatic effect on its solubility, dissolution rate (and therefore bioavailability), physical stability, and interaction with excipients. Analysis of these systems typically requires the application of several analytical techniques, one or two of which may be particularly helpful. In this thesis work, solid-state NMR spectroscopy (SSNMR) was found to be a particularly powerful method for characterizing proline enantiomers in the solid state. Several of the major conclusions of the work in this dissertation are summarized below.

7.1.1 *Crystallization of proline enantiomers (Chapter 3)*

Using SSNMR, we evaluated the differences in crystal forms of proline that resulted from changes in enantiomeric ratio and crystallization conditions. Various ratios of D- and L-proline (0–50% L-proline with 100–50% D-proline) were crystallized from aqueous solution and by lyophilization, spray drying, and cryogrinding.

A racemic cocrystal (DL-proline) is the thermodynamically favored product upon concurrent crystallization of both D- and L-proline, and any excess enantiomer

crystallizes separately in an enantiopure crystal lattice. Only one form of the racemic cocrystal (denoted DL-I) had been reported previously.

In our studies, concurrent crystallization of D- and L-proline from aqueous solution always resulted in mixtures of DL-I and enantiopure proline. However, preparation by other methods resulted in several additional crystalline forms, including two previously unreported polymorphs, termed DL-II and III. DL-III was found to be metastable to the previously reported form (DL-I), and DL-II was determined to be more thermodynamically stable than DL-I above room temperature. Additional studies were performed in order to understand the formation of this more thermodynamically stable form, DL-II.

7.1.2   *Formation of DL-I versus DL-II (Chapters 3 and 5)*

Although DL-II was shown to be more thermodynamically stable than DL-I, the kinetic stability of DL-I was very high. This allowed DL-I to remain the dominant crystal form in the bulk material, even in the presence of DL-II seed crystals.

Whereas DL-I was the major product upon crystallization from solution, DL-II was the predominant form when samples were prepared by lyophilizing nonequimolar mixtures of D- and L-proline enantiomers. The hypothesized explanation for the preferential crystallization of DL-II versus DL-I involved: 1) the molecular mobility associated with a given crystallization process and 2) the degree of molecular translation necessary to create a racemic cocrystal lattice structure.

In solution, there is a high degree of molecular mobility that allows D and L molecules to pair with one another and then pack to form the DL lattice. On the other

hand, in the lyophilization method, the proline molecules are "frozen" in the ice lattice. As the water molecules are removed by sublimation, the proline molecules, now in the solid state, are left behind. Molecular mobility is greatly restricted in a solid as compared to in solution, resulting in a large reduction in the translational motion associated with pairing of D and L molecules.

When an equimolar ratio of the two proline enantiomers is present, assuming that D and L molecules are homogeneously distributed throughout the solution prior to freezing, the probability of finding a D and an L molecule neighboring each other is quite high. This means that forming the hetero-enantiomeric pair (and others around it) to create the DL lattice requires little translational motion. In contrast, at lower concentrations of L-proline (e.g., 25% L-proline), the translational movement necessary to form a DL crystal lattice becomes much greater.

At the 25% L-proline level, a homogeneous distribution of D and L molecules means that every L molecule is likely very close to a D molecule. As a result, upon solidification, the formation of DL pairs does not require much translational motion. That said, these DL pairs are physically separated from each other by the presence of the excess D molecules, and translational motion is necessary for DL pairs to pack together to form the crystal lattice. Growth of the crystal lattice is therefore inhibited. By slowing down the crystallization process, it is possible to form the thermodynamically stable crystal form (DL-II), not just the kinetically favorable form (DL-I).

This hypothesis was supported by observation of a possible intermediate, "frustrated" state, in which the racemic cocrystal DL-pairs and D-proline molecules could not completely separate from one another in order to form their own thermodynamically

stable crystal lattices. This "frustrated" state was observed when lyophilized proline samples were maintained in low-RH conditions through the use of dry nitrogen, but exposure to either ambient water vapor or elevated temperature increased molecular mobility sufficiently to facilitate crystallization to more thermodynamically stable D and DL crystal forms.

7.1.3   Observation of L-proline chiral defects (Chapters 3 and 4)

In order to detect low levels of proline crystal forms, a spectral-subtraction method was applied to the proline system. This method provided sufficient sensitivity and selectivity as to observe and quantitate L-proline molecules that were kinetically trapped, substitutional chiral defects within the D-proline crystal lattice. Previous studies have investigated chiral defects, but no direct observations of these defects have been made.[1,2] We provided support for the observation of L-proline chiral defects in the host crystal lattice of D-proline through use of SSNMR methods (including relaxation measurements) and by assessing thermal and RH stability of the defects. The amount of this L-proline chiral defect was quantitated in lyophilized samples and found to exist up to a 1.4% level in the D-proline host crystal. This is the first direct solid-state observation and quantitation of chiral defects incorporated into a three-dimensional crystal lattice of an enantiopure system.[3,4]

7.1.4   Crystallization of amorphous proline (Chapter 6)

Crystallization of proline enantiomers from an amorphous phase also was investigated. Proline samples of three different compositions were cryoground:

enantiopure D-proline, DL-I, and an equimolar physical mixture of D- and L-proline (D+L). Low-temperature SSNMR analysis allowed for stabilization and analysis of metastable forms, including an amorphous phase, that were produced upon cryogrinding the proline samples. After an initial spectral acquisition at low temperature, sample temperatures were increased in order to identify thermal transitions within the samples, and the observed transitions were compared to corresponding DSC analyses.

D-proline could not be amorphized, even after 60 min of cryogrinding. However, cryogrinding either DL-I or D+L for 30 min resulted in partial amorphization. The crystallization of cryoground DL-I and cryoground D+L produced DL-I and DL-II respectively. Residual crystalline material in each sample likely seeded the amorphous phase to produce the observed differences in polymorphism upon crystallization. However, another possible explanation involves the potential influence of mixing homogeneity on the crystallization process, where the metastable DL-I is the major crystal product when both enantiomers are homogeneously distributed, allowing for rapid crystallization of the cocrystal. This is in contrast to an inhomogeneous distribution of the enantiomers, which results in slower crystallization kinetics, therein allowing the thermodynamically stable form, DL-II, to crystallize as the major product. Further study is necessary to elucidate this possible mechanism and determine the effect of seeding on the crystallization of amorphous material in this system.

7.1.5 Conclusion

Crystallization of L-proline with D-proline in various ratios with different crystallization methods produced multiple crystalline forms, including new polymorphs

and chiral defects. SSNMR was highly suited for investigating proline enantiomers in the solid state. Different solid forms, including crystal defects and amorphous material, gave rise to different peaks in SSNMR spectra. Additionally, isotopic labeling, combined with spectral subtraction, allowed for identification and relative quantitation of the various forms under a wide range of enantiomeric ratios. Phase separation among these forms was confirmed by ^{1}H T_1 relaxation measurements, and 2D-SSNMR experiments possess the potential to provide structural information in future studies.

7.2   Suggestions for future work

7.2.1   Proline

The work reported in this thesis is the first work to characterize proline enantiomers in the solid state. As outlined previously (§ 3.1.2), proline possessed many favorable properties for SSNMR experiments, and it proved to be an interesting and complex system with many different solid forms.

Additional studies of the proline system are of interest and were noted at various points throughout this work. These studies include:

- Lyophilizing proline enantiomers with a polymer. Our hypothesis for the production of DL-II versus DL-I was based on the idea that the enantiomeric excess slowed the crystallization process and allowed crystallization of the more thermodynamically favored product (DL-II) versus the kinetic product (DL-I). If this is indeed the case, then the presence of a polymer should also "frustrate"/slow the crystallization process and result in the formation of DL-II as the major product.

- Additional cryogrinding experiments should be performed to complement the studies that used lyophilization as a preparation method. Understanding the effect of enantiomeric ratio and cryogrinding time on the amorphization and crystallization process is of interest due to its potential to produce additional solid forms of proline.

- Perhaps of greatest interest is further characterization of amorphized cocrystals. As mentioned in Chapter 6, the production of cocrystals by grinding has garnered attention recently as a rapid method for producing cocrystals during the solid-form screening/drug development process.[6] Studies have demonstrated that this type of cocrystal formation can occur through an intermediate amorphous phase. Although this type of amorphous phase has been observed, including in this thesis work, this state has not been fully characterized (i.e., What homo- and hetero-intermolecular interactions exist within these systems? How important is the mixing homogeneity of the two components during the cocrystallization process?). This lack of understanding was highlighted by our cryogrinding studies, in which a transition was observed (by VT SSNMR) between 20 and 30ºC among cryoground DL-proline samples. This transition, which appeared to be an amorphous–amorphous transition due to the broad peak shapes in the ^{13}C CP-MAS NMR spectrum, could not be definitively identified. Understanding such systems is highly relevant for the production of future pharmaceutical solids, which increasingly include cocrystals due to favorable pharmaceutically relevant properties.[7]

7.2.2 *Future model chiral compound: Pseudoephedrine*

Pseudoephedrine has been proposed as a future model chiral compound due to its pharmaceutical relevance and the presence of two chiral centers within its structure, which leads to the existence of both enantiomers and diastereomers. Initial experiments using the free base form of pseudoephedrine (PE) indicated that its high vapor pressure led to sample changes. Figure 7.1 shows that an equimolar mixture of (+)- and (-)-PE (free base) transformed via sublimation of the individual enantiomers and subsequent crystallization of the racemic cocrystal during SSNMR analysis. In order to overcome this unacceptable instability, we converted the free base to the hydrochloride salt.

The hydrochloride salt form was relatively easy to prepare and possessed several desirable properties. By converting the compound to the HCl salt, the sublimation tendency of the compound was greatly reduced. This is demonstrated in Figure 7.2, which shows TGA analysis of PE free base versus the HCl salt, where the weight loss due to sublimation is plotted as a function of time during an isothermal hold at 150ºC. Whereas the free base completely sublimed within 25 min, the HCl salt only lost ~2.3% over 2 hr at this elevated temperature. Additionally, as shown in Figures 7.3 and 7.4, DSC and SSNMR analyses indicated that PE HCl forms a racemic cocrystal when crystallized from aqueous solution, similar to proline. This makes it a good model for following up the proline work.

Unfortunately, despite the increased stability relative to the free base, the HCl salt still lacked sufficient stability against sublimation. Lyophilization of the enantiopure form resulted in a 100% yield. However, lyophilization of the racemic cocrystal yielded ~50%, indicating that 50% of the product sublimed during the preparation
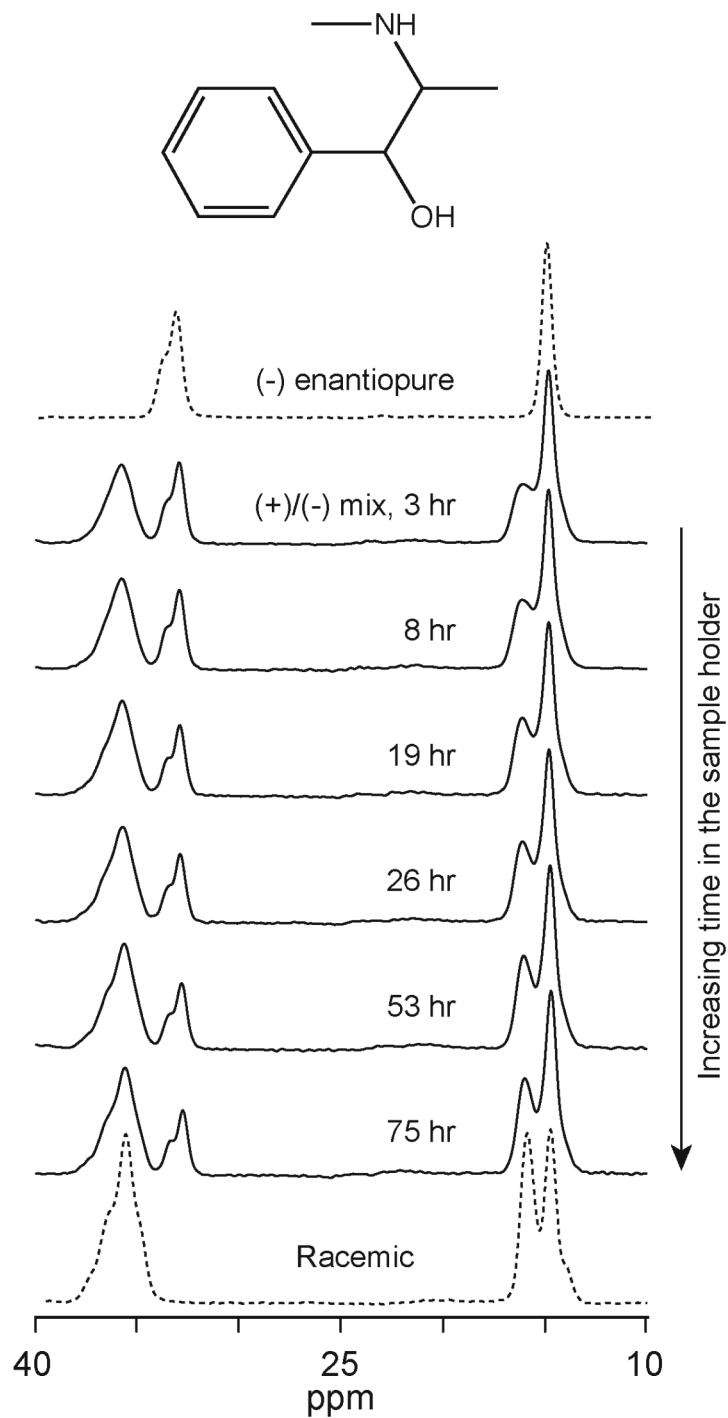
Figure 7.1. ^{13}C CP-MAS NMR spectra of enantiopure and racemic pseudoephedrine free base (dashed) and a lightly ground equimolar mixture of (+)- and (-)-pseudoephedrine, analyzed over time in the instrument.
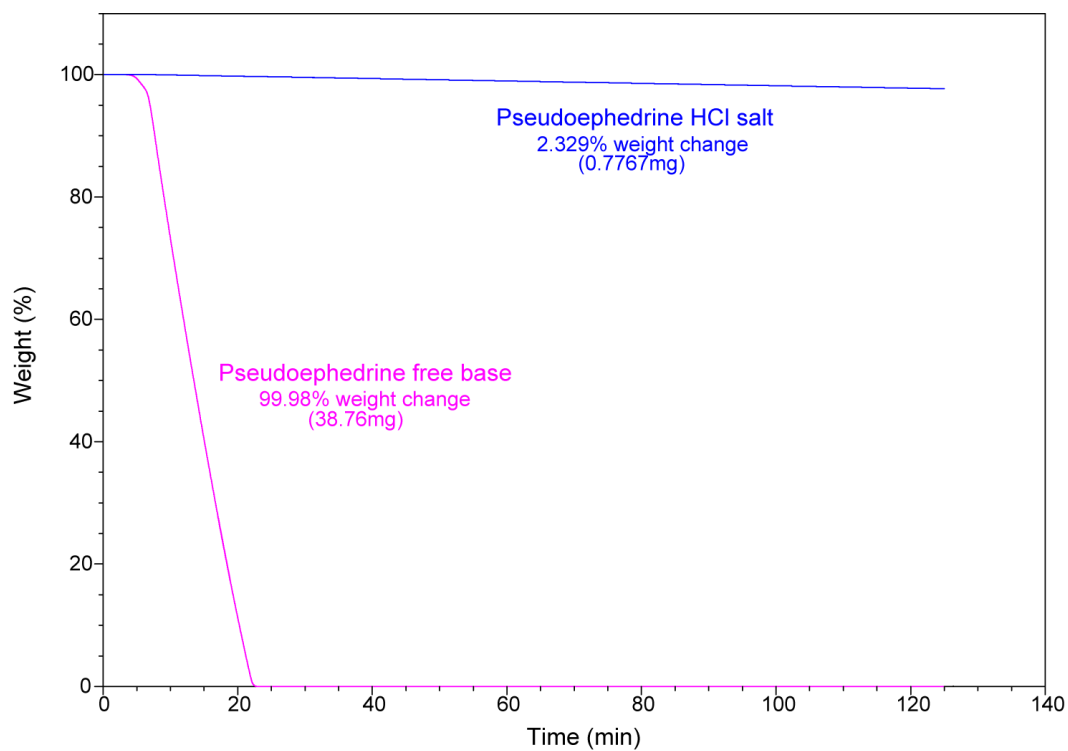
Figure 7.2. Thermogravimetric analysis, demonstrating weight loss due to sublimation of pseudoephedrine free base versus the hydrochloride salt during an isothermal hold at 150ºC.

Figure 7.3. DSC thermograms of pseudoephedrine HCl samples containing various enantiomeric ratios, crystallized from aqueous solution.

Figure 7.4. ^{13}C CP-MAS NMR spectra of pseudoephedrine HCl samples prepared with various enantiomeric ratios by crystallization from aqueous solution.

269

method, which uses low pressure to sublime frozen water. This means that lyophilization, and likely spray drying, are not feasible preparation methods for PE HCl. Because these methods were shown to be very useful in preparing proline samples, we wish to continue using them for the prepa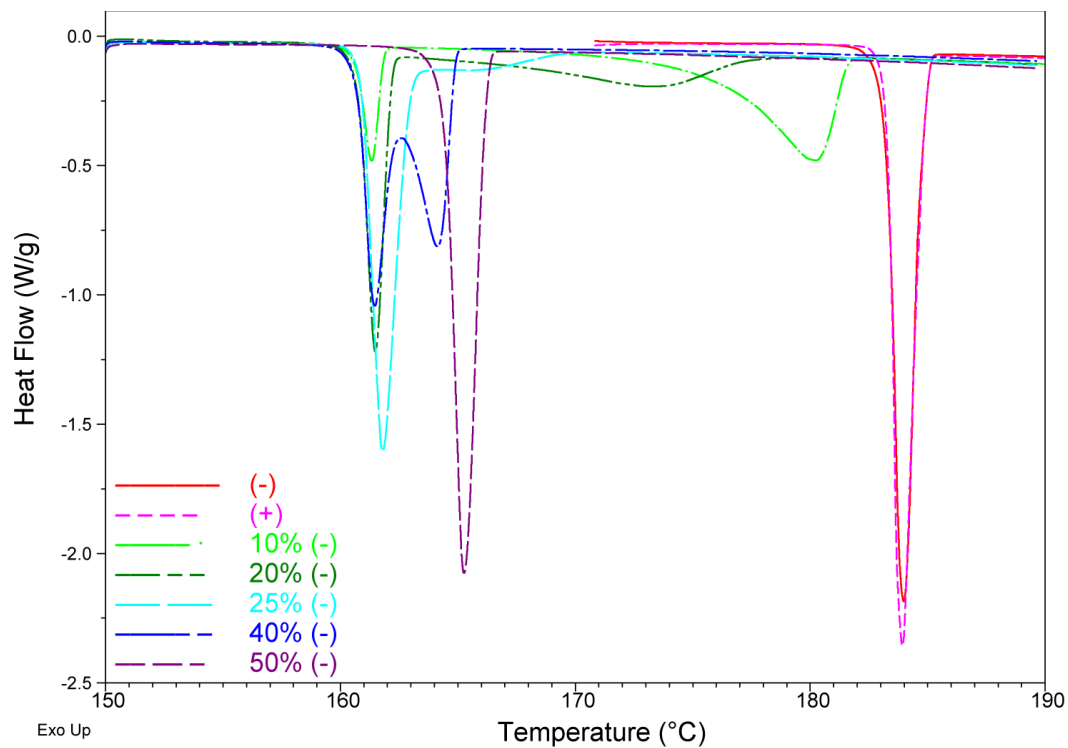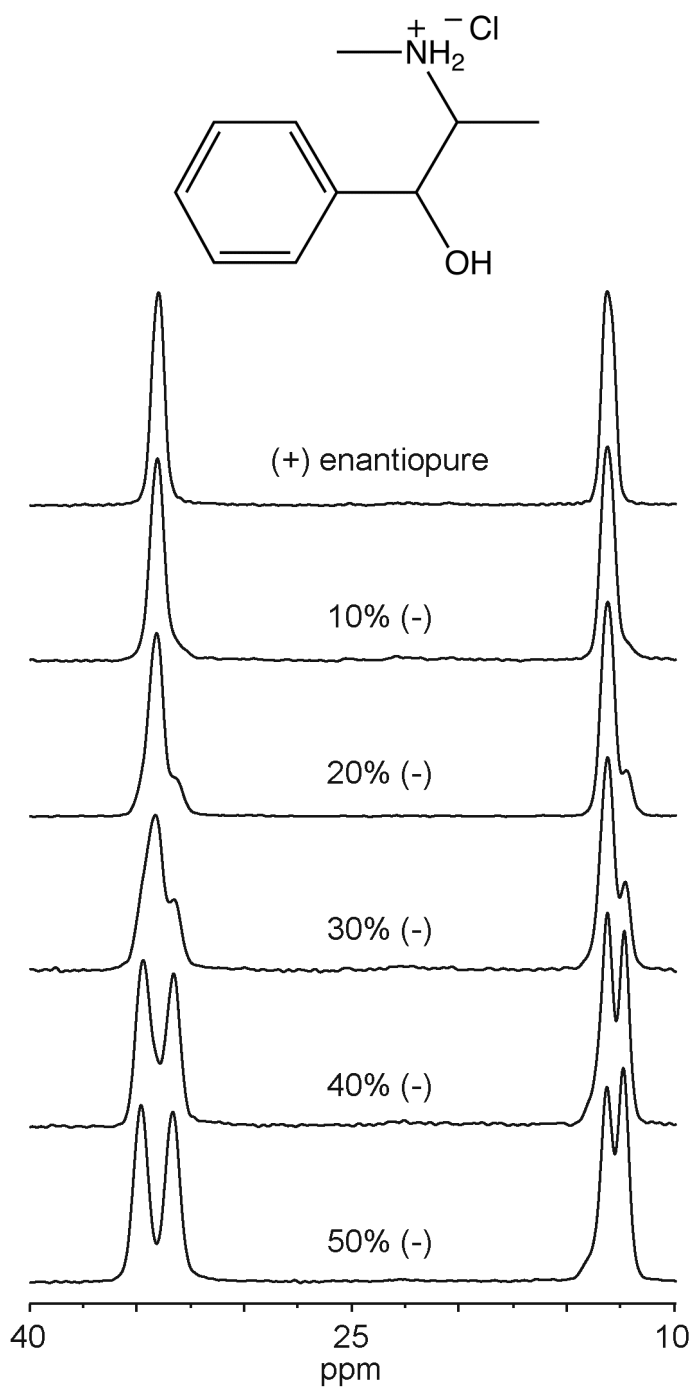ration of other enantiomeric systems. Thus, the PE model would require conversion to a more stable salt form before it could be used as a proper model in future studies.

7.2.3 *Crystal defects, nanocrystals, and amorphous materials*

As illustrated by the observation of L-proline chiral defects in the D-proline host lattice, the sensitivity of SSNMR to the electronic environment of a molecule makes it a very good tool for studying crystal defects. One of the interesting questions about chiral defects is their potential to affect physicochemical stability of the host crystal lattice. Aspartyl phenylalanine is a potential model, as its thermal lability might make it a good model for studying the effect of defect site inclusion on changes in chemical stability.

In addition to future studies of chiral defects, mechanically induced crystal defects (i.e., defects caused by grinding) are also of interest. A great deal of research has been focused on detecting and distinguishing crystal defects, nanocrystals, and amorphous materials.[5,8-10] These high-energy sites/forms can be produced unintentionally during common pharmaceutical processing techniques and can negatively affect product performance.[10] Thus there is a need for analytical tools that are capable of detecting and characterizing these systems. Due to the unique ability for SSNMR to identify components within a mixture, quantitate, and provide information about the structure and mobility within a system, it will no doubt be a valuable tool for analyzing such systems.

7.3   Implications of this work

This thesis work has significant implications for the development of pharmaceutical solids. Upon discovering a new active pharmaceutical compound, it is necessary to identify and characterize solid forms of that molecule in order to determine which form should be used in the final product. This requires intensive solid-form/polymorphic screening.

Whereas typical polymorphic screening assays involve crystallizing from various solvents, we used lyophilization, spray drying, and cryogrinding in our studies. These nontraditional crystallization methods produced high-energy solid forms (e.g., defects, amorphous material, metastable polymorphs) and also a more thermodynamically stable cocrystal polymorph that had not previously been reported. Due to the ability for common pharmaceutical processing techniques to accidentally cause changes in physical form,[10] it is essential to understand the potential for producing such forms as well as their possible effects on product performance. This idea is highlighted by the "quality by design" FDA imperative, which states that "quality should be built into a product with a thorough understanding of the product and process by which it is developed and manufactured along with a knowledge of the risks involved in manufacturing the product and how best to mitigate those risks."

Additionally, as we demonstrated in the proline system, the presence of the opposite enantiomer altered crystallization kinetics in the system, therein affecting the crystal product. Because of the prevalence of enantiopure pharmaceutical compounds, this type of "chiral doping" scheme is highly relevant to the polymorphic screening

271

process that occurs during the development of new pharmaceuticals, as it may produce forms that would not be observed during normal screening methods.

Not only is the production of new crystal forms very important, but also the detection of such forms is key. In this work, we demonstrated the ability for SSNMR to be applied to enantiomeric systems and toward the characterization of solids in general. Its ability to detect and quantitate the presence of different polymorphic forms, cocrystals, amorphous material, and even crystal defects makes it very useful in understanding physicochemical properties of a material (e.g., an increased dissolution rate may be attributed to the presence of defects versus the presence of amorphous material). Additionally, its ability to assess molecular mobility (relaxation measurements) and provide structural information (1D and 2D SSNMR experiments) make it especially valuable for characterizing solid systems in which traditional structural elucidation techniques (i.e., X-ray diffraction methods) cannot be applied.

7.4 References

1. Duddu SP, Fung FKY, Grant DJW 1993. Effect of the opposite enantiomer on the physicochemical properties of (-)-ephedrinium 2-naphthalenesulfonate crystals. Int J Pharm 94(1-3):171-179.

2. Li ZJ, Grant DJW 1996. Effects of excess enantiomer on the crystal properties of a racemic compound: ephedrinium 2-naphthalenesulfonate. Int J Pharm 137(1):21-31.

3. Fasel R, Parschau M, Ernst K-H 2006. Amplification of chirality in two-dimensional enantiomorphous lattices. Nature 439(7075):449-452.

4.   Weissbuch I, Lahav M, Leiserowitz L, Meredith GR, Vanherzeele H 1989. Centrosymmetric crystals as host matrices for second-order optical nonlinear effects. Chem Mater 1(1):114-118.

5.   Suryanarayanan R, Mitchell AG 1985. Evaluation of two concepts of crystallinity using calcium gluceptate as a model compound. Int J Pharm 24(1):1-17.

6.   Lu E, Rodriguez-Hornedo N, Suryanarayanan R 2008. A rapid thermal method for cocrystal screening. CrystEngComm 10(6):665-668.

7.   Rodríguez-Hornedo N, Nehm SJ, Jayasankar A 2007. Cocrystals: design, properties, and formation mechanisms.   Encyclopedia of Pharmaceutical Technology: Informa Healthcare USA, Inc. p 615-635.

8.   Bates S, Zografi G, Engers D, Morris K, Crowley K, Newman A 2006. Analysis of amorphous and nanocrystalline solids from their X-ray diffraction patterns. Pharm Res 23(10):2333-2349.

9.   Byard SJ, Jackson SL, Smail A, Bauer M, Apperley DC 2005. Studies on the crystallinity of a pharmaceutical development drug substance. J Pharm Sci 94(6):1321-1335.

10.   Wildfong PLD, Hancock BC, Moore MD, Morris KR 2006. Towards an understanding of the structurally based potential for mechanically activated disordering of small molecule organic crystals. J Pharm Sci 95(12):2645-2656.

Appendix

Characterization of Thiamine Hydrochloride Hydrates

by Solid-State NMR Spectroscopy

A.1   Introduction

The purpose of this work was to characterize the dehydration of thiamine hydrochloride crystals using complementary structural and spectroscopic analyses. Only solid-state NMR analysis is reported here. Please refer to relevant publications (§ A.1.1) for additional details.

A.1.1   Relevant publications

Chakravarty, P.; Berendt, R.T.; Munson, E.J.; Young, V.G.; Govindarajan, R.; Suryanarayanan, R. 2010. Insights into the dehydration behavior of thiamine hydrochloride (vitamin B1) hydrates: Part I. J. Pharm. Sci. 99(2), 816-827.

Chakravarty, P.; Berendt, R.T.; Munson, E.J.; Young, V.G.; Govindarajan, R.; Suryanarayanan, R. 2010. Insights into the dehydration behavior of thiamine hydrochloride (vitamin B1) hydrates: Part II. J. Pharm. Sci. 99(4), 1882-1895.

A.1.2   Pharmaceutical hydrates

Crystalline hydrates are relatively common among pharmaceutical compounds.[1] The hydrated and anhydrous states of a particular compound may possess significantly different physicochemical properties (e.g., solubility, dissolution rate/bioavailability, stability).[2,3]   This means that changes in the hydration state of a pharmaceutical compound can significantly alter product performance. Figure A.1. demonstrates some of the possible changes that can occur upon dehydration of a crystal lattice: 1) the lattice collapses, resulting in amorphous or disordered crystalline material, which can be
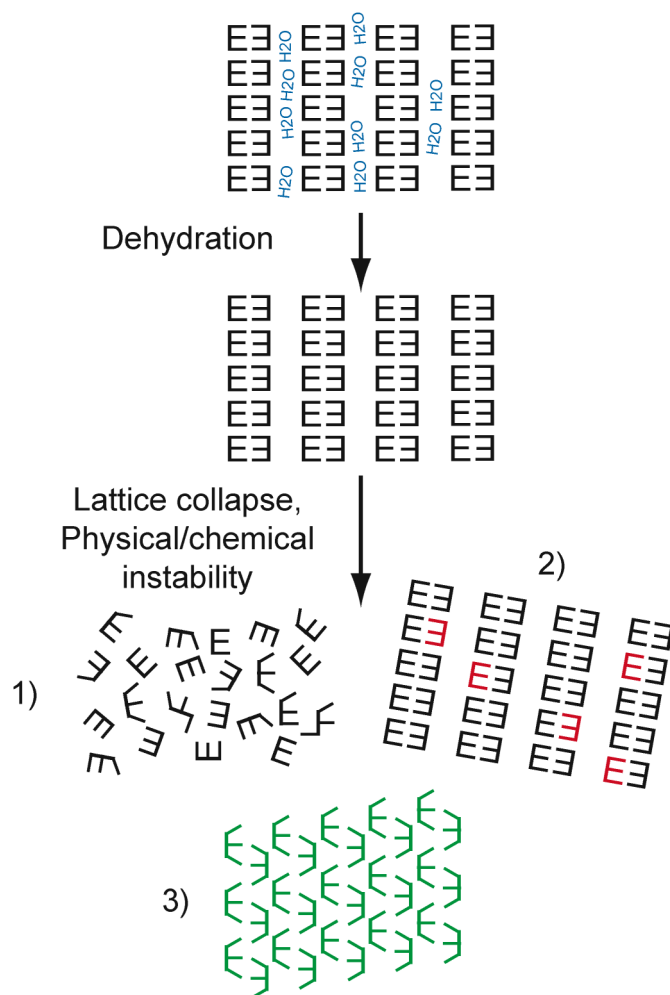
Figure A.1. Potential effects of dehydration: 1) Lattice collapse and formation of amorphous material, 2) reduced chemical stability, and 3) reduced physical stability, leading to formation of a different crystal form.

chemically and physically less stable than the parent material; 2) the lattice structure is unaltered, but the empty channels may result in decreased chemical stability, due to the ability for reactants, such as oxygen, to enter the crystal lattice; or 3) the lattice packing may be altered, resulting in a crystal structure that may possess different physicochemical properties than the parent hydrate crystal.

The active pharmaceutical compound/product is exposed to a range of temperatures and water vapor pressures during pharmaceutical manufacturing processes and subsequent storage. The physical stability of a hydrate and its propensity to dehydrate are dictated by the temperature and water vapor pressure. Because of this, it is important to understand the dehydration behavior of pharmaceutical hydrates.

A.1.3 *Stoichiometric versus nonstoichiometric hydrates*

Hydrates are a specific type of multiple-component crystal in which the ratio of the active pharmaceutical ingredient and water molecules can be either stoichiometric (e.g., monohydrate, 1:1 ratio) or nonstoichiometric (e.g., channel hydrate, where water content varies as a function of the environmental % RH). Figure A.2 shows examples of stoichiometric and nonstoichiometric hydrates and illustrates the effect of % RH on the hydration state of each.

Thiamine hydrochloride (**THCl**) can exist as both a nonstoichiometric hydrate (**NSH**, 0 to ~1 mole water) and a hemihydrate (**HH**, 0.5 mole water per mole **THCl**). ^{13}C CP-MAS NMR spectra of the **NSH**, **HH**, and anhydrous (**ID**) crystal forms are shown in Figure A.3. In order to understand the dehydration behavior of **NSH** and **HH**, these crystal forms were analyzed by solid-state NMR spectroscopy.

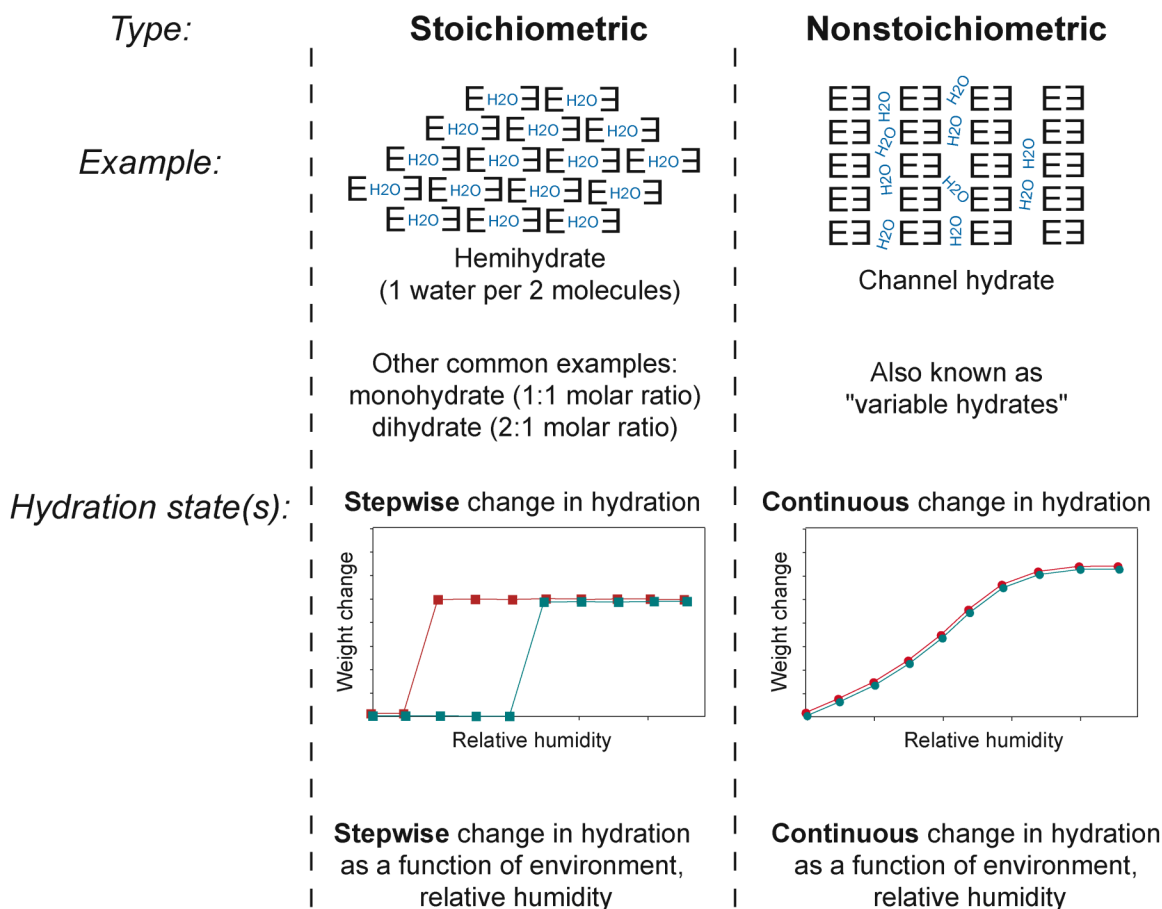|	**Stoichiometric**	**Nonstoichiometric**
Type:		
Example:	Hemihydrate (1 water per 2 molecules) Other common examples: monohydrate (1:1 molar ratio) dihydrate (2:1 molar ratio)	Channel hydrate Also known as "variable hydrates"
Hydration state(s):	**Stepwise** change in hydration Stepwise change in hydration as a function of environment, relative humidity	**Continuous** change in hydration Continuous change in hydration as a function of environment, relative humidity

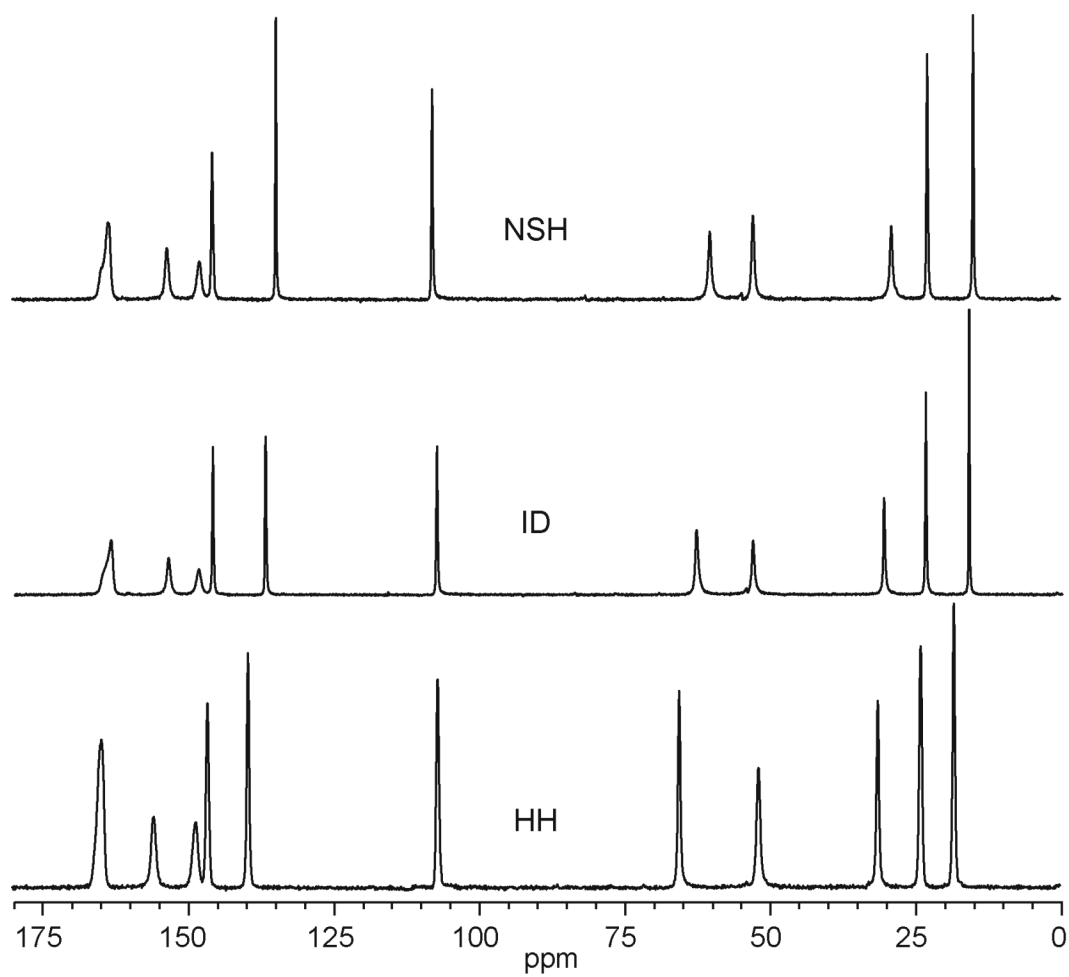**Figure A.2.** Stoichiometric versus nonstoichiometric hydrates.

278

Figure A.3. ^{13}C CP-MAS NMR spectra of thiamine hydrochloride nonstoichiometric hydrate (NSH), isomorphic desolvate (ID), and hemihydrate (HH) crystal forms.

A.2 Experimental

A.2.1 Materials

Bulk **THCl** was purchased from Sigma-Aldrich (St. Louis, MO) and determined to be a nonstoichiometric hydrate (**NSH**).

A.2.2 Sample preparation

Nonstoichiometric hydrate (NSH). **NSH** samples of intermediate water content were prepared by dehydrating **NSH** (~1 mole water) at 50ºC under ambient pressure and were then packed into zirconia rotors with Teflon® end caps. **ID** was prepared by heating **NSH** over anhydrous $CaSO_4$ at 40ºC. For the VT SSNMR experiment, a sample was prepared by mixing **NSH** and **ID** in a 1:1 (w/w) ratio and equilibrating the mixture at 50ºC for 12 hr within a zirconia rotor sealed with ribbed Kel-F® end caps. The water contents of all samples were determined before and after SSNMR analysis by thermogravimetric analysis (Q50 TGA, TA Instruments).

Hemihydrate (HH). **HH** was obtained by suspending **NSH** in water for ~12 hr, followed by drying at 40ºC for ~4 hr.

HH_2: Dehydration of HH by thermal treatment. **HH** decomposition was observed when heated to temperatures >120ºC,[4] so dehydration was attempted at temperatures <100ºC under reduced pressure. **HH** was dried at 60ºC in a bench top freeze dryer (Unitop 400L, Virtis, Gardiner, NY, USA) under reduced pressure (20–60 mtorr) for 7 days. This product phase will be referred to as **HH_2**. A sample of **HH** also was subjected to forced degradation by storing at 180ºC for 4 hr and analyzed by SSNMR.

Cryogrinding THCl. Amorphous thiamine hydrochloride was obtained by cryogrinding **HH** or **ID** in a Freezer/Mill (SPEX 6750, SPEX CertiPrep, Metuchen, NJ). The total milling time was 60 min. This was done in 30 cycles; each cycle consisted of 2 min of grinding followed by a 2-min rest interval. Amorphous–crystalline physical mixtures were prepared by physically mixing 5–50% (w/w) cryoground **ID** with **HH**. Unless otherwise noted, samples were prepared and packed into zirconia rotors in a dry nitrogen glove box. Where applicable, the water content of samples was determined by KFT before and after SSNMR analysis.

A.2.3 Solid-state NMR spectroscopy

[13]C spectra were acquired at 75 MHz (Tecmag Apollo HF-3 and Chemagnetics CMX-300 spectrometers), and at 100 MHz (Infinity-400 spectrometer). All the instruments used a double-resonance probe fitted with a 7-mm spinning module (Revolution NMR, Fort Collins, CO) and approximately 3.0 μs [1]H 90º pulse durations. Pulse sequences included ramped-amplitude cross polarization,[5,6] total sideband suppression (TOSS),[7] and SPINAL64 decoupling.[8] Acquisition parameters included 4 kHz MAS,[9] a contact time of 1.5 ms, and pulse delays at least 1.5 times the [1]H T_1 value of each sample. The ^{1}H relaxation measurements were performed using a saturation–recovery pulse sequence, and T_1 values were calculated using KaleidaGraph (Synergy, version 4.01) with the equation y = amp(1-exp(-τ/T_1)), where y is the integrated signal intensity, amp is the amplitude constant, τ is saturation–recovery time, and T_1 is the spin–lattice relaxation time. 3-methylglutaric acid (MGA) was used to optimize the spectrometer settings as well as to set the reference.[10] For ambient temperature (~20ºC)

experiments, a double-resonance probe fitted with a 7-mm spinning module (Revolution NMR, Fort Collins, CO) was used with a 3.1-μs ^{1}H 90° pulse duration. Variable-temperature SSNMR was performed with a double-resonance probe fitted with a 7.5-mm spin module (Varian, Palo Alto, CA) using a 3.9-μs ^{1}H 90° pulse duration. Lead nitrate was used for temperature calibration.[11] Strict quantitation methods were not used to collect spectra of amorphous–crystalline physical mixtures; however, the same acquisition and processing parameters, including contact time, pulse delay, acquisition length, and 30 Hz of exponential line broadening, were used for all samples.

A.3   Results: Characterization of the nonstoichiometric hydrate (NSH)

A.3.1   Dehydration of NSH

Figure A.4 shows ^{13}C CP-MAS NMR spectra of **NSH** at three levels of hydration. There is only one peak per carbon in each spectrum, indicating that there is one inequivalent site per unit cell, in agreement with the single-crystal structure data. Peak assignments are shown above each peak.[4] The peaks moved downfield and changed line width at lower water contents. The line width reached a maximum breadth at ~0.4 moles water, followed by narrowing as further dehydration occurred.

Figure A.5 highlights the most pronounced spectral changes upon water loss. The largest changes were observed in the carbon atoms closest to the water molecule in the crystal lattice – the β, α, 5, and 4-CH$_3$ carbons. All of the individual peaks (Figure A.5a) have been scaled to the same intensity. The changes in chemical shift and line width of these peaks were plotted as a function of the lattice water content in Figures A.5b and c respectively. The gradual peak shifts indicate that the **NSH** lattice exists as a continuum,
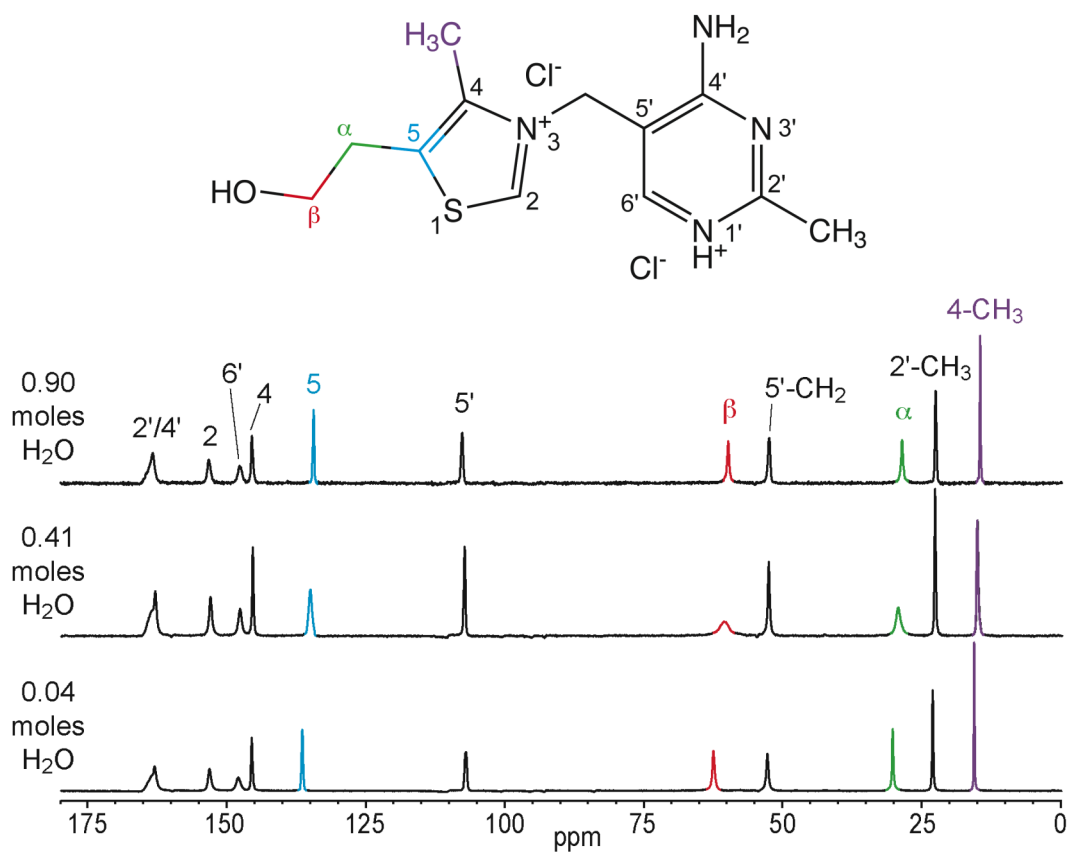
282

Figure A.4. ^{13}C CP-MAS NMR spectra of THCl NSH at various stages of dehydration (0.90–0.04 moles water). Only a few representative spectra are shown. Adapted from Chakravarty et al.[12]
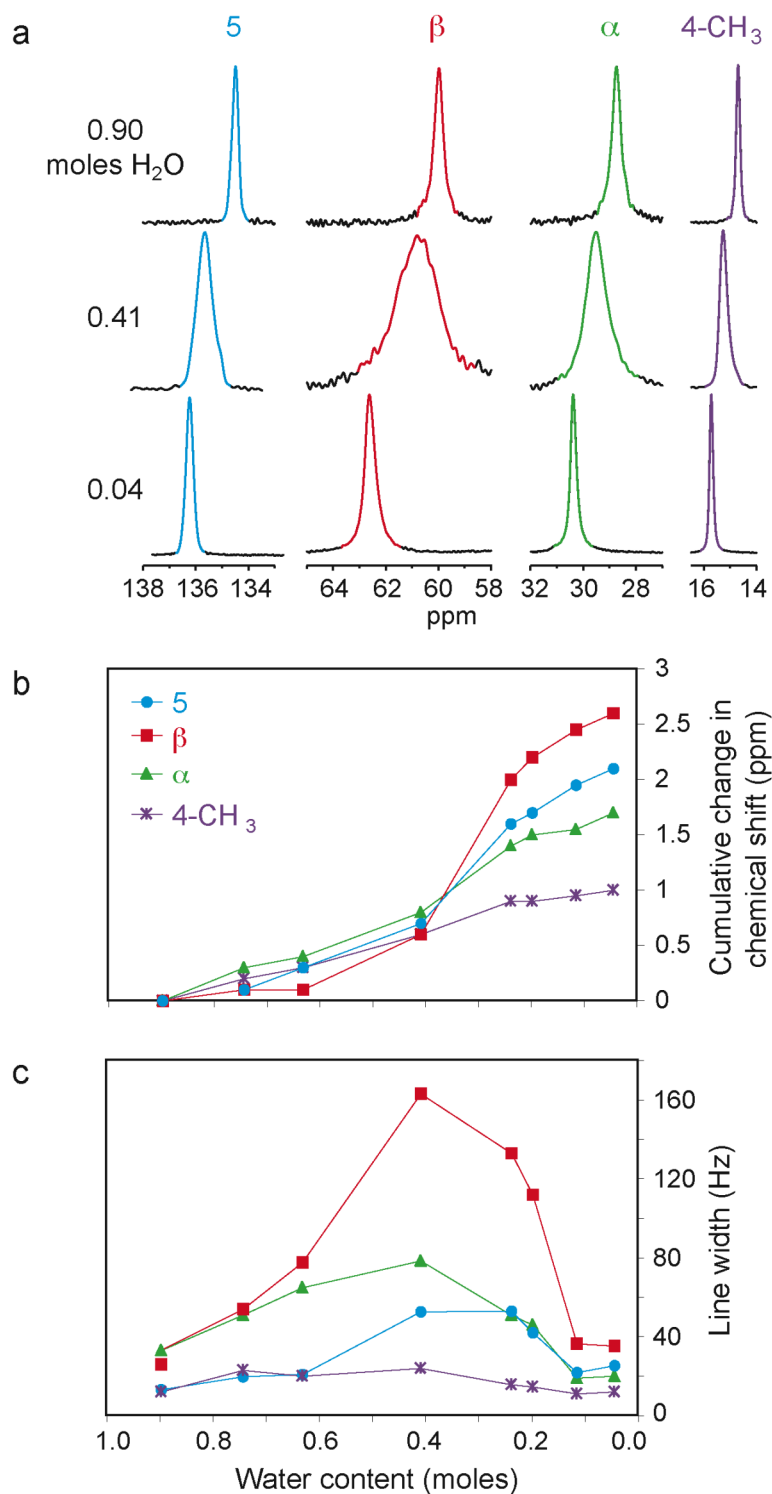
Figure A.5. ^{13}C CP-MAS NMR spectra of NSH in partially dehydrated states. a) Expanded spectral regions of the 5-, β-, α-, and 4-CH$_3$- carbon peaks at water contents of 0.90, 0.41, and 0.04 moles. Plots of the change in b) chemical shift and c) line width as a function of water content (0.90–0.04 moles). Adapted from Chakravarty et al.[12]

rather than a mixture of discrete hydrated and dehydrated crystalline phases. If two phases existed, multiple peaks would have been observed (vide infra). Changes in line width suggest the presence of disorder – either dynamic or static – when the lattice is partially dehydrated (Figure A.6). Dynamic disorder would exist if the observed broad SSNMR peaks represent an average state that appears due to the constant movement of water in the lattice so that changes in conformation between the hydrated and dehydrated states occur too rapidly to be observed as separate peaks in the SSNMR spectrum (Figure A.7). Alternatively, the line broadening could be due to static disorder, in which molecules in the lattice are conformationally disordered within a specific molecular conformation range between that of the hydrated and dehydrated crystalline states (Figure A.7). Both dynamic and static disorder models could be consistent with the results from other techniques. These spectra demonstrate that the hydration state of this system exists in a continuum that contains either dynamic or static disorder.

Figure A.8 is a plot of ^{1}H T_1 relaxation times as a function of hydration state. Relaxation times decreased gradually from ~15 seconds (**NSH**, 0.9 moles water) to ~2 seconds (0.04 moles water), indicating increased mobility as the water content decreased. The dashed line in the plot is the theoretical relaxation curve for a dynamic two-state model. The curve is based on the idea that the observed relaxation time actually represents a combined relaxation of two different sites that are located within a single phase (i.e., intimately mixed). It was created using the known relaxation times at the 0.90 and 0.04 moles hydration states. For example, at a 0.50 moles hydration state, 50% of the thiamine molecules are in the hydrated state (~15 sec ^{1}H T_1), and 50% are in the dehydrated state (~2 sec). Since relaxation is exponential, the observed relaxation time
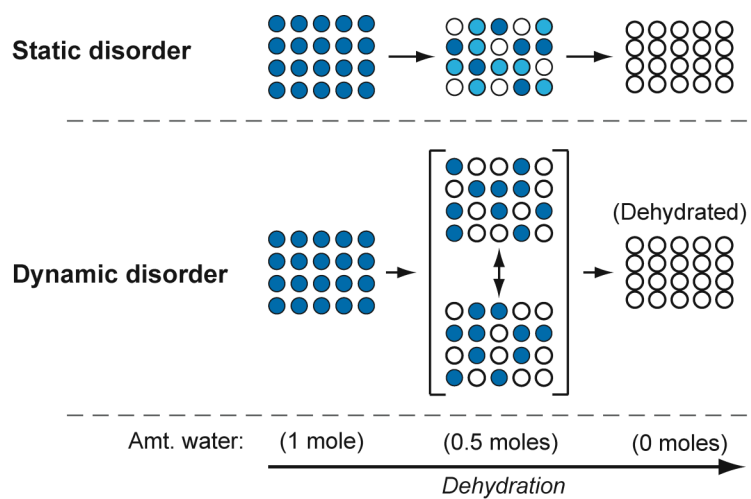
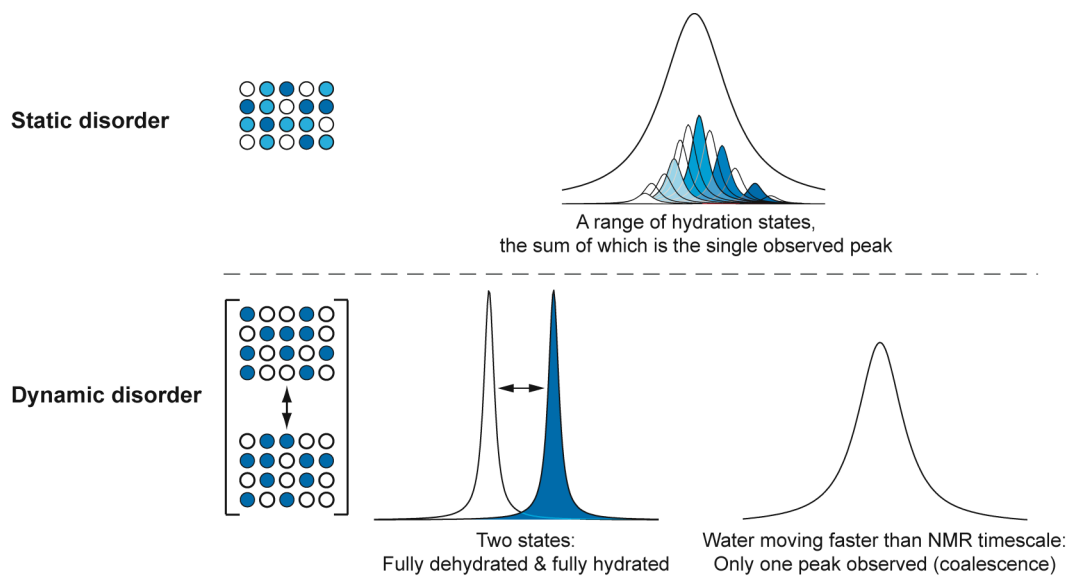**Figure A.6.** Theoretical illustration of dynamic versus static disorder during dehydration of a hydrate.

Figure A.7. Theoretical illustration of dynamic versus static disorder during dehydration of a hydrate, as observed by SSNMR.
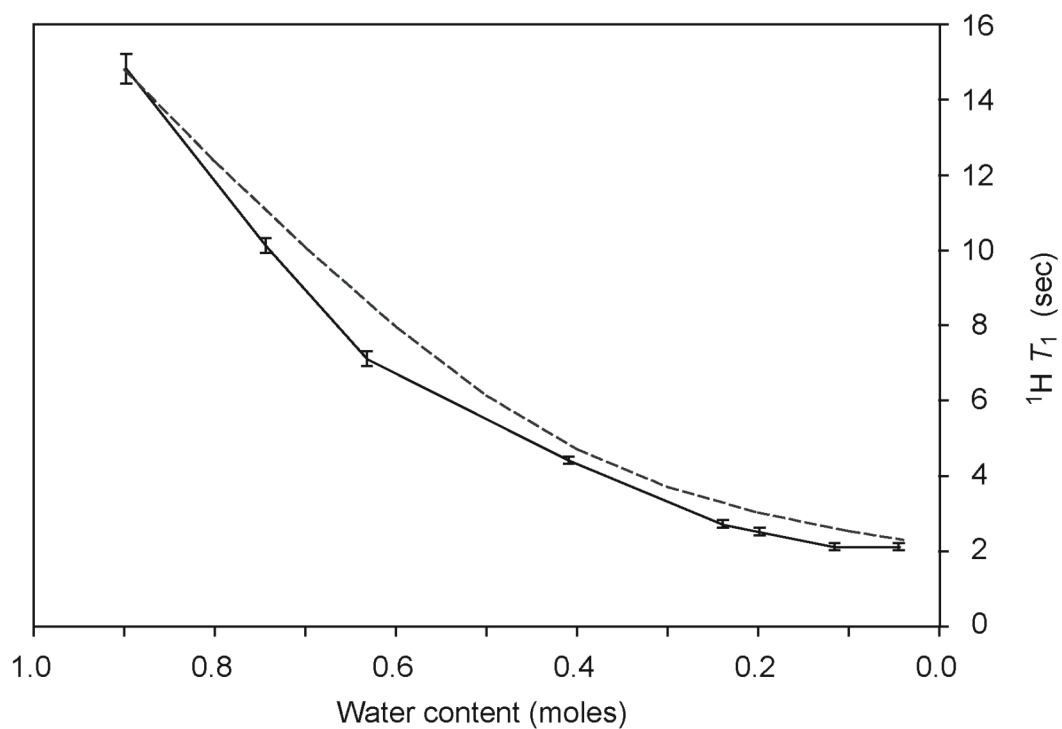
Figure A.8. Plot of NSH ^{1}H T_1 spin–lattice relaxation time (seconds) as a function of water content. Solid line represents ^{1}H T_1 values calculated from experimental data, and error bars indicate error associate with the calculations. Dashed curve represents the theoretical relaxation for a two-site model. Decreased relaxation time indicates an increase in lattice mobility. Adapted from Chakravarty et al.[12]

for the 0.5 moles hydration state is biased toward the lower relaxation time. In this case, the theoretical relaxation time would be ~6 sec. The two-site dynamic model agrees very well with the experimental relaxation times. However, it is possible for a static-disorder model to fit the experimental data as well. The ^{1}H T_1 data are consistent with the presence of either static or dynamic disorder in a continuum.

A.3.2 Variable-temperature SSNMR of NSH

Figure A.9 shows variable-temperature ^{13}C CP-MAS NMR spectra that were collected to distinguish between static and dynamic disorder in the partially dehydrated **NSH** system. Due to the temperature dependence of molecular motion, changes in temperature should have a pronounced effect on a system with dynamic disorder, with little to no effect on a sample with static disorder. The sample was a 1:1 (w/w) physical mixture of **NSH**:**ID** (overall water content of 0.42 moles). A spectrum of the non-equilibrated physical mixture was obtained at 20ºC (not shown). Two peaks for several of the carbons were present in the spectrum, corresponding to a mixture of separate hydrated and dehydrated phases. The temperature was increased to 50ºC, at which point spectra were acquired every hour until equilibration was complete (~12 hr), as indicated by coalescence of fully hydrated and fully dehydrated peaks into a single peak for each carbon (not shown). Immediately following equilibration, ^{13}C spectra of the sample were acquired in the temperature range of 100 to -80ºC (Figure A.9, collected in the following order: 100, -80, -40, and 30ºC). The spectra show a single narrow peak for each carbon atom at 100ºC, then peak broadening at 30ºC, followed by peak splitting at -40ºC. The likely explanation for this observed splitting is that cooling the **NSH** sample
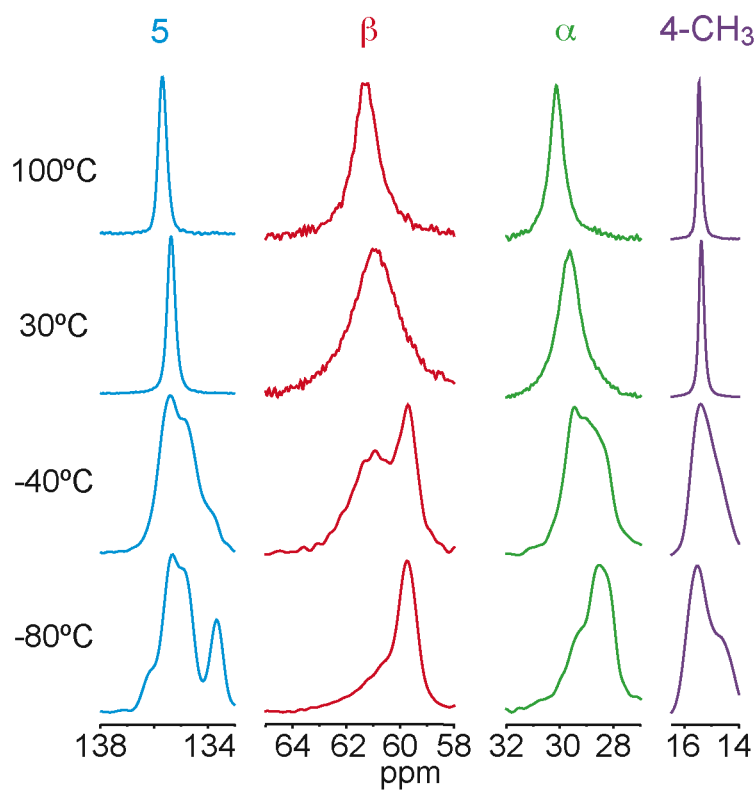
Figure A.9. Variable-temperature ^{13}C CP-MAS NMR spectra of THCl NSH with 0.42 moles of water, acquired from 100 to -80ºC. Spectral regions for carbons 5, β, α, and 4-CH$_3$ are shown. Adapted from Chakravarty et al.[12]

to -40ºC sufficiently slowed the movement of the water molecules such that SSNMR detected the individual hydrated and dehydrated states, resulting in two peaks for several of the carbon atoms. The temperature dependence of the peak width demonstrates that dynamic disorder exists in the **NSH** system, and it is this dynamic disorder that causes the broad peaks in partially dehydrated samples at room temperature (Figures A.5a and c). In addition to the changes in peak width, temperature-dependent peak shifts and additional peak splitting at -80ºC were observed. The peak shifts were not influenced by the state of hydration (data not shown), and they are likely the result of a change in either the lattice density or interactions with quadrupolar chloride ions. The additional peak splitting at -80ºC, which does not correspond to peaks for the **NSH** or **ID** forms, is attributed to carbon–chlorine quadrupolar coupling. Typically, chloride-ion nuclei are able to self-decouple due to rapid movement at room temperature. Upon cooling, this self-decoupling mechanism can be inhibited, resulting in peak splitting.[13,14]

A.3.3   Overview of NSH characterization

Conceptually, one can think of the **NSH** (~1 moles water) and **ID** as the two extremes in a system exhibiting a continuum in the state of hydration. Partial dehydration of **NSH** produced gradual peak shifts in SSNMR spectra. Observation of peak shifts, as opposed to the appearance of new peaks, indicated that the hydration state of all crystallites in the powder exist as a single, continuous phase and not a mixture of separate fully hydrated and fully dehydrated phases.

 SSNMR studies show that this system can be defined as a dynamic two-site model, in which the thiamine molecules transiently exist in either hydrated or dehydrated

states. The ^{1}H T_1 relaxation data is consistent with this model, and low temperatures slowed the movement of water molecules to the point where the individual hydrated and dehydrated states were observed in the SSNMR spectra. At higher temperatures, including room temperature, the water molecules move faster than the SSNMR timescale, giving rise to the broad peaks observed in partially dehydrated **NSH**.

The SSNMR studies reported here only included observation of ^{13}C nuclei. However, chlorine–carbon coupling effects were observed during the VT SSNMR studies. Although the presence of this quadrupolar coupling complicated the ^{13}C spectra at low temperature, it highlights the potential use of analyzing this system by ^{35}Cl SSNMR.[15] Because the chloride ions are directly bonded to a water molecule, changes in the water content will have a significant effect on the chlorine nuclei, as well as neighboring nuclei. In addition, thiamine contains four nitrogen nuclei, which also might be significantly affected (directly or indirectly) by water loss. Future studies of this system might benefit from use of ^{35}Cl and ^{15}N SSNMR spectroscopy.

Dehydration of the nonstoichiometric hydrate (**NSH**) form of **THCl** results in the formation of an isomorphic desolvate (**ID**) where the lattice packing is minimally affected by the departure of water. This dehydration behavior is not readily evident from its structure due to lack of connecting pathways that facilitate the smooth departure of water from the lattice. **NSH** (with ~1 moles water) and **ID** represent the two extremes of a system exhibiting a continuum in the state of hydration. On the basis of structural and mobility data, it is hypothesized that the variable-hydrate nature of **THCl NSH** arises from the ability of the thiamine molecules to cooperatively deform, therein allowing rapid movement of water throughout the lattice, despite the lack of continuous channels.[16]

A.4 Results: Characterization of the hemihydrate (HH)

A.4.1 Dehydration of HH

Figure A.10 shows ^{13}C CP-MAS NMR spectra of **HH** subjected to different treatments. Partial dehydration of **HH** under low pressure for 7 days (**HH₂**) resulted in a new peak at 157 ppm and the appearance of shoulders on the peaks at 148, 138, 65, and 18 ppm. In an effort to identify the source of these new peaks, two additional samples were prepared: 1) forcefully degraded **HH**, prepared by heating **HH** at 180ºC for 4 hr; and 2) amorphous **HH**, prepared by cryogrinding. In the forcefully degraded sample, there was a visible color change (from white to dark yellow), which was not observed in **HH₂** samples. However, the spectra of **HH₂** and the forcefully degraded **HH** were very similar; both contained the additional peak at 157 ppm as well as shoulders on other peaks throughout the spectrum. Only the forcefully degraded sample contained a small amount of anhydrous **NSH/ID**, evidenced by the low-intensity peaks at ~15 and 136 ppm. The lack of an observable color change in **HH₂** suggests that the observed spectral changes, in particular the appearance of the peak at 157 ppm, cannot be attributed to the presence of thermal degradant. The yellow thermal degradant likely existed at levels below the limit of detection of the SSNMR method, as no peaks in the spectrum of the forcefully degraded sample could be attributed to the degradant. The 157-ppm peak in the spectra of **HH₂** and forcefully degraded **HH** also cannot be attributed to amorphous THCl, since this peak is absent in the spectrum of cryoground **HH**. The water content of **HH₂** and forcefully degraded **HH** were below the stoichiometric water content of the hemihydrate (KFT), which suggests that the loss of water is responsible for the appearance of the new peak and shoulders. Additional SSNMR studies were performed
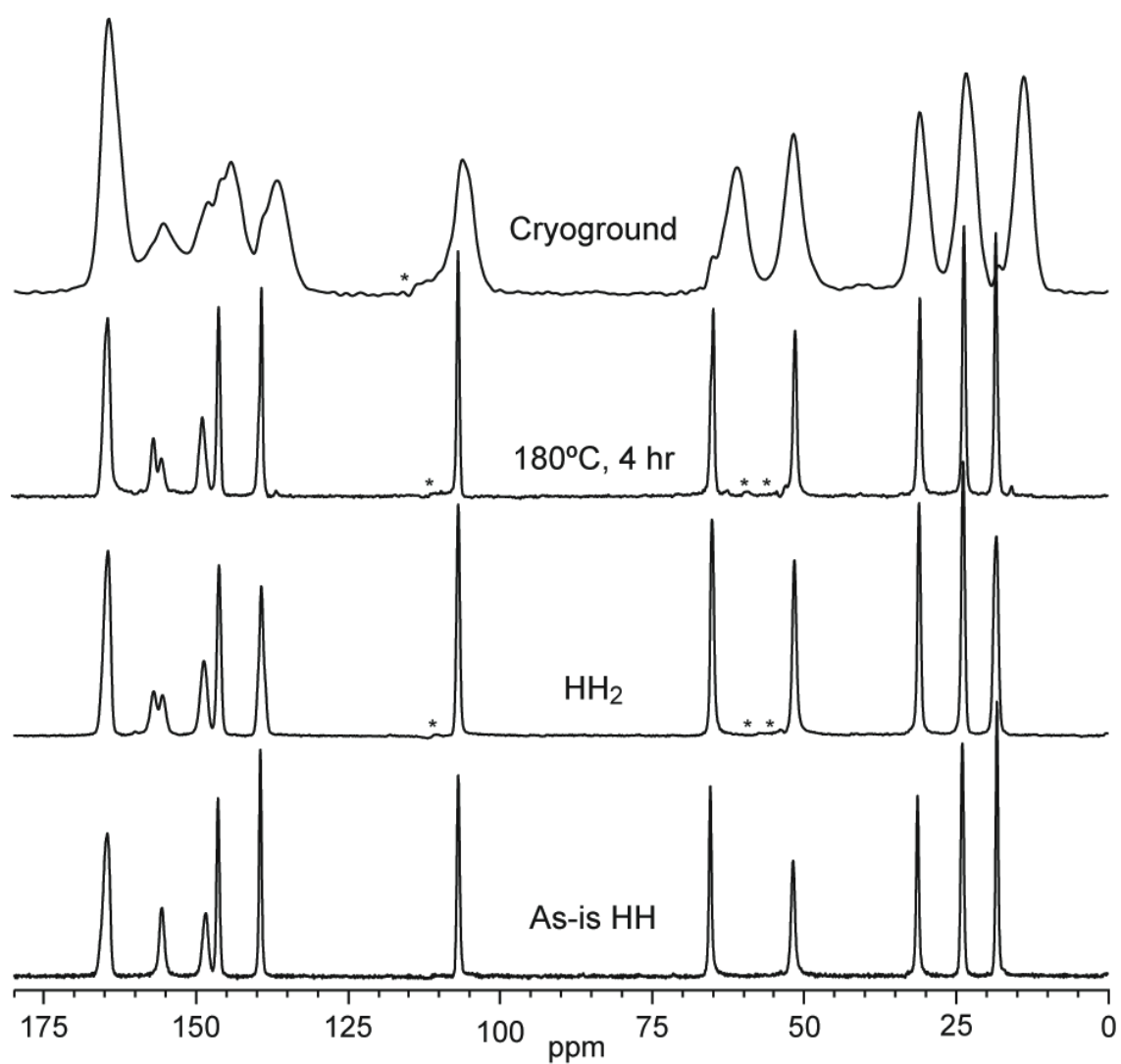
Figure A.10. ^{13}C CP-MAS NMR spectra of various samples of THCl HH. Asterisks denote spinning sideband artifacts. Adapted from Chakravarty et al.[17]

in order to characterize the stability and reversibility of the spectral changes that occurred upon partial dehydration of the **HH** lattice.

Figure A.11 contains the ^{13}C CP-MAS NMR spectra of a single **HH$_2$** sample progressively analyzed following exposure to different storage conditions, and the spectrum of **HH** is included for comparison. The region from 130 to 170 ppm was expanded in order to better observe spectral changes. The second-from-the-top spectrum is that of freshly prepared **HH$_2$** (same sample shown in Figure A.10). Following spectral acquisition, the sample was removed from the instrument (but not unpacked from the SSNMR rotor) and stored for 6 weeks (RT) in a desiccator containing anhydrous CaSO$_4$. SSNMR analysis following this dry storage showed only a slight change in the relative intensities of the peaks at ~157 ppm, indicating that the sample was fairly stable under these storage conditions. Following analysis, the sample was unpacked from the rotor into a glass vial, which was left uncapped for ~24 hr at ambient laboratory conditions. The powder sample was then repacked into the rotor (under ambient conditions) and analyzed. The spectrum shows significant changes in the intensity of the peak at 157 ppm and the shoulder at ~138 ppm (arrows in Figure A.11) and results in a spectrum that more closely resembles that of **HH**. This supports that the additional peak and shoulders (157, 148, 138, 65, and 18 ppm) in the **HH$_2$** spectrum arise from partial dehydration of the **HH** lattice and that this dehydration is reversible upon storage in the presence of water vapor.

Since partial dehydration did not significantly change the spectrum, it is unlikely that the water removal significantly affected the thiamine molecular conformation/packing. Instead, two possible causes for the additional SSNMR peaks
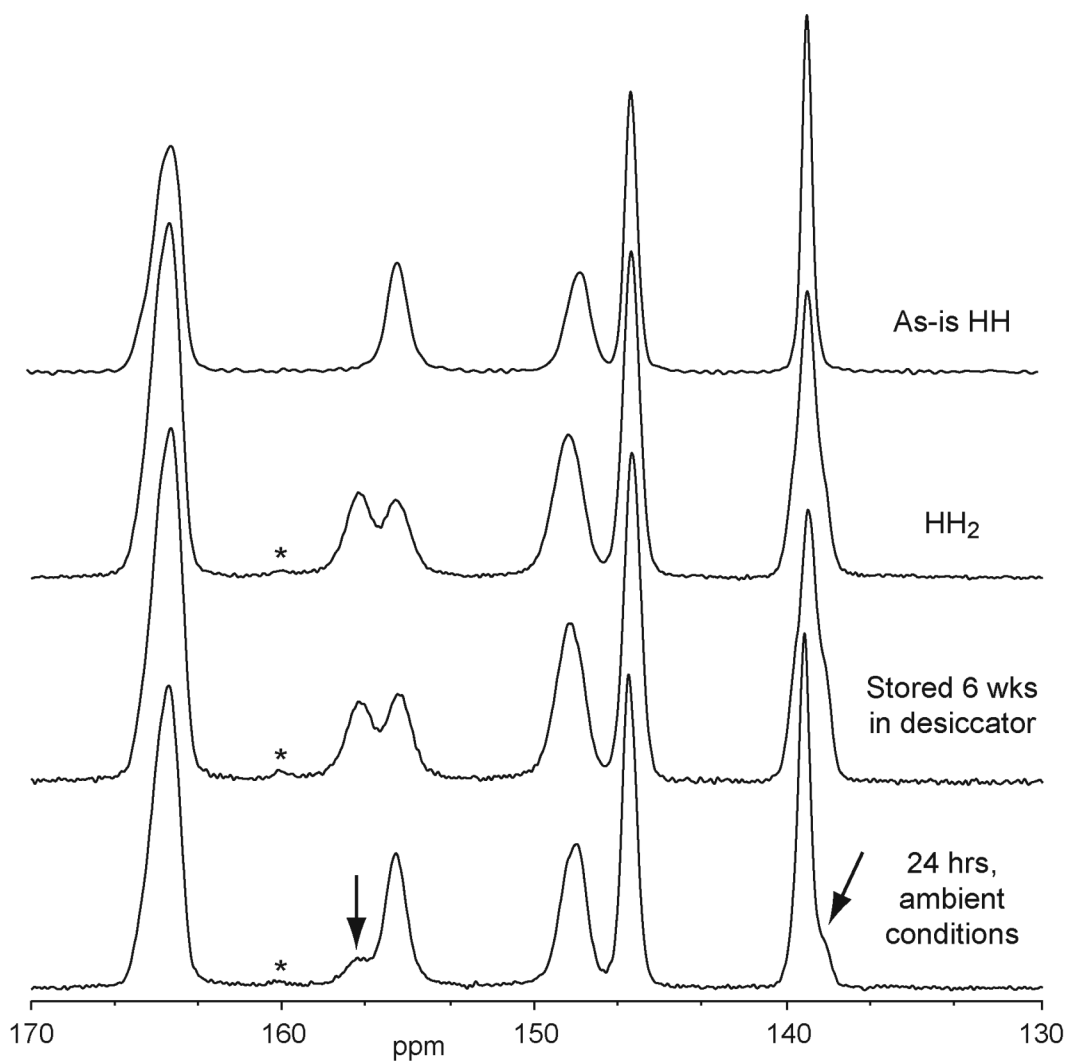
Figure A.11. ^{13}C CP-MAS NMR spectra of a single HH_2 sample, progressively analyzed upon exposure to different storage conditions. Arrows highlight spectral changes. Asterisks denote spinning sideband artifacts. Adapted from Chakravarty et al.[17]

were hypothesized: 1) the loss of water caused changes in ^{13}C–^{14}N coupling and/or 2) the removal of water changed the electronic field and/or physical location of the chloride ions within the crystal lattice. The potential for altered ^{13}C–^{14}N coupling upon water loss is relevant due to the presence of four nitrogen nuclei in the thiamine molecule. Spectra of a single **HH$_2$** sample were acquired on both 300 and 400 MHz spectrometers in order to determine if the new peaks were associated with changes in ^{13}C–^{14}N coupling. The line widths (in ppm) of the peaks should be different at different field strengths if such coupling is present. The differences in line widths at the two field strengths were not significant enough to make definitive conclusions (data not shown). Another potential cause of the new peaks/shoulders upon partial dehydration is movement of the chloride ion within the lattice. X-ray structural data shows that the chloride ions are hydrogen-bonded to water and electrostatically bound to the thiamine molecule. Upon removal of water, the chloride ion may interact differently with the thiamine molecule due to changes in the charge distribution and/or physical location of the ion. Molecular modeling studies will be necessary to further understand the observed dehydration-induced SSNMR spectral changes.

A.4.2 *Assessing the crystallinity of partially dehydrated HH*

SSNMR also was used to investigate the effect of partial dehydration of **HH** on the crystallinity of the product phase, **HH$_2$**. A broad halo was observed in the PXRD pattern of **HH$_2$** (not shown), and the sample also showed significant water uptake upon exposure to high relative humidity. However, these results could not distinguish between the two models of crystallinity: i) the two-state model, which assumes the existence of

the lattice in either a perfectly ordered (100% crystalline) or a totally disordered (100% amorphous) state and expresses the degree of crystallinity of a sample in terms of the fractions of these two states; and ii) the one-state model, which assumes a gradual and continuous decrease in lattice order during the progression from a completely ordered to a completely disordered lattice.[18,19] If the PXRD halos were due to amorphous material (two-state model), the amorphous fraction should be high enough to be detected by SSNMR.

Figure A.12 contains the ^{13}C CP-MAS NMR spectra of physical mixtures of **HH** and amorphous **THCl**. The region from 5–35 ppm has been expanded in order to clearly show the separate crystalline **HH** peak (~18 ppm) and amorphous peak (~14 ppm) of the **THCl** 4-CH$_3$ carbon. In the 50% amorphous sample, the low-intensity peak at ~15 ppm indicates residual **ID** in the amorphous material. This impurity is attributed to incomplete amorphization by cryogrinding and is not particularly disruptive since the objective was not the rigorous quantitation of the different physical forms. The purpose of the SSNMR study was to: (i) demonstrate that low levels of amorphous material could be detected by SSNMR, (ii) determine if amorphous material was present in **HH$_2$**, and (iii) estimate the amorphous content of **HH$_2$**. As observed in the top three spectra of Figure A.12, the peak attributed to amorphous **THCl (~**15 ppm) was discernible down to 5% amorphous level. In the **HH$_2$** spectrum, it is difficult to assign the signal at this chemical shift to a peak. Thus, even if in **HH$_2$** contains amorphous **THCl**, its concentration is significantly lower than 5%. Such a low concentration of amorphous material is unlikely to yield the pronounced halo observed in the PXRD pattern (not shown). It is therefore hypothesized that the halos exists due to partial loss of long-range order (one-state model), and not due
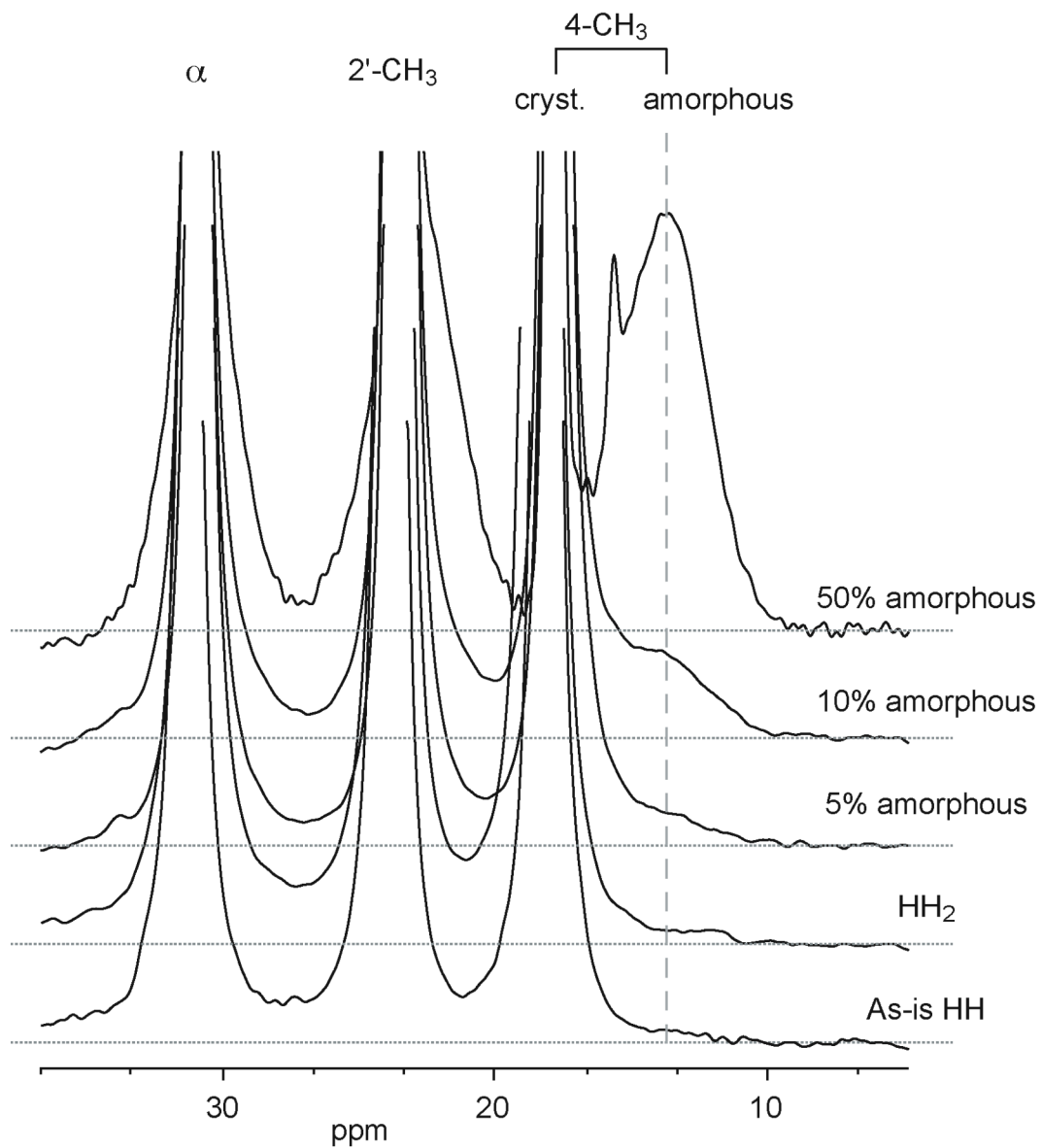
Figure A.12. ^{13}C CP-MAS NMR spectra of HH with varying levels of amorphous content. Crystalline and amorphous peaks for the 4-CH$_3$ carbon are well resolved. The dashed vertical line indicates the amorphous peak position, and dotted horizontal lines display the spectral baseline. Adapted from Chakravarty et al.[17]

to the formation of an amorphous phase (two-state model), upon removal of water from the lattice.

A.4.3 *Overview of HH characterization*

THCl HH is extremely stable and demonstrates slow dehydration kinetics in the solid state. Attempts to dehydrate **HH** at low temperatures (<100ºC) and reduced pressure caused incomplete dehydration and loss of long-range order within the crystal lattice, while, at elevated temperatures (>120ºC), water loss was accompanied by decomposition. **NSH** and **HH** show pronounced differences in their physical stability, which is attributed to the differences in the water-binding in their respective crystal lattices.

A.5 References

1. Cui Y, Yao E 2008. Evaluation of hydrate-screening methods. J Pharm Sci 97(7):2730-2744.

2. Khankari RK, Grant DJW 1995. Pharmaceutical hydrates. Thermochim Acta 248:61-79.

3. Byrn SR, Pfeiffer RR, Stowell JG 1999. Solid-State Chemistry of Drugs. 2nd ed., West Lafayette, Indiana: SSCI, Inc.

4. Te RL, Griesser UJ, Morris KR, Byrn SR, Stowell JG 2003. X-ray diffraction and solid-state NMR investigation of the single-crystal to single-crystal dehydration of thiamine hydrochloride monohydrate. Cryst Growth Des 3(6):997-1004.

5.   Metz G, Wu X, Smith SO 1994. Ramped-amplitude cross polarization in magic-angle-spinning NMR. J Magn Reson, Ser A 110(2):219-227.

6.   Pines A, Gibby MG, Waugh JS 1973. Proton-enhanced NMR of dilute spins in solids. J Chem Phys 59(2):569-590.

7.   Dixon WT, Schaefer J, Sefcik MD, Stejskal EO, McKay RA 1982. Total suppression of sidebands in CPMAS carbon-13 NMR. J Magn Reson 49(2):341-345.

8.   Fung BM, Khitrin AK, Ermolaev K 2000. An improved broadband decoupling sequence for liquid crystals and solids. J Magn Reson 142(1):97-101.

9.   Andrew ER, Bradbury A, Eades RG 1959. Removal of dipolar broadening of nuclear magnetic resonance spectra of solids by specimen rotation. Nature 183:1802-1803.

10.   Barich DH, Gorman EM, Zell MT, Munson EJ 2006. 3-Methylglutaric acid as a 13C solid-state NMR standard. Solid State Nucl Magn Reson 30(3-4):125-129.

11.   Bielecki A, Burum DP 1995. Temperature dependence of 207Pb MAS spectra of solid lead nitrate. An accurate, sensitive thermometer for variable-temperature MAS. J Magn Reson, Ser A 116(2):215-220.

12.   Chakravarty P, Berendt RT, Munson EJ, Young VG, Jr., Govindarajan R, Suryanarayanan R 2010. Insights into the dehydration behavior of thiamine hydrochloride (Vitamin B1) hydrates: Part I. J Pharm Sci 99(2):816-827.

13.   Spiess HW, Haeberlen U, Zimmermann H 1977. Proton multiple-pulse study of a single crystal of trans-diiodoethylene: example of self-decoupling. J Magn Reson 25(1):55-66.

14.   Harris RK, Olivieri AC 1992. Quadrupolar effects transferred to spin-1/2 magic-angle spinning spectra of solids. Prog Nucl Magn Reson Spectrosc 24(5):435-456.

15.   Hamaed H, Pawlowski JM, Cooper BFT, Fu R, Eichhorn SH, Schurko RW 2008. Application of solid-state 35Cl NMR to the structural characterization of hydrochloride pharmaceuticals and their polymorphs. J Am Chem Soc 130(33):11056-11065.

16.   Petit S, Coquerel G 1996. Mechanism of several solid-solid transformations between dihydrated and anhydrous copper(II) 8-hydroxyquinolinates. Proposition for a unified model for the dehydration of molecular crystals. Chem Mater 8(9):2247-2258.

17.   Chakravarty P, Berendt RT, Munson EJ, Young VG, Jr., Govindarajan R, Suryanarayanan R 2010. Insights into the dehydration behavior of thiamine hydrochloride (vitamin B1) hydrates: Part II. J Pharm Sci 99(4):1882-1895.

18.   Suryanarayanan R, Mitchell AG 1985. Evaluation of two concepts of crystallinity using calcium gluceptate as a model compound. Int J Pharm 24(1):1-17.

19.   Huettenrauch R 1978. Molecular galenics as the basis of modern drug formation. Acta Pharm Technol, Suppl 6:55-127.